Segmented π-Conjugated Polymers For Optical and Biomedical Applications

A Thesis

Submitted in Partial Fulfillment of the Requirements
Of the Degree of
Doctor of Philosophy

By

Karnati Narasimha

Reg. No. 20113142

Department of Chemistry

INDIAN INSTITUTE OF SCIENCE EDUCATION AND RESEARCH, PUNE

Pune 411008, Maharashtra, India

July 2017

Dedicated to…

My Parents

भारतीय विज्ञान शिक्षा एवं अनुसंधान संस्थान पुणे
INDIAN INSTITUTE OF SCIENCE EDUCATION AND RESEARCH PUNE
(An Autonomous Institution of Ministry of Human Resource Development, Govt. of India)
Dr. Homi Bhabha Road, Pune - 411 008.

Prof. M. Jayakannan
Professor and Chair
Department of Chemistry

CERTIFICATE

Certified that the work incorporated in the thesis entitled "*Segmented π-Conjugated Polymers for Optical and Biomedical Applications*" Submitted by **Mr. Karnati Narasimha** was carried out by the candidate under my supervision. The work presented here or any part of it has not been included in any other thesis submitted previously for the award of any degree or diploma from any other University or Institution.

Date: 12/07/2017.
Pune (MH) India

Prof. M. Jayakannan
(Thesis Supervisor)

DECLARATION

I declare that this written submission represents my ideas in my own words and where others' ideas have been included; I have adequately cited and referenced the original sources. I also declare that I have adhered to all principles of scientific honesty and integrity and have not misrepresented or fabricated or falsified any idea/data/fact/source in my submission. I understand that violation of the above will be cause for disciplinary action by the institute and can also evoke penal action from the sources which have thus not been properly cited or from whom proper permission has not been taken when needed.

K. Narasimha

Date: 12/07/17

Pune (MH) India

Karnati Narasimha

Roll No: 20113142

ACKNOWLEDGEMENTS

I would like to express my sincere gratitude to my supervisor **Prof. M. Jayakannan** for his continuous support, patience, motivation and immense knowledge during my PhD study and related research. His guidance helped me in all the time of research and writing of this thesis. I will be always grateful to him for teaching, guiding and counseling me for all these years of my PhD at IISER, Pune.

I am extremely thankful to my research advisory committee (RAC) members; Dr. S. G. Srivatsan, Dr. K. Krishnamoorthy and Dr. J. Nithyanandhan for their insightful comments and encouragement during RAC meetings.

My sincere thanks goes to Prof. K.N. Ganesh, Director, and IISER-Pune for providing the research facilities at IISER Pune for carrying out this research work.

I would also like to thanks Dr. Asha, S. K. from NCL Pune, for her constant support, intellectual scientific discussions, and for giving the flavour of homely environment during my stay at IISER.

I would like to thank all the faculty members in the department of chemistry for extending their research facilities, interactive scientific discussions and teaching me various courses.

I specially thanks my present and former lab mates for their support and cooperation especially, Balamurugan, Mahima, Smita, Ananthraj, Moumita, Pramod, Bapu, Rajendra, Bhagyashree, Mehak, Sonashree, Nilesh, Dheeraj, Nitesh, Shraddha, Hemlata, Ruma, Mishika, Shurpuddhin, Khushboo, Vikas, Uma, Kaushalendra, Rekha, Nagesh, Chinmay, Shekhar, Nisha, Senthil, Saibal, Prajitha, Swapnil, Sarabjot, Sandeep and Jhansi.

I take this opportunity to say my sincere thanks to my labmates Dr. Bapurao surnar, Nilesh, and Sonashree for helping me with cytotoxicity studies, and confocal microscope imaging. I also wish to thanks my labmate Dr. Anantharaj for his wonderfull guidance and helping with my experiments during my initial days of Ph.D.

I would like to thank all instruments' technicians of IISER Pune for their support: Pooja, Deepali, Chinmay (NMR), Swati (MALDI), Nayna (HRMS), Megha (AFM), Anil, Yatish

(FE-SEM), Mayuresh, Nithin, and Mahesh (Department staff). I thank National Chemical Laboratory (NCL) Pune for HR TEM facilities.

A heartfull thanks to all my friends who made the IISER Pune experience more funfull, specially Telugu friends Kishor, Gopal, Sivakoti, Harikrishna, Ashok, Sandeep, Rajkumar, Subrahmanyam, Dinesh, Jagan, Naveen, Gayatri, Mahesh, jagadish, shiva, sharath, Gurivireddy, Chenna reddy, Ranga reddy, and Narendraprasad reddy. I also like to thank my labmate Dheeraj for keeping my taste buds alive with his wonderfull dal, rice and also for countless joyfull evenings.

I would like to thank my parents and mom for everything that I have achieved in life, without her none of this would have been possible. I thanks my brothers (Ravi, Punnaiah) and for their whole hearted support and encouragement.

Financial support from UGC and IISER Pune is greatly acknowledged.

.

Narasimha

Synopsis

The development of π-conjugated polymers and study their self-assembly process through non-covalent interactions such as aromatic π-stacking is an important area of research due to their ability to exhibit diverse nano-assemblies for applications in material science and biomedical field. Self-assembly of π-conjugated polymers that are responsive to undergo changes in the chain backbone with respect to the topology is particularly important since it would provide new fundamental understanding on chain folding phenomena and also facilitate the design of new materials. Segmented π-conjugated polymers are unique classes of materials with rigid aromatic π-core and flexible alkyl or oligoethyelene spacers in the backbone. In this design, the aromatic rigid core and flexible units can be selectively segregated in the polymer matrix via weak non-covalent interactions such as aromatic π-stacking and van der Waals forces. The thesis work aims to design and develop new classes of amphiphilic and non-amphiphilic segmented π-conjugated polymer deign based on oligo-phenylenevinylene (OPV) π-core. These segmented polymers were demonstrated for their applications in π-conjugated photonic switches (or photonic wave plates), fluorescent nanoparticle bio-probes for cancer cell imaging, and also producing room temperature charge transfer complexes with color-tunable absorbance in the entire solar spectrum. The thesis has been divided into four major sections:

1. **Chapter-1:** The introduction chapter provides literature survey on the π-conjugated polymers and their application in devices, self-assembly of amphiphilic polymers, and emphasized the need for the development of segmented π-conjugated polymers.
2. **Chapter-2:** First attempts on the building of π-conjugated photonic switches (or optical wave plates) from concept to reality is demonstrated. New series of semi-crystalline segmented π-conjugated polymers were designed and developed and their self-assembled organogel was constructed as thermo-reversible photonic switches for imaging technology.
3. **Chapter-3:** Amphiphilic π-conjugated polymer was designed and their stable aqueous luminescence nanoparticles were employed as bio-imaging probe in cancer cells. Solvent-induced chain aggregation studies were studies in detail to trace the morphological transitions from one dimensional helical nano-fibrous to three dimensional spherical nano-assemblies.
4. **Chapter 4:** Room temperature charge transfer complexes based on segmented OPV polymers and arylene bisimides were developed. Thermal analysis, electron and light microscope imaging, steady state photophysical studies were carried out us to establish the donor-acceptor self-assembly in charge transfer complexes.

The chapter 2 demonstrates one of the first examples of π-conjugated photonic switches (or photonic wave plates) based on the tailor made π-conjugated polymer anisotropic organogel. New semi-crystalline segmented π-conjugated polymers were designed with rigid aromatic OPV π-core and flexible alkyl chain along the polymer backbone. These polymers are found to be self-assembled as semi-crystalline or amorphous with respect to the number of carbon atoms in the alkyl units. These semi-crystalline polymers produce organogel having nano-fibrous morphology of 20 nm thickness with length up to 5 μm. The polymer organogel is aligned in a narrow glass capillary and this anisotropic gel device is further demonstrated as photonic switches. The glass capillary device behaves as typical λ/4 photonic wave plates upon the illumination of the plane polarized light. The λ/4 photonic switching ability is found to be maximum at θ = 45° angle under the cross-polarizers. The orthogonal arrangements of the gel capillaries produce dark and bright spots as on-and-off optical switches waves. Thermo-reversibility of the polymer organogel (also its xerogel) was exploited to construct thermo-responsive photonic switches for the temperature window starting from 25 to 160 °C. The organic photonic switch concept can be adapted to large number of other π-conjugated materials for optical communication and storage.

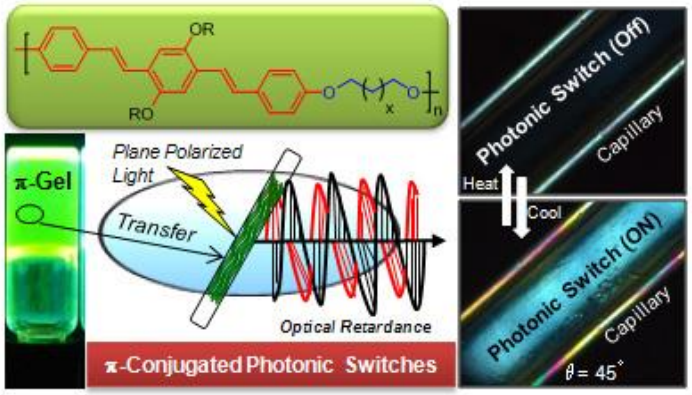

In chapter 3, color tunable amphiphilic segmented π-conjugated polymer design was developed and demonstrated their application as luminescent nanoparticle probes for bio-imaging in cervical and breast cancer cells. Oligo-phenylenevinylene (OPV) was employed as rigid luminescent π-core and oligo-ethyleneoxy chains were used as flexible spacers to constitute new amphiphilic segmented π-conjugated polymers by Witting-Horner polymerization route. The rigidity of the π-core was varied using tricyclodecanemethyloxy, 2-etheylhexyloxy or methoxy pendants. Solvent-induced chain aggregation of the polymers exhibited morphological transition from one dimensional helical nano-fibrous to three dimensional spherical nano-assemblies in good/bad solvent combinations. This morphological transformation was accompanied by the fluorescence colour change from blue-to-white-to-yellow. Electron and atomic microscopes, steady state photophysical studies, time resolved fluorescent decay analysis and dynamic light scattering method enabled us to establish the precise mechanism

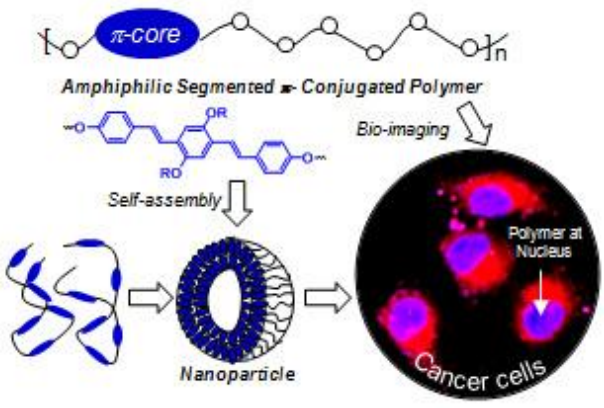

for the self-assembly of segmented OPV polymers. The polymers produced stable and luminescent aqueous nanoparticles of < 200 nm in diameter in water. Cytotoxicity studies in cervical and breast cancer cells revealed that these new aqueous luminescent polymer nanoparticles are highly biocompatible and non-toxic to cells up to 60 μg/mL. Cellular uptake studies by confocal microscope further exposed that these nanoparticles were internalized in the cancer cells and they were predominantly accumulated at the nucleus.

In chapter 4, room temperature stable solid state charge transfer (CT) complexes based on electron rich oligo-phenylenevinylene (OPV) and electron deficient arylenebisimides were reported. Semi-crystalline or amorphous segmented OPVs polymers were complexed with naphthalene (NDI) and phenylene (PDI) biimides to produce red and green colored CT complexes having absorbance from the visible to NIR region in the solar spectrum. The donor-acceptor interaction exhibited thermo-reversibility and also produced 1:1 complexation with respect to long range order of …D-A-D-A.. aromatic π-stacks. Interestingly, the solid state alignment of the D-A interaction was highly selective to the acceptor units, and the OPV polymer-NDI complex exclusively showed two dimensional lamellar packing. Electron microscope, polarizing microscope and x-ray diffraction analysis provided direct evidence for the lamellar D-A self-assembly in the solid state. The polymer based CT bands was found to be stable irrespective of the nature of the segmented OPV polymers whether it was semi-crystalline or amorphous. This enabled the accomplishment of room temperature CT complexes in π-conjugated polymer system having absorption from 350 to 1100 nm. These stable room temperature donor-acceptor CT self-assemblies are processed under solvent free melt crystallization process; thus, they are very good materials for processing in optoelectronics.

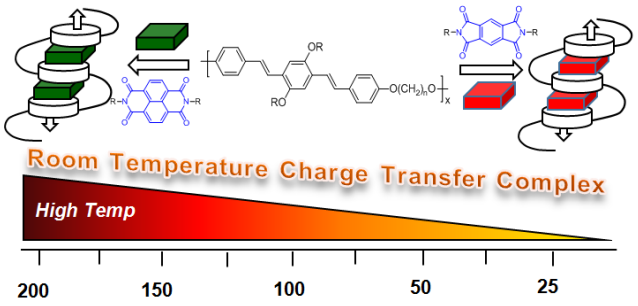

The last chapter summarized the overall thesis work and also describes the future direction.

TABLE OF CONTENTS

Chapter 1

Introduction

1.1. Introduction to Conducting Polymers

Polymers are a quintessential class of materials due to high tensile strength, non-wettability, high mechanical strength, elasticity, resistance towards acids and alkalis, facile processibilty used in wide range of applications in plastics, textiles, nano sensors, cosmetics, life sciences, coatings, paints, electric insulation and so on. Easy synthetic procedures make polymers an attractive class of materials. Typically, polymers are insulator in nature; for example, polyethylene, polypropylene and polyvinylchloride are some of the widely used polymers for electrical insulator applications. Recent discoveries by three eminent scientists MacDiarmid, Heeger, and Shirakawa showed that a selective group of polymers having extended π-conjugation can conduct electricity like metals, which changed the entire way of looking at polymers as insulators.[1] Polymeric materials with these special features were used for newer applications in molecular electronics and bio-medical applications. The Molecular electronics such as light emitting diodes (LEDs), photovoltaic (PVs), field effect transistor (FETs),[2-6] and room-temperature organic ferroelectric devices[7] and on the other hand bio-medical applications such as bio-imaging,[8-9] DNA binding,[10] carbohydrate-protein interaction,[11] gene,[12] and drug delivery.[13-15]

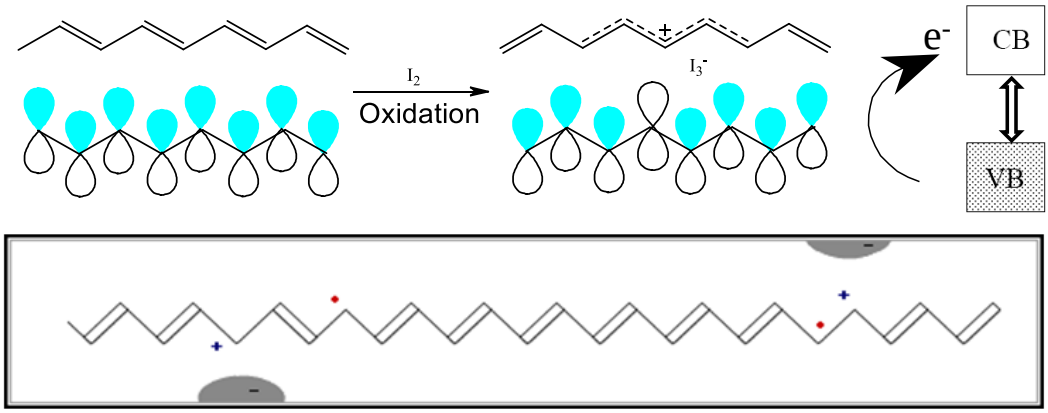

Figure 1.1. *Electrically conducting polyacetylene and mobility of the charges in the backbone (adapted from* Heeger, et al. *J. Chem. Soc., Chem. Commun.* **1977**, 578)

These polymers could replace metals traditionally used in constructing electronic devices and has added advantages such as better mechanical stability, easy processibilty, low density and high impact, which are completely absent in metals or normal inorganic materials. The essential structural feature for a polymer to be conducting was that, it should have extended π-conjugated system. For example, this

process has been explained in polyacetylene as shown in the figure 1.1. Polyacetylene is not conducting in its nascent form; however, it could be converted from an insulator to conductor by exposing to iodine vapour. The chemical oxidation of polyacetylene chains led to removal of an electron from valance band; as a result, radial cation or holes (positive chares) started migrating along the polymer chain. This process converted insulating polyacetylene chains in to electrically conducting polymeric material as shown in the scheme 1.1. This breakthrough discovery of conducting polyacetylene was recognized by the award of the Nobel Prize in chemistry in the year 2000. Polyacetylene showed amazingly interesting conducting properties and could be doped to achieve conductivity as high as that of copper. In spite of high conductivity, polyacetylene was air-sensitive and insoluble in common organic solvents. These drawbacks led to the need for other conjugating materials, which could show similar behavior but were stable and processable.[16-17] The conducting polymers are emerging as potential candidates for various applications since they combine high electrical conductivity and processibility. In 1990, the field received a major boost when Richard Friend and Andrew Holmes discovered electroluminescence (EL) in π-conjugated polymers.[18-19] They showed that polymers such as poly(phenylenevinylene)s emitted light on applying voltage between two metallic electrodes. This led to first polymer based light-emitting diode and the subsequent introduction of π-conjugated systems in molecular devices.[20] Chemical structures of various conducting oligomers and polymers showed in figure 1.2.

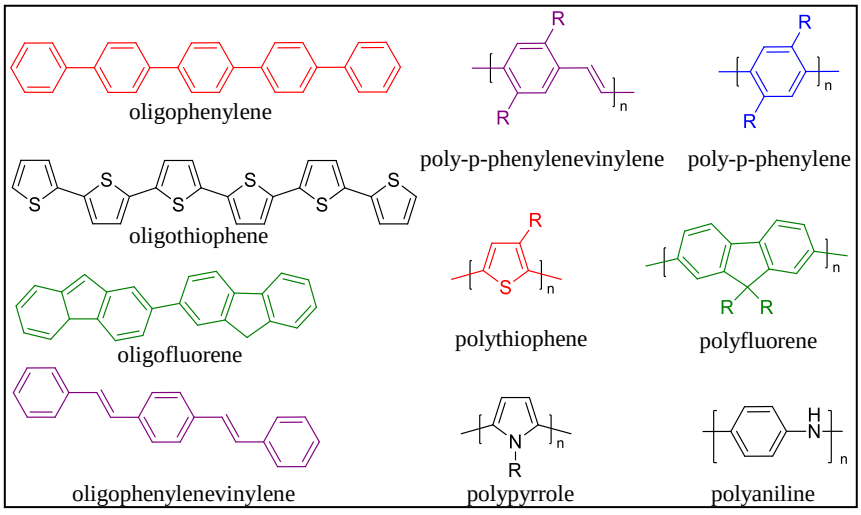

Figure 1.2. *Chemical structures of various conducting oligomers and polymers (adapted from* Greenham et al. *Nature* **1993**, *365,* 628).

Light Emitting Diodes:

A polymer light emitting diode works on the principle of electroluminescence, which involves emission of light when a π-conjugated material is excited by flow of electric current. The schematic diagram for single-layer electroluminescent device using a polymer layer has been shown in the figure 1.3.

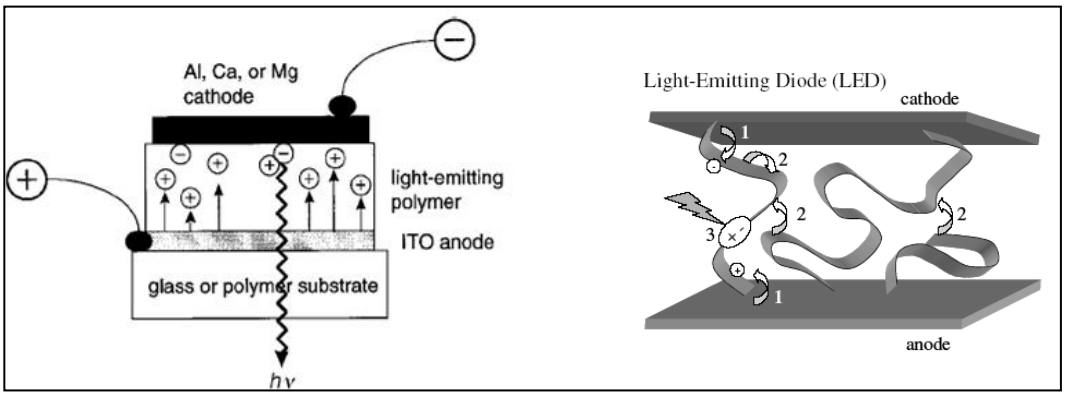

Figure 1.3. *Device set up and conduction mechanism of light emission from a PLED (adapted from* Akcelrud, L. *Prog. Polym. Sci*. **2003**, *28,* 875).

A thin film of π-conjugated material is sandwiched between two electrodes. The anode consists of a layer of PEDOT-PSS coated on an ITO patterned glass substrate and the polymer layer is spin casted above it. The cathode[21] is made up of a low-work function material such as calcium, magnesium or aluminium. In a polymer LED, electrons are injected into the LUMO (to form radical anions) and holes into the HOMO (to form radical cations) of the electroluminescent polymer, as diagrammatically represented in figure 1.3. The resulting charges migrate from polymer chain to polymer chain under the influence of the applied electric field. When a radical anion and a radical cation combine on a single conjugated segment, light is emitted. Some examples of π-conjugated polymers used in electroluminescent devices with different emission colors have been shown in the figure 1.4. These π-conjugated polymers have significant properties like colour tuning ability, mechanical stability, and flexibility etc.[22], which were not there in inorganic and organic crystals.

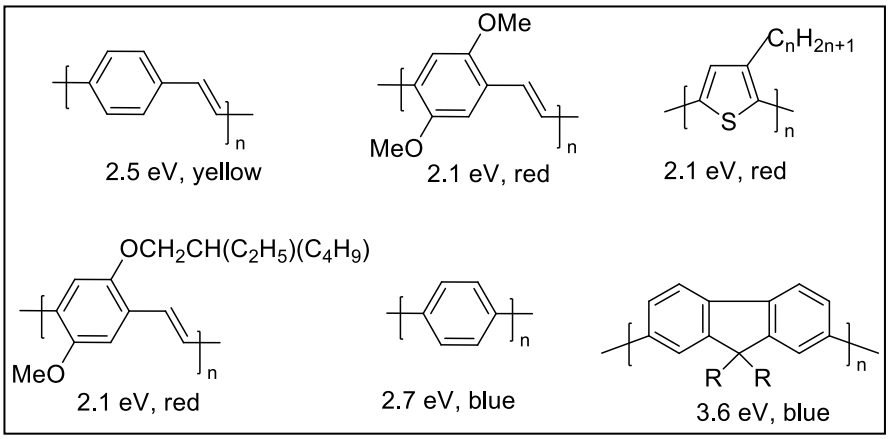

Figure 1.4. *Polymers with different emission colors and their π-π*band gaps are given (adapted from Akcelrud, L. Prog. Polym. Sci.* **2003**, *28*, 875).

Photovoltaics:

The general device setup for an organic solar cell is similar to that of a light emitting diode.[23] An organic solar cell consists of an electron donating (D) and electron acceptor (A) layer. Upon absorption of light, an electron is transferred from an electron donor (p-type semiconductor) to electron acceptor (n-type semiconductor). This photoinduced electron transfer results in the formation of radical cation of the donor (D•+) and the radical anion of the acceptor (A•-) as shown in the figure 1.5. The photogenerated charges are then transported and collected at opposite electrodes leading to the flow of current.[24] Different conjugated polymers and oligomers used in organic solar cells showed in figure 1.6.[25]

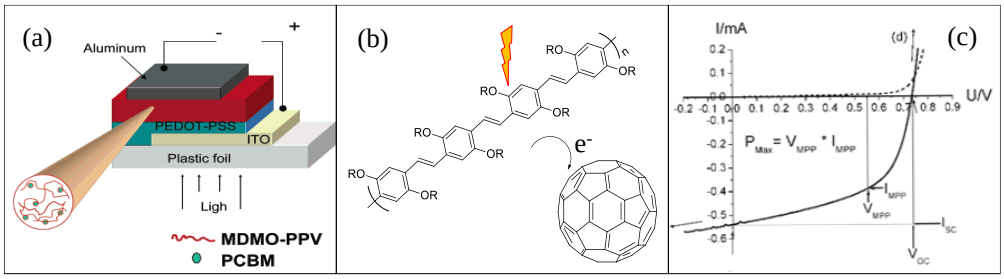

Figure 1.5. *(a) Device set up of a solar cell. (b) Electron transfer from donor to acceptor. (c) Current-voltage (I-V) curves of an organic solar cell (dark-dashed; illuminated-full line)(Adopted from Hoppe et al. J. Mater. Res.* ***2004****, 19, 1924-1945; Gunes et al. Chem. Rev.* ***2007****, 107, 1324-1338).*

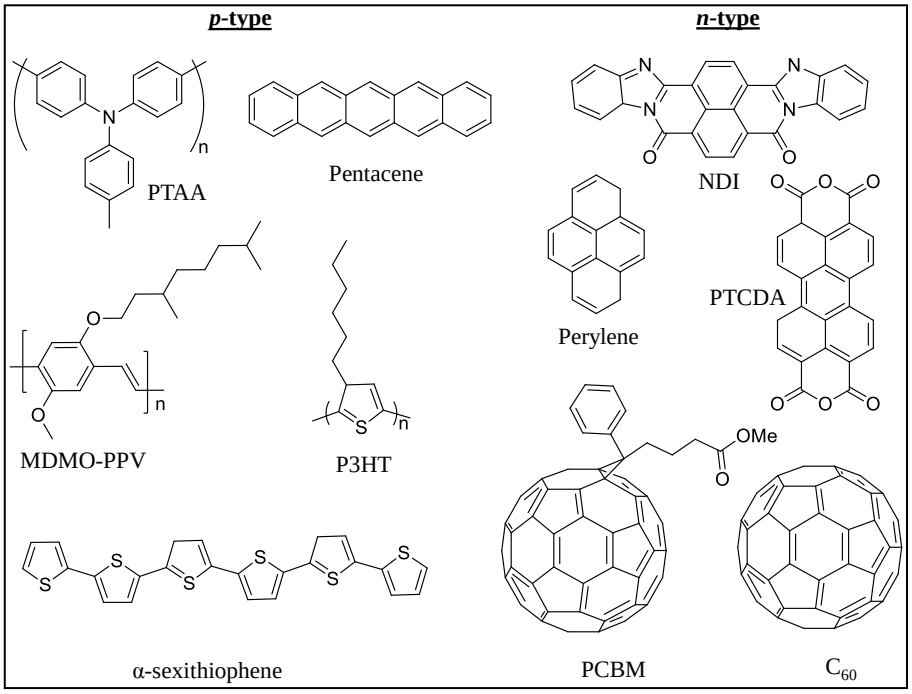

Figure 1.6. *Various conjugated polymers and oligomers used in organic solar cells ((Adapted from Chem. Rev.* ***2007****, 107, 1324-1338).*

Organic Field Effect Transistors:

Organic field-effect transistors consisting of organic π-conjugated molecules as active layers are emerging as next generation solid state electronics.[26-27] Two metal electrodes called source and drain are placed on top of the π-conjugated layers at each ends. Electrode materials are typically chosen from a variety of materials including metals (e.g., Au, Ag), heavily doped silicon and metallic conductive oxides (e.g., indium tin oxide), etc. An insulator separates the active layer from the gate electrode, and three terminals drain, source, and gate electrodes constitute the OFET configuration.[28] The device set-up of an OFET has been shown in figure 1.7. The mobility of the OFET is determined by the effective flow of charges from the source electrode to the drain electrode through the π-conjugated active layer. In this process, charge carrier accumulation is highly localized at the interface between the organic semiconductor and the gate dielectric.

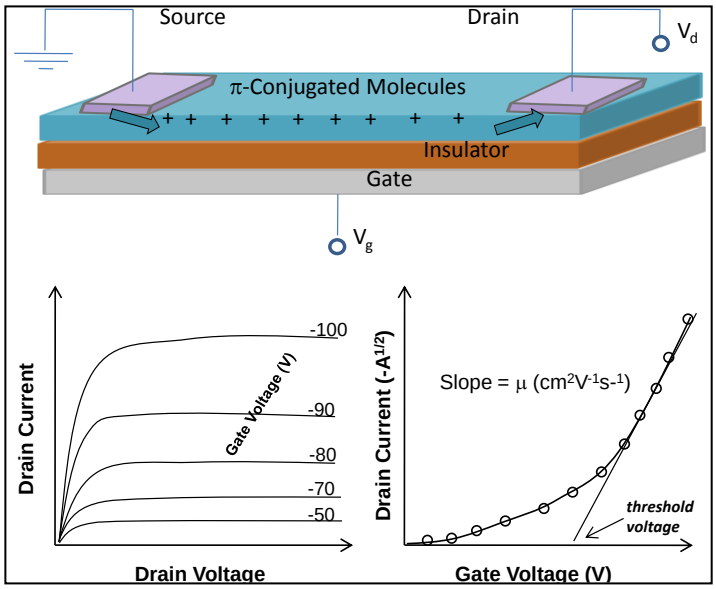

Figure 1.7. *OFETs device configuration and typical I-V characteristics (*Zhu, et al. *J. Mater. Chem.* **2005**, *15*, 53-65).

Therefore, OFET could be regarded as a capacitor in which the semiconductor layer and the gate electrode act as electrodes to sandwich the gate insulator. In figure 1.3, a typical OFET data output for the plots of drain current (I_D) vs drain voltage (V_D) for various applied gate voltage (V_G) are shown for π-conjugated molecules. The drain current is expressed as:[28]

$$I_D = \{WC_i/ 2L\} \times \{\mu (V_G - V_T)^2$$

where, C_i is the capacitance per unit area of the dielectric layer, V_T is the threshold voltage, and μ is the field-effect mobility. From the plot of gate voltage versus square root of drain current, the field-effect mobility could be calculated. The inter-section point in the x-axis provides the threshold voltages of the devices.

Lastly, the development in π-conjugated polymers last 40 years and futuristic applications reported by Swagar and schematic representation showed in figure 1.8.[29]

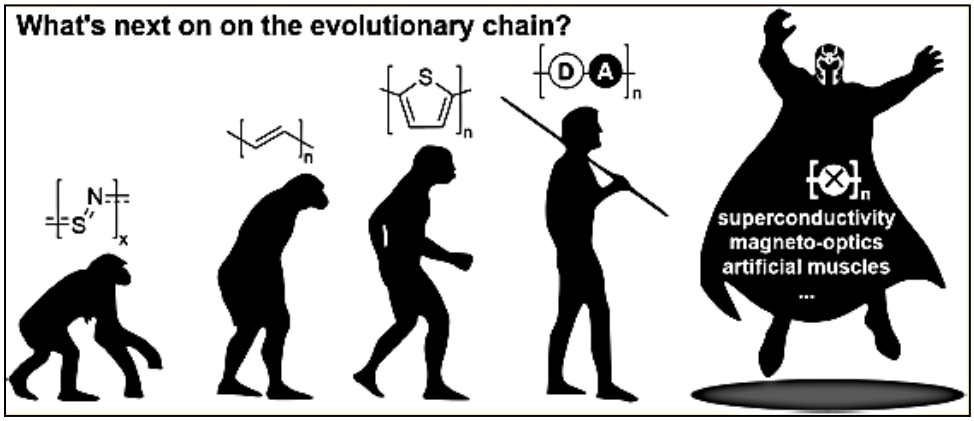

Figure 1.8. *Evolution in π-conjugated polymers (adapted from Swager, T. M. Macromolecules* **2017** ASAP (**DOI:** 10.1021/acs.macromol.7b00582).

1.2. Self-Assembly of Donor-Acceptor Systems by charge -transfer interactions

Electron rich systems called as electron donors and electron deficient systems called as electron acceptor systems. Recent development in the area of π-conjugated organic materials for optoelectronic applications has been the introduction of supramolecular assembly of donor (D) and acceptor (A) molecules.[30-34] Electron rich donor-type semiconducting polymers such as poly(pheynelevinylene)s (PPV), poly(3-alkylthiophenes), and polyfluorenes were blended with electron deficient molecules like fullerene (C_{60}) derivatives, perylenebisimide, and naphthalene derivatives and TCNQ.[35-43] The various types of D and A used in D-A complex for charge-transfer interactions. Charge-transfer (CT) interactions between alternately stacked electron donor (D) and electron acceptor (A) molecules have been cleverly employed for the construction of various molecular and macromolecular assemblies such as foldamers, catenanes/rotaxanes and supramolecular polymers.[42,43, 44-49]

Jian Pei and co-workers reported the synthesis of C_3 symmetric donor–acceptor truxene derivative (Tr_3) and it's oxidized counterpart, the truxenone derivative (TrO_3) and studied one-dimensional microwires formed by the co-assembly of complementary aromatic donors and acceptors. The formation of donor–acceptor assembly in solution (see figure 1.9) and solid state confirmed by ^{1}H NMR, photoluminescence Scanning electron microscopy, powder X-ray diffraction analysis.[50]

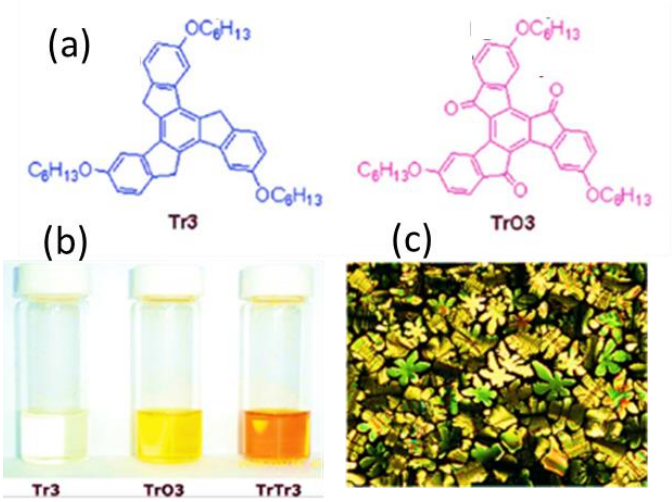

Figure 1.9. *(a) Structures of Tr3, and TrO3. (b) Photograph of Tr3, TrO3, and the 1:1 mixture TrTr3 in CH_2Cl_2 at room temperature. (c) PLM images of the 1:1 mixture TrTr3 (at170 °C) (adapted from jian pei et al. Adv. Funct. Mater.* **2009**, *19*, 1746-1752).

Ghosh et al. reported the NDI and pyrene based H-bonded donor-acceptor assembly in water and demonstrated due to vesicular self-assembly of acceptor can intercalate with pyrene donor form alternate D-A assembly with charge transfer interactions. Due to D-A charge transfer assembly observed the 1-D nanofibers and also reported the H-bonded between π-complementary aromatic acceptor NDI and dialkoxy naphthalene (DAN) donors and they form D–A co-assembly through π-π stacking, charge transfer and hydrogen bonding (see figure 1.10). Same group also reported the naphthalene based D and A systems and studied the D–A complexes with high association constant in charge-transfer complexes.[51-53]

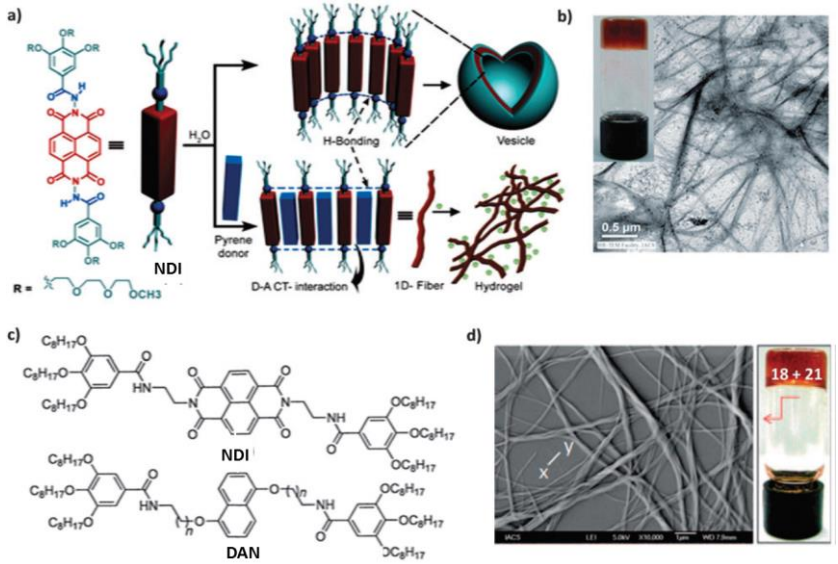

Figure 1.10. (a) *Chemical structure of NDI based acceptor and a schematic representation of inclusion of pyrene donor into the NDI self-assembled matrix, leading to a morphology transition from vesicles to fibers. (b) Photograph of the MS-CT gel of NDI with pyrene and corresponding TEM image of the CT fibers. (c) Molecular structure of NDI and DAN derivatives with the gallic amide as a gelator. (d) SEM images and the photograph of the MS-CT gel formed between DAN and NDI (1:1) (adapted from George, et* al. *Phys. Chem. Chem. Phys.* **2014**, 16, 1300).

George and co-workers reported formation of a hydrogel by co-assembly of a coronene tetracarboxylate salt as a donor and dodecyl methyl viologen as an acceptor. They also showed D-A co-assembly of a perylenebisimide acceptor which produces cylindrical micelles leading to hydrogelation at higher concentrations. D-A assembly showed nanotube morphology and remarkably high conductivity (0.02 Scm^{-1}). Same group also reported novel D-A pairs of coronene and naphthalenediimide (NDI) and studied the alternately stacked CT assemblies. Highly ordered one-dimensional nanostructural assemblies observed (see figure 1.11).[54-56]

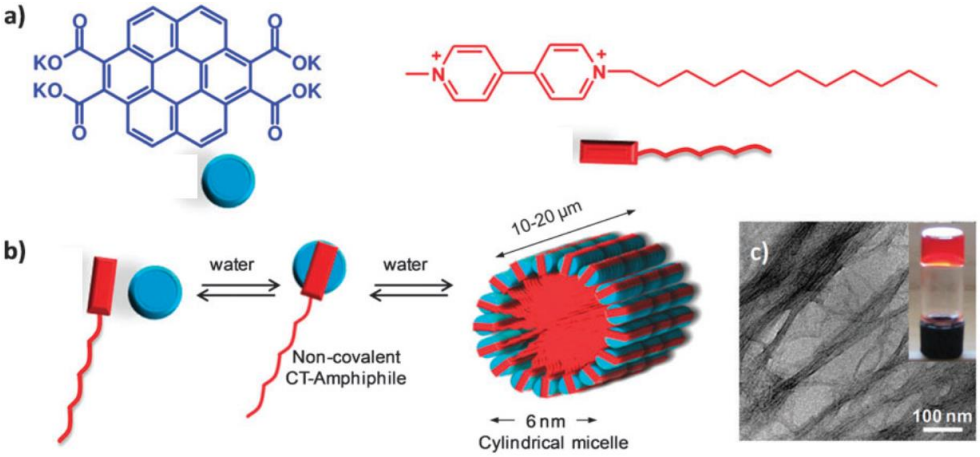

Figure 1.11 *(a) Molecular structures of the polycyclic aromatic corone tetracarboxylate (D) donor and viologen (A). (b) Schematic representation of the non-covalent amphiphile and its self-assembly into high aspect ratio cylindrical micelles (adapted from George, et al. Phys. Chem. Chem. Phys.* **2014**, 16, 1300).

Xi Zhang and co-workers reported naphthalene the new amphiphilic donor and acceptor systems and demonstrated tuning the structures of the building blocks, X-shape or H-shape superamphiphiles (see figure 1.12) were successfully assembled, which can be used to create tunable supramolecular nanostructures.[57-59]

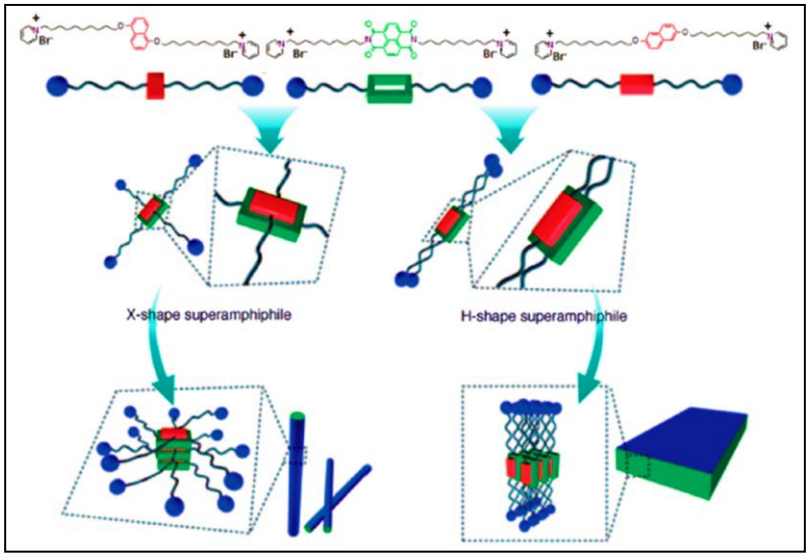

Figure 1.12 *Molecular structures of amphiphilic donor and acceptor. Schematic representation of the X- and H-shape assembly of donor and acceptor and their one-dimensional and two-dimensional nanostructures, respectively (adapted from George, et al. Phys. Chem. Chem. Phys.* **2014**, 16, 1300).

Govindaraju and co-workers demonstrated naphthalene and pyrene based H-bonded D-A hydrogel for multi stimuli responsive. These extended supramolecular chiral mixed-stack CT hydrogels with nanofibrous 3D networks as a promising room-temperature thin-film organic ferroelectric material (see figure 1.13).[60]

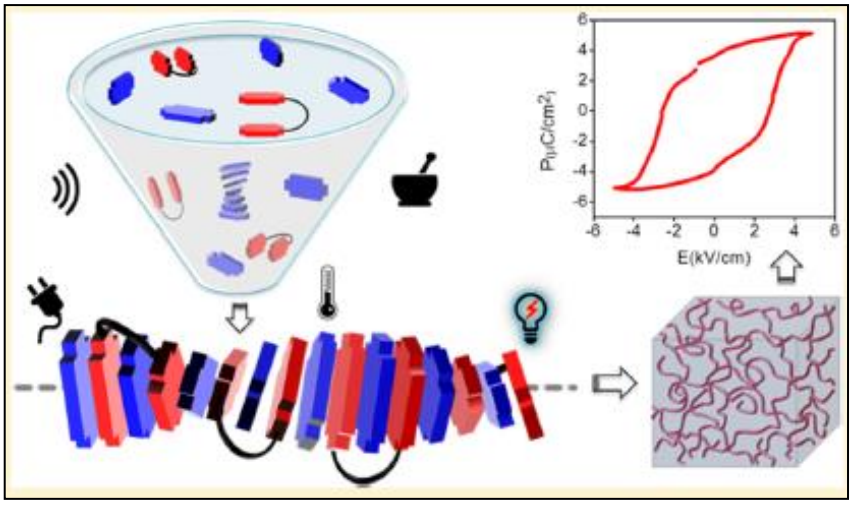

Figure 1.13. *Schematic representation of self assembly of donor-acceptor and ferroelectrcity plot (adapted from Govindaraju et al. J. Am. Chem. Soc.* **2016**, *138*, 8259−8268).

Iverson and co-workers came with new idea reported the different class of amino acid based segmented donor-acceptor π-conjugated systems and demonstrated

the folding of a series of D–A oligomers with varying flexible chain length where the DAN and NDI chromophores were linked by flexible amino acid linkers containing a pendant carboxylic acid functional group. UV/vis studies showed a reduction in band intensities and the appearance of CT band, thus suggesting the existence of the folded structure by intrachain D–A stacking (Figure 1.14), also confirmed by a change in the chemical shift values of the aromatic ring protons and NOE studies.[61] They also demonstrated that such folding can be achieved by interchain CT interactions between structurally similar oligomers containing either NDI or DAN units.[62]

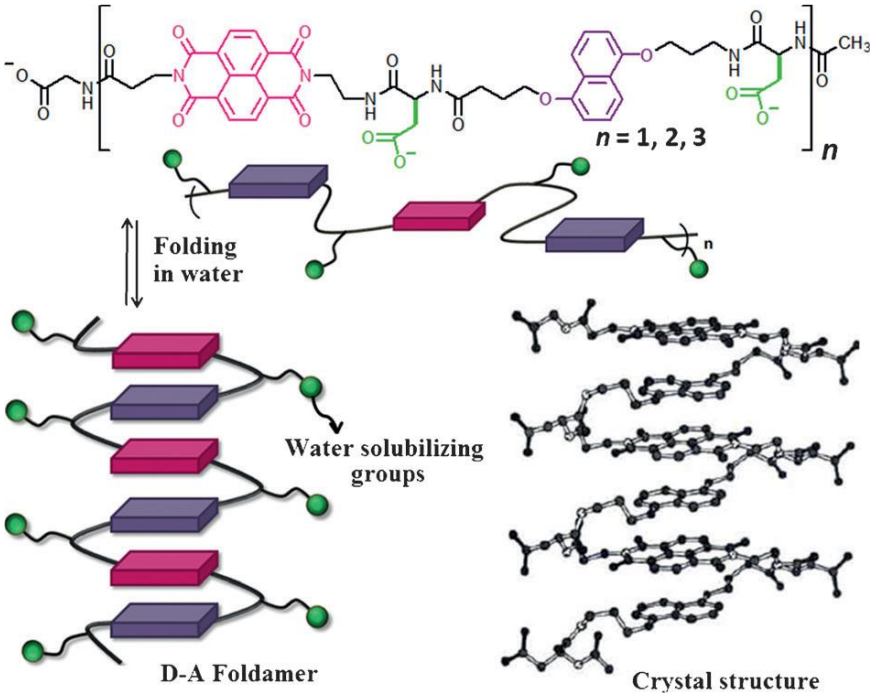

Figure 1.14. *Folding of D–A oligomers (top) in aqueous medium by intrachain CT interactions. Crystal structure is shown at bottom right* ***(****adapted from Iverson et al. Nature* ***1995****, 375, 303-305.; Das* et al. *Angew Chem. Int. Ed.* **2014**, *53*, 2038–2054).

Ramakrishnan and co-workers designed flexible amphiphilic donor-acceptor based polymer and demonstrated the folding phenomena, formation of charge-transfer complex, and metal-ion complexation. The maximum probability of folded state was seen in the presence of an alkali-metal ion, and stacked donor and acceptor.[63] Ramakrishnan and co-workers also designed new flexible synthetic polymer and demonstrated a folding of polymer in solution by utilizing a small molecule as a folding agent. An ammonium cation in the folding agent forms a complex with a hexaoxyethylene spacer thereby aiding the CT interaction between a

naphthalene donor and a pyromellitic diimide acceptor in the polymer (see figure 1.15). Importantly, the folding was also shown to be completely reversible checked by using [18] crown-6.[64] Same group also reported a novel class of ionenes that contains alternating donor and acceptor aromatic units within the alkylene segments. They studied the formation of charge transfer complex in enhanced in polar solvents. The flat pancake like aggregates observed in AFM analysis in dilute aqueous solutions.[65]

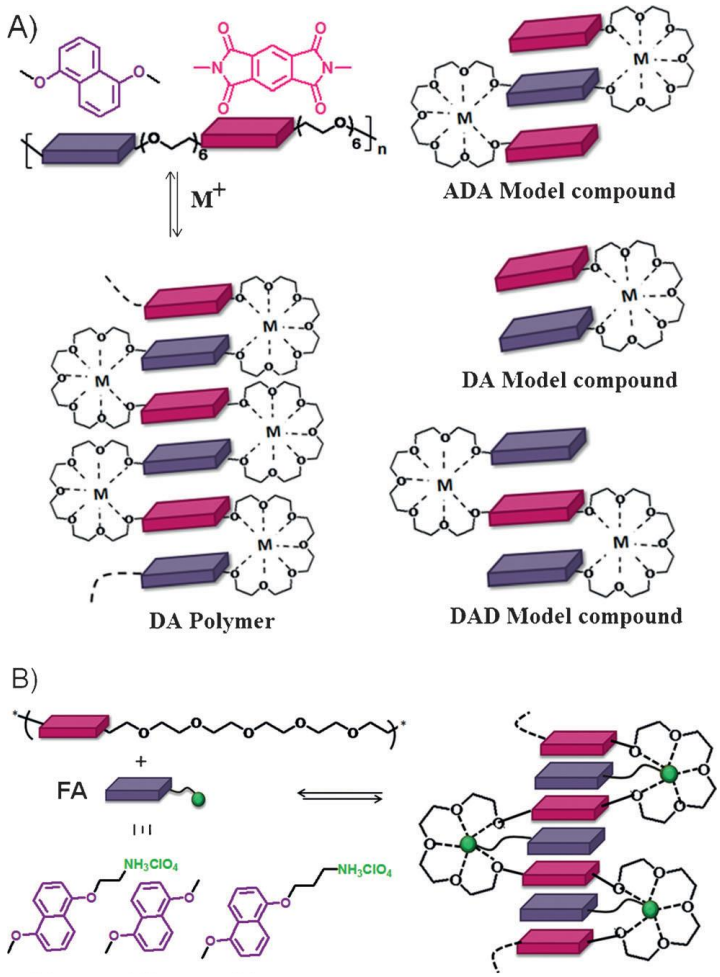

Figure 1.15. *(A) Metal ion complexation induced CT interaction and folding of D–A polymers and model compounds. (B) External FA induced folding of a flexible polymer* ***(****adapted from Das et al. Angew Chem. Int. Ed.* **2014**, *53*, 2038–2054*).*

Edward A. McGehee et al reported studies of cocrystalisation of Complementary C_3-Symmetric Donor-Acceptor Components like hexaalkoxytriphenylene(D) and mellitic triimide (A) in 1:1 ratio and studied the mesophase behaviour of D-A assembly in solid state.[66] Bent L. Iverson and co-workers reported studies of cocrystallisation of Complementary C_2-Symmetric

electron rich 1,5-dialkoxynaphthalene (Dan) donors and relatively electron deficient 1,4,5,8-naphthalenetetracarboxylic diimide (Ndi) acceptors in 1:1 ratio and studied alternating stacks of Dan and Ndi derivatives produced columnar mesophase with a deep red color with charge transfer band and predictable mesophase transition.[67-68] Klaus Mullen and co-workers[69] reported studies of columanar mesophase behaviour of donor-acceptor assembly of the derivative of hexaperihexabenzocoronene and derivative of perylenediimide in the solid state. Recently Joseph J. Reczek and co-workers reported a series of aromatic donor-acceptor columnar liquid crystal materials was developed whose charge-transfer absorption completely spans the visible spectrum.[70]

Charge-transfer D-A single crystal used for room-temperature organic ferroelectric devices.[71] In a very recent breakthrough result of Stupp et al. have shown, for the first time, room temperature ferroelectric CT crystals, constructed from a pyromellitic diimide as an acceptor (1a) with pyrene (1b), naphthalene and TTF as donors (see figure 1.16).[71] The donor (D) and acceptor (A) used for highly ordered D-A assembly have being exploited to measure the photoconductivity and ambipolar charge transport of DA material.[72-74]

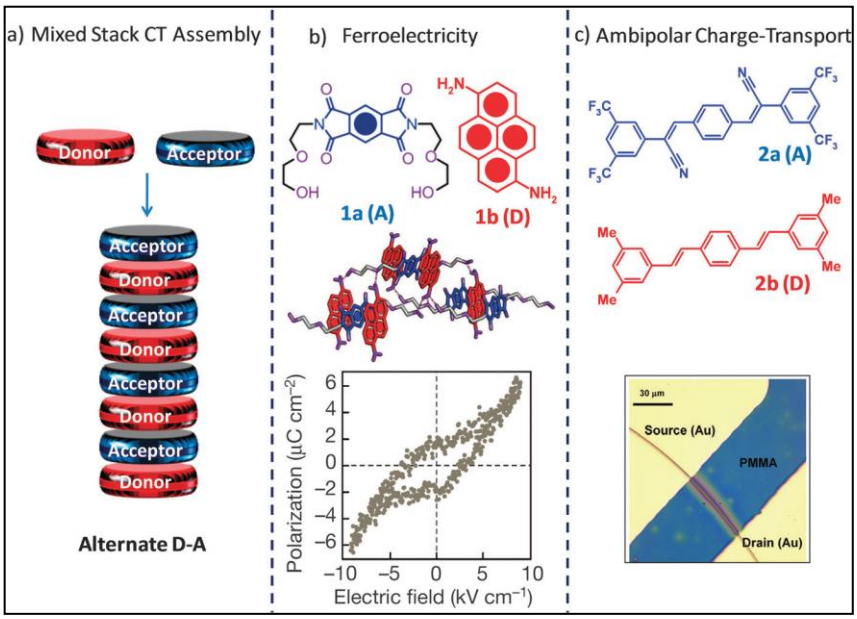

Figure 1.16. *(a) Schematic representation of alternately stack of donor and acceptor molecules CT assembly. (b) The 1a–1b co-crystal showed room temperature organic ferroelectricity. (c) Optical photograph of the CT co-crystal of 2a–2b, which shows ambipolar charge transport* (Adapted from George et al. *Phys. Chem. Chem. Phys.* **2014**, *16*, 1300).

Nazario Martín and co-workers[75] recently demonstrated the formation of highly ordered functional materials from π-extended tetrathiafulvalene (exTTF) as electron-donor and perylene-bisimide (PBI) as electron-acceptor. These n-and p-materials are endowed with ionic groups with opposite charges on their surfaces, carboxylic acid and guanidinium or quaternary ammonium. A controlled alignment of the n/p-material is bestowed by the electrostatic co-assembly of two complementary self-assembling nanofibers (see figure 1.17) which results in high values of photoconductivity. Photoconductivity measurements show values for these n/p-co-assembled materials up to 0.8 $cm^2\ V^{-1}\ s^{-1}$.

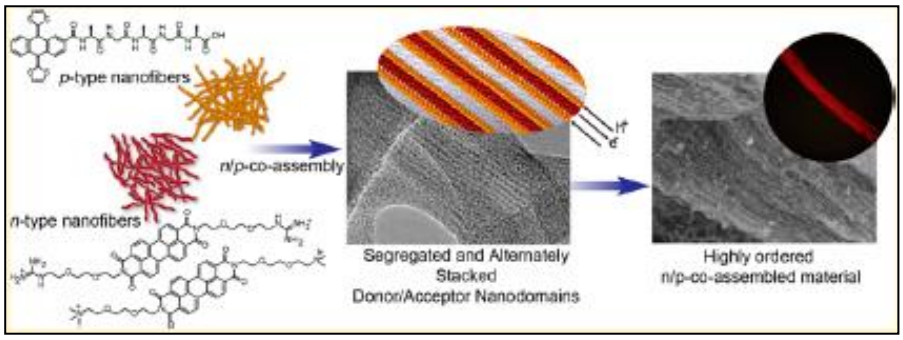

Figure 1.17. *Structures of donor and acceptor and their nano-fibres morphology* (adapted from Nazario Martín et al. *J. Am. Chem. Soc.* **2015**, *137*, 893-897).

Ajayaghosh and co-workers studied the D-A assembly of p-type π-gelator trithienylenevinylene derivative (TTV) with an n-type semiconductor perylene-bisimide (PBI) derivative and resulted in the formation of self-sorted fibers which are coaxially aligned to form interfacial p–n heterojunctions (see figure 1.18). By using flash photolysis time-resolved microwave conductivity (FP-TRMC) technique, they measured the anisotropic photoconductivity of D-A (TTV/PBI). Helin Huang et al reported the morphology control of nanofibril D-A assemblies and measured their photoconductivity.[76]

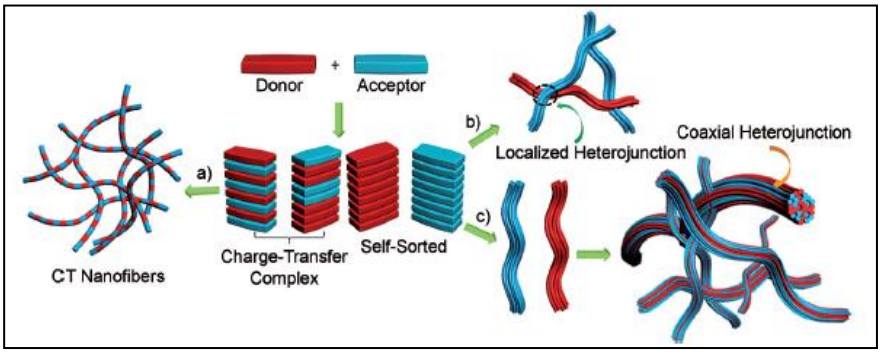

Figure 1.18. *A conceptual representation showing the possible interactions between a p-type donor and an n-type acceptor leading to different possible hierarchical structures (adapted from Ajayaghosh et al Angew. Chem., Int. Ed.* **201**5, *54*, 946-950).

1.3. Aggregation control in π-conjugated systems

Aggregation is an important and widely observed phenomenon in π-conjugated polymers which makes the aggregated polymer chains exhibit distinct properties compared to the isolated chains and also the aggregation properties are different in solution and solid state.[77-78] The molecular aggregation properties of polymers (π-conjugated systems) are generally monitored by absorption or emission spectroscopy, time resolved photoluminescence techniques, electron microscopic studies etc. In solution state the molecular aggregation can be traced by a number of methods which includes using a good solvent/bad solvent combination, concentration or temperature dependant studies etc.[79-85] The polymers completely dissolve in a good solvent (in which it is fully soluble), to which upon addition of the poor solvent a clear color change will be observed indicating the formation of new aggregates. The main possibility of this change may be the π-π stacking of conjugated systems and also conformational change of the π-conjugated chains by chain folding process. In bad solvents, the polymer forms rigid and stable structures and the excitation of which will result in lower energy emissive species. The concentration dependant studies are based on the formation of aggregates by self-coiling of the polymer chains. A lot of work has been done on the PPVs (poly(phenyleneethynylene)s, PPEs) based on the aforementioned concept. Usually THF, $CHCl_3$ etc. are used as the good solvents, whereas methanol (MeOH), and water act as the bad solvent in most cases.[86-88] An alternative way to reduce the quality of the solvent in a controlled and continuous way is to reduce the temperature. The aggregation of π-conjugated materials significantly impacts the photophysics and performance of optoelectronic devices.[84] Bunz group

are the pioneers in PPE-based polymers and their study based on the above concept showed the development of a red shifted peak corresponding to the aggregation in the solvent/temperature induced studies.[85-86]

Claudio Resta et al, reported the poly[2-methoxy-5(2-ethylhexoxy)-p-phenylenevinylene](MEH-PPV) and studied the aggregation in chloroform/methanol combinations. The aggregation of polymer is confirmed by deduction of absorbance and quenching of fluorescence spectroscopy (see figure 1.19).[87]

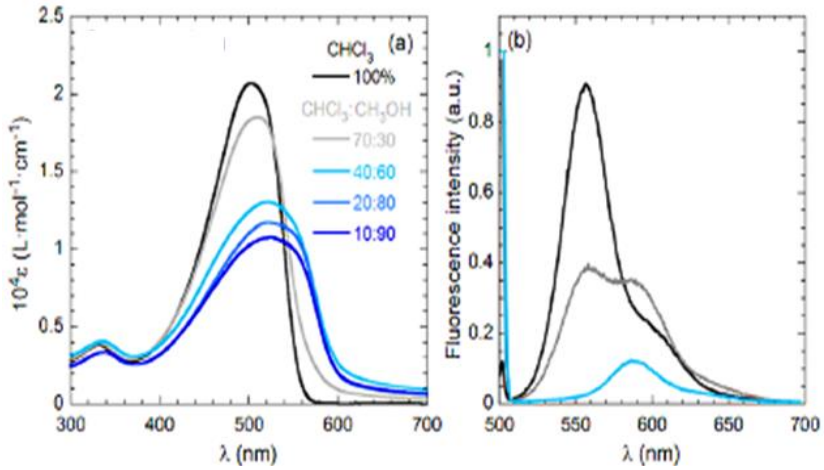

Figure 1.19. (a) *Absorption, and (b) emission in chloroform/methanol mixtures (adapted from* Resta et al. *Macromolecules* **2014**, *47*, 4847−4850).

Therefore, noticeable changes will be there in the absorption and fluorescence spectra by the presence of the molecular aggregates. The red shift observed in the absorption and emission spectra has known to be caused by the interchain aggregation, but there still exists debates about this process. One reason for this red shift was explained due to the delocalization of the π-electrons over multiple stacked segments of different chains in the aggregated state because of the close proximity.[86]Another factor for the red shift is attributed to the collapse of isolated chains and planarization of the phenyl rings due to confinement in conjugation.[86-87] But in brief, the molecular aggregates formed in the presence of high amount of poor solvent, in highly concentrated polymer solution or in low temperature conditions, resemble like the polymers in the solid state. The segmental association of the polymer chains was also found to be different in various solvents and it was demonstrated by Li et al. that in a good solvent the PPV chains forms looser network aggregates whereas in a poor solvent tightly packed aggregates are formed.[89] These interchain aggregations are mainly driven by aromatic π-π interactions. Fakis and

coworkers have studied the influence of aggregates and solvent aromaticity on the photophysical properties of the PPV derivatives.[90]

The molecular aggregation in the solid state can also be followed by many methods like time-resolved decay measurements, SEM, TEM, etc. including the absorption and luminescence measurements. Recently Chen et al. have shown that the molecular aggregation in MEH-PPV results in the nematic textures which causes a red shift in the emission maxima. In this case the molecular aggregation is assumed to be driven by the aromatic π- π interactions in which the small methoxy unit is unable to provide necessary shielding for the polymer backbone.[91-92]

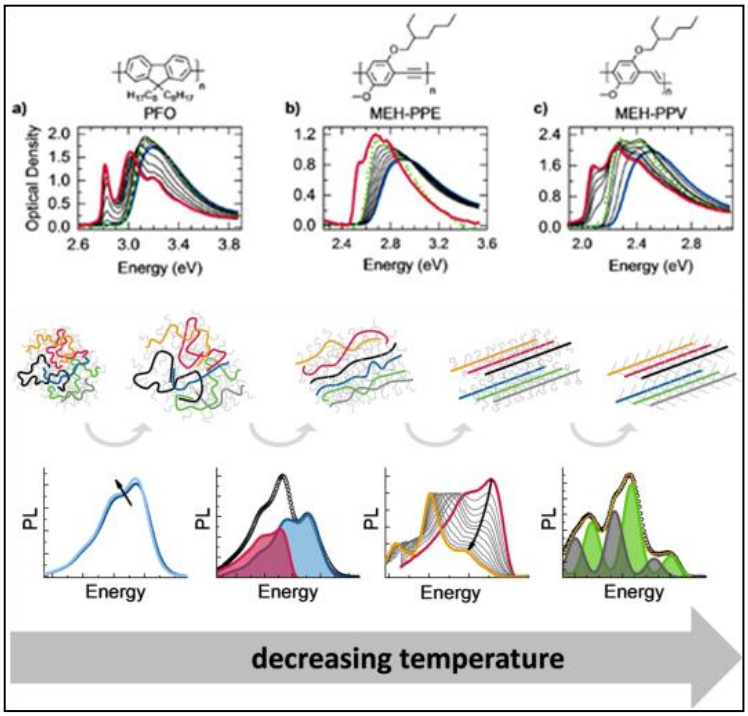

Figure 1.20. (*a-c) Temperature-dependent absorption spectra of the investigated material systems in MTHF solution showing aggregation behavior. The chemical structure is indicated on top of each panel. Schematic representation of change in PL intensity and corresponding aggregates with temperature (*adapted from Fabian Panzer et al. *J. Phys. Chem. Lett.* **2017**, *8*, 114−125).

In short, PPVs are highly luminescent class of conducting polymers that are found to have wide applications in optical and electronic industry. The above discussions are mainly pointed on towards the necessity of structural modification and control of molecular aggregation for the designing of highly luminescent and efficient materials The temperature-dependent optical spectroscopy is powerful tool to investigate aggregate formation. Mostly, the π-conjugated molecules or polymers the

formation of aggregates can be understood in terms of an order-disorder transition. Most of the π-conjugated polymers in good solvents the polymer chains exist as expanded conformation, where as in bad solvents the polymer chains exist as coil like conformation at lower temperatures (see figure 1.20). The aggregation phenomena are important for organic solar cells or field effect transistors. Notably, the chain expands before it collapses into a highly ordered compact state. For a given non interacting polymer chain or π-conjugated molecule, an increased conjugation length suggests that conjugated segments have become more planar and, in the case of a polymer, more elongated.[84] McCullough,[93] Yamamoto,[94] and Leclerc[95-96] extensively studied the self-assembly of poly(3-alkylthiophene)s in solution and solid state, exploring the effect of temperature, regioregularity, and solvent by means of spectroscopy and light scattering techniques. Similar studies on polymer chain aggregation of poly(methoxyethylhexyloxyphenylenevinylene)s and poly(*p*-phenyleneethynylene)s reported by Schwartz[97] and Bunz,[98] respectively. In a polymer high number of substituents can prevent π- stacking between polymer backbones, as a resulting in a wormlike cylindrical conformation. The concentration of the side chains is reduced, planarity increases as a result in stronger π-stacking, leading to lamellar arrangements. The properties these solution were compared to the optical properties of the same polymers in film state.

Self-Assembly of Block Copolymers

Different polymers is synthetically link to the oligomer or polymeric conjugated building blocks to other blocks that are able to enhance the positioning of the conjugated blocks in the active layer and improve the mechanical and processing properties. Block copolymers involve two or more homopolymer parts connected together through covalent bonds. The synthesis of these block copolymers primarily involves the homo polymerization of a single monomer and subsequently another monomer is added which grows beside the homopolymer to yield a block copolymer. In this process, depending on the monomers used, polymers can be subdivided in to diblock (two monomers) and triblock (three different monomers). Block copolymers with two, three, or more blocks are called as di, tri, and multi block copolymers respectively. The block copolymer approach can show phase separation, and so, a variety of self-assembled nano structure are available ranging from lamellar, spherical, cylindrical, to vesicular morphology etc.[99] François et al., reported the

honeycomb morphology made from rod-coil poly(*p*-phenylene)-polystyrene block copolymer and observed micelle morphology formed by evaporating the solvent CS_2 resulted in regular pores arranged in a hexagonal array (see figure 1.21).[100]

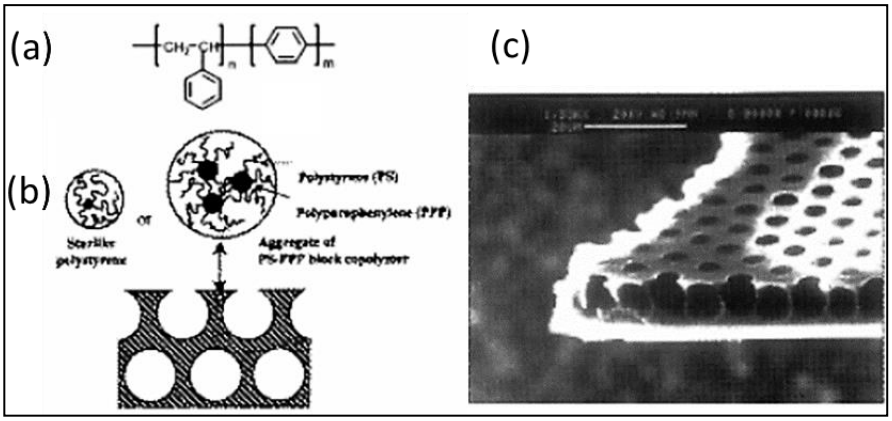

Figure 1.21. (a) *Structure of the block copolymer. (b) Schematic representation for the cross section and (c) SEM image of a honeycomb structure of polymer* ***37*** ***(****adapted from François et al. Nature* **1994**, *369*, 387-389; Hoeben et al. *Chem. Rev.* **2005,** *105*, 1491-1546).

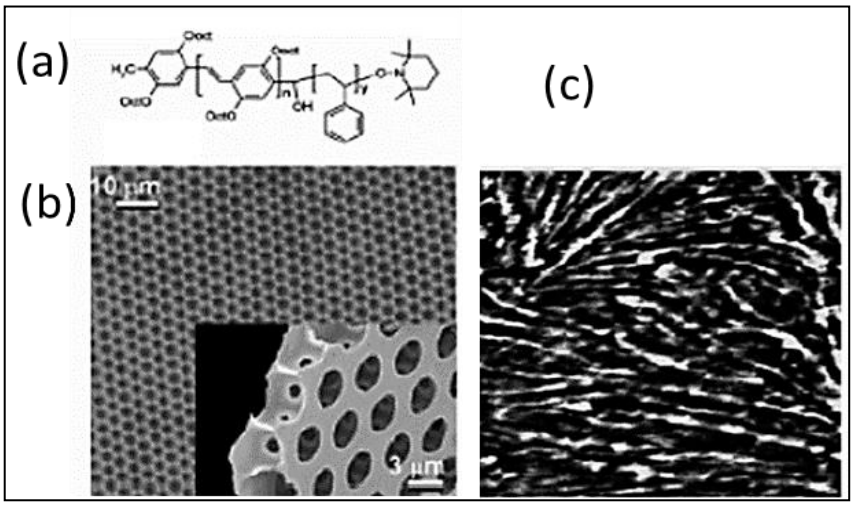

Figure 1.22. *(a) Structure of the block copolymer. (b) Fluorescence and SEM (inset) images of a honeycomb-structured film of PPV-b-PS obtained by drop casting from CS2 and (c) lamellar morphology as obtained by drop casting from dichlorobenzene* ***(****adapted from Hadziioannou et al. Polymer* ***2001****, 42, 9097-9109.; Hoeben et al. Chem. Rev.* ***2005,*** *105, 1491-1546).*

Similarly, Hadziioannou et al. reported a honeycomb morphology for block copolymers of polystyrene and poly(p-phenylenevinylene) when cast from CS_2, a poor solvent (Figure 1.22).[101] However, when cast from a good solvent dichlorobenzene, a bilayered lamellar morphology was observed of stacked PPV

blocks.[102-103] The honeycomb morphology could also be reproduced by François et al. with block copolymers of polystyrene and polythiophene.[104-106] McCullough et al. were reported the self-assembly of regioregular poly-3-hexylthiophenes made from copolymerisation with polystyrene, polymethacrylate, and polyurethane.[107] Nanowire morphologies of the copolymers were obtained by slow evaporation from toluene (see figure 1.23).

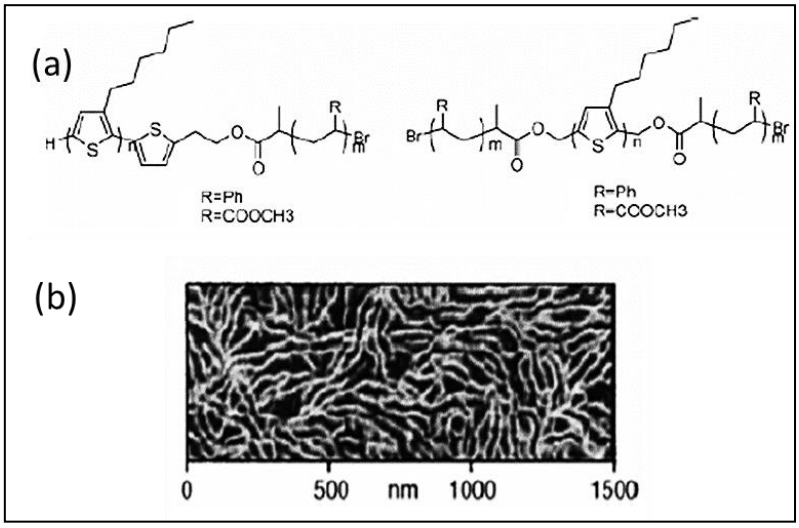

Figure 1.23. *(a) Structure of the block copolymer. (b) AFM image of Nanowire morphology of poly(3-hexylthiophene) copolymers drop casted from toluene (adapted from McCullough et al. Angew. Chem., Int. Ed.* **2002**, *41*, 329-332.; Hoeben et al. *Chem. Rev.* **2005,** *105*, 1491-1546).

Hempenius et al. used the same units by synthesizing a triblock copolymer of polystyrene-undecathiophene-polystyrene, and phase separation was observed in a poor solvent. TEM and AFM show that the copolymer is self-assembled into irregular, spherical, micellar structures having an average diameter of 12 nm (Figure 1.24). [108]

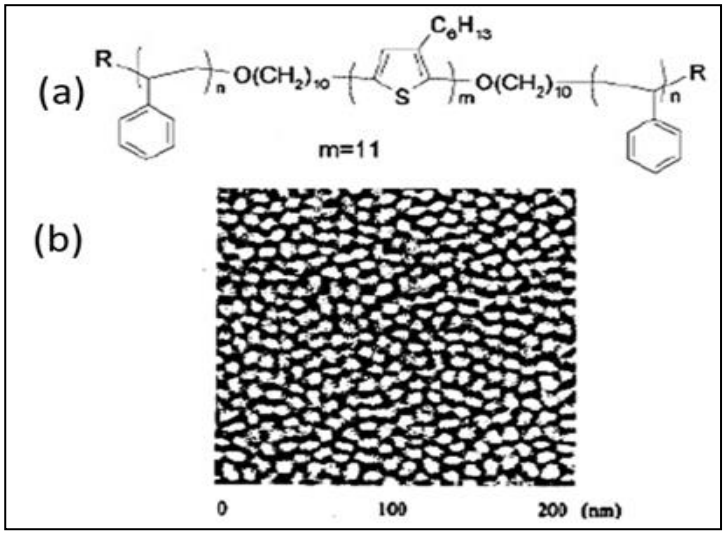

Figure 1.24. (a) *Triblock copolymer of polystyrene and oligothiophene blocks. (b) The AFM image shows that phase separates into micellar aggregates* ***(****adapted from Hempenius et al. J. Am. Chem. Soc*. **1998**, *120*, 2798-2804.; Hoeben et al. *Chem. Rev.* **2005,** *105*, 1491-1546).

1.4. Amphiphilic π-conjugated systems

Amphiphilic π-conjugated systems are the π-conjugated systems having rigid aromatic π-core and flexible oligo ether spacers or highly polar functional group in the back bone. Mostly Amphiphilic π-conjugated systems contains hydrophilic (water-loving) oligo ethylene glycol chains and hydrophobic (water-hating) π-conjugated systems. The self-assembly of amphiphilic π-conjugated systems have been widely studied amphiphilic derivatives of π-conjugated systems such as naphthalene,[109-111] oligophenylenevinylene,[112-113] perylene,[114-115] and thiophenes[116-118] etc. Amphiphilic π-conjugated molecules are water soluble or water dispersible eco-friendly and the self-assembled nano structure of amphiphilic π-conjugated molecules used for variety of applications like metal ion sensing,[119-123] D-A assembly,[43-44,124] bio-medical applications.[125-131] Nowadays, most of amphiphilic nano structures used for bio-medical applications like bio-imaging, drug delivery, gene delivery, and DNA binding. The supramolecular architectures have a well-defined size and shape including fibers, ribbons, tubes, helices, cylindrical micelles, vesicles, spherical micelles, bilayers, and toroids.[44, 132-133] Different types of amphiphilic π-conjugated systems shown in figure 1.25

Examples of π-amphiphilic conjugated systems

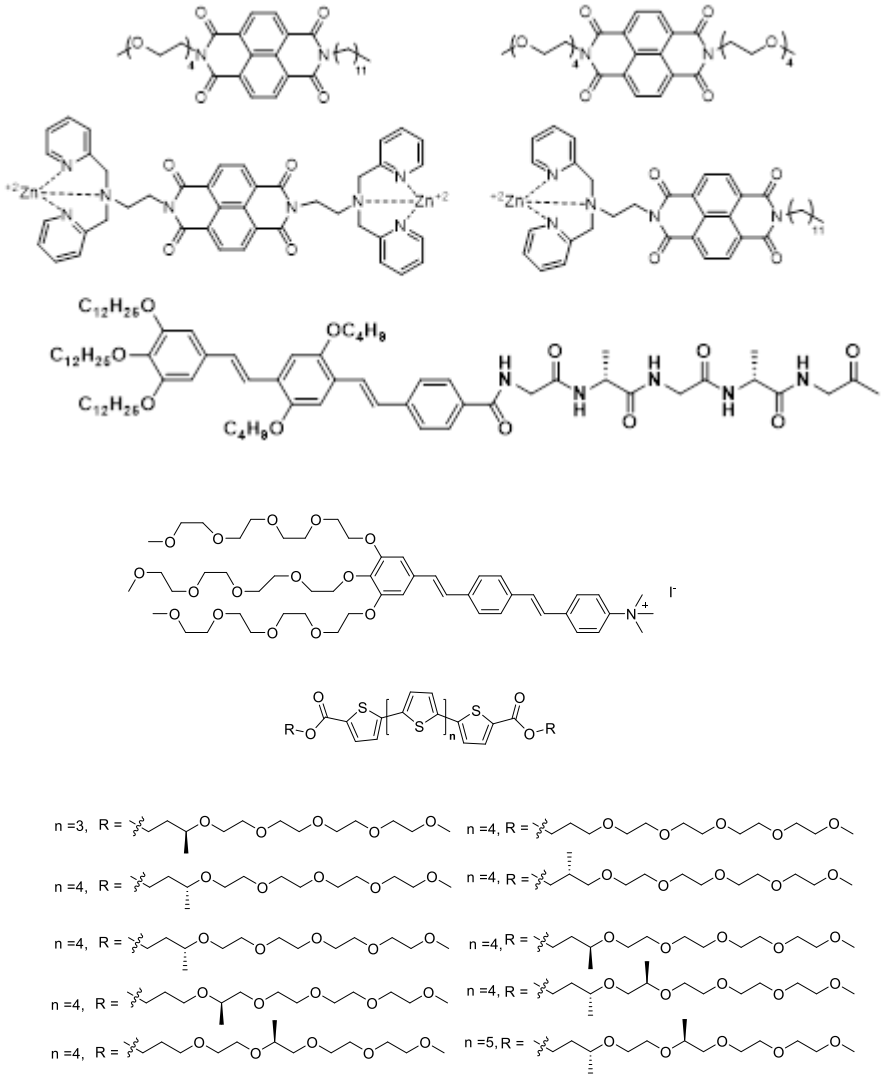

Figure 1.25. *Structure of few amphiphilic π-conjugated systems (adapted from ref. 112-113, 115, and 119).*

The rigid amphiphilic small molecules are composed of rigid aromatic segments and flexible coil segments. They can form supramolecular structures with dimensions as small as a few nanometers, the rigid-flexible amphiphilies can be excellent candidates for creating well-defined supramolecular architectures. These amphiphilic systems leads to the formation of a nanostructure with a rigid hydrophobic core surrounded by flexible hydrophilic chains in an aqueous solution.[140] Myongsoo Lee and co-workers have reported the three different rigid amphiphilic small molecules and studied the nano structure assembly in water. In an aqueous

solution, molecule 1 self-assembles into planar sheets, whereas molecule 2 forms a ribbonn due to a different ratio of hydrophilic chain length. When 1 or 2 was coassembled with 3 in aqueous solution, observed toroidal nano structure with decrease in size of the aggregates upon the addition of 3 confirmed by dynamic light scattering (DLS) and transmission electron microscopy (TEM) analysis and demonstrated the propeller-shaped amphiphilic molecules based on a conformationally peripheral flexible chains with aromatic core and studied the aggregation behavior in water–THF mixed solutions (see figure 1.26).[133]

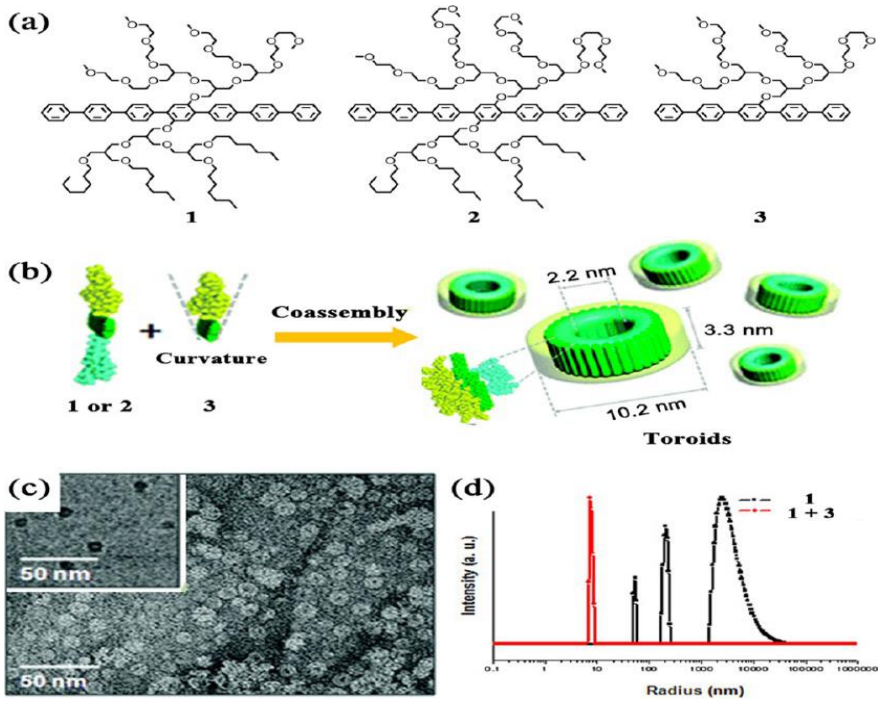

Figure 1.26. (a) *Chemical structures of 1, 2, and 3. (b) Schematic representation of the formation of toroids via the coassembly of 1 or 2 with 3. (c) TEM image of toroidal nanostructures of 1 containing 3 (90 mol % relative to 1) in aqueous solution; the inset is a cryo-TEM image of the toroids. (d) Size distribution graphs of 1 and 1 containing 3 (*adapted from Myongsoo Lee et al. *Acc. Chem. Res.* **2013**, *46, 2888−2897*).

Myongsoo Lee reported the synthetic nanometer-scale tubular assembly and these nanotubules undergo a reversible contraction-expansion motion accompanied by an inversion of helical chirality. The aromatic bent-shaped amphiphiles self-assemble into hexameric macrocycles in aqueous solution, forming chiral tubules by spontaneous one-dimensional stacking with a mutual rotation in the same direction. The adjacent aromatic segments within the hexameric macrocycles reversibly slide along one another in response to external triggers, resulting in pulsating motions of

the tubules accompanied by a chiral inversion. The aromatic interior of the self-assembled tubules encapsulates hydrophobic guests such as C60. Using a thermal trigger, they could regulate the C60-C60 interactions through the pulsating motion of the tubules (see figure 1.27).[134]

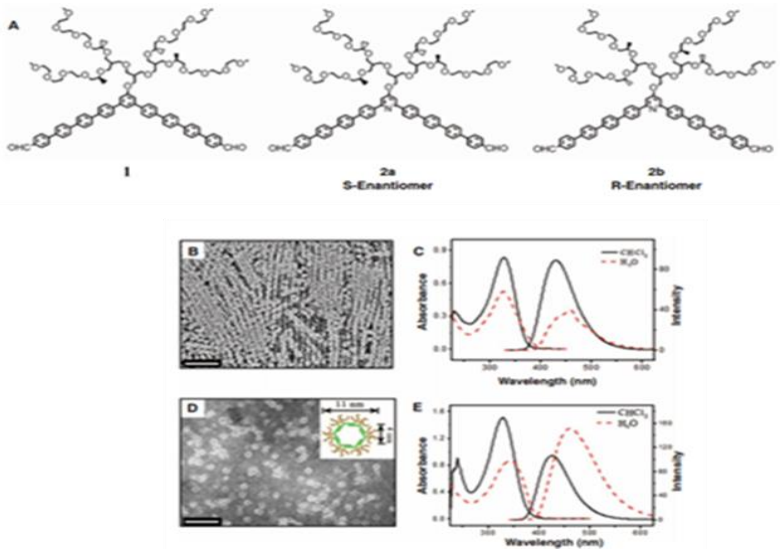

Figure 1.27. *(A) Molecular structure of bent-shaped amphiphiles. (B) TEM image of 1 from 0.01 wt % aqueous solution (scale bar, 50 nm). (C) Absorption and emission spectra of 1 in $CHCl_3$ (black and solid line) and in aqueous solution (red and dashed line). (D) TEM image of 2a from 0.002 wt % aqueous solution (scale bar, 50 nm). (E) Absorption and emission spectra of 2a in $CHCl_3$ (black and solid line) and in aqueous solution (red and dashed line) (*adapted from Myongsoo Lee et al. *Science* **2012**, *337*, 1521-1526).

Stupp and coworkers synthsized the series of amphiphilic oligo(p-phenylene vinylene)s (OPV)s containing oligo(phenylene vinylene) (OPV) rod like structure asymmetrically substituted with a hydrophilic poly(ethylene glycol) (PEG) unit and a hydrophobic alkyl chain and demonstrated the self-assembly of amphiphilic oligo(p-phenylene vinylene)s. These amphiphilic OPVs (Fig. 1.28) with different hydrophobic/hydrophilic balances which showed chain-length dependent thermotropic and lyotropic liquid crystalline phases. Among them, 18d and 18e were found to be soluble in aqueous medium and the latter formed a transparent self-supporting gel with J-aggregation among the OPV units and enhanced photoluminescence.[135]

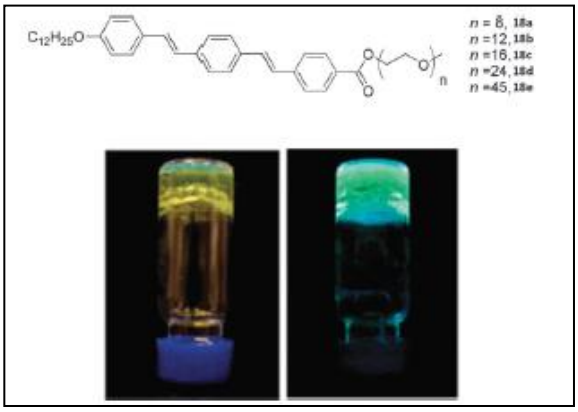

Figure. 1.28. *Top: structure of OPV amphiphiles; bottom: images of OPV hydrogel of 18e in daylight (left) and under UV light (right) (adapted* Stupp et al. from *J. Am. Chem. Soc*., **2005**, *127*, 366).

Bhattacharya and coworkers reported43 the aqueous self-assembly of a phenylenedivinylenebis- N-octyl pyridinium salt (Fig. 1.19) which showed gelation in water and interesting emission properties in the aggregated state. The self-assembled structures fibers, coils and tubes, tuned by varying the concentration. The emission properties changed drastically depending on the extent of aggregation, which could be tuned in presence of added NaBr by a predictable Hofmeister effect resulting in different emission colors (sky blue, orange or even white) under different conditions (see figure 1.29).[136]

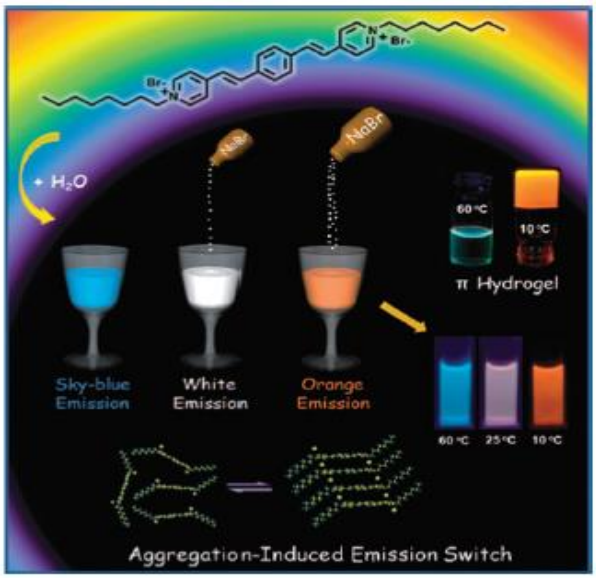

Figure 1.29. *Aggregation induced emission switching of a phenylenedivinylene-bis-N-octyl pyridinium salt (adapted from* Bhattacharya et al. *Chem.- Eur. J.* **2012**, *18,* 16632).

George and co-workers reported the different class of coronene based amphiphilic unsymmetrical diimides and studied self-assembly in water-tetrahydrofuran medium. This bisimide showed a signature of strong self-assembly in THF–H_2O medium and also observed the by intense π-π interactions and solvophobic repulsive forces confirmed by spectroscopic studies. By varying the composition of the THF–H_2O mixture, tuned the emission colour of the solution from green to orange–red as a result of aggregation (Fig. 8) which was also reflected in a solvent dependent morphology change from nano-tape to nanotubes with increasing water content (see figure 1.30).[137] Luping Yu and co-workers developed a series of rod-coil diblock and coil-rod-coil triblock copolymers amphiphilic diblock copolymers with different lengths of oligo(phenylene vinylene) as the rod block and poly(ethylene oxide) as the coil block and studied aggregation of diblock copolymers in good and bad solvent combination. THF as good solvent and water as a bad solvent for aggregation study. This diblock copolymer self-assemble into cylindrical micelles observed in TEM, AFM analysis and confirmed by small-angle neutron scattering (SANS) technique (see figure 1.31). These OPV-PEG micelles have acylindrical OPV core surrounded by a PEG corona and also showed liquid crystal property in thermal analysis.[138]

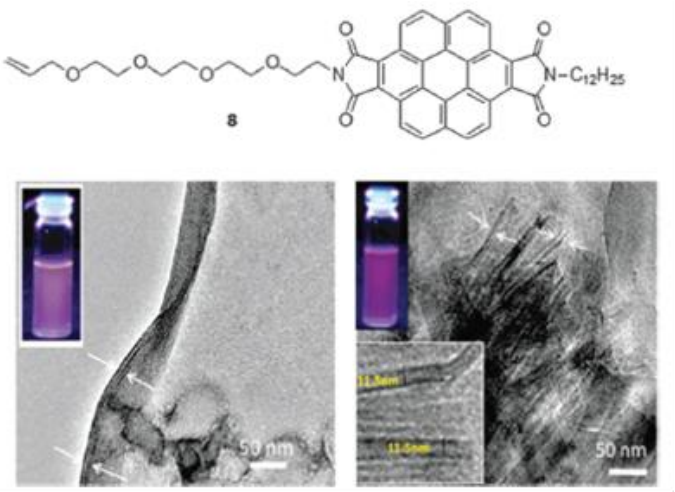

Figure 1.30. *Top: structure of amphiphilic coronene bisimide. Bottom: solvent dependent morphology (adapted from George et al. Org. Lett.* **2010**, *12*, 2656).

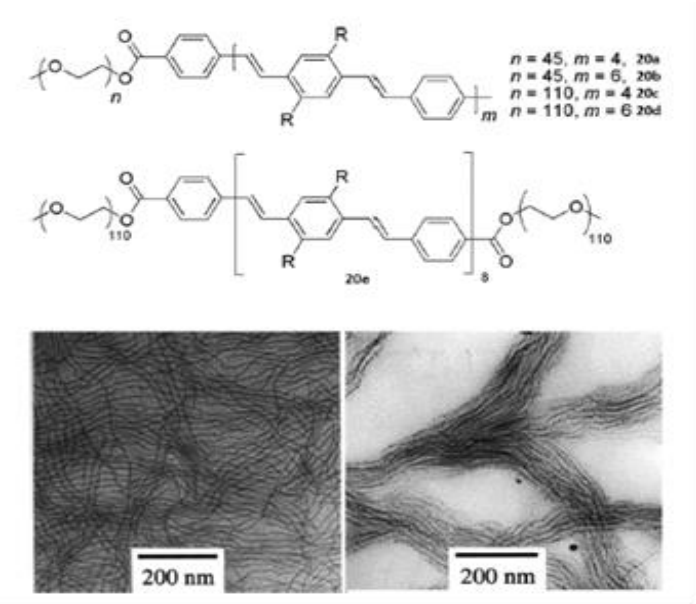

Figure. 1.31. *Top: structures of OPV containing rod–coil block copolymers (ref. 62); bottom: TEM image of 20b before (left) and after (right) complexation with silver triflate (adapted from Luping et al. J. Am. Chem.* Soc. **2000**, *122*, 6855).

Zong-Quan Wu and co-workers reported the conjugated block copolymers containing poly(3-hexylthiophene) (P_3HT) and poly(triethyl glycol allene) (PTA) segments which were synthesized in one pot using Ni(dppp)Cl_2 as a single catalyst via sequential polymerization of the two (or three) monomers. Interestingly, the P3HT-b-PTA diblock copolymers showed excellent thermoresponsive properties in water, and the lower critical solution temperature (LCST) is dependent on concentration of polymer and ratio of the block. In addition, the diblock copolymer showed highly tunable emission properties depending on the solvents used and the pH value of the solution. Both P3HT-b-PTA and P3HT-b-PTA-b-P3HT block copolymers exhibit solvatochromism properties. However, the triblock copolymer exhibit tunable light emissions with emission color widely expanded from red to blue due to the distinct self-assembly structures in different solvents. Very interestingly, white-light emission can be readily achieved from the P3HTb- PTA-b-P3HT triblock copolymer in composition of 25 % THF / methanol (see figure 1.32).[139]

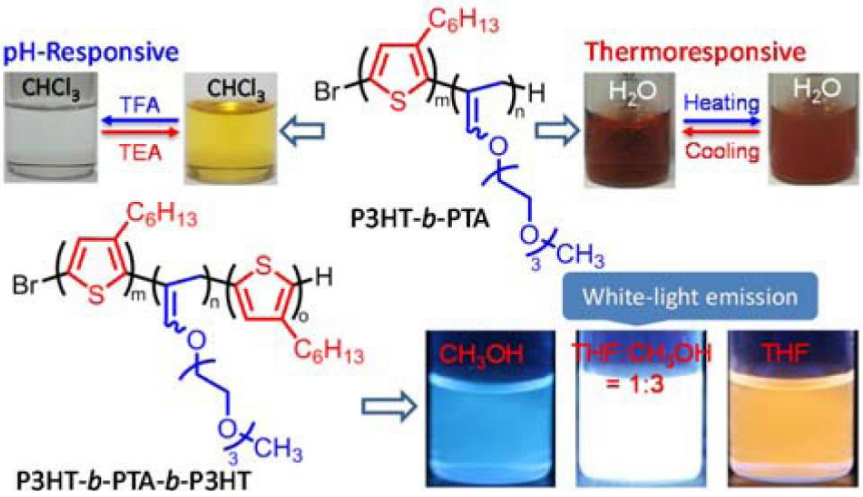

Figure 1.32. *Photographs of polymer in pH responsive, thermoresponsive, and in different solvents under room light UV light at 365 nm (Adapted from Wu et al. Macromolecules* ***2015****, 48, 5204-5212).*

Zong-Quan Wu and co-workers reported the multiresponsive poly(3-hexylthiophene) based amphiphilic triblock copolymers and also studied helical as well as color tunable assembly (see figure 1.33). Remarkably, achieved the white-light emission in solution, gel, and also solid state.[140-142]

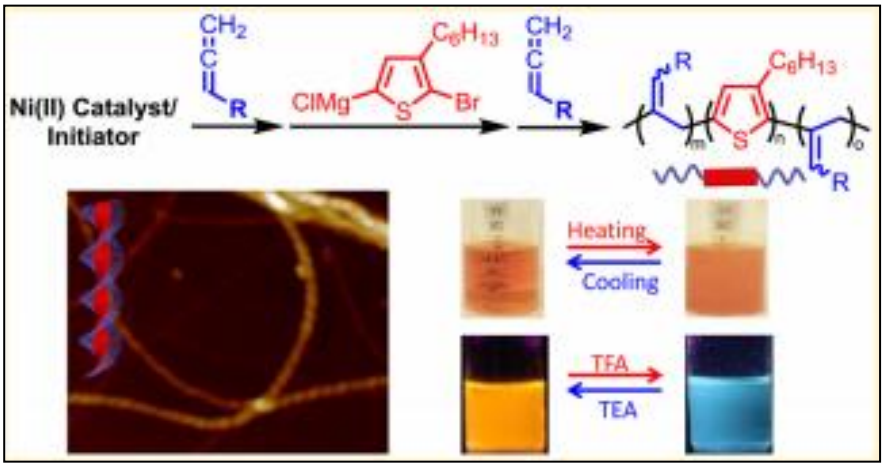

Figure 1.33. *Top structure of the polymer, bottom helical nanowires, photographs of polymer in pH responsive, thermoresponsive, and in different solvents under room light UV light at 365 nm (Adapted from Wu et al. Macromolecules,* **2016***, 49,* 1180–1190).

Frank Wurthner and coworkers developed the water-soluble nanocapsule system composed of enclosed energy-donor molecules and a bilayer dye membrane as an energy acceptor. The loaded vesicles are stabilized by in situ photopolymerization to give nanocapsules that are stable over the entire aqueous pH range. On the basis of

pH-tunable spectral overlap of donors and acceptors, the donor loaded polymerized vesicles showed pH-dependent fluorescence resonance energy transfer from the encapsulated donors to the bilayer dye membrane, providing ultrasensitive pH information on their aqueous environment with fluorescence colour changes covering the whole visible light range with a white light emission observed at pH 9.0. At pH 9.0, quite exceptional white fluorescence could be observed for such water-soluble donor-loaded perylene vesicles (see figure 1.34).[143]

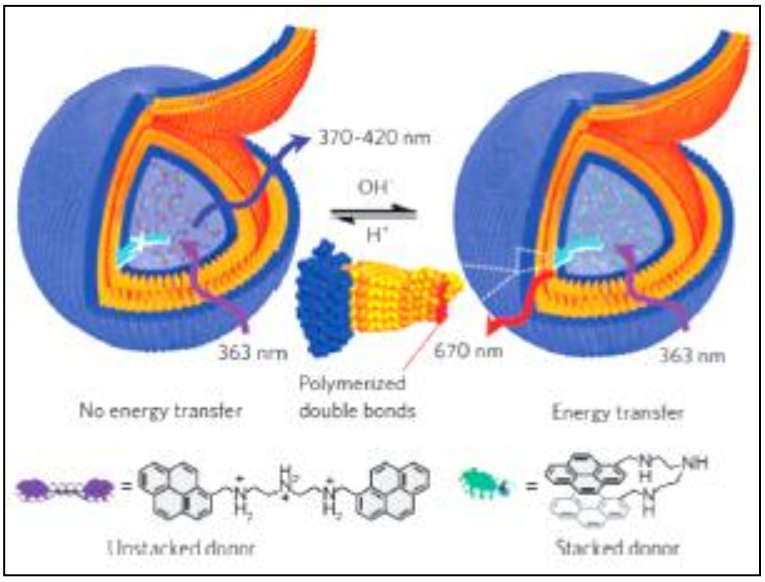

Figure. 1.34. *Schematic showing encapsulation of pH responsive pyrene dimer in a PBI vesicle and pH-dependent emission due to conformational change of the guest. (Adapted from Wurthner et al. Nat. Chem.,* **2009**, *1,* 623*).*

Swager et al. extended this concept to crown-ether functionalized poly(*p*-phenyleneethynylene) that π-π stacks upon adding potassium, whereas upon adding sodium a planar nonaggregated polymer backbone was obtained that is highly emissive. PPVwith crown ether substituents could form wormlike nanoribbons through complexation with potassium in dilute chloroform solution. The growth of nanoribbons enhanced by long time exposure to potassium. TEM and AFM revealed that width and length of nanoribbons is 15 nm and a few micrometers respectively (Figure 1.35).[144-145]

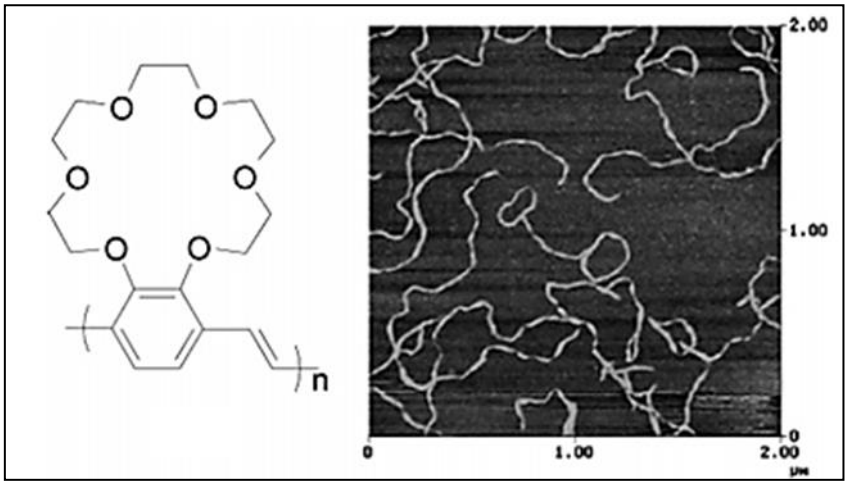

Figure 1.35. *AFM picture showing wormlike morphologies obtained from poly(p-phenylenevinylene) with pendant crown ethers in the presence of potassium (adapted from Hoeben et al*. *Chem. Rev.* **2005,** *105,* 1491-1546.; Luo et al. *J. Am. Chem. Soc.* **2003**, *125*, 6447−6451)

Ryan C. Hayward and co-workers reported the solution-state assembly of π-conjugated polythiophene diblock copolymers containing nonpolar (hexyl) and polar (triethylene glycol) side chains and studied the aggregation of this polymer in different ratio of good and bad solvent combinations. Chloroform chosen as good solvent and methanol chosen as bad solvent. As increasing bad solvent combination new aggregated peak appeared in higher wavelength region and the color of solution changes to orange to purple and the size of the aggregates increased in DLS analysis and also observed formation of nanofabrils in TEM and AFM analysis. When this polymer complexed with KI ions the TEG side chains drives the formation of helical ribbons, which further associate into superhelical structures showed in TEM analysis (see figure 1.36).[146] Hui-Feng Jiao et al, synthesized amphiphilic di block π-conjugated copolymers with thiophene units containing hydrophobic unit via a nickel-catalyzed quasi-living polymerization. These copolymers dispersed in water via a slow dialysis method produced molecular-level self-assembled core–shell nanospheres with a crystallized hydrophobic core and a hydrophilic amorphous shell, which was proved by TEM images. By changing ratio of copolymers tuned size and quantum yield of polymer micelles. These polymers showed high quantum yield (19% in aqueous medium), good photostability and low cytotoxicity. By using a far-red/near-infrared (FR/NIR) cellular probe, BP40 is internalized efficiently by the cells and accumulated in the cytoplasm to give bright fluorescence (see figure 1.37).[147]

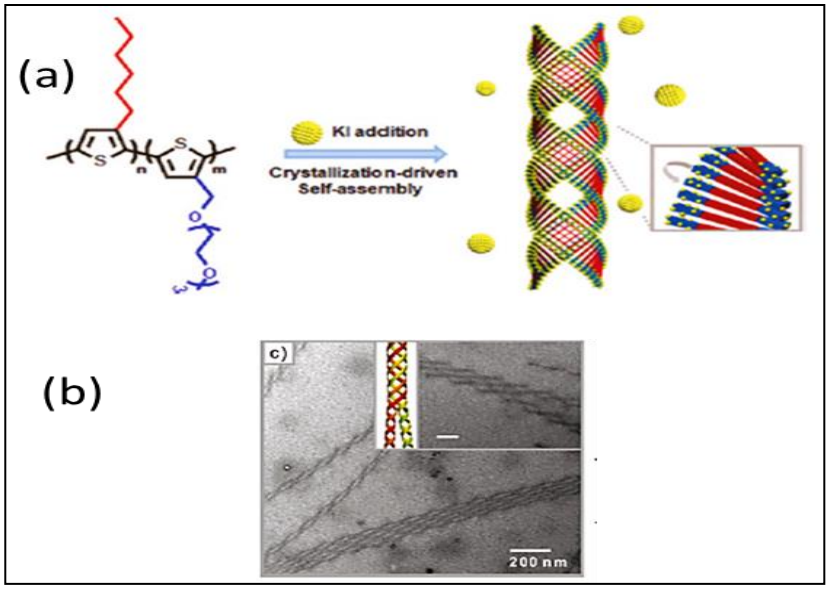

Figure 1.36. (a) *Molecular structure of P3HT-b-P3(TEG)T diblock copolymers and schematic representation of their assembly into super helical structures through crystallization in the presence of potassium ions. (b) multiple-stranded helices. Inset: TEM image and schematic showing association of double helices into quadruple superhelices (scale bar, 100 nm) (adapted from Hayward et al. J. Am. Chem. Soc.* **2011**, *133*, 10390-10393).

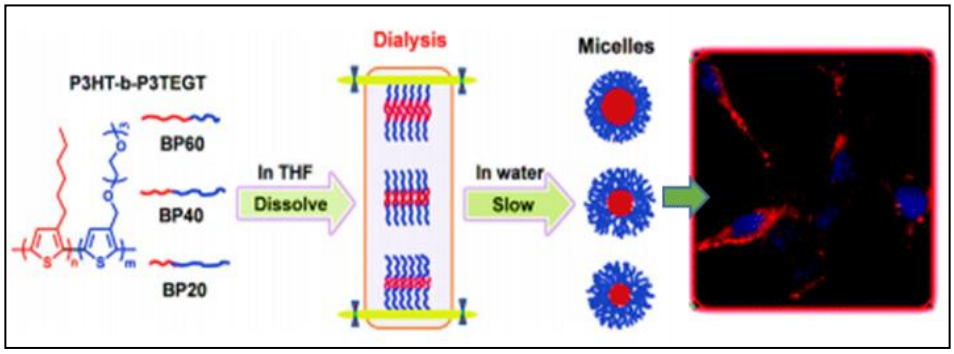

Figure 1.37. *Schematic illustration of the self-assembly processes during the dialysis process of various block copolymers and the fluorescence image of HEK 293 cells incubated with BP40 (5 mM) after being stained by DAPI (adapted from Jiao et al. J. Mater. Chem. B*, **2016**, *4*, 7882-7887).

Futher, from our group Kulkarni et al. reported the Oligophenylenevinylene (OPV) and polycaprolactone based ABA tri block copolymer and demonstrated the cellular imaging and delivering drugs to intracellular compartments. These triblocks self-assembled in organic solvents to produce well-defined helical nanofibers, whereas in water they produced blue luminescence spherical nanoparticles (size ~150 nm) and loaded anticancer drug such as doxorubicin (DOX). In vitro studies revealed

that the biodegradable PCL arm was susceptible to enzymatic cleavage at the intracellular lysosomal esterase under physiological conditions to release the loaded drugs. The nascent nanoparticles were found to be nontoxic to cancer cells and the DOX-loaded nanoparticles accomplished more than 80% killing in HeLa cells. Confocal microscopic analysis confirmed the cell penetrating ability of the blue luminescent polymer nanoparticles and their accumulation preferably in the cytoplasm. The DOX loaded red luminescent polymer nanoparticles were also taken up by the cells, and the drug was found to be accumulated at the perinuclear environment (see figure 1.38).[148]

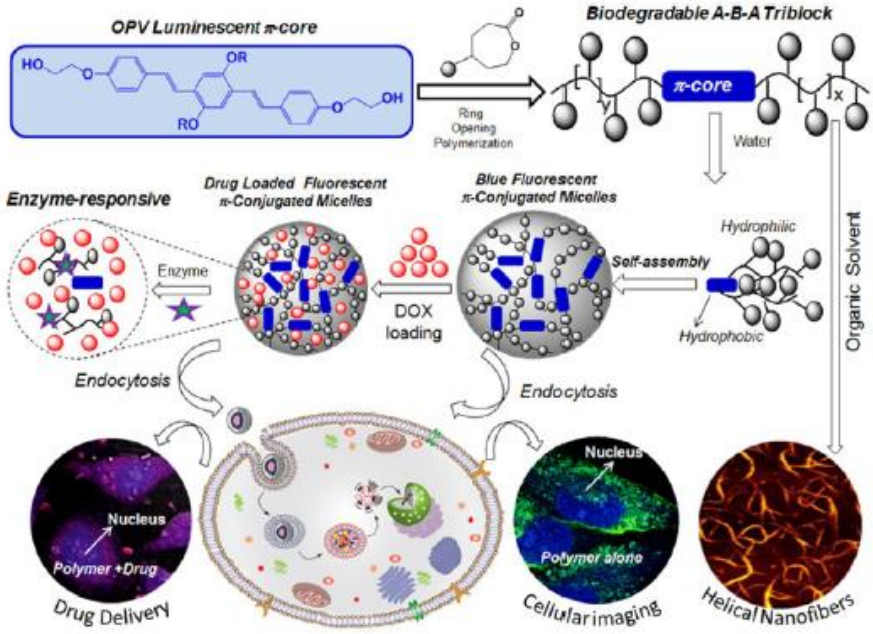

Figure 1.38. *Schematic representation of biodegradable conjugated chromophore triblock copolymer approach for drug delivery and imaging in cancer cells (adapted from Kulkarni* et al. *Bio macromolecules* **2016**, *17*, 1004-1016).

1.5. Segmented π-conjugated systems

In conjugated polymers, the aromatic parts are separated by flexible units named as segmented π-conjugated polymers. The flexible units could be alkyl or oligoether units. Most of the π-conjugated systems used for LED and metal ions sensing and D-A with white light emission and these are fold to form higher order aggregates/structures. These are new class of conjugated systems and first soluble Oligophenylenevinylene based segmented π-conjugated polymers developed by F.E. Karasz and coworkers in 1992. F.E. Karasz and coworkers developed a new segmented polymer by witting route and uniform conjugated units of specified length with flexible-chain aliphatic oligomeric segments. The basic design concepts can be extended to produce useful soluble materials emitting in other regions of the spectrum and possessing optimized mechanical, optical, and electrical properties. Franco Cacialli et al, synthesized the soluble two different segmented π-conjugated polymers via witting reaction and named as block copolymers. One of block copolymer contains distyrylbenzene as chromophore and hexa (ethylene oxide) units arranged alternative fashion in polymer backbone and another polymer contains hexa (ethylene oxide) and dodecafluoro- distyrylbenzene. Studied the solid-state photoluminescence efficiency for LED applications and measured the optical energy gap for both polymers (see figure 1.40).[149-151]

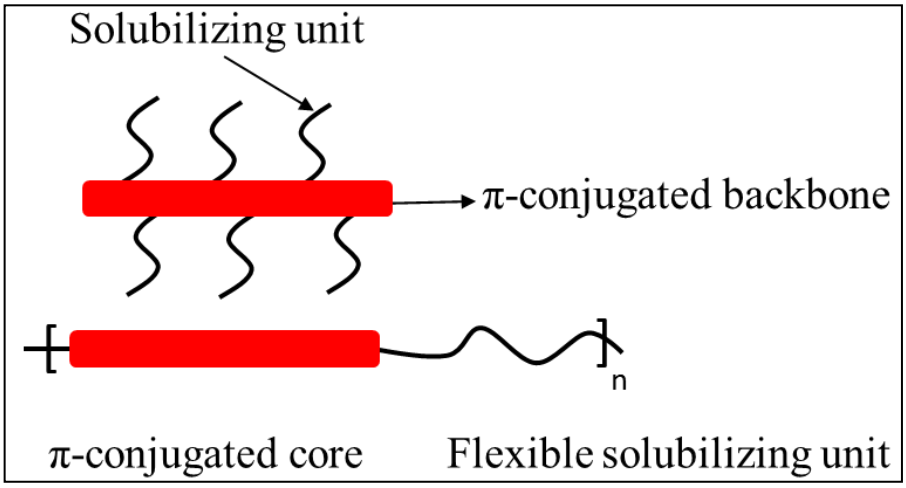

Figure 1.39. *Schematic representation of segmented π-conjugated polymer.*

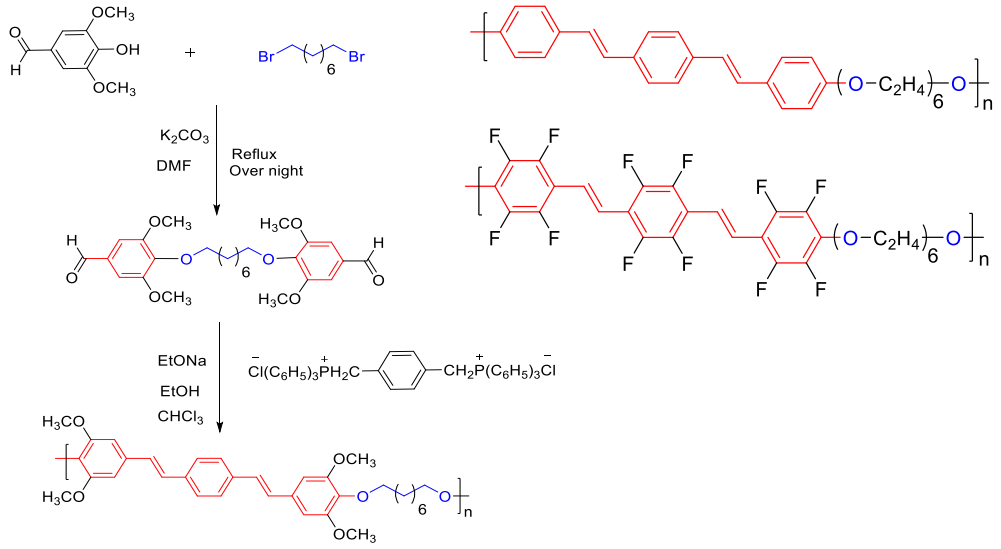

Figure 1.40. *Left: Synthesis of segmented polymers. Right: Structure of segmented polymers (adapted from ref. 149-151).*

Further, from our group Mahima et al. designed a new series of different chain length flexible TCD based oligo-1,4-phenylenevinylenes (OPV) segmented polymers. By having flexible the segments on polymer back bone produced J-type aggregates through chain folding and the OPV π-core aggregation in methanol/THF solvent mixtures. Polymer formed helical fibers (see figure 1.41) observed in electron microscopic analysis and complexation of flexible polymer with electron deficient molecule perylenebisimide derivative produced well-ordered helical donor−acceptor assemblies by simple solution blending techniques. The formations of the helical D−A stacks were further confirmed by detailed FRET studies and TCSPC analysis.[152]

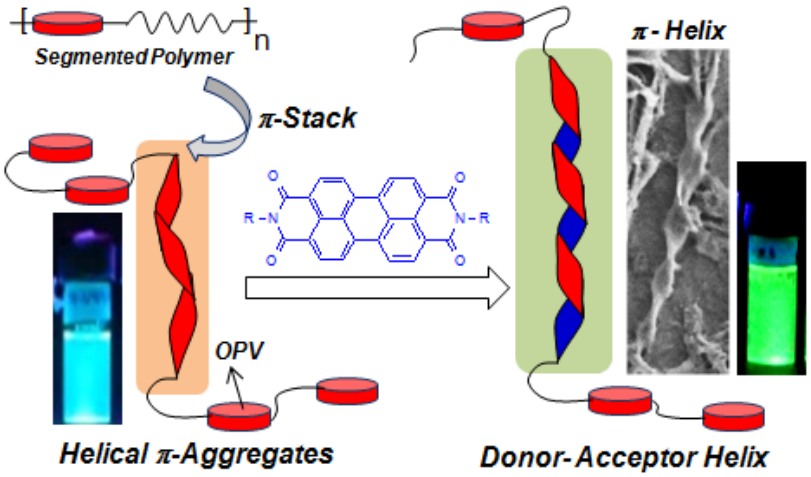

Figure 1.41. *Approache for helical segmented polymers and donor-acceptor helix* (adapted from Mahima et al. *Macromolecules* **2014**, *47*, 2592−2603).

Further, from our group Balamurugan et al, also designed a new series of amphiphilic segmented π-conjugated luminescent thermo-sensitive carboxylic acid functionalised OPV polymers and demonstrated as efficient photosensitizers for Eu^{3+} ions. Upon photoexcitation, the excitation energy transfer from the blue luminescent polymeric ligand to metal center (LMET) produced strong and sharp metal centered red-emission. These π-conjugated polymer–Eu^{3+} ion complexes were found to be thermo-sensitive and behaved as reversible 'turn-on' or 'turn-off' luminescent switches in solution and in solid state and also demonstrated the concept of triple-action molecular probe for sensing applications (see figure 1.42). A triple-action p-conjugated polymer chemosensor is developed for sensing temperature, selective detection of copper (II) metal-ion and biological species-amino acids.[153-154]

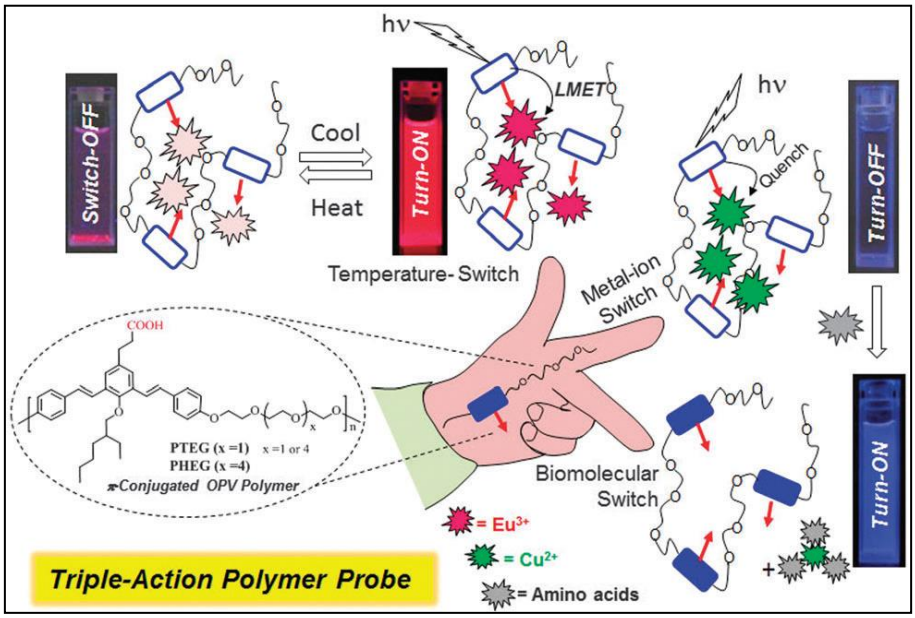

Figure. 1.42 *Triple-action distilbene chromophore bearing polymer as temperature, metal-ion and biomolecular fluorescent probes* ***(****adapted from Balamurugan et al Chem. Commun.* **2014,** *50,* 842-845*).*

Asha and co-workers designed carboxyl functional group as a side chain containing an 1, 3-oligo(phenylenevinylene) (OPV) based segmented polymer. By using this polymer studied the hydrogen bonded D-A assembly with acceptor pyridine functionalized perylene bisimide in tetrachloroethane with white light emission. These polymer D-A complexes formed lamellar morphology. The polymer additionally showed thermosensitive emission color tuning due to its polymer chain coiling and uncoiling in solvent upon heating and cooling process.[155] Ghiggino and co-workers recently developed the segmented polymers and demonstrated the photoinduced

charge separation in oligo-1,4-phenylenevinylenes (OPV) segmented polymers with PCBM and alt-*co*-MEH-PPV:PCBM blends confirmed by transient absorption measurements and Fluorescence spectroscopy.[156] Ullrich Scherf and co-workers reported the segmented the series of cationic polyelectrolytes main-chain polyelectrolytes containing pyridinium-based *p*-phenylenevinylene chromophores that are connected via alkylene spacers of varying length by a base-catalyzed aldol-type coupling reaction and studied the thermoreversible gelation property as well as morphological analysis (see figure 1.43).[157]

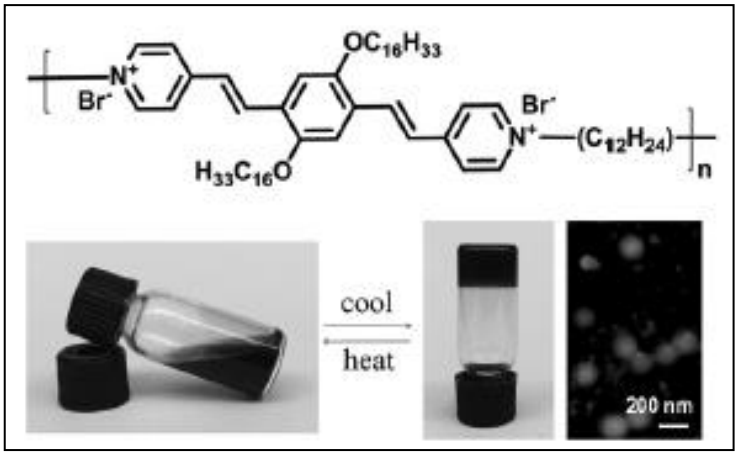

Figure. 1.43. *Structure of segmented polymer, Sol-Gel transition and FE-SEM image of polymer at gel state* ***(****adapted from Ullrich et al. Macromol. Chem. Phys.* **2017**, *218*, 1600374).

Rene´ A. J. Janssen and coworkers reported new series of electron deficient three polymers consisting of alternating perylene bisimide chromophores and flexible polytetrahydrofuran segments of different length studied using absorption and (time-resolved) photoluminescence spectroscopy. The perylene bisimide chromophores form H-type aggregates in ODCB (o-di chloro benzene) solution. The tendency to form aggregates increases for shorter polyTHF segments.[158-159] Another class of segmented π-conjugated systems are thiophene systems and are aggregates in dioxane or dioxane-water systems monitored by UV-visible and fluorescence spectroscopy.[160-165]

1.7. Aim of the Thesis work

π-Conjugated polymers are currently extensively studied for applications in photovoltaics, light emitting diodes, field effective transistors, etc; however, only very few efforts have taken to construct segmented π-conjugated materials polymers for thes above applications. Since π-conjugated materials have charge carrier mobility, color tenability, processability and mechanical stability; the development of new π-conjugated materials would open up new avenue for current and futuristic photonic-cum-electronic devices. In the last few decades, significant amount of works have been done on π-conjugated oligomers to understand their self-organization through aromatic π-stacking. However, translating the self-assembly knowledge gained in the small molecular building blocks to polymer systems is very challenging due to the large anisotropy associated with macromolecular chain folding phenomena. Thus, new strategies are required to design aligned 2D and 3D π-conjugated materials in the solid state (or thin-film) that are crucial for the performance in devices. Further, the development of amphiphilic π-conjugated polymers and study their water soluble nano-assemblies are also emerging as new area of research in bio-imaging applications.

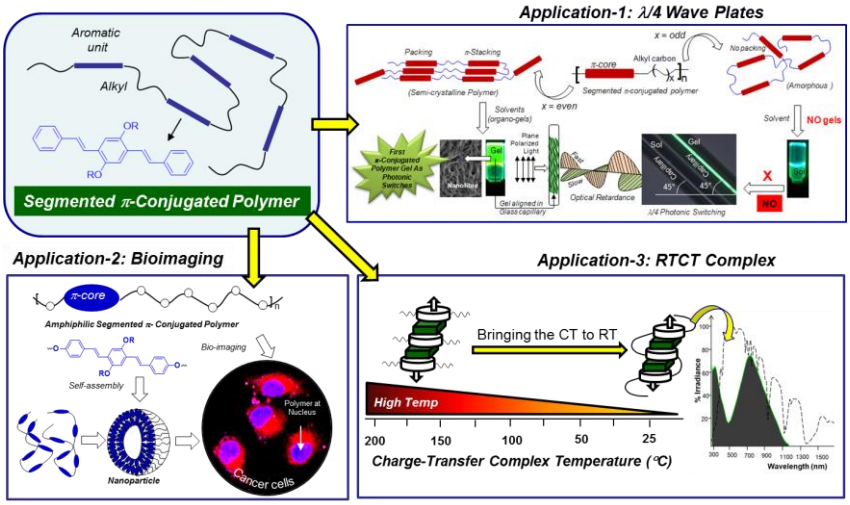

Figure 1.44. *New classes of segmented polymers and their application in thermoresponsive photonic switches, bio-imaging in cancer cells, and room temperature donor-acceptor charge-transfer materials.*

Among these, self-assembly of π-conjugated polymers that are responsive to undergo changes in the chain backbone is particularly important since it would provide new fundamental understanding on chain folding phenomena. The thesis work is aimed to address this important problem based on segmented π-conjugated polymers having rigid aromatic π-core and flexible alkyl or oligoethyelene spacers. This concept is schematically shown in Figure 1.44.

In this thesis work, π-conjugated photonic switches (or photonic wave plates) based on polymer anisotropic organogel was developed. This concept was achieved based on two important factors: (i) successful development of semi-crystalline π-conjugated polymer and (ii) their ability to produce transparent self-organized anisotropic organogel that can be processed into desire objects for photonic switching capabilities. Further, amphiphilic segmented π-conjugated polymers were designed for studying their unique π- stacking driven self-assembly and also successfully employ their color tubable luminescent aqueous nanoparticles as non-toxic probes for bio-imaging in cervical and breast cancer cells. Appropriate oligo-phenylenevinylene π-core was chosen and flexible oligo-ethyelenoxy segments were employed as spacers to make new classes of segmented OPV polymers. The polymers were obtained in high molecular weights, with very good solubility in and also dispersable into aqueous stable nanoparticles of < 200 nm in size. Cytotoxicity in cervical and breast cancer cells revealed that these segmented polymer nanoparticles are non-toxic to cells. Confocal microscope imaging confirmed their selectively accumulation at the nucleus of the cancer cells. Efforts were also taken to make new classes of room temperature charge transfer (CT) complex based on segmented OPV polymers and arylene bisimides. The solid state CT band absorbance was found to be much higher in intensify compared to their solution CT band. It is important to mention that the new combination of OPV polymer+NDI donor-acceptor solid state assemblies is one of the first examples to produce CT band capable of absorption the light entire solar spectrum at the room temperature. The CT band the D-A complexes in the solid state was observed to very stable for more than 6 months at room temperature in normal laboratory conditions. The final chapter concludes the overall thesis work and put forward new concepts for futuristic research in the above research area.

1.7. References

1. Shirakawa, H.; Louis, E. J.; MacDiarmid, A. G.; Chiang, C. K.; Heeger, A. J. *J. Chem. Soc., Chem. Commun.* **1977**, 578.
2. Wise, D. L. *Electrical and Optical Polymer Systems: Fundamentals: Methods and Applications* CRC Press, **1998**.
3. Skotheim, T. A. *Handbook of Conducting Polymers*, Marcel Dekker, New York, **1986.**
4. Salamone, J. C. *Polymeric Materials Encyclopedia* CRC Press, **1996**.
5. Nalwa, H. S. *Handbook of Advanced Electronic and Photonic Materials and Devices*, Academic Press, **2000.**
6. Bredas, J. L. *Conjugated Oligomers, Polymers and Dendrimers: From Polyacetylene to DNA*, Proceedings of the Fourth Francqui Colloquium, Brussels, **1998**.
7. Tayi, A. S.; Kaeser, A.; Matsumoto, M.; Aida, T.; and Stupp, S. I. *Nature Chem.* **2015**, *7*, 281.
8. Li, K.; Liu, B. *Chem. Soc. Rev.* **2014**, *43*, 6570−6597.
9. Zhu, C.; Liu, L.; Yang, Q.; Lv, F.; Wang, S. *Chem. Rev*. **2012**, *112*, 4687−4735.
10. Xia, f.; Zuo, X.; Yang, R.; Xiao, Y.; Kang, D.; Valle-Blisle, A.; Gong, X.; Heeger, A. J.; Plaxco, K. W.; J. Am. Chem. Soc. 2010, 132, 1252-1254.
11. Zeng, X.; Qu, K.; and. Rehman, A. *Acc. Chem. Res.* **2016**, *49*, 1624−1633.
12. Xu, X.; Liu, R.; Li, L. *Chem. Commun.* **2015** *51*, 16733-16749.
13. Ding, D.; Li, K.; Zhu, Z.; Pu, K.; Hu, Y.; Jiang, X.; Liu, B. *Nanoscale*, **2011**, *3*, 1997-2002.
14. Feng, L.; Liu, L.; Lv, F.; Bazan, G.C.; Wang, S. *Adv. Mater.* **2014**, *26*, 3926-3930.
15. Feng, X.; Tang, Y.; Duan, X.; Liu, L.; Wang, S. *J. Mater. Chem.* **2010**, *20*, 1312-1316.
16. Shirakawa, H. *Angew. Chem. Int. Ed.* **2001**, *40*, 2574.
17. Sun, S. S.; Sariciftci, N. S. *Organic Photovoltaics: Mechanism, Materials and Devices* CRC Press, **2005**.

18. Burroughes, N. N.; Bradley, D. D. C.; Brown, A. R.; Marks, N. N.; Mackay, K.; Friend, R. H.; Burns, P. L.; Holmes, A. B. *Nature*, **1990**, *347*, 539.
19. Burn, P. L.; Holmes, A. B.; Kraft, A.; Bradley, D. D. C.; Brown, A. R.; Friend, R. H.; Gymer, R. W. *Nature* **1992**, *356*, 47.
20. Greenham, N. C.; Moratti, S. C.; Bradley, D. D. C.; Friend, R. H.; Holmes, A. B. *Nature* **1993**, *365*, 628.
21. Akcelrud, L. *Prog. Polym. Sci*. **2003**, *28*, 875.
22. Mueller, G. *Electroluminescence I (Semiconductors and Semimetals)*, Academic Press, USA, **1999**.
23. Hoppe, H.; Sariciftci, N. S. *J. Mater. Res.* **2004**, *19*, 1924-1945. (b) Cheng, Y.J.; Yang, S. H.; Hsu, C. S. *Chem. Rev.***2009**, *109*, 5868-5923.
24. Ouali, L.; Krasnikov, V. V.; Stalmach, U.; Hadziioannou, G. *Adv. Mater.* **1999**, *11*, 1515-1518. (b) Gu¨nes, S.; Neugebauer, H.; Sariciftci, N. S. *Chem. Rev.* **2007**, *107*, 1324-1338.
25. Lu, L.; Zheng, T.; Wu, Q.; Schneider, A.M.; Zhao, D.; Yu, L. *Chem. Rev.* **2015**, 115, 12666,
26. Wu, W.; Liu, Y.; Zhu, D. *Chem. Soc. Rev.* **2010**, *39*, 1489-1502.
27. Wang, C.; Dong, H.; hu, W.; Liu, Y.; Zhu, D. *Chem. Rev.* **2012**, *112*, 2208-2267.
28. Sun, Y.; Liu, Y.; Zhu, D. *J. Mater. Chem.* **2005**, *15*, 53-65.
29. Swager, T. M. *Macromolecules* **2017** ASAP (**DOI:** 10.1021/acs.macromol.7b00582).
30. Hoeben, F. J. M.; Jonkheijm, P.; Meijer, E. W.; Schenning, A. P. H. J. *Chem. Rev*. **2005**, *105*, 1491-1546.
31. Oksana Ostroverkhova *Chem. Rev.*, **2016**, *116*, 13279-13412.
32. Hedley, G. J.; Ruseckas, A.; Samuel, I. D. W. *Chem. Rev.* **2017**, *117*, 796−837.
33. Sommer, M.; Huettner, S.; Thelakkat, M. *J. Mater. Chem.* **2010**, *20*, 10788-10797.
34. Hunter, C. A.; Lawson, K. R.; Perkins, J.; Urch, C. J. *J. Chem. Soc. Perkin Trans.* **2001**, *2*, 651–669.
35. Huettner, S.; Hodgkiss, J. M.; Sommer, M.; Friend, R. H.; Steiner U.; Thelakkat, M. *J. Phys. Chem. B* **2012**, *116*, 10070−10078.

36. Eckert, J. F.; Nicoud, J. F.; Nierengarten, J. F.; Liu, S. G.; Echegoyen, L.; Barigelletti, F.; Armaroli, N.; Ouali, L.; Krasnikov, V.; Hadziioannou, G. *J. Am. Chem. Soc.* **2000**, *122*, 7467-7479.

37. Peeters, E.; Hal, P. A. V.; Knol, J.; Brabec, C. J.; Sariciftci, N. S.; Hummelen, J. C.; Janssen, R. A. J. *J. Phys. Chem. B* **2000,** *104*, 10174-10190.

38. Wang, L.; Wu, C-F.; Wang, H-Y.; Chen, Q-D.; Han, W.; Qin, W-P.; McNeill, J.; Sun, H-B. *Nanoscale*, **2013**, *5*, 7256-7270

39. Neuteboom, E. E.; Meskers, S. C. J.; Hal, P. A. V.; Duren, J. K. J. V.; Meijer, E. W.; Janssen, R. A. J.; Dupin, H.; Pourtois, G.; Cornil, J.; Lazzaroni, R.; Bredas, J. L.; Beljonne, D. *J. Am. Chem. Soc.* **2003**, *125*, 8625-8638.

40. L. Ouali, L.; Krasnikov V. V., Stalmach, U.; Hadziioanno, G. *Adv. Mater.* **1999**, *11*, 1515-1518.

41. Asha, S. K.; Schenning, A. P. H. J.; Meijer, E. W. *Chem. Eur. J.* **2002**, *8*, 3353-3361.

42. Das, A.; Ghosh, S. *Angew Chem. Int. Ed.* **2014**, *53*, 2038–2054.

43. Kumar, M.; Venkata Rao, K.; George, S. J. *Phys. Chem. Chem. Phys.* **2014**, 16, 1300.

44. Jalani, K.; Kumar, M.; George, S. J. Chem. Commun. 2013, 49, 5174 –5176;

45. Scott Lokey, R.; Iverson, B. L. *Nature* **1995**, *375*, 303 –305;

46. Kaiser, G.; Jarrosson, T.; Otto, S.; Ng, Y.-F.; Bond, A. D.; Sanders, J. K. M. *Angew. Chem. Int. Ed*. **2004,** *43*, 1959 –1962;

47. Vignon, S. A.; Jarrosson, T.; Iijima, T.; Tseng, H.-R.; Sanders, J. K. M.; Stoddart, J. F. *J. Am. Chem. Soc.* **2004**, *126*, 9884 – 9885.

48. De Greef, T. F. A.; Smulders, M. M. J.; Wolffs, M.; Schenning, A. P. H. J.; Sijbesma,; R. P., Meijer, E. W. *Chem. Rev.* **2009**, *109*, 5687.

49. Huang, F.; Scherman, O. A. *Chem. Soc. Rev*. **2012**, *41*, 5879.

50. Wang, J.-Y.; Yan, J.; Ding, L.; Ma, Y.; Pei, J. *Adv. Funct. Mater.* **2009**, *19*, 1746-1752

51. Molla, M. R.; Ghosh, S. *Chem.-Eur. J.*, **2012**, *18*, 9860.

52. Das, A.; Molla, M. R.; Banerjee, A.; Paul, A.; Ghosh, S. *Chem.-Eur. J.*, **2011**, *17*, 6061.

53. Chakraborty, S.; Kar, H.; Sikder, A.; Ghosh, S. *Chem. Sci*.**, 2017**, *8*, 1040-1045.

54. Rao, K. V.; Jayaramulu, K.; Maji, T. K.; George, S. J. *Angew. Chem.* **2010**, *122*, 4314;

55. Rao, K. V.; George, S. J. *Chem. Eur. J.* **2012**, *18*, 14286.

56. Kumar, M.; George, S. J. *Chem. Asian J.* **2014**, *9*, 2427-2431.

57. Liu, K.; Wang, C.; Li, Z. B. Zhang, X. *Angew. Chem., Int. Ed*., **2011**, *50*, 4952;

58. Liu, K.; Yao, Y.; Wang, C.; Liu, Y.; Li, Z.; Zhang, X. *Chem.–Eur. J.,* **2012**, *18*, 8622;

59. Liu, K.; Yao, Y.; Wang, C.; Liu, Y.; Li, Z.; Zhang, X. *Langmuir*, **2012**, *28*, 10697.

60. Pandeeswar. M.; Senanayak. S. P.; Narayan. K. S.; Govindaraju. T. *J. Am. Chem. Soc.* **2016**, *138*, 8259−8268.

61. Scott Lokey, R.; Iverson, B. L. *Nature* **1995**, *375*, 303 –305.

62. Gabriel, G. J.; Iverson, B. L.; *J. Am. Chem. Soc.* **2002**, *124*, 15174.

63. Ghosh, S.; Ramakrishnan, S. *Angew. Chem. Int. Ed.* **2004**, *43*, 3264-3268

64. Ghosh, S.; Ramakrishnan, S. *Angew. Chem. Int. Ed.* **2005**, *44*, 5441-5447.

65. De, S.; Ramakrishnan, S.; *Macromolecules* **2009**, *42*, 8599.

66. Park. L. Y.; Hamilton. D. G.; McGehee. E. A.; McMenimen. K. A. *J. Am. Chem. Soc.* **2003**, *125*, 10586-10590.

67. Alvey, P. M.; Reczek, J. J.; Lynch, V.; Iverson, B. L. *J. Org. Chem.* **2010**, *75*, 7682- 7690.

68. Reczek, J. J.; Villazor, K. R.; Lynch, V.; Swager, T. M.; Iverson, B. L. J. Am. Chem. Soc. **2006,** *128* 7995-8002.

69. Pisula, W.; Kastler, M.; Wasserfallen, D.; Robertson, J. W. F.; Nolde, F.; Kohl, C.; Müllen, K. *Angew. Chem., Int. Ed.* **2006**, *45*, 819.

70. Leight, K. R.; Esarey, B. E.; Murray, A. E.; Reczek, J. J. *Chem. Mater.* **2012**, *24*, 3318– 3328.

71. Tayi, A. S.; Shveyd, A. K.; Sue, A. C.-H.; Szarko, J. M.; Rolczynski, B. S.; Cao, D.; Kennedy, T. J.; Sarjeant, A. A.; Stern, C. L.; Paxton, W. F.; Wu, W.; Dey, S. K.; Fahrenbach, A. C.; Guest, J. R.; Mohseni, H.; Chen, L. X.; Wang, K. L.; Stoddart, J. F.; Stupp, S. I. *Nature* **2012**, *488*, 485

72. Diez-Perez, I.; Li, Z. H.; Guo, S. Y.; Madden, C.; Huang, H. L.; Che, Y. K.; Yang, X. M.; Zang, L.;Tao, N. J. *ACS Nano* **2012**, 6, 7044-7052.

73. Park, S. K.; Varghese, S.; Kim, J. H.; Yoon, S. J.; Kwon, O. K.; An, B. K.; Gierschner, J.; Park, S. Y. *J. Am. Chem. Soc.* **2013**, *135*, 4757– 4764.

74. Guan, Y.-S.; Qin, Y.; Sun, Y.; Chen, J.; Xu, W.; Zhu, D. *Chem. Commun.*, **2016**, *52*, 4648.
75. López-Andarias, J.; Rodriguez, M. J.; Atienza, C.; López, J. L.; Mikie, T.; Casado, S.; Seki, S.; Carrascosa, J. L.; Martín, N *J. Am. Chem. Soc.* **2015**, *137*, 893-897.
76. Prasanthkumar, S.; Ghosh, S.; Nair, V. C.; Saeki, A.; Seki, S.; Ajayaghosh, A. *Angew. Chem., Int. Ed*. **201**5, *54*, 946-950.
77. Traiphol, R.; Charoenthai, N.; Srikhirin, T.; Kerdcharoen, T.; Osotchan, T.; Maturos, T. *Polymer* **2007**, *48*, 813.
78. Belletete, M.; Bouchard, J.; Leclerc, M.; Durocher, G. *Macromolecules* **2005**, *38*, 880.
79. Zhang, H.; Lu, X.; Li, Y.; Ai, X.; Zhang, X.; Yang, G. *J. Photochem. Photobiol. A Chem.* **2002,** *147*, 15.
80. Traiphol, R.; Sanguansat, P.; Srikhirin, S.; Kerdcharoen, T.; Osotchan, T. *Macromolecules* **2006,** *39*, 1165.
81. Quan, S.; Teng, F.; Xu, Z.; Qian, L.; Zhang, T.; Liu, D.; Hou, Y.; Wang, Y.; Xu, X. *J. Luminescence* **2007**, *124* , 81.
82. Panzer, F.; Bassler, H.; Kohler, A. *J. Phys. Chem. Lett.* **2017**, *8*, 114−125.
83. Halkyard, C. E.; Rampey, M. E.; Kloppenburg, L.; Studer-Martinez, S. L.; Bunz, U. H. F. *Macromolecules* **1998**, *31*, 8655.
84. Miteva, T.; Palmer, L.; Kloppenburg, L.; Neher, D.; Bunz, U. H. F. *Macromolecules* **2000**, *33*, 652.
85. Hu, Y.; Su, M.; Ma, C.; Yu, Z.; Liu, N.; Yin, J.; Ding, Y.; Wu, Z. *Macromolecules* **2015**, *48*, 5204−5212.
86. Li, Y. C.; Chen, K. B.; Chen, H. L.; Hsu, C. S.; Tsao, C. S.; Chen, J. H.; Chen, S. A. *Langmuir* **2006,** *22*, 11009.
87. Resta, C.; Di Pietro, S. D.; MajerićElenkov, M.; Hamersak, Z.; Pescitelli, G.; Di Bari, L. D. *Macromolecules* **2014**, *47*, 4847−4850.
88. Fakis, M.; Anestopoulos, D.; Giannetas, V.; Persephonis, P. *J. Phys. Chem. B.* **2006**, *110*, 24897.
89. Chen, S. H.; Su, A. C.; Huang, Y. F.; Su, C. H.; Peng, G. Y.; Chen, S. A. *Macromolecules* **2002**, *35*, 4229.
90. Chen, S. H.; Su, A. C.; Chou, H. L.; Peng, K. Y.; Chen, S. A. *Macromolecules* **2004**, *37*, 167.

91. McCullough, R. D.; Tristram-Nagle, S.; Williams, S. P.; Lowe, R. D.; Jayaraman, M. *J. Am. Chem. Soc.* **1993**, *115*, 4910-4911.
92. Yamamoto, T.; Komarudin, D.; Arai, M.; Lee, B.-L.; Suganuma, H.; Asakawa, N.; Inoue, Y.; Kubota, K.; Sasaki, S.; Fukuda, T.; Matsuda, H. *J. Am. Chem. Soc.* **1998**, *120*, 2047-2048.
93. Faı¨d, K.; Fre´chette, M.; Ranger, M.; Mazerolle, L.; Le´vesque, I.; Leclerc, M.; Chen, T.-A.; Rieke, R. D. *Chem. Mater.* **1995**, *7*, 1390-1396.
94. Le´vesque, I.; Leclerc, M. *Chem. Mater.* **1996**, *8*, 2843-2849.
95. Schwartz, B. J. *Annu. Rev. of Phys. Chem.* **2003**, *54*, 141-172.
96. Bunz, U. H. F. *Chem. Rev.* **2000**, *100*, 1605-1644.
97. Hoeben, F. J. M.; Jonkheijm, P.; Meijer, E. W.; Schenning, A. P. H. J. *Chem. Rev*. **2005**, *105*, 1491-1546.
98. Widawski, G.; Rawiso, M.; Francüois, B. *Nature* **1994**, *369*, 387-389.
99. de Boer, B.; Stalmach, U.; van Hutten, P. F.; Melzer, C.; Krasnikov, V. V.; Hadziioannou, G. *Polymer* **2001**, *42*, 9097-9109.
100. de Boer, B.; Stalmach, U.; Nijland, H.; Hadziioannou, G. *Adv. Mater.* **2000**, *12*, 1581-1583.
101. Ng, S.-C.; Chan, H. S. O.; Xia, J.-F.; Yu, W. *J. Mater. Chem.* **1998**, *8*, 2347-2352.
102. Francüois, B.; Pitois, O.; Francois, J. *Adv. Mater.* **1995**, *7*, 1041-1044.
103. Francüois, B.; Widawski, G.; Rawiso, M.; Cesar, B. *Synth. Met*.**1995**, *69*, 463-466.
104. Olinga, T.; Francüois, B. Makromol. *Chem., Rapid Commm.* **1991**, *12*, 575-582.
105. Brabec, C. J.; Winder, C.; Scharber, M. C.; Sariciftci, N. S.; Hummelen, J. C.; Svensson, M.; Andersson, M. R. *J. Chem. Phys.* **2001**, *115*, 7235-7244.
106. Camaioni, N.; Ridolfi, G.; Casalbore-Miceli, G.; Possamai, G.; Maggini, M. *Adv. Mater*. **2002**, *14*, 1735-1739.
107. Padinger, F.; Rittberger, R. S.; Sariciftci, N. S. *Adv. Funct. Mater.* **2003**, *13*, 85-88.
108. Liu, J.; Guo, T.-F.; Yang, Y. *J. Appl. Phys.* **2002**, *91*, 1595-1600.
109. Hempenius, M. A.; Langeveld-Voss, B. M. W.; van Haare, J. A. E. H.; Janssen, R. A. J.; Sheiko, S. S.; Spatz, J. P.; Mo¨ller, M.; Meijer, E. W. *J. Am. Chem. Soc.* **1998**, *120*, 2798-2804.

110. Kumar, M.; George, S. J. *Chem. – Eur. J*., **2011**, *17*, 11102.

111. Kumar, M.; George, S. J. *Nanoscale*, **2011**, *3*, 2130.

112. Molla, M. R.; Ghosh, S., *Chem. – Eur. J.*, **2012**, *18*, 9860.

113. Hulvat, J. F.; Sofos, M.; Tajima, K.; Stupp, S. I.; *J. Am. Chem. Soc*., **2005**, *127*, 366.

114. Matmour, R.; DeCat, I.; George, S.J.; Adriaens, W.;Leclère, P.; Boman s, P. H. H.; Sommerdijk, N. A. J. M.; Gielen, J. C.; Christianen, P. C. M.; Heldens, J. T.;van Hest, J. C. M.; Löwik, D. W. P. M.; De Feyter, S.; Meijer, E. W.; Schenning, A. P. H. J. *J. Am. Chem. Soc.* **2008**, *130*, 14576– 14583.

115. Wu¨rthner, F. *Chem. Commun.*, **2004**, 1564.

116. Zhang, X.; Chen, Z.; Wu¨rthner, F. *J. Am. Chem. Soc*., **2007**, *129*, 4886.

117. P. V. Rijn, D. Janeliunas, A. L. M. Brizard, M. C. A. Stuart, G. J. M. Koper, R. Eelkemaa and J. H. van Esch, *New J. Chem*., **2011**, *35*, 558.

118. O. Henze, W. J. Feast, F. Gardebien, P. Jonkheijm, R. Lazzaroni, P. Lecle´re, E. W. Meijer and A. P. H. J. Schenning, *J. Am. Chem. Soc*., **2006**, *128*, 5923.

119. S. Schmid, E. M. Osteritz, A. Kopyshev and P. Bau¨erle, *Org. Lett.*, **2009**, *11*, 5098.

120. Kumar, M.; Venkata Rao, K.; George, S. J. *Phys. Chem. Chem. Phys.* **2014**, 16, 1300.

121. Bunz, U. H. F.; Seehafer, K.; Bender, M.; Porz, M*Chem. Soc. Rev.* **2015**, *44*, 4322-4336.

122. Thomas III, S. W.; Joly, G. D.; Swager, T. M. *Chem. Rev*. **2007**, *107*, 1339-1386.

123. Kim, H. N.; Ren, W. X.; Kim, J. S.; Yoon, J. *Chem. Soc. Rev.* **2012**, *41*, 321-3244.

124. Wu, Y.; Tan, Y.; Wu, J.; Chen, S.; Chen, Y. Z.; Zhou, X.; Jiang, Y.; Tan, C.; M. *ACS Appl. Mater. Interfaces* **2015**, 7, 6882−6888.

125. McQuade, D. T.; Pullen, A. E.; Swager, T. M. *Chem. Rev*. **2000**, *100*, 2537−2574.

126. Kumar, M.; Venkata Rao, K.; George, S. J. *Phys. Chem. Chem. Phys.* **2014**, 16, 1300.

127. Li, K.; Liu, B.; Yang, Q.; Lv, F.; Wang, S. *Chem. Rev*. **2014**, *43*, 6570.
128. Zhu, C.; Liu, L.; Yang, Q.; Lv, F.; Wang, S. *Chem. Rev*. **2012**, *112*, 4687−4735.
129. Xu, X.; Liu, R.; Li, L. *Chem. Commun.* **2015** *51*, 16733-16749.
130. Ding, D.; Li, K.; Zhu, Z.; Pu, K.; Hu, Y.; Jiang, X.; Liu, B. *Nanoscale*, **2011**, *3*, 1997-2002.
131. Feng, L.; Liu, L.; Lv, F.; Bazan, G.C.; Wang, S. *Adv. Mater.* **2014**, *26*, 3926-3930.
132. Kim, Y.; Li, W.; Shin, S.; Lee, M. *Acc. Chem. Res*. **2013**, *46*, 2888−2897.
133. Rahaman, M.; Ghosh, S.; *Phys. Chem. Chem. Phy.* **2014**, 16, 26672-26683.
134. Kim, H.-J.; Kim, T.; Lee, M. *Acc. Chem. Res.* **2011**, *44*, 72–82.
135. Huang, Z.; Kang, S.-K.; Banno, M.; Yamaguchi, T.; Lee, D.; Seok, C.; Yashima, E.; Lee, M. *Science* **2012**, *337*, 1521-1526.
136. S. Bhattacharya and S. K. Samanta, *Chem. - Eur. J.* **2012**, *18*, 16632.
137. K. V. Rao and S. J. George, *Org. Lett.* **2010**, *12*, 2656.
138. Wang, H.; Wang, H. H.; Urban, V. S.; Thiyagarajan, K. C. L. P.; Yu, L.; *J. Am. Chem.* Soc. **2000**, *122*, 6855.
139. Hu, Y.; Su, M.; Ma, C.; Yu, Z.; Liu, N.; Yin, J.; Ding, Y.; Wu, Z. *Macromolecules* **2015**, *48*, 5204−5212.
140. Yu, Z.-P.; Ma, C.-H.; Wang, Q.; Liu, N.; Yin, J.; Wu, Z.-Q. *Macromolecules* **2016**, *49*,1180
141. Su, M.; Shi, S.-Y.; Wang, Q.; Liu, N.; Yin, J.; Liu, C.; Ding, Y.; Wu, Z.-Q. *Polym. Chem.* **2015**, 6, 6519.
142. Yu, Z.-P.; Liu, N.; Yang, L.; Jiang, Z.-Q.; Wu, Z.-Q. *Macromolecules* **2017**, *50*, 3204–3214.
143. Zhang, X.; Rehm, S.; Safont-Sempere, M. M.; Wu¨rthner, F. *Nat. Chem.* **2009**, *1*, 623.
144. Morgado, J.; Cacialli, F.; Friend, R. H.; Chuah, B. S.; Moratti, S. C.; Holmes, A. B. *Synth. Met.* **2000**, *111-112*, 449-452.
145. Luo, Y.-H.; Liu, H.-W.; Xi, F.; Li, L.; Jin, X.-G.; Han, C. C.; Chan, C.-M. *J. Am. Chem. Soc.* **2003**, *125*, 6447-6451.
146. Lee, E.; Hammer, B.; Kim, J. K.; Page, Z.; Emrick, T.; Hayward, R. C. *J. Am. Chem. Soc*. **2011**, *133*, 10390-10393.

147. Jiao, H.-F.; Wang, X.; Yao, K.; Chen, P.; Ji, Z.; Peng, Z.; and Li, F.; *J. Mater. Chem. B*, **2016**, *4*, 7882-7887.
148. Kulkarni, B.; Surnar, B.; Jayakannan, M. *Biomacromolecules* **2016**, *17*, 1004-1016.
149. Yang, Z.; Sokolik, I.; Karasz, F. E. A *Macromolecules* **1993**, *26*, 1188−1190.
150. Cacialli, F.; Feast, W. J.; Friend, R. H.; de Jong, M.; Lovenich, P. W.; Salaneck, W. R. Polymer **2002**, *43*, 3555-3561.
151. Cacialli, F.; Friend, R. H.; Feast, W. J.; Lovenich, P. W. *Chem. Commun.* **2001**, 1778-1779.
152. Goel, M.; Narasimha, K.; Jayakannan, M. *Macromolecules* **2014**, *47*, 2592−2603.
153. Balamurugan A.; Reddy, M. L. P.; Jayakannan, M.. J. *Mater. Chem. A.* **2013**, *1*, 2256-2266.
154. Balamurugan, A.; Kumar, V.; Jayakannan, M. *Chem. Commun.* **2014**, *50*, 842−845.
155. Shinde. S.; Asha. S. K.; *Macromolecules* **2016**, *49*, 8134−8145.
156. Tan, T. A. T.; Clarke, T. M.; James, D.; Durrant, J. R.; White, J. M.; Ghiggino, K. P.; *Polym. Chem.* **2013**, *4*, 5305–5309
157. . Samanta, S. K.; Scherf. U. *Macromol. Chem. Phys.* **2017**, *218*, 1600374.
158. Neuteboom, E. E.; Meskers, S. C. J.; Meijer, E. W.; Janssen, R. A. J. *Macromol. Chem. Phys.* **2004**, *205*, 217-222.
159. Neuteboom, E. E.; Janssen, R. A. J.; Meijer, E. W. *Synth. Met.* **2001**, *121*, 1283-1284.
160. Hong, Y.; Miller, L. L. *Chem. Mater.* **1995**, *7*, 1999-2000.
161. Kunugi, Y.; Miller, L. L.; Maki, T.; Canavesi, A. *Chem. Mater.* **1997**, *9*, 1061-1062.
162. Donat-Bouillud, A.; Mazerolle, L.; Gagnon, P.; Goldenberg, L.; Petty, M. C.; Leclerc, M. *Chem. Mater.* **1997**, *9*, 2815-2821.
163. Henze, O.; Feast, W. J. *J. Mater. Chem.* **2003**, *13*, 1274-1278.
164. Kilbinger, A. F. M.; Feast, W. J. *J. Mater. Chem.* **2000**, *10*, 1777-1784.
165. Henze, O.; Fransen, M.; Jonkheijm, P.; Meijer, E. W.; Feast, W. J.; Schenning, A. P. H. J. J. *Polym. Sci., Part A: Polym. Chem*. **2003**, *41*, 1737-1743.

Chapter 2

π-Conjugated Polymer Anisotropic Organogel Assemblies as Thermoresponsive Photonic Switches

Abstract:

In this chapter one of the first examples of π-conjugated photonic switches (or photonic wave plates) is demonstrated based on the tailor made π-conjugated polymer anisotropic organogel. New semicrystalline segmented π-conjugated polymers are designed with rigid aromatic oligophenylenevinylene π-core and flexible alkyl chain along in polymer backbone. These polymers are found to be self-assembled as semicrystalline or amorphous with respect to the number of carbon atoms present in the alkyl units. These semicrystalline polymers produce organogels having nanofibrous morphology of 20 nm thickness with length up to 5 μm. The polymer organogel is aligned in a narrow glass capillary and this anisotropic gel device is further demonstrated as photonic switches. The glass capillary device behaves as typical λ/4 photonic wave plates upon the illumination of the plane polarized light. The λ/4 photonic switching ability is found to be maximum at $\theta = 45^\circ$ angle under the cross-polarizers. The orthogonal arrangements of the gel capillaries produce dark and bright spots as on-and-off optical switches waves. Thermoreversibility of the polymer organogel (also its xerogel) was exploited to construct thermoresponsive photonic switches for the temperature window starting from 25 to 160 ℃. The organic photonic switch concept can be adapted to large number of other π-conjugated materials for optical communication and storage.

2.1. Introduction:

Photonic switches (or photonic wave plates) are materials that are capable of transforming the wavelength of light or trafficking optical information for doing specific job or storage.[1-3] Commercial photonic wave plates are made up of silica (quartz) or inorganic crystals and they are routinely employed as half-wave plates (λ/2) or quarter-wave plates (λ/4) with respect to their function and applications.[4] Owing to the limitation in the processability of the inorganic materials; there is an emerging trend in the last four years for the development of organic photonic switches. Recently, Bing Xu et al. reported the oligopeptide based enzymatic hydrogel and demonstrated by utilizing aromatic-aromatic interactions and enzyme catalysis, resulted a spontaneously aligned supramolecular nanofibers for producing anisotropic hydrogel that exhibits significant birefringence (see figure 2.1).[5] Polypeptide gels,[6] and alginate gels[7] are some of the examples that are recently reported for the above purpose. Photopolymerizable anionic polyterephthalamide hydrogel was also developed for optical sensor applications[8].

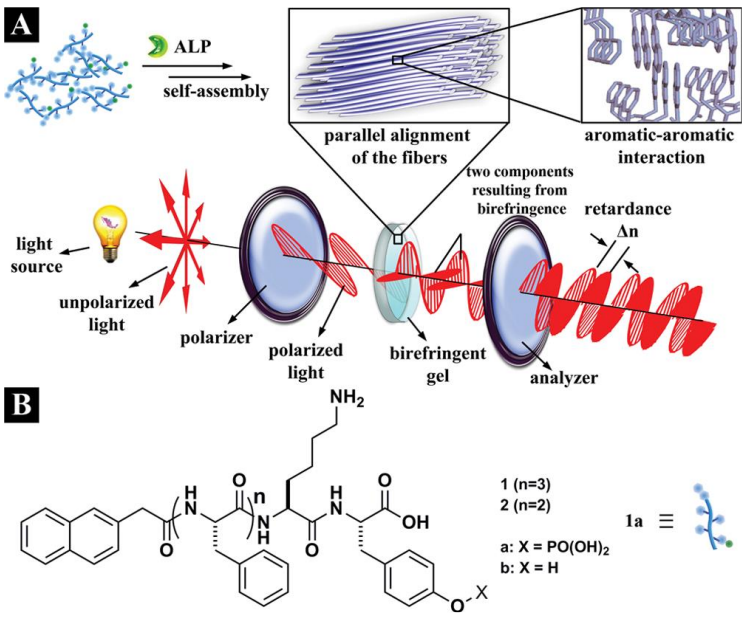

Figure 2.1. *(A) Illustration of aromatic-aromatic interactions, in a hydrogel (Gel1b) formed by treating the solution of a precursor (1a) with an enzyme (ALP), to enhance interfiber interactions that favors alignment of nanofibers and results in an inherently anisotropic hydrogel that causes optical retardance. (B) Structures of two hydrogelators, differing only in the number of phenylalanine residues. (Adopted from* Bing Xu et al *J. Am. Chem. Soc.***2014**, *136,* 2970−2973*).*

Samuel I. Stupp et al.[6] reported the polypeptide based hydrogel and demonstrated the thermal pathway that converts isotropic solutions of peptide-containing molecules to liquid crystals in which molecules in group into long filaments of bundled nanofibers (see figure 2.2). These oligo-peptide materials are nonconducting and nonluminescent; thus, they restrict their exploration for photonic switching in tunable optical wavelength and electro-optic devices.

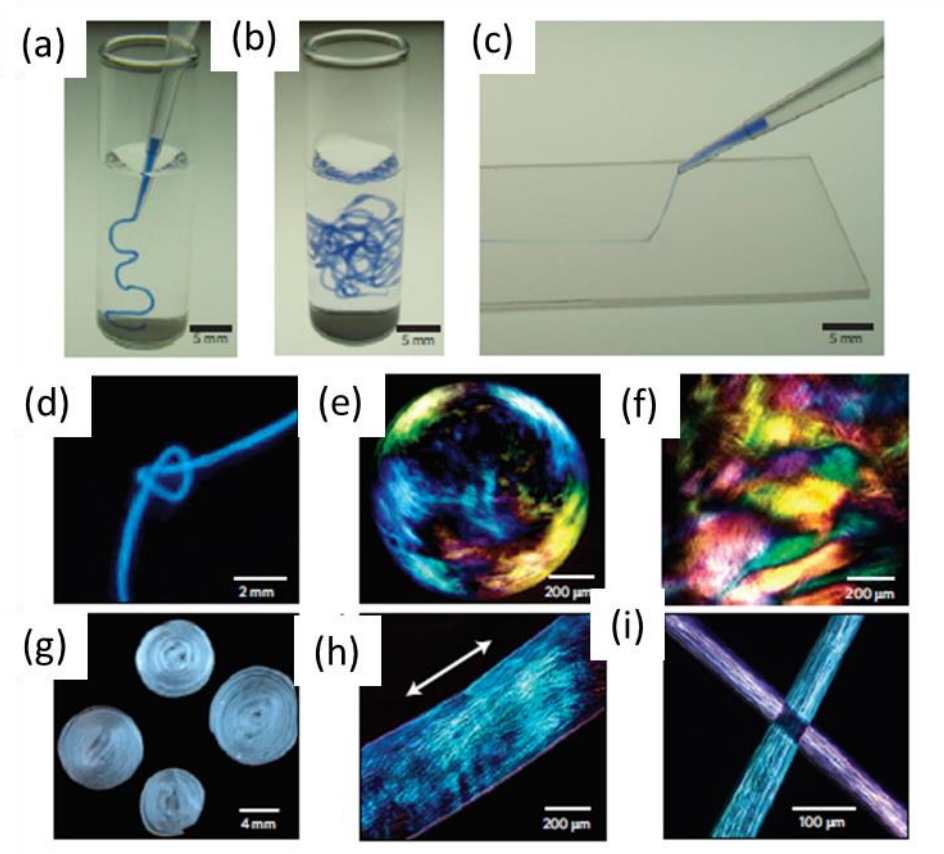

Figure 2.2. *Strings and gels with long-range internal alignment (a), and b. A peptide amphiphile solution coloured with trypan blue injected into phosphate-buffered saline after heat treatment. (c) The same solution dragged through a thin layer of aqueous CaCl2 to form a noodle-like string. (d) A knot made with peptide amphiphile string. (e) Birefringence of a bubble gel observed between cross polars suggesting the presence of macroscopically aligned domains. (f) Similar domains in a gel film.* ***g****, Peptide amphiphile noodle spirals prepared on a spin coater. (h) Birefringence of a single string suggesting alignment along the string axis. (i) Light extinction between cross polars at the crosspoint of two noodles demonstrating uniform alignment in each (Adopted from Nat. Mater.,* **2010***, 9,* 594-601*).*

π-Conjugated polymers are important classes of materials and they have both electronic charge mobility as well as tunable absorbance and luminescence properties in the entire visible light and near-IR region.[9] The π-conjugated polymers (or

oligomers) are currently extensively tested for applications in photovoltaics,[10] light emitting diodes,[11] field effective transistors,[12] etc; however, there is no attempt to use π-conjugated materials as photonic switches (or photonic wave plates). Further, for the photonic switching application; it is necessary to choose semicrystalline π-conjugated polymers that would allow the anisotropic alignment of the polymer chains or fibres which is essential for producing optical retardance[5] with the incident light (see Figure 2.3). Among the various problems, the chain entanglement in the π-conjugated polymers is very difficult process to control; consequently, more than 95 % of the reported π-conjugated polymers were found to be sluggish to crystalize.[13] Partial alignment of the π-conjugated backbone was achieved by the interdigitations of the alkyl side chains substitution that were primarily introduced for the solubility purpose.[14-16] Unfortunately, these microcrystalline domains (or π-conjugated aggregates) were behaved as quenching pockets for diminishing the emission characteristics of π-conjugated core.[17-19] As a result, most often it was rather difficult to find trade-off between the luminescence properties and crystallinity in π-conjugated polymeric materials for photonic applications.[20]

Segmented π-conjugated polymers based on main-chain substituted analogues is an alternative attractive approach to resolve the above problem. This polymer design provides new opportunity for retaining the photophysical characteristics of the π-core and also induces molecular self-assembly along the backbone through chain folding. Karasz and coworkers reported the p-and m-phenyelenevinylene π-conjugated polymers with polymethylene spacers as light emitting materials.[21, 22] Very recently, Pang and coworkers developed new nano-composites based on functionalized 1,3-meta poly(phenyelenevinylene)s with single-walled carbon nanotubes.[23, 24] From our research group, Balamurugan et al. reported carboxylic functionalized segmented π-conjugated polymers and their polymer-Eu^{3+} ions complex as thermosensor as well as chemosensor for metal ions and amino acids.[25, 26] Mahima et al. from our group[27] and Ghiggino and coworkers[28] were reported independently the donor-acceptor assemblies based on segmented p-phenyelenevinylene chromophores with perylenebisimide and C_{60} derivatives, respectively. These segmented polymers were also found to be amorphous, and they were found to be not suitable for photonic switches. Hence, there is an urgent need to

design new semicrystalline segmented π-conjugated polymers for the development of first π-conjugated photonic switches.

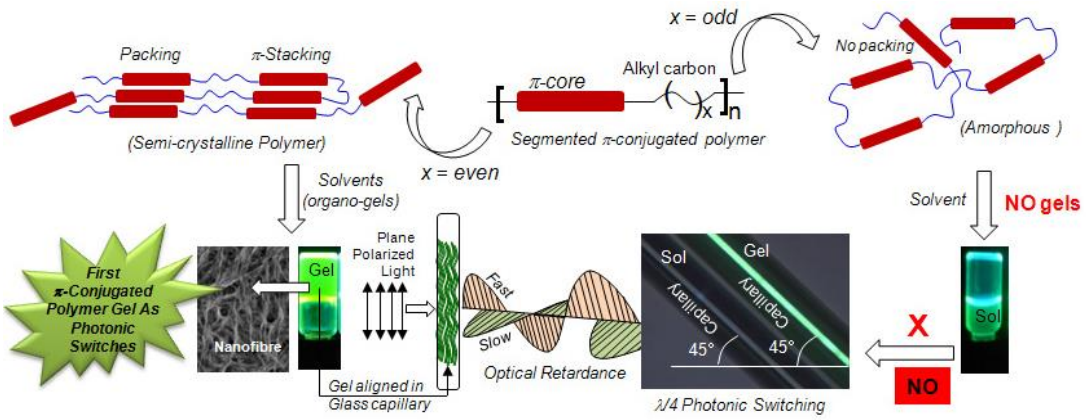

Figure 2.3. *Approaches to develop the first organic photonic switches based on segmented π-conjugated polymer anisotropic organogel.*

The present investigation is emphasized to develop π- photonic switches based on π-conjugated polymer through molecular self-organization approach (see Figure 2.3). This concept was based on two important factors: (i) successful development of semicrystalline π-conjugated polymer and (ii) their ability to produce transparent self-organized anisotropic organogel that can be processed into desired objects for testing their photonic switching capabilities. A new segmented π-conjugated polymer strategy was developed in which rigid oligophenylenevinylene (OPV) chromophores were tied in the polymer backbone by flexible alkyl chain bearing carbon atoms 2 to 12. The polymer structures were adopted in such a way that they were devoid of any functional groups (OH, COOH, amide, etc.) and only capable of undergoing self-organization through aromatic π-stacking (or van der Waals forces).[29] On the basis of our previous experience,[27] the structures of the segmented polymers were carefully designed with 2-ethylhexyl units on the OPV core so that complete polymer solubility was achieved for characterization and organogel formation.[30] The present polymer design is unique in that all even-polymers (having even number of alkyl carbons C_n (n = 2, 4,...,12) self-organized to produce semicrystalline polymers. Further, the semicrystalline even-analogues self-assembled in organic solvents to produce stable polymer organogels having anisotropic nanofibrous network (see Figure 2.3). These new semicrystalline anisotropic polymer organogels were aligned in narrow glass capillaries and they were demonstrated as photonic switches, more specifically as λ/4 photonic wave plates. Further, the thermoreversibility of the organogel (or xerogel)

was also demonstrated as thermo-responsible optical switches for the temperature range of 25 - 160 °C.

2.2. Experimental section

2.2.1. Materials: Hydroquinone, ethylhexyl bromide, triethylphosphite, dibromalkanes, 4-hydroxybenzaldehyde, potassium tert-butoxide (1 M in tetrahydrofuran (THF)), and 1-bromodecane were purchased from Aldrich Chemicals. HBr in glacial acetic acid, paraformaldehyde, K_2CO_3, and KOH were purchased locally. Solvents were purchased locally and were purified by standard procedures.

2.2.2. Instrumentation: ^{1}H and ^{13}C NMR were recorded using 400 MHz JEOL NMR spectrometer. Infrared spectra were recorded using a Thermo-Scientific Nicolet 6700 FT-IR spectrometer in solid state in KBr in the range of 4000 - 600 cm^{-1}. Mass analysis of precursors was determined by the Applied Biosystems 4800 PLUS MALDI TOF/TOF analyzer using TiO_2 as matrix. The molecular weights of polymers were determined using gel permeation chromatography (GPC) which was performed by Viscotek triple detector setup and tetrahydrofuran as solvent. Thermogravimetric analysis (TGA) analysis was done using PerkinElmer STA 6000 simultaneous Thermal Analyzer. Differential scanning calorimetry (DSC) measurements were performed on TA Q20 DSC. The data were recorded at heating and cooling rate of 10 °C/min. The first heating cycle data were discarded since they possessed prehistory of the sample. Powder X-ray diffraction patterns were recorded by Philips Analytical Diffractometer using CuKα emission. The spectra were recorded in the range of 2θ = 3 – 40° and analyzed using X'pert software. Variable-temperature X-ray diffraction studies were performed using a Rigaku Dmax 2500 diffractometer with a copper target. Absorption spectra were recorded using a PerkinElmer Lambda 45 UV spectrophotometer. Steady state emission and excitation spectra were recorded using Fluorolog HORIBA JOBIN VYON fluorescence spectrophotometer. The solid state quantum yield was measured using a Model F-3029, Quanta-Phi 6″ Integrating Sphere connected with a Horiba Jobin Yvon Fluorolog 3 spectrophotometer. Field emission scanning electron microscope (FESEM) images were recorded using Zeiss Ultra Plus scanning electron microscope and the samples were prepared by drop casting on silicon wafers and coated with gold. TEM images were recorded using a Technai-300 instrument by drop casting the sample on Formvar-coated copper grid.

Atomic force microscope (AFM) images were recorded using Veeco Nanoscope IV instrument. The sample was drop-cast on freshly cleaved mica surface. The imaging was carried out in tapping mode using TAP-190AL-G50 probe from Budget sensors with a nominal spring constant of 48 N/m and resonance frequency of 163.5. LIECA DM2500 P polarized light microscope equipped with Linkam TMS 94 heating and freezing stage was used. Rheology measurements were done in Anton Paar Physica MCR 301 instrument. A 25 mm Parallel plate was used and measuring system PP08 (d = 0.5 mm) with Peltier control temperature device was used.

Single Crystal Analysis of OPV-10: For single crystal X-ray analysis, the good quality crystals were grown in a mixture of chloroform and methanol (1:1 v/v). Crystals were subjected to data collection at 100 K on Bruker APEX duo CCD-X- ray diffractometer equipped with graphite monochromated Mo Kα radiation (λ=0.71073 Å). The frames were integrated with Bruker APEX software package. The structures were solved by direct methods and refined with a full matrix least squares techniques using SHELXS v97 programs. One oxygen and eight carbon atoms of the ethylhexyloxy moiety were disordered. Atom positions of the disordered groups were refined isotropically over two positions using the similar distances and similar U-restraints of the shelx. There is a slightly higher Uiso(max)/Uiso(min) values for the constrained H atoms of the ethylhexyloxy motif owing to the disordered atom positions. The R-factor of the crystal analysis is 8.31% which is in range acceptable to larger sized organic crystals.[31-32] The disordered atoms are refined isotropically.

Synthesis of 4,4'-(alkoxy)-bisbenzaldehyde (4c): The synthesis is described in detail for **4c** and all other compounds were made following identical procedure. 4-Hydroxybenzaldehyde (6.2 g, 51.0 mmol), 1,4-dibromobutane (2.7 mL, 23.2 mmol), and anhydrous K_2CO_3 (12.7 g, 92.0 mmol) were taken in dry acetonitrile (60.0 mL). The reaction mixture was refluxed for 48 h under nitrogen atmosphere. It was cooled, and the mixture was diluted with dichloromethane (30.0 mL). The solution was filtered, and the solvent was removed under vacuum. Water (50.0 mL) was added to the residue and the content was extracted with dichloromethane (100.0 mL). The organic layer was dried over anhydrous Na_2SO_4 and the solvent was removed to get product as white solid. The product was further purified by passing through silica gel column using ethyl acetate (18 % v/v) in hexane as eluent. Yield = 4.9 g (72 %). mp = 107-109 °C. ^{1}H NMR ($CDCl_3$, 400 MHz) δ: 9.89 ppm (s, 2H, C**H**O), 7.85 ppm (d,

2H, **Ar-H**), 7.03 ppm (d, 2H, **Ar-H**), 4.29 ppm (t, 4H, O**C**$\mathbf{H_2}$), and 2.36 ppm (m, 2H, C$\mathbf{H_2}$**).** ^{13}C NMR ($CDCl_3$, 100 MHz)δ: 190.4 (**C**HO), 163.4, 131.7, 129.7, 114.4 (Ar-**C**), 64.2 (O**C**H_2), and 28.6 ppm (**C**H_2). FT-IR (KBr, cm^{-1}): 2926, 2852, 1675, 1597, 1570, 1500, 1460, 1425, 1387, 1304, 1241, 1206, 1147, 1106, 1035, 960, 822, 731, and 645. MALDI-TOF-TOF-MS (MW = 298.33): *m*/*z* = 321.0 (M+ Na^+) and *m*/*z* = 337.0 (M + K^+).

Synthesis of 4, 4'-(ethane-1, 2-diylbis(oxy))dibenzaldehyde (4a): 4-Hydroxybenzaldehyde (1.0 g, 12.0 mmol), was reacted with 1,2-dibromoethane (0.45 mL, 5.0 mmol) and anhydrous K_2CO_3 (2.7 g, 20.0 mmol) in dry acetonitrile (30.0 mL) **as described for 4c**. It was further purified by passing through silica gel column using ethyl acetate (20 % v/v) in hexane as eluent. MP = 127-129 °C. Yield= 0.85 g (59%).^{1}H-NMR ($CDCl_3$, 400 MHz) δ: 9.9 ppm (s, 2H, C**H**O), 7.87 ppm (d, 2H, **Ar-H**), 7.07ppm (d, 2H, **Ar-H**), 4.46 ppm (s, 4H, OC$\mathbf{H_2}$) . ^{13}C-NMR ($CDCl_3$, 100 MHz) δ: 190.44 (C**H**O), 163.06, 131.7, 130.06, 114.54 (Ar-**C**), and 66.15 ppm (OC$\mathbf{H_2}$). FT-IR (KBr, cm^{-1}): 2923, 2946, 2752, 1676, 1593, 1498, 1453, 1425, 1391, 1305, 1242, 1206, 1147, 1110, 926, 816, and 649. Molecular formula: $C_{16}H_{14}O_4$, MALDI-TOF-MS (MW=270.28) *m*/*z* = 293.0 (M+ Na^+) and *m*/*z* = 309.0 (M + K^+).

Synthesis of 4, 4'-(propane-1, 3-diylbis(oxy))dibenzaldehyde (4b) : 4-Hydroxybenzaldehyde (5 g, 54mmol) was reacted with 1,3-dibromopropane (2.5mL, 25mmol) , and K_2CO_3 (7.5 g, 54m mol) in dry acetonitrile(60 mL) **as described for 4c**. The product was further purified by passing through silica gel column using ethyl acetate (20 % v/v) in hexane as eluent. Yield = 4.55 mg (64 %). MP = 131-133 ºC. ^{1}H-NMR ($CDCl_3$, 400 MHz) δ: 9.89 ppm (s, 2H, C**H**O), 7.85 ppm (d, 2H, **Ar-H**), 7.03 ppm (d, 2H, **Ar-H**), 4.29 ppm (t, 4H, OC$\mathbf{H_2}$) and 2.36 ppm(m, 2H, OC$\mathbf{H_2}$**).** ^{13}C-NMR ($CDCl_3$, 100 MHz) δ: 190.4 (**C**HO), 163.4, 131.7, 129.7, 114.4 (Ar-**C**), 64.2 (O**C**H_2) and 28.6 ppm (**C**H_2). FT-IR (KBr, cm^{-1}): 2922, 2845, 2752, 1686, 1595, 506, 1462, 1426, 1387, 1305, 1244, 1213, 1153, 1111, 1046, 987, 959, 860, 821, and 649. Molecular formula: $C_{17}H_{16}O_4$, MALDI-TOF-MS (MW = 284.306): *m*/*z* = 307.0 (M+ Na^+) and *m*/*z* = 323.0 (M + K^+).

Synthesis of 4,4'-(pentane-1,5-diylbis(oxy))dibenzaldehyde (4d): 4-Hydroxybenzaldehyde (5.8 g, 48 mmol), was reacted with 1,5-dibromopentane (2.9 ml, 22 mmol), and K_2CO_3 (6.6 g, 48 mmol) in dryacetonitrile (60ml) **as described**

for 4c. The product was further purified by passing through silica gel column using ethyl acetate (15 % v/v) in hexane as eluent. Yield =5.1 g (76 %). MP = 93-95 °C. ^{1}H-NMR ($CDCl_3$, 400 MHz) δ: 9.89 ppm (s, 2H, C**H**O), 7.84 ppm (d, 2H, **Ar-H**), 7.0 ppm (d, 2H, **Ar-H**), 4.1 ppm (t, 4H, OC**H₂**) , 1.94 ppm (m, 4H, C**H₂)** and 1.74 ppm (m, 2H, C**H₂)**. ^{13}C-NMR ($CDCl_3$, 100 MHz) δ: 190.83 (**C**HO), 164.12, 132.0, 129.78, 114.7 (Ar-**C**), 68.15 (O**C**H_2), 28.97 (**C**H_2), and 25.77ppm (**C**H_2). FT-IR (KBr, cm^{-1}): 2932, 2853, 1685, 1601, 1509, 1466, 1427, 1308, 1252, 1154, 1112, 1065, 1029, 984, 935, 835, 799, and 650. Molecular formula: $C_{19}H_{20}O_4$, MALDI-MS (MW = 312.36): *m*/*z* = 335.0 (M+ Na^+) and *m*/*z* = 351.0 (M + K^+).

Synthesis of 5,5'-(hexane-1,6-diylbis(oxy))dibenzaldehyde (4e): 4-Hydroxybenzaldehyde (4.40 g, 38 mmol) was reacted with 1,6-dibromohexane (2.7 mL, 17 mmol) , and K_2CO_3 (8.96 g, 38 mmol) in dryacetonitrile**as described for 4d.** The product was further purified by passing through silica gel column using ethyl acetate (12 % v/v) in hexane as eluent. Yield = 4.3 g (75 %). MP = 113-115°C. ^{1}H-NMR ($CDCl_3$, 400 MHz) δ: 9.89 ppm (s, 2H, C**H**O), 7.84 ppm (d, 2H, **Ar-H**), 7.0 ppm (d, 2H, **Ar-H**), 4.1 ppm (t, 4H, OC**H₂**) , 1.88 ppm (m, 4H, C**H₂)** and 1.58 ppm (m, 4H, C**H₂).** ^{13}C-NMR ($CDCl_3$, 100 MHz) δ: 190.5 (**C**HO), 163.8, 131.7, 129.5, 114.4 (Ar-**C**), 67.8 (O**C**H_2), 28.65 (**C**H_2) and 25.45ppm (**C**H_2). FT-IR (KBr, cm^{-1}): 2935, 2850, 1680, 1590, 1509, 1474, 1395, 1305, 1248, 1150, 1004, 1029, 829, and 725. Molecular formula: $C_{20}H_{22}O_4$, MALDI-TOF-MS (MW = 326.38): *m*/*z* = 349.0 (M+ Na^+) and *m*/*z* = 365.0 (M + K^+).

Synthesis of 4, 4'-(heptane-1,7-diylbis(oxy))dibenzaldehyde (4f): 4-Hydroxybenzaldehyde (0.52 g, 4 mmol) was reacted with 1,7-dibromoheptane (0.33 mL, 2 mmol) , and K_2CO_3 (0.6 g, 8 mmol) in dryacetonitrile**as described for 4c.** The product was further purified by passing through silica gel column using ethyl acetate (12 % v/v) in hexane as eluent. Yield = 0.58 g (88 %). MP = 86-88 °C. ^{1}H-NMR ($CDCl_3$, 400 MHz) δ : 9.89 ppm (s, 2H, C**H**O), 7.8 ppm (d, 2H, **Ar-H**), 7.0 ppm (d, 2H, **Ar-H**), 4.1 ppm (t, 4H, OC**H₂**) , 1.85 ppm (m, 4H, C**H₂)** and 1.51 ppm (m, 4H, C**H₂).** ^{13}C-NMR ($CDCl_3$, 100 MHz) δ: 191.1 (**C**HO), 164.5, 132.3, 130.1, 115.40 (Ar-**C**), 68.6 (O**C**H_2), 29.34 (**C**H_2), 29.3 (**C**H_2), and 26.2 ppm (**C**H_2). FT-IR (KBr, cm^{-1}): 2928, 2857, 1678, 1587, 1495, 1300, 1246, 1207, 1140, 1103, 819, and 723. Molecular formula: $C_{21}H_{24}O_4$, MALDI-TOF-MS (MW = 340.41): *m*/*z* = 363.0 (M+ Na^+) and *m*/*z* = 379.0 (M + K^+).

Synthesis of 4, 4'-(octane-1,8-diylbis(oxy))dibenzaldehyde (4g): 4-Hydroxybenzaldehyde (4.9 g, 40 mmol) was reacted with 1,8-dibromooctane (3.4 mL, 20 mmol) , and K_2CO_3 (5.6 g, 40 mmol) in dryacetonitrile(50mL) **as described for 4c.** The product was further purified by passing through silica gel column using ethyl acetate (12 % v/v) in hexane as eluent. Yield = 5.0 g (76 %). MP = 90-92 °C. ^{1}H-NMR ($CDCl_3$, 400 MHz) δ : 9.9 ppm (s, 2H, C**H**O), 7.8 ppm (d, 2H, **Ar-H**), 7.0 ppm (d, 2H, **Ar-H**), 4.05 ppm (t, 4H, OC**H₂**), 1.8 ppm (m, 4H, C**H₂)**, 1.5 ppm (m, 4H, C**H₂)** and 1.4 ppm (m, 4H, C**H₂**). ^{13}C-NMR ($CDCl_3$, 100 MHz) δ: 190.1 (**C**HO), 164.2, 132.0, 129.7, 114.7 (Ar-**C**), 68.3 (O**C**H_2), 29.2 (**C**H_2), 29.0 (**C**H_2), and 25.9 ppm (**C**H_2). FT-IR (KBr, cm^{-1}): 2930, 2859, 1677, 1591, 1455, 1302, 1253, 1213, 1149, 1013, 826, and 695. Molecular formula: $C_{22}H_{26}O_4$, MALDI-TOF-MS (MW = 354.44): *m*/*z* = 377.1 (M+ Na^+) and *m*/*z* = 393.07 (M + K^+).

Synthesis of 4,4'-(nonane-1,9-diylbis(oxy))dibenzaldehyde (4h): 4-Hydroxybenzaldehyde (0.52 g, 4 mmol) was reacted with 1,9-dibromononane (0.35 mL, 2 mmol) , and K_2CO_3 (0.6 g, 8 mmol) in dry acetonitrile**as described for 4c.** The product was further purified by passing through silica gel column using ethyl acetate (12 % v/v) in hexane as eluent. Yield = 0.48 g (71 %). MP = 103-105°C. ^{1}H-NMR ($CDCl_3$, 400MHz) δ: 9.9 ppm (s, 2H, C**H**O), 7.8 ppm (d, 2H, **Ar-H**), 7.0 ppm (d, 2H, **Ar-H**), 4.05 ppm (t, 4H, OC**H₂**), 1.8 ppm (m, 4H, C**H₂)** 1.5 ppm (m, 4H, C**H₂)** and 1.4 ppm (m, 6H, C**H₂**). ^{13}C-NMR ($CDCl_3$, 100 MHz) δ: 190.8 (**C**HO), 164.2, 131.1, 129.7, 114.7 (Ar-**C**), 68.3 (O**C**H_2), 29.4 (**C**H_2), 29.2 (**C**H_2), 29.0 (**C**H_2), and 25.9 ppm (**C**H_2). FT-IR (KBr, cm^{-1}): 2925, 2847, 1675, 1590, 1499, 1465, 1382, 1310, 1256, 1210, 1148, 1109, 1057, 1008, 965, 823, and 728. Molecular formula: $C_{23}H_{28}O_4$, MALDI-TOF-MS (MW = 368.46): *m*/*z* = 391.087 (M+ Na^+) and *m*/*z* = 407.064 (M + K^+).

Synthesis of 4, 4'-(decane-1, 10-diyl bis(oxy))dibenzaldehyde (4i): 4-Hydroxybenzaldehyde (4.47 g, 36 mmol) was reacted with 1,10-dibromodecane (3.7 mL, 16 mmol) , and K_2CO_3 (5.06 g, 36 mmol) in dryacetonitrile **as described for 4c.** The product was further purified by passing through silica gel column using ethyl acetate (10 % v/v) in hexane as eluent. Yield = 5.4 g (85 %). MP = 91-93°C.^{1}H-NMR ($CDCl_3$, 400 MHz) δ: 9.9 ppm (s, 2H, C**H**O), 7.8 ppm (d, 2H, **Ar-H**), 7.0 ppm (d, 2H, **Ar-H**), 4.0ppm (t, 4H, OC**H₂**), 1.8 ppm (m, 4H, C**H₂)**, 1.5 ppm (m, 4H, C**H₂)** and 1.35 ppm (m, 8H, C**H₂**). ^{13}C-NMR ($CDCl_3$, 100 MHz) δ ppm: 190.8 (**C**HO), 164.2,

132.0, 129.7, 114.7 (Ar-**C**), 68.4 (O**C**H_2), 29.4 (**C**H_2), 29.3 (**C**H_2), 29.0 (**C**H_2), and 25.9 (**C**H_2). FT-IR (KBr, cm^{-1}): 2926, 2851, 1683, 1590, 1500, 1460, 1388, 1306, 1251, 1206, 1145, 999, 831, 791, and 728. Molecular formula: $C_{24}H_{30}O_4$, MALDI-TOF-MS (MW = 382.49): *m*/*z* = 405.12 (M+ Na^+) and *m*/*z* = 421.1 (M + K^+).

Synthesis of 4, 4'-(undecane-1, 11-diyl bis(oxy))dibenzaldehyde (4j): 4-Hydroxybenzaldehyde (0.43 g, 3 mmol) was reacted with 1,11-dibromoundecane (0.37 mL, 2 mmol) , and K_2CO_3 (0.5 g, 3 mmol) in dryacetonitrile (30mL) **as described for 4c.** The product was further purified by passing through silica gel column using ethyl acetate (10 % v/v) in hexane as eluent. Yield = 0.59 g (95 %). MP = 87-89°C. ^{1}H-NMR ($CDCl_3$, 400 MHz) δ: 9.9 ppm (s, 2H, C**H**O), 7.8 ppm (d, 2H, **Ar-H**), 7.0 ppm (d, 2H, **Ar-H**), 4.1 ppm (t, 4H, OC**H₂**), 1.8 ppm (m, 4H, C**H₂**), 1.5 ppm (m, 4H, C**H₂)** and 1.3 ppm (m, 10H, C**H₂**). ^{13}C-NMR ($CDCl_3$, 100 MHz) δ: 190.8 (**C**HO), 164.2, 132.0, 129.7, 114.7 (Ar-**C**), 68.4 (O**C**H_2), 29.49 (**C**H_2), 29.47 (**C**H_2), 29.3 (**C**H_2), 29.0 (**C**H_2), and 26.0 ppm (**C**H_2). FT-IR (KBr, cm^{-1}): 2919, 2846, 1678, 1585, 1461, 1390, 1309, 1252, 1203, 1140, 1102, 1032, 991, 826, 782, and 728. Molecular formula: $C_{25}H_{32}O_4$, MALDI-TOF-MS (MW = 396.52): *m*/*z* = 419.133 (M+ Na^+) and *m*/*z* = 435.1 (M + K^+).

Synthesis of 4,4'-(dodecane-1,12-diyl bis(oxy))dibenzaldehyde (4k): 4-Hydroxybenzaldehyde (4.1 g, 33 mmol) was reacted with 1,12-dibromododecane (4.9g, 15 mmol) , and K_2CO_3 (4.6 g, 0.008 mol) in dryacetonitrile **as described for 4c.** The product was further purified by passing through silica gel column using ethyl acetate (10 % v/v) in hexane as eluent. Yield = 5.0g (81%). MP = 81-83 °C. ^{1}H-NMR ($CDCl_3$, 400 MHz) δ: 9.9 ppm (s, 2H, C**H**O), 7.8 ppm (d, 2H, **Ar-H**), 7.0 ppm (d, 2H, **Ar-H**), 4.0 ppm (t, 4H, OC**H₂**) , 1.8 ppm (m, 4H, C**H₂**) 1.5 ppm (m, 4H, C**H₂**) and 1.3 ppm (m, 12H, C**H₂**). ^{13}C-NMR ($CDCl_3$, 100 MHz) δ: 190.8 (**C**HO), 164.2, 132.0, 129.7, 114.7 (Ar-**C**), 68.4 (O**C**H_2), 29.5 (**C**H_2), 29.3 (**C**H_2), 29.0 (**C**H_2), and 26.0 ppm (**C**H_2). FT-IR (KBr, cm^{-1}): 2919, 2848, 1683, 1592, 1505, 1465, 1428, 1390, 1310, 1258, 1210, 1150, 1107, 998, 832, 788, and 728. Molecular formula: $C_{26}H_{34}O_4$, MALDI-TOF-MS (MW = 410.54): *m*/*z* = 433.163 (M+ Na^+) and *m*/*z* = 449.137 (M + K^+).

Synthesis of 4-(decyloxy)benzaldehyde (5): 4-Hydroxybenzaldehyde (3.6g, 30 mmol), 1-bromodecane (6.8 mL, 30 mmol) and K_2CO_3 (8.3 g, 60mmol) have taken in

a two neck round bottom flask dry acetonitrile (40 mL) added into it under inert atmosphere. Reflux the reaction mixture 24 hrs under inert atmosphere. The reaction mixture cool to room temperature, dichloromethane (30 mL) added into it and filtered the solution concentrated under vaccum. Water (50mL) added into the residue extracted with dichloromethane (50 ml). Again aqueous layer washed with dichloromethane (50ml) the organic layer was dried over anhydrous sodiumsulphate and the solvent was evaporated to get product as colorless liquid. It was further purified by passing through silica gel column using ethyl acetate (5 % v/v) in hexane as eluent. Yield = 84 %. ^{1}H-NMR ($CDCl_3$, 400 MHz) δ: 9.9 ppm (s, 1H, C**H**O), 7.83ppm (d, 2H, **Ar-H**), 7.0 ppm (d, 2H, **Ar-H**), 4.05 ppm (t, 2H, OC**H$_2$**) , 1.82 ppm (m, 2H, C**H$_2$)** 1.47 ppm (m, 2H, C**H$_2$),** 1.38-1.28 ppm (m, 12H, C**H$_2$)** and 0.9 ppm (t, 3H, C**H$_3$**). ^{13}C-NMR ($CDCl_3$, 100 MHz) δ: 190.84 (**C**HO), 164.3, 132.0, 129.7, 114.73 (Ar-**C**), 68.42 (O**C**H_2), 31.87 (**C**H_2), 29.53 (**C**H_2), 29.32 (**C**H_2), 29.3 (**C**H_2), 29.04(**C**H_2), 25.94 (**C**H_2), 22.66 (**C**H_2), and 14.10 ppm (**C**H3). FT-IR (KBr, cm^{-1}): 2924, 2854, 2731, 1694, 1601, 1577, 1509, 1467, 1428, 1393, 1311, 1258, 1215, 1159, 1109, 1016, 832, 721, and 651. HRMS (ESI): Calculated (M+H) 263.2011, measured 263.2013.

Synthesis of 4,4'-((1E,1'E)-(2,5-bis((2-ethylhexyl)oxy)-1,4-phenylene)bis(ethene-2,1-diyl))bis((decyloxy)benzene) (OPV-10): Compound **3** (0.3 g, 0.47 mmol) and 4--decyloxybenzaldehyde (0.31 g, 1.2 mmol) were taken in dry THF (15 mL),purged nitrogen in 30 min. and kept under ice cold condition. Potassium *tert*-butoxide (6.0 mL, 1M THF solution) was added dropwise to the reaction mixture under a nitrogen atmosphere and the stirring was continued at 30°C for 12 hrs. The resultant yellow green solution was concentrated and poured into a large amount of methanol. The yellow green precipitate was filtered and washed with a large amount of methanol. The product was further purified by passing through silica gel column using ethyl acetate (5 % v/v) in hexane as eluent. Yield = 0.33g (82 %). ^{1}H NMR ($CDCl_3$, 400 MHz), δ: 7.46 ppm (d, 4H, **Ar-H**), 7.36 ppm (d, 2H, C**H=**C**H,** J = 16), 7.11 ppm (s, 2H, **Ar-H**), 7.09 ppm (d, 2H, C**H=**C**H,** J = 16), 6.90 ppm (d, 4H, Ar-**H**),4.0 ppm (t, 4H, OC**H$_2$**), 3.95 ppm (d, 4H, OC**H$_2$**), 1.81 (m, 6H,2C**H,** 2C**H$_2$**), 1.64-1.28 ppm (m, 44H, C**H$_2$**), 1.0 ppm (t, 6H, C**H$_3$**), and 0.95-0.88 ppm (m, 12H, C**H$_3$**) .^{13}C-NMR ($CDCl_3$,100 MHz) δ: 158.7, 151.0, 130.67, 128.03, 127.57, 126.70, 121.27, 114.67, 110.04, 71.75, 68.06, 39.77, 31.90, 30.93,29.58, 29.56, 29.41, 26.28, 26.05,24.22,

23.11, 22.68, 14.13 and 11.33 ppm. FT-IR (KBr, cm^{-1}): 3787, 2919, 2853, 2350, 1600, 1503, 1461, 1418, 1384, 1292, 1239, 1177, 1020, 959, 842, 812, 723, and 664. MALDI-TOF-MS (MW = 851.35): *m*/*z* = 851.6 (M^+).

Synthesis of 1, 4-bis (2-ethyl-hexyloxy) benzene (1): Hydroquinone (10.0 g, 91 mmol) and KOH (20.4 g, 364mmol) were taken in 80 mL of DMSO at room temperature. 2-Ethylhexylbromide (32.5mL, 182mmol) was added drop wise to this reaction mixture. This reaction mixture was then stirred at 80 ^{O}C for 48 h, extracted in dichloromethane, and washed with 5% NaOH solution. The organic layer was dried over anhydrous sodium sulphate and condensed to get product. It was further purified by passing through silica gel column using ethyl acetate (1 % v/v) in hexane as eluent. Yield =75 % (33.0 g). ^{1}H-NMR ($CDCl_3$, 400 MHz) δ: 6.8 ppm (s, 4H, **Ar-H**), 3.8 ppm (m, 4H, OC**H**$_2$), 1.7 ppm (m, 2H, OCH_2C**H**), 1.56 -1.3 ppm (m, 16H, **aliphatic-H**) and 0.95-0.9 ppm (m, 12H, C**H**$_3$). ^{13}C-NMR ($CDCl_3$, 100 MHz) δ: 153.4, 115.3 (Ar-**C**), 71.15 (OC**H**$_2$), 39.45, 30.52, 29.1, 23.8, 23.06, 14.1, and 11.1 ppm. FT-IR (KBr, cm^{-1}): 2957, 2924, 2864, 1506, 1464, 1382, 1285, 1221, 1109, 1037, 928, 822, and 779. Molecular formula: $C_{22}H_{38}O_2$, MALDI-TOF-MS (MW = 334.54): *m*/*z* = 334.25 (M^+).

Synthesis of 1, 4-bis(bromomethyl)-2,5-bis(2-ethylhexyloxy)benzene (2): Compound **1** (10 g, 30 mmol) and paraformaldehyde (3.5 g, 120 mmol) were taken in 100 ml of glacial acetic acid and HBr in glacial acetic acid (33 ml, 66 mmol) was added using a pressure equalizing funnel. The reaction mixture was then refluxed for 8 h, cooled to room temperature and poured into large amount of water. The product precipitated as white solid, which was repeatedly washed with cold water to remove acidic impurities. The product was filtered and recrystallized from a hot isopropyl alcohol. Yield = 60 % (9.3 g). ^{1}H-NMR ($CDCl_3$, 400 MHz) δ: 6.86 ppm (s, 2H, **Ar-H**), 4.5 ppm (s, 4H, **C**H_2Br), 3.89-3.88 ppm (d, 4H, O**C**H_2), 1.76 ppm (m, 2H, OCH_2**CH**), 1.6-1.34 ppm (m, 16H, **aliphatic**), and 0.98-0.92 ppm (t, 12H, **C**H_3). ^{13}C-NMR ($CDCl_3$, 100 MHz) δ: 150.7, 127.35, 114.2 (Ar-**C**), 70.9 (Ar-O-**C**H_2), 39.6, 30.6, 29.1, 28.76, 24.0, 23.05, 14.1, and 11.24 ppm. FT-IR (KBr, cm^{-1}): 2957, 2923, 2865, 1505, 1462, 1444, 1313, 1220, 1115, 1086, 1033, 902, 871, 770, 731 and 686.

Synthesis of tetraethyl (2, 5-bis (2-ethylhexyloxy)-1, 4-phenylene)bis(methylene)diphosphonate (3) : Compound **2** (8 g, 15.4 mmol) and

triethylphosphite (6.4g, 38.5 mmol) were kept for 12h at 120 ^{O}C under inert atmosphere. Excess triethylphosphite was removed by applying high vacuum and the product was finally obtained as a colourless liquid. The product was further purified by passing through silica gel column using ethyl acetate (50 % v/v) in hexane as eluent. Yield: 93 % (9.0 g). ^{1}H-NMR ($CDCl_3$, 400 MHz) δ: 6.9 ppm (s, 2H, **Ar-H**), 4.0 ppm (m, 8H, PO**CH$_2$**CH_3) ; 3.8 ppm (t, 4H, O**CH$_2$**), 3.25-3.20 ppm (d, 4H, C**H$_2$**P), 1.71 ppm (m, 2H, OCH_2**CH**), 1.55-1.3 ppm (m, 16H, **aliphatic CH$_2$**), 1.23 ppm (t, 12H, $POCH_2$**CH_3**) and 0.94-0.9 ppm (m, 12H, **aliphatic** C**H$_3$**). ^{13}C-NMR ($CDCl_3$, 100 MHz) δ: 150.4, 119.3, 114.65, 71.2 (OC**H$_2$**), 61.8 (PO**C**H_2CH_3), 39.65, 30.6, 29.1, 26.8, 25.4, 23.9, 23.04, 16.34, 14.1 and 11.14 pm. FT-IR (KBr, cm^{-1}): 3472, 2957, 2925, 2868, 1647, 1510, 1465, 1393, 1248, 1211, 1163, 1097, 1025, 957, 890, 824, 783, 727, and 650. Molecular formula: $C_{32}H_{60}O_8P_2$, MALDI-TOF-MS (MW = 634.76): *m*/*z* = 657.47 (M^+ + 23)

General procedure for Synthesis of Polymers (P-n)s: All Polymers were synthesized using the general method as described for **P-4**. Monomer (3) (0.508 g, 0.8 mmol) and 4,4'-(butane-1,4-diylbis(oxy))dibenzaldehyde (0.238 g, 0.8 mmol, for polymer P-4) were taken in dry THF (30 mL) and kept under ice condition. Potassium *tert*-butoxide (6.0 mL, 1 M THF solution) was added dropwise to the reaction mixture under a nitrogen atmosphere and the stirring was continued at 30 °C for 24 h. The resultant yellow-green solution was concentrated and poured into a large amount of methanol. The yellow- green precipitate was filtered and washed with a large amount of methanol. The polymer was dissolved in THF and solvent was filtered and concentrated to 10 mL. The polymer solution was precipitated into methanol to obtain fibrous polymer as product. Yield= 0.312 g. ^{1}H NMR ($CDCl_3$, 400 MHz) δ: 7.47 ppm (d, 4H, **Ar-H**), 7.37 ppm (d, 2H, J = 16 Hz, C**H**=C**H**), 7.11 ppm (s, 2H, **Ar-H**), 7.09 ppm (d, 2H, J = 16 Hz, **CH=CH**), 6.91 ppm (d, 4H, **Ar-H**), 4.08 ppm (t, 4H, OC**H$_2$**), 3.95 ppm (d, 4H, OC**H$_2$**), 2.02 ppm (m, 4H, OCH_2-C**H$_2$**- C**H$_2$**), 1.82 ppm (m, 2H, OCH_2-C**H**-CH_2), 1.64-1.38 ppm (m, 18H, **aliphatic-H**),1.0 ppm (t, 6H, C**H$_3$**), and 0.93 ppm (t, 6H, C**H$_3$**). ^{13}C-NMR ($CDCl_3$, 100 MHz) δ: 158.51, 151.0, 130.84, 128.0, 127.61, 126.67, 121.37, 114.65, 110.03, 71.72, 67.50, 39.75, 30.92, 29.25, 26.02, 24.21, 23.11, 14.13, and 11.32 ppm. FT-IR (KBr, cm^{-1}): 3778, 3692, 2922, 2859, 2337, 1600, 1458, 1372, 1338, 1294, 1240, 1173, 1031, 957, 839, 802, 722, and 675.

Synthesis of P-2: Compound **3 (**0.504 g, 0.79 mmol) was reacted with 4,4'-(ethane-1,2-diylbis(oxy))dibenzaldehyde (0.215 g, 0.79 mmol) **as described for P-4.** Yield = 0.10 g. ^{1}H NMR ($CDCl_3$, 400 MHz), δ: 7.5 ppm (d, 4H, **Ar-H**), 7.4 ppm (d, 2H, J = 16 Hz, C**H**=C**H**), 7.1 ppm (s, 2H, **Ar-H**), 7.0 ppm (d, 2H, J = 20 Hz, C**H**=C**H**), 6.88 ppm (d, 4H, **Ar-H**), 4.4 ppm (s, 4H, OC**H**$_2$), 3.96-3.95 ppm (d, 4H, OC**H**$_2$), 1.8 ppm (m, 2H, OCH_2-C**H**$_2$$CH_2$), 1.56 ppm (m, 8H, **aliphatic-H**),1.38 ppm (m, 8H, **aliphatic-H**) 1.0 ppm (t, 6H, **CH**$_3$) and 0.93 ppm (t, 6H, **CH**$_3$). ^{13}C-NMR ($CDCl_3$, 100 MHz) δ: 158.13, 151.02, 131.33, 127.93, 127.64, 126.7, 121.67, 114.89, 110.09, 71.77, 66.58, 39.77, 30.94, 29.26, 24.23, 23.11, 14.13 and 11.33 ppm. FT-IR (KBr, cm^{-1}): 3775, 3693, 2925, 2848, 1598, 1453, 1379, 1298, 1233, 1176, 1120, 1025, 955, 838, 871, 721, and 659.

Synthesis of P-3: Compound **3 (**0.51 g, 0.8 mmol) was reacted with 4, 4'-(propane-1,3-diylbis(oxy))dibenzaldehyde (0.23 g, 0.8 mmol) **as described for P-4.** Yield = 0.10 g. ^{1}H NMR ($CDCl_3$, 400 MHz), δ: 7.47 ppm (d, 4H, **Ar-H**), 7.36 ppm (δ, 2H, J = 20 Hz, **CH=CH**), 7.11 ppm (s, 2H, **Ar-H**), 7.09 ppm (d, 2H, J = 16 Hz, **CH=CH**), 6.93 ppm (d, 4H, **Ar-H**), 4.21 ppm (t, 4H, OC**H**$_2$), 3.95 ppm (d, 4H, OC**H**$_2$), 2.31 ppm (m, 2H, OCH_2-C**H**$_2$- OCH_2), 1.82 ppm (m, 2H, OCH_2-**CH**$_2$-CH_2), 1.64-1.38 ppm (m, 16H, **aliphatic-H**), 1.01ppm (t, 6H, **CH**$_3$), and 0.93 ppm (t, 6H, **CH**$_3$). ^{13}C-NMR ($CDCl_3$, 100 MHz) δ: 158.37, 151.0, 130.97, 128.1, 127.96, 126.61, 126.68, 121.45, 114.68, 110.04, 71.73, 64.50, 39.76, 30.92, 29.32, 29.25, 24.22, 23.11, 14.13, and 11.33 ppm. FT-IR (KBr, cm^{-1}): 3784, 3685, 2922, 2862, 2338, 1599, 1561, 1461, 1414, 1380, 1297, 1237, 1112, 1114, 1031, 958, 807, 720, and 672.

Synthesis P-5: Compound **3** (0.508 g, 0.8mmol) was reacted with 4,4'-(pentane-1,5-diylbis(oxy))dibenzaldehyde(0.25 g, 0.8 mmol) **as described for P-4.** Yield = 0.213 g. ^{1}H NMR ($CDCl_3$, 400 MHz), δ: 7.46 ppm (d, 4H, **Ar-H**), 7.36 ppm (d, 2H, J = 16 Hz, **CH=CH**), 7.11 ppm (s, 2H, **Ar-H**), 7.09 ppm (d, 2H, J = 16 Hz, **CH=CH**), 6.91 ppm (d, 4H, **Ar-H**), 4.03 ppm (t, 4H, OC**H**$_2$), 3.95 ppm (d, 4H, OC**H**$_2$), 1.93-1.79 ppm (m, 6H, OCH_2-C**H**$_2$- C**H**$_2$), 1.69 ppm (m, 2H, OCH_2-C**H**-CH_2), 1.62-1.29 ppm (m, 18H, **aliphatic-H**), 1.0 ppm (t, 6H, C**H**$_3$**),** and 0.93 ppm (t, 6H, C**H**$_3$). ^{13}C-NMR ($CDCl_3$, 100 MHz) δ: 158.57, 151.0, 130.76, 128.0, 127.60, 126.67, 121.32, 114.64, 110.01, 71.71, 67.78, 39.75, 30.91, 29.25, 26.06, 24.21, 23.11, 14.13, and 11.32 ppm. FT-IR (KBr, cm^{-1}): 2922, 2862, 1602, 1506, 1465, 1417, 1239, 1171, 1024, 960, 844, 810, 729, and 667.

Synthesis of P-6: Compound **3 (**0.501 g, 0.79 mmol) was reacted with 5, 5'-(hexane-1,6-diylbis(oxy)) dibenzaldehyde (0.26 g, 0.79 mmol) **as described for P-4.** Yield = 0.39 g. ^{1}H NMR ($CDCl_3$, 400 MHz), δ: 7.46 ppm (d, 4H, **Ar-H**), 7.36 ppm (d, 2H, J = 16 Hz, **CH=CH**), 7.11 ppm (s, 2H, **Ar-H**), 7.09 ppm (d, 2H, J = 16 Hz, **CH=CH**), 6.91 ppm (d, 4H, **Ar-H**), 4.01 ppm (t, 4H, O**CH$_2$**), 3.95-3.94 ppm (d, 4H, O**CH$_2$**), 1.84 ppm (m, 6H, OCH_2-**CH$_2$- CH$_2$**), 1.64-1.36 ppm (m, 20H, **aliphatic-H**),1.0 ppm (t, 6H, **CH$_3$),** and 0.93 ppm (t, 6H, **CH$_3$**). ^{13}C-NMR ($CDCl_3$, 100 MHz) δ: 158.62, 151.98, 130.74, 128.01, 127.60, 126.69, 121.32, 114.66, 110.04, 71.74, 67.88, 39.76, 30.92, 29.26, 25.92, 24.22, 23.11, 14.13, and 11.32 ppm. FT-IR (KBr, cm^{-1}): 3885, 3774, 3721, 3566, 3419, 3335, 3221, 3166, 2903, 2857, 2311, 1647, 1602, 1506, 1464, 1396, 1240, 1168, 1016, 968, 918, 841, 801, 725, and 667.

Synthesis of P-7: Compound **3 (**0.52 g, 0.82 mmol) was reacted with 4,4'-(heptane-1,7-diylbis(oxy))dibenzaldehyde (0.28 g, 0.82 mmol) **as described for P-4.** Yield = 0.17 g. ^{1}H NMR ($CDCl_3$, 400 MHz), δ: 7.46 ppm (d, 4H, **Ar-H**), 7.36 ppm (d, 2H, J = 16 Hz, C**H**=C**H**), 7.10 ppm (s, 2H, **Ar-H**), 7.08 ppm (d, 2H, J = 12 Hz ,**CH=CH**), 6.90 ppm (d, 4H, **Ar-H**), 4.0 ppm (t, 4H, OC**H$_2$**), 3.95-3.94 ppm (d, 4H, O**CH$_2$**), 1.82 ppm (m, 6H, OCH_2-C**H$_2$**-C**H$_2$**), 1.64-1.36 ppm (m, 22H, **aliphatic-H**),1.0 ppm (t, 6H, C**H$_3$),** and 0.93 ppm (t, 6H, C**H$_3$**). ^{13}C-NMR ($CDCl_3$, 100 MHz) δ: 158.65, 151.0, 130.72, 128.02, 127.58, 126.7, 121.31, 114.66, 110.05, 71.76, 67.96, 39.77, 30.93, 29.26, 29.19, 26.02, 24.22, 23.11, 14.13, and 11.32 ppm. FT-IR (KBr, cm^{-1}): 3923, 3715, 3570, 3424, 2913, 2861, 2308, 1603, 1506, 1466, 1420, 1293, 1241, 1175, 1110, 1023, 960, 917, 807, 765, and 729.

Synthesis of P-8: Compound **3 (**0.502 g, 0.79 mmol) was reacted with 4, 4'-(octane-1,8-4-diylbis(oxy))dibenzaldehyde (0.28 g, 0.79 mmol) **as described for P-4.** Yield = 0.312 g. ^{1}H NMR (CDCl3, 400 MHz), δ: 7.46 ppm (d, 4H, **Ar-H**), 7.36 ppm (d, 2H, J = 16 Hz, C**H**=C**H**), 7.10 ppm (s, 2H, **Ar-H**), 7.10-7.07 ppm (d, 2H, J = 16 Hz, C**H**=C**H**), 6.90 ppm (d, 4H, **Ar-H**), 4.0 ppm (t, 4H, OC**H$_2$**), 3.95-3.94 ppm (d, 4H, OC**H$_2$**), 1.82 ppm (m, 6H, OCH_2-C**H$_2$**-C**H$_2$**), 1.64-1.36 ppm (m, 24H, **aliphatic-H**),1.0ppm(t, 6H, C**H$_3$),** and 0.93 ppm (t, 6H, C**H$_3$**). ^{13}C-NMR ($CDCl_3$, 100 MHz) δ: 158.66, 151.0, 130.70, 128.02, 127.58, 126.7, 121.3, 114.66, 110.05, 71.75, 68.0, 39.77, 30.93, 29.34, 29.26, 29.02, 24.22, 23.11, 14.13, and 11.32 ppm. FT-IR (KBr, cm^{-1}): 3889, 3776, 3719, 3572, 3473, 3427, 2907, 2852, 2311, 1603, 1507, 1239, 1193, 959, 908, 803, 763, 723, and 729.

Synthesis of P-9: Compound **3** (0.51 g, 0.8 mmol) was reacted with 4,4'-(nonane-1,9-diylbis(oxy))dibenzaldehyde (0.28 g, 0.8 mmol) **as described for P-4.** Yield = 0.06 g. ^{1}H NMR ($CDCl_3$, 400 MHz), δ: 7.46 ppm (d, 4H, **Ar-H**), 7.36 ppm (d, 2H, J = 16 Hz, C**H**=C**H**), 7.10 ppm (s, 2H, **Ar-H**), 7.10-7.07 ppm (d, 2H, J = 16 Hz, C**H**=C**H**), 6.90 ppm (d, 4H, **Ar-H**), 4.0 ppm (t, 4H, OC**H**$_2$), 3.95-3.94 ppm (d, 4H, OC**H**$_2$), 1.81 ppm (m, 6H, OCH$_2$-C**H**$_2$-C**H**$_2$), 1.64-1.36 ppm (m, 26H, **aliphatic-H**), 1.0 ppm (t, 6H, C**H**$_3$**),** and 0.92 ppm (t, 6H, C**H**$_3$). ^{13}C-NMR ($CDCl_3$, 100 MHz) δ: 158.66, 151.0, 130.67, 128.0, 127.57, 126.68, 121.26, 114.65, 110.01, 71.72, 68.02, 39.75, 30.91, 29.50, 29.35, 29.28, 29.25, 26.07, 24.21, 23.11, 14.13, and 11.32 ppm. FT-IR (KBr, cm^{-1}): 3889, 3773, 3716, 3666, 3568, 3421, 2916, 2858, 2311, 1602, 1505, 1466, 1421, 1293, 1240, 1174, 1023, 960, 807, 719, and 672.

Synthesis of P-10: Compound **3** (0.53 g, 0.83mmol) was reacted with 4,4'-(decane-1,10-diylbis(oxy))dibenzaldehyde (0.317 g, 20.83mmol) **as described for P-4.** Yield = 0.35 g. ^{1}H NMR ($CDCl_3$, 400 MHz), δ: 7.46 ppm (d, 4H, **Ar-H**), 7.36 ppm (d, 2H, J = 16 Hz, C**H**=C**H**), 7.10 ppm (s, 2H, **Ar-H**), 7.09 ppm (d, 2H, J = 16 Hz, C**H**=C**H**), 6.90 ppm (d, 4H, **Ar-H**), 4.0 ppm (t, 4H, OC**H**$_2$), 3.95 - 3.94 ppm (d, 4H, OC**H**$_2$), 1.80 ppm (m, 6H, OCH$_2$-C**H**$_2$- C**H**$_2$), 1.64-1.36 ppm (m, 28H, **aliphatic-H**), 1.0 ppm (t, 6H, C**H**$_3$), and 0.93 ppm (t, 6H, C**H**$_3$). ^{13}C-NMR ($CDCl_3$, 100 MHz) δ: 158.68, 151.0, 130.68, 128.02, 127.57, 126.70, 121.28, 114.66, 110.04, 71.74, 68.04, 39.77, 30.93, 29.52, 29.41, 29.29, 29.26, 26.06, 24.22, 23.11, 14.13, and 11.33 ppm. FT-IR (KBr, cm^{-1}): 3859, 3721, 3664, 3520, 3471, 3420, 3353, 2960, 2902, 2850, 2383, 2310, 1606, 1240, 1180, 957, 886, 804, 762, 726, and 682.

Synthesis of P-11: Compound **3 (**0.503 g, 0.79 mmol) was reacted with 4, 4'-(undecane-1, 11-diylbis(oxy))dibenzaldehyde (0.314 g, 0.79 mmol) **as described for P-4.** Yield = 0.19 g. ^{1}H NMR ($CDCl_3$, 400 MHz), δ: 7.45 ppm (d, 4H, **Ar-H**), 7.35 ppm (d, 2H, J = 16 Hz, C**H**=C**H**), 7.10 ppm (s, 2H, **Ar-H**), 7.08 ppm (d, 2H, J = 16 Hz, C**H**=C**H**), 6.90 ppm (d, 4H, **Ar-H**), 4.0 ppm (t, 4H, OC**H**$_2$), 3.95-3.94 ppm (d, 4H, OC**H**$_2$), 1.80 ppm (m, 6H, OCH$_2$-C**H**$_2$- C**H**$_2$), 1.64-1.27 ppm (m, 30H, **aliphatic-H**), 1.0 ppm (t, 6H, C**H**$_3$**),** and 0.93 ppm (t, 6H, C**H**$_3$). ^{13}C-NMR ($CDCl_3$, 100 MHz) δ: 158.67, 151.0, 130.66, 128.01, 127.57, 126.68, 121.26, 114.65, 110.01, 71.72, 68.04, 39.76, 30.92, 29.57, 29.42, 29.29, 29.25, 26.06, 24.21, 23.11, 14.13, and 11.32 ppm. FT-IR (KBr, cm^{-1}): 3720, 3567, 3468, 3419, 2912, 2857, 2308, 1604, 1505, 1449, 1241, 1179, 1111, 1033, 964, 809, and 726.

Synthesis of P-12: Compound **3** (0.524 g, 0.83 mmol) was reacted with 4,4'-(dodecane-1,12-diylbis(oxy))dibenzaldehyde (0.34 g, 0.83 mmol) **as described for P-2.** Yield = 0.51 g. ^{1}H NMR ($CDCl_3$, 400 MHz), δ: 7.46 ppm (d, 4H, **Ar-H**), 7.36 ppm (d, 2H, J = 16 Hz ,C**H**=C**H**), 7.10 ppm (s, 2H, **Ar-H**), 7.09 ppm (d, 2H, J = 16 Hz ,C**H**=C**H**), 6.90 ppm (d, 4H, **Ar-H**), 4.0 ppm (t, 4H, OC**H**$_2$), 3.95-3.94 ppm (d, 4H, OC**H**$_2$), 1.80 ppm (m, 6H, OCH_2-C**H**$_2$-C**H**$_2$), 1.64-1.27 ppm (m, 32H, **aliphatic-H**), 1.0 ppm(t, 6H, C**H**$_3$**),** and 0.92 ppm (t, 6H, C**H**$_3$). ^{13}C-NMR ($CDCl_3$, 100 MHz) δ: 158.69, 151.0, 130.68, 128.03, 127.57, 126.71, 121.28, 114.67, 110.05, 71.76, 68.06, 39.77, 30.93, 29.58, 29.42, 29.26, 26.06, 24.22, 23.11, 14.12, and 11.32 ppm. FT-IR (KBr, cm^{-1}): 3895, 3723, 3570, 2913, 2858, 2310, 1604, 1509, 1469, 1241, 1178, 1105, 1038, 970, 803, and 734.

2.3. Results and Discussion

2.3.1. Synthesis and Structural Characterization

A homologous series of segmented polymers having rigid oligophenylenevinylene (OPV) aromatic core with different flexible units (C_n, n= 2,3..,.12) along the longitudinal polymer backbone was synthesized as shown in Scheme-2.1. Hydroquinone was reacted with ethylhexylbromide in the presence of base to give 1,4-bis((2-ethylhexyl)oxy)benzene which was further reacted with paraformaldehyde and HBr in acetic acid to give corresponding bis-bromomethylated derivative. It was further converted to its corresponding 1, 4-bis[(alkyloxy)]-2,5-xylenediphosphonate (**3**). Bis-benzaldehydes were synthesized by reacting 4-hydroxybenzaldehyde with appropriate ω-dibromoalkanes in the presence of potassium carbonate as base in dry acetonitrile.

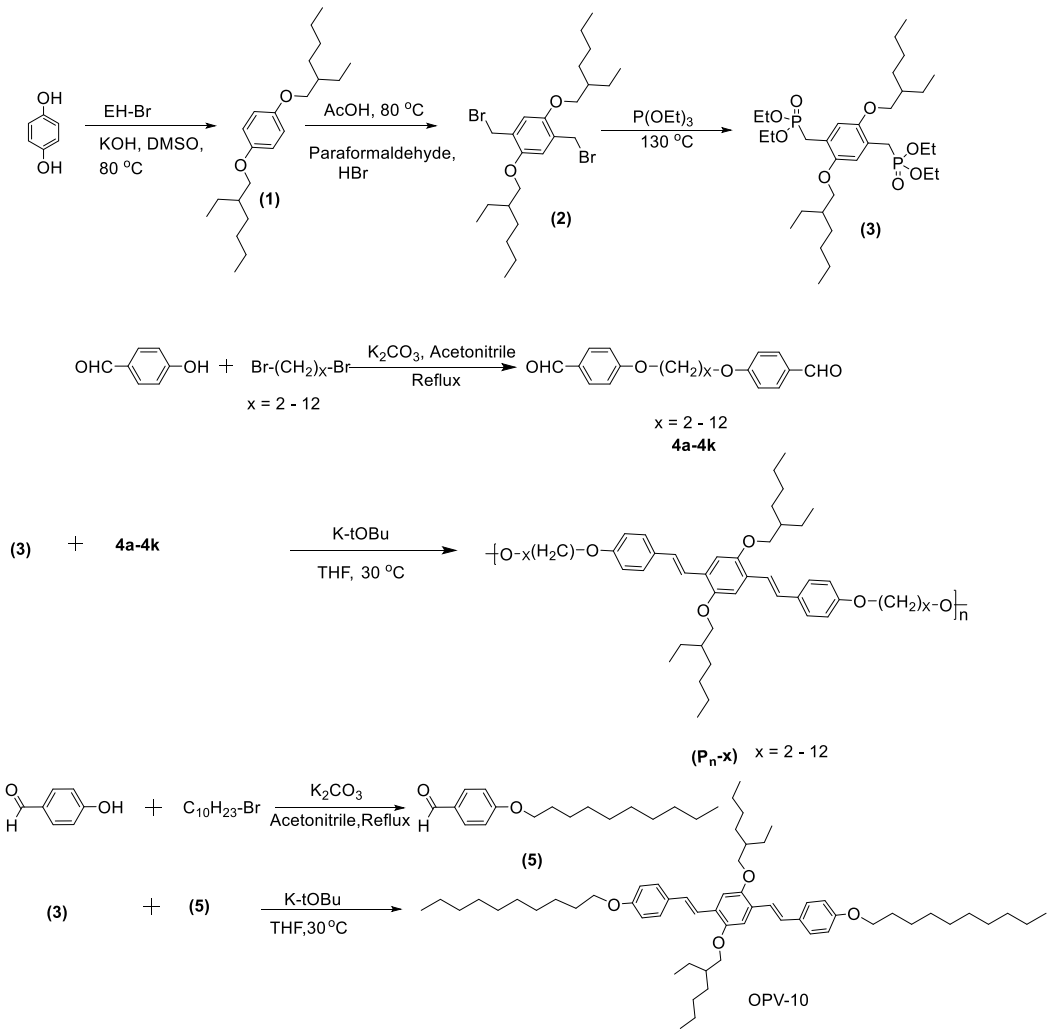

Scheme 2.1. *Synthesis of Segmented OPV Polymers P-n and OPV-10.*

The polymerization of monomer **1** with equimolar amounts of bis-benzaldehydes under Wittig-Horner conditions produced segmented polymers, **P-n**, where n is the number of carbon atoms present in the flexible alkyl chains. The structures of the polymers were confirmed by ^{1}H NMR, ^{13}C NMR and FT-IR. The ^{1}H-NMR spectra of the polymers showed peaks at 7.46 and 6.90 ppm with appropriate splitting pattern corresponding to aromatic phenylene protons (see Figure 2.4). The two doublets belonging to *trans*-vinylene protons appeared at 7.36 and 7.09 ppm and the protons in the middle aromatic ring appeared as a singlet at 7.11 ppm. The broad triplets at 4.0 ppm and the doublet in the range of 3.96-3.94 ppm were attributed to Ar-OC**H**$_2$-alkyl and Ar-OC**H**$_2$-EH protons, respectively. The peaks for all other protons appeared below 1.90 ppm. Similarly, ^{13}C-NMR spectra of the polymers exhibited aromatic and aliphatic carbons (see Figure 2.4).

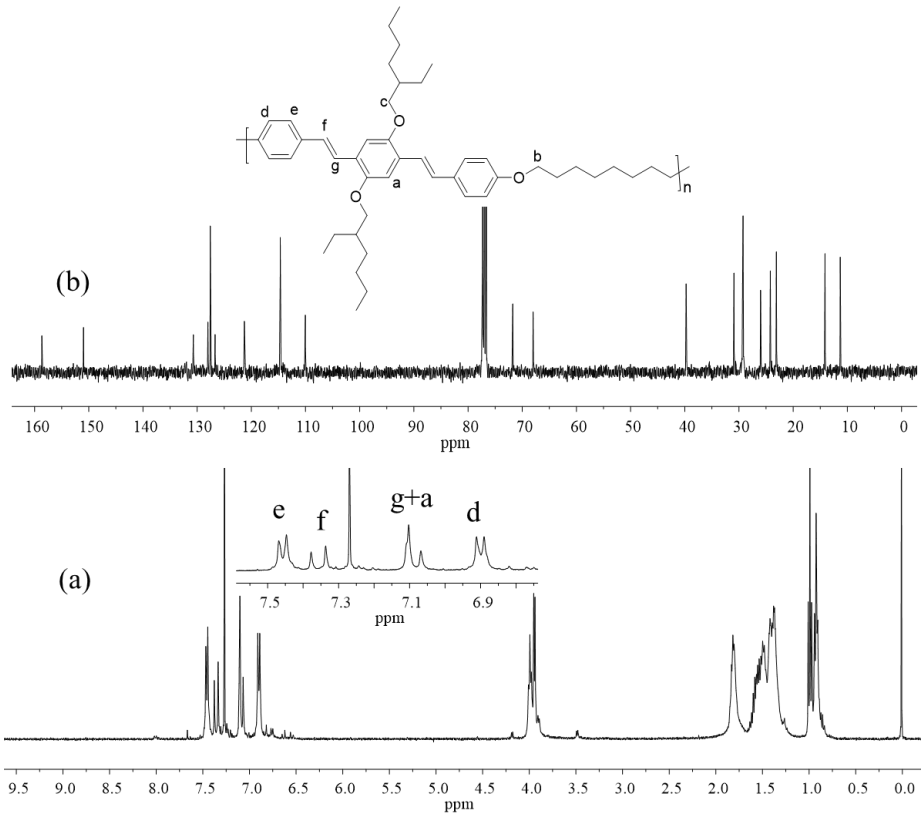

Figure 2.4. *^{1}H-NMR (a) and ^{13}C-NMR (b) spectra of polymerP-8 in $CDCl_3$.*

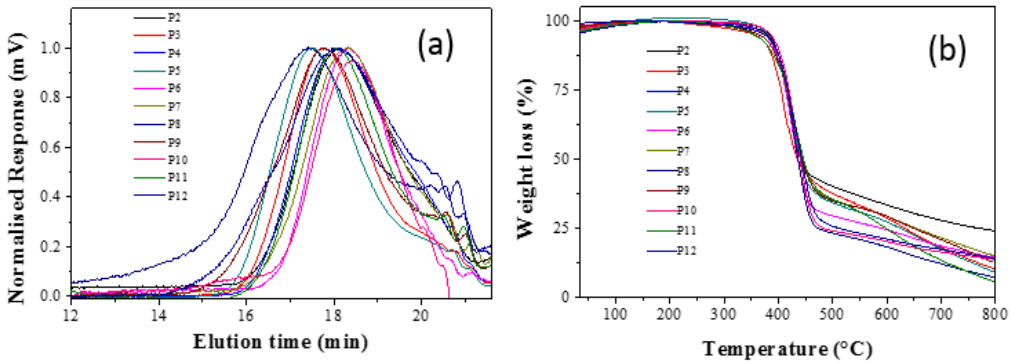

Figure 2.5. ***(a)*** *GPC chromatograms of the segmented polymers P-2 to P-12 in THF. (b) TGA of the polymers under nitrogen at 10 °/min hetaing.*

Table 2.1. Molecular weights of the segmneted polymers

Sample	M_p	M_n	M_w	M_w/M_n	n[a]
P-2	38,700	14,000	44,200	3.1	23
P-3	51,000	14,000	50,500	3.6	23
P-4	38,000	11,500	38,900	3.3	18
P-5	65,000	15,200	62,500	4.1	23
P-6	30,300	14,900	32,600	2.2	23
P-7	30,800	9,900	35,000	3.5	15
P-8	54,000	12,700	52,800	4.1	19
P-9	50,100	12,500	62,100	4.9	18
P-10	21,200	9,200	20,900	2.3	13
P-11	40,000	11,000	39,800	3.6	15
P-12	40,200	18,500	30,400	1.6	25

(a) n = number of repeating units detmined from M_n/repetaing unit mass.

The molecular weights of the polymers were determined by gel permeation chromatography (GPC), and the details are given in Figure 2.6. All the GPC chromatograms appeared as a single peak confirming their monomodel distribution. The molecular weights of the polymers were obtained as M_w = 21000 to 62000 g/mol with polydispersities from 1.6 to 4.0 (see Table -2.1). The number average degrees of polymerization (n) of the polymers were calculated by dividing their M_n/repeating unit mass (see Table-2.1). These segmented polymers were found to have n = 13 to 25 repeating units indicating that the molecular weights of the polymers obtained were moderate to high. TGA of the polymer confirmed that all the polymers were thermally stable up to 350 °C (see Figure 2.5b).

2.3.2. Odd-Even Effect in Polymer Crystallization

Segmented polymers were analyzed by DSC to trace their thermal properties and solid state packing. DSC thermograms of the polymers at 10 ^{o}C/min heating are shown in Figure 2.6a and 2.6b (see Figure 2.6c and 2.6d for their cooling cycles). The segmented polymers with even number of carbon atoms in the alkyl chains (P-n, n= 2, 4, 6, 8, 10 and 12) were found to be semicrystalline and they showed glass transition (T_g) and melting transitions in the heating cycle (see Figure 2.6a). In the subsequent cooling cycles, they showed melt crystallization transitions as well as T_g (see Figure 2.6).

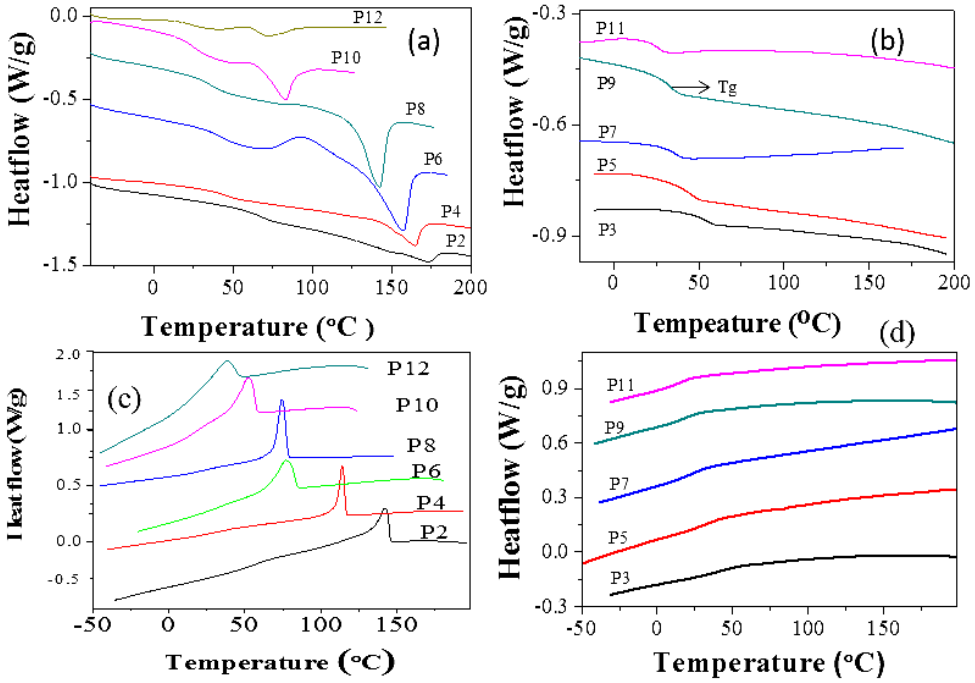

Figure 2.6. *DSC thermograms of the even (a), and odd (b) segmented polymers in the heating cycle at 10 °/min. DSC thermograms of even (c), and odd polymers in the cooling cycles at 10 °/min.*

In Figure 2.6a, both the melting transitions and the T_g's of the polymers decreased with increase in the spacer length. Surprisingly, the segmented polymers with odd number of carbon atoms in the flexible unit (P-n, n= 3, 5, 7, 9 and 11) were found to be amorphous and showed only T_g (see Figure 2.6b).

Table 2.2. DSC thermal data of all polymers the heating and cooling rate is 10/min.

POLYMER	P2	P3	P4	P5	P6	P7	P8	P9	P10	P11	P12
T_g (K)	340	327	318	318	315	308	309	304	297	299	296

Polymer	ΔH_m (kJ/mol)	ΔHc (kJ/mol)	Tm (K)	Tc (K)	$T_g(m)$ (K)	ΔS_m kJ/mol/K	ΔS_c kJ/mol/K
P-2	1.42	2.53	446.2	416.1	340.2	0.0032	0.0061
P-4	3.8	3.65	437.6	388.7	318.5	0.0087	0.0094
P-6	5.74	4.1	430.3	351.3	315.6	0.013	0.0116
P-8	8.4	7.42	415.3	349	309.5	0.020	0.0213
P-10	4.5	3.84	355.9	325.9	297.3	0.0126	0.0118
P-12	3.9	2.5	346.5	316.0	296.2	0.0113	0.008

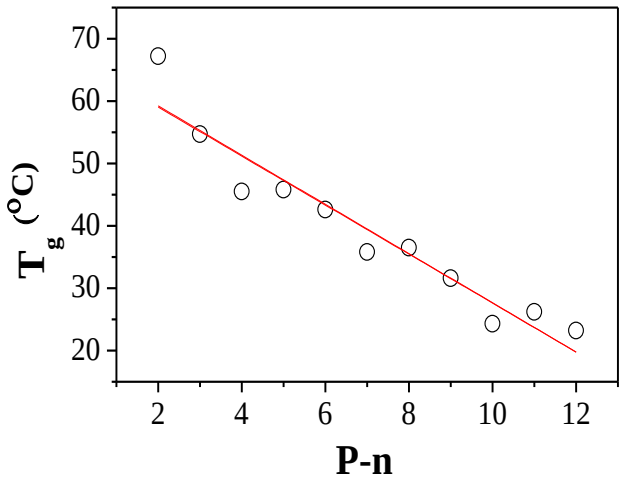

Figure 2.7. *Plot of T_g versus the number of carbon atoms in the P-n.*

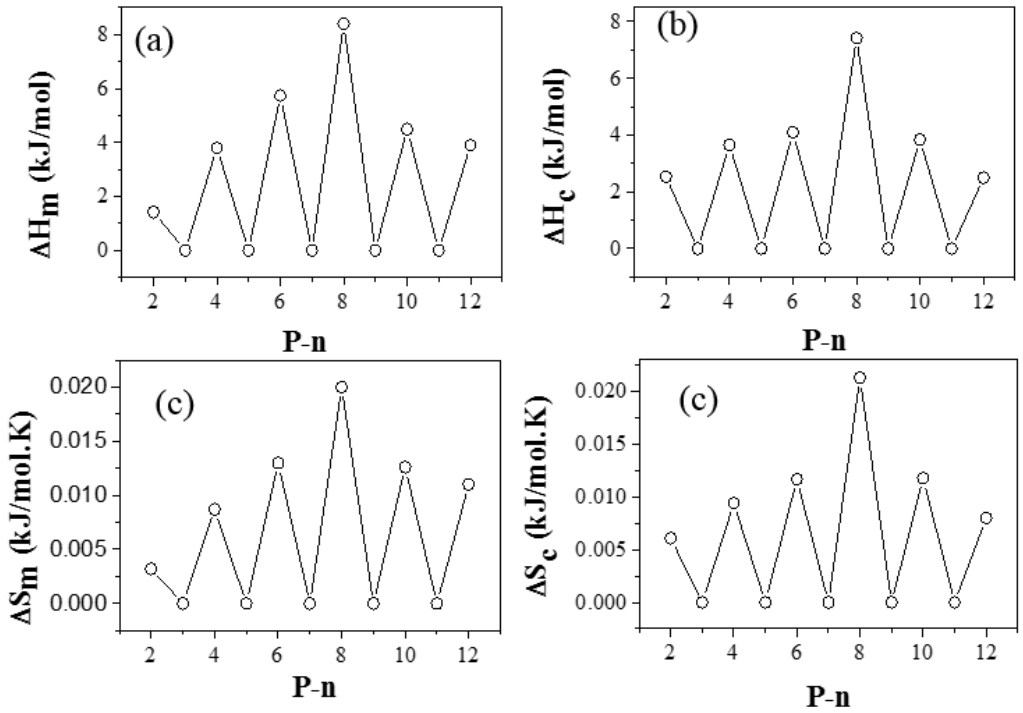

Figure 2.8. *Plots of enthalpy of melting versus (a), crystallization (b), entropy of melting (c) and crystallization (d) versus the number of carbon atoms in the alkyl chain unit in P-n. (for odd-segmented polymer, the values are taken as zero due to their amorphous nature).*

The plot of T_g versus number of carbon atom in the alkyl chains revealed that the polymers almost followed a linear trend for the decrease in T_g with increase in the spacer length irrespective of their semicrystalline or amorphous natures (see Figure 2.7). The polymer with longer flexible spacer showed low T_g compared to that of the shorter chains. The decrease in T_g was observed as 3.3°/carbon atom in the backbone (see Figure 2.7). The semicrystalline and amorphous natures of the segmented polymers were driven by the odd or even number of carbon atoms irrespective of the lengths of spacers (shorter or longer). Enthalpies of the melting transition (ΔH_m) and crystallization (ΔH_c) for the even polymers were determined from DSC thermograms (see Table -2). The plot of ΔH_m versus the number of carbon atom is shown in Figure 2.8a. The ΔH_m increases with the spacer length and attained maxima at P-8. This trend indicated that the alkyl chains facilitated the OPV π-core packing at an optimum alkyl spacer length (from P-2 to P-8 polymer). Further increase in the spacer length decreased the chain packing (from P-8 to P-12). A similar trend was observed in the plot of ΔH_c versus the carbon atoms (see Figure 2.8b). The entropies of the phase transitions were calculated using the following equation:[33] $\Delta S = \Delta H/T$, where, ΔH is the enthalpy of the transition at the temperature T (in Kelvin scale, see table-2 for

data). The plot of ΔS versus number of carbon atom (see Figure 2.8) showed similar trend as seen in Figure 2.8. All the segmented polymers have identical OPV core; thus the semicrystalline or amorphous nature of the polymers was believed to be driven by the packing of the alkyl chains in the backbone. The polymers with shorter alkyl chains predominantly have large contents of aromatic core; thus aromatic π-interaction is expected to dictate the solid state self-assembly.

2.3.3. Segmented Polymer Lamellar Packing

Solid state packing of the segmented polymers was further investigated by powder wide angle X-ray diffraction. WXRD patterns of even-polymers P-2 to P-12 are shown in Figure 2.9a (see Figure 2.9c for odd-polymers P-3 to P-11). The even-spacer semicrystalline polymer P-6 showed sharp crystalline peaks at 2 θ = 8.6, 17.93 and 23.2 with respect to order crystalline domains (see table-4). The odd-polymers P-3 to P-11 did not show any diffraction pattern (see Figure 2.11) which as an indicative of to their amorphous nature as observed in their DSC analysis (see Figure 2.6). The d-spacing of the crystalline peaks in even polymers (for P-4) were determined as 11.05 Å with respect to 1st layer of diffractions. Further, these samples did not show any other peaks in the small angle X-diffraction pattern; thus, the first peak at 2θ = 8.0 (d-spacing 11.05 Å) was assigned to first order crystalline peak. Variable temperature WXRD analysis was done for the P-8 to check their thermoreversible packing in the heating and cooling cycles. The variable WXRD patterns of P-8 (see Figure 2.9b) showed the disappearance of the crystalline peaks at the molten state at 150° C. In the subsequent cooling, the peaks reappeared and this trend confirmed their thermoreversible crystallization nature. Thus, the even-spacer segmented analogues are very good semicrystalline π-conjugated polymers. To gain more insight into the packing of crystalline lattices in the WXRD peaks of the segmented polymer, structurally identical OPV oligomer OPV-10 was synthesized. Among the various OPV-n attempted for this purpose; OPV-10 with decyl chain substitution in the longitudinal positions produced good quality crystals in chloroform/methanol. OPV-10 single crystal was resolved and its structure is shown in Figure 2.10. All three aromatic rings occupied in the same plane. The molecules were packed in triclinic system and their unit cell parameters are given in the table-3 and Figure-10.

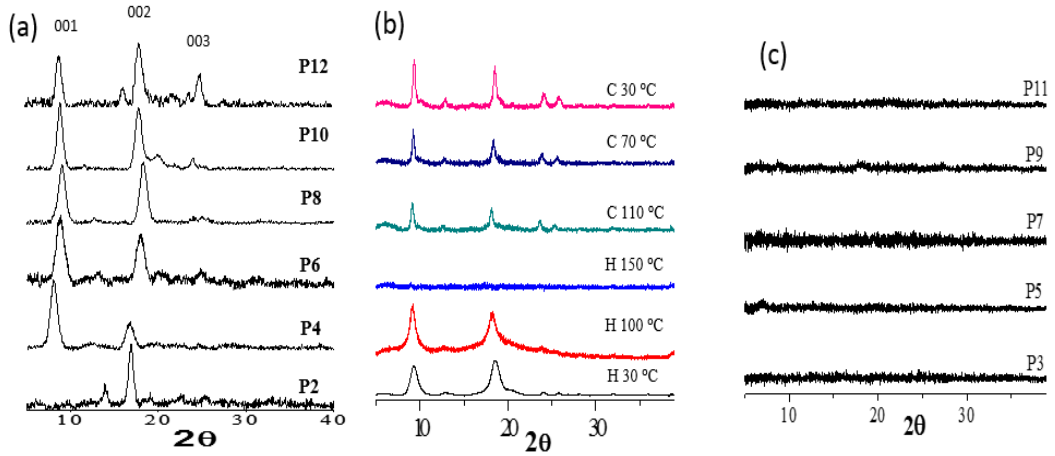

Figure 2.9. *(a) Wide angle X-ray diffraction pattern for even-polymers P-2 to P-12. (b) Variable temperature WRXD patterns for P-8 in heating and cooling cycles. (c) Wide Angle X-ray Diffraction (WAXD) of odd-polymers.* ***Note:*** *there is no peak in WAXD patten conforming their amorphous nature.*

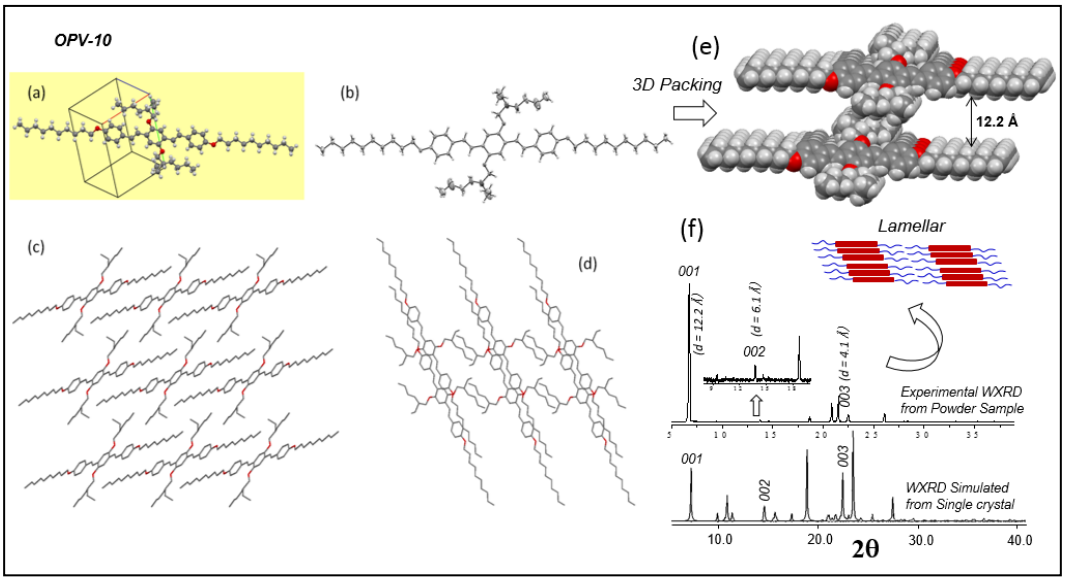

Figure 2.10. *Unit cell (a) and ORPET diagram (b) of OPV-10. Three dimensional packing of the molecules along the a-xis (c) and b-axis (d). 3D packing Single crystal structure of oligomer OPV-10. (d) Simulated WXRD pattern for OPV-10 (bottom) and its experimental WXRD plot (top) with assigned miller indices.*

Table 2.3. Single crystal data for OPV-10.

Compound	OPV-10
formula	$C_{58}H_{90}O_4$
Solvent	Chloroform/MeOH
Molwt	851.35
Color, habit	Yellow green, needle
temp(K)	100
system	triclinic
space group	P-1
a, (Å)	8.8300
b, (Å)	12.7274
c, (Å)	12.7974
α, (deg)	81.000
β, (deg)	72.859
γ, (deg)	72.567
V, $Å^3$	1307.53
d_{cacl},g cm^{-1}	1.121
μ(mm^{-1})	0.07
GOF	0.984
Z	1
no. of unique reflections	8972
Reflections collected	27196
θ range	1.34 to 24.04
No. of refined parameters	651
R_1 (on F, I>2σ (I))	0.1317
wR_2 (on F^2, all data)	0.4437

Each OPV-10 molecule was separated apart in the b-axes and c-axes equally by 12.7 Å (see Figure 2.10). Based on our earlier approach,[31-32] powder WXRD for the OPV-10 was computationally simulated from its single crystal structure and the Miller indices were assigned in the WXRD pattern (see Figure 2.10 bottom). Powder WXRD pattern for the OPV-10 was recorded experimentally and it is shown in Figure 2.10 (top). The Miller indices for peak in the simulated XRD plot (based on single crystal) matched very well with that of the OPV-10 experimental powder WXRD patterns.[31] The 001 first fundamental peak in the OPV-10 with d = 12.2 Å closely matched with the first diffraction pattern at 2θ = 8.0° (d = 11.05 Å) in the

semicrystalline polymer P-4 (see Figure 2.10). The 1.1 Å difference between the 001 planes for OPV-10 and P-4 polymer was attributed to the structural difference between the polymer repeating units and OPV-10. Unlike, the small OPV molecules, the polymer chains have to undergo chain folding to produce crystalline lattices; thus, the 1.1 Å could account for the polymer crystallization phenomena. This concept was further validated by plotting the d-spacing values for 001 peak in the even-segmented polymers (see Figure 2.13 and table-4). The d-spacing decreased from 11.05 to 9.2 Å with increase in the number of carbon atoms from 2 to 12. Thus, the increase in the spacer length was found to slightly decrease the interlayer distance in the lamella. The other two peaks in Figure 9a at 2θ ~18° (d = 4.9 Å) and 2θ ~ 24° (d = 3.57 Å) were assigned to 002 and 003 planes (see table-4).

Table 2.4. WXRD data of the polymers

Sample	2θ (°)	d-spacing (Å)
P-2	7.9, 16.86	11.1, 5.25
P-4	8.0, 16.69	11.05, 5.3
P-6	8.6, 17.93, 23.2	10.17, 4.94, 3.7
P-8	9.0, 18.3, 23.6	9.83, 4.84, 3.7
P-10	8.76, 17.74, 23.9	10.1, 5.0, 3.7
P-12	8.83, 18.0, 24.9	10, 4.9, 3.57

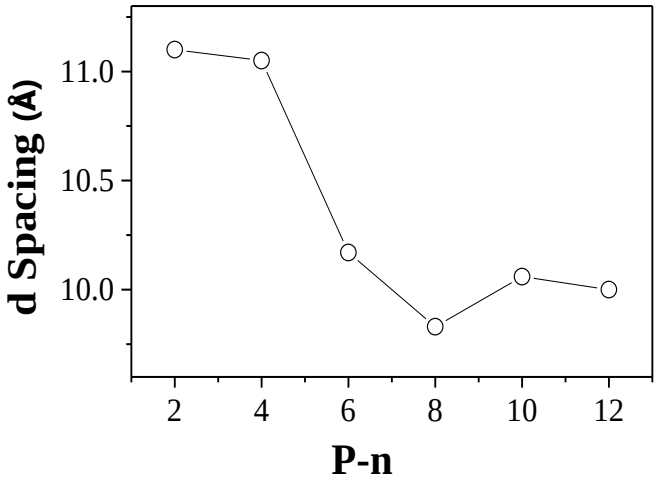

Figure 2.11. *Wide Angle X-ray Diffraction d-spacing of polymers plotted against P-n. For P-2, the 001 plane was calculated based on the secondary peak 002 at 2θ =16.86°*

To visualize the morphology of the lamellar packed semicrystalline polymers, these polymers were further subjected to polarizing light microscope (PLM) and FESEM. In the PLM experiment, the polymers were melted and control cooled at 10 °/min using programmed hot stage. PLM images of the polymer P-8 captured during their crystallization process are shown in Figure 2.12. The PLM images showed the existence of layered crystalline packing with respect to lamellar-structure. These lamellar structures were reproducible in the repetitive heating and cooling cycles (see more PLM images in Figure 2.14). On the other hand, the odd-polymers did not show any crystalline domains rather than they appeared as glassy solid with respect to their amorphous nature (see Figure 2.14).

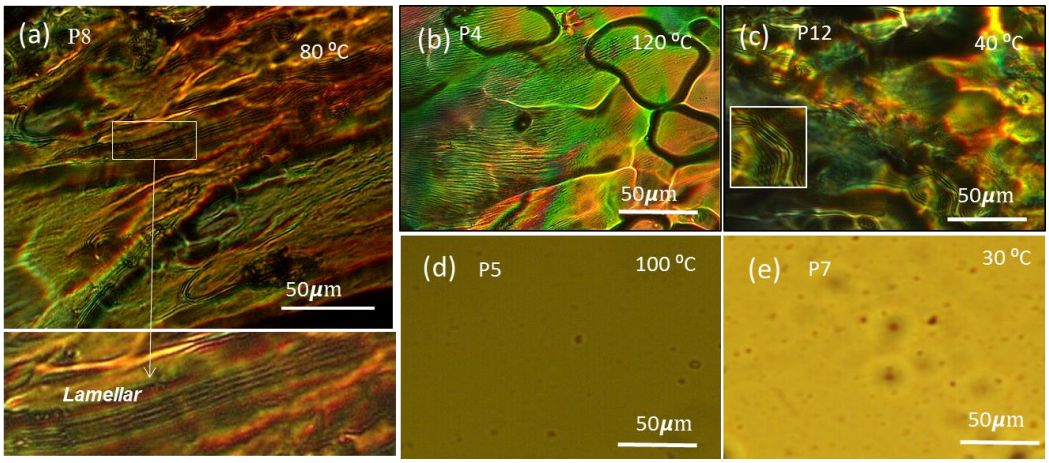

Figure 2.12. *PLM pictures of even polymers P-8, P-4 and P-12 odd polymers P-5 and P-7. PLM image of the polymers captured on glass substrate at crystallization temperature at 10 °/min cooling rate. The expanded PLM images showed the lamellar crystalline domains.*

For FESEM imaging (see Figure 2.13), the samples were prepared under the identical PLM conditions on the silicon wafer surface at 10 °/min cooling from the molten state. The FESEM image of P-8 showed the bundles of submicrometer thick fibers of layered arrangements (see Figure 2.13, for FE-SEM images of P-4, P-5 and P-12). These thick-fibres were entangled with each other as typically observed in thermoplastics. In FE-SEM of the odd polymer P-5 did not show any fiber which conformed the amorphous nature. On the basis of the above techniques such as DSC, WXRD, variable temperature WXRD, single crystal structure, PLM and FE-SEM images; it can be concluded that even-spacer OPV polymers were self-organized as lamellar crystalline solids.

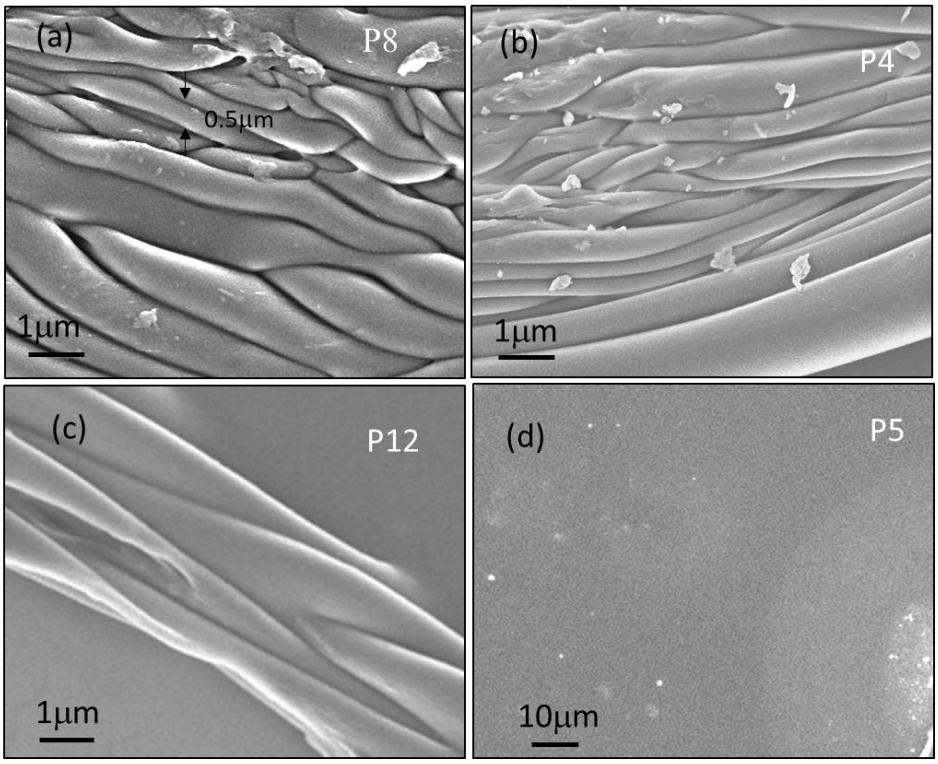

Figure 2.13. *FE-SEM images of P-8, P-4, P-12, P-12 and P-5. FESEM image of polymers sample on the silicon wafer substrate after crystallization at 10 °/min cooling.*

2.3.4. Photophysical Characterization

The photophysical properties of the polymers were studied in solution (toluene) as well as in solid state (in film). In toluene, at dilute concentration, all the polymers showed almost identical absorbance and emission maxima (see Figure 2.14. The solution quantum yields of the polymers were determined in the range of 0.3-0.4 using quinine sulfate as standard (ϕ = 0.54 in 0.1 N H_2SO_4,[29] also see table-5). The absorbance and emission spectra of the polymer thin films are shown in Figure 2.15a and 2.15b. The absorbance maxima of the polymers were plotted against the number of the carbon atoms in the alkyl spacer and shown in Figure 2.5. The overall absorbance of the segmented polymers did not change drastically and they absorb light in the same range of 400-420 nm. Among them, the even-spacer polymers showed slightly higher absorbance maxima (red-shifted) compared to their neighbouring odd-counterparts (typically ± 5 to 8 nm). The comparison of the enthalpies of the melting (see Figure 2.8) and the absorbance maxima shift (see Figure 2.15) revealed that the highly packed polymer chain showed red-shift with

respect to strong π-interactions among the OPV chromophores. The plot of the emission maxima versus the number of carbon atoms (see Figure 2.15) showed no-clear trend for the odd and even spacers. Therefore, absolute solid state photoluminescence quantum yield (PLQY) was determined using integrating sphere setup to study the role of the lamellar packing on the OPV chromophore emission.

Table 2.5. Photophysical properteis of polymers in solution and solid state.

SAMPLE	In TOLUENE			In film		PLQY[b] (%)
	λabs(nm)	*λem (nm)*	ϕ[a]	*Λabs (nm)*	*Λem (nm)*	
P-2	398	446, 474	0.31	405	500	19
P-3	397	446, 477	0.31	401	500	25
P-4	397	445, 477	0.32	410	503	21
P-5	395	446, 481	0.40	405	505	27
P-6	400	446, 476	0.33	418	499	20
P-7	395	445, 475	0.33	409	500	20
P-8	394	446, 473	0.35	416	496	15
P-9	396	446, 474	0.36	400	496	19.1
P-10	396	446, 473	0.36	419	499	15.5
P-11	397	446, 474	0.36	400	497	20
P-12	397	445, 474	0.36	405	498	19

a) *Quantum yield (Toluene) of all polymes are determined using quinine sulphate as standarad (ϕ = 0.54 in 0.1 N H_2SO_4,[29]) b) solid state photoluminescence quantum yields are deterined using integrated sphere setup following the report Palsson et al. (Ref. 34).*

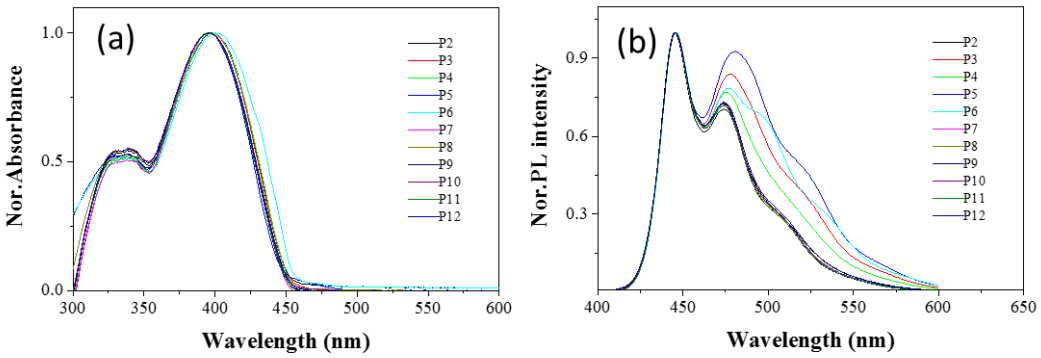

Figure 2.14. *Absorbance and emission of polymer samples in Toluene.*

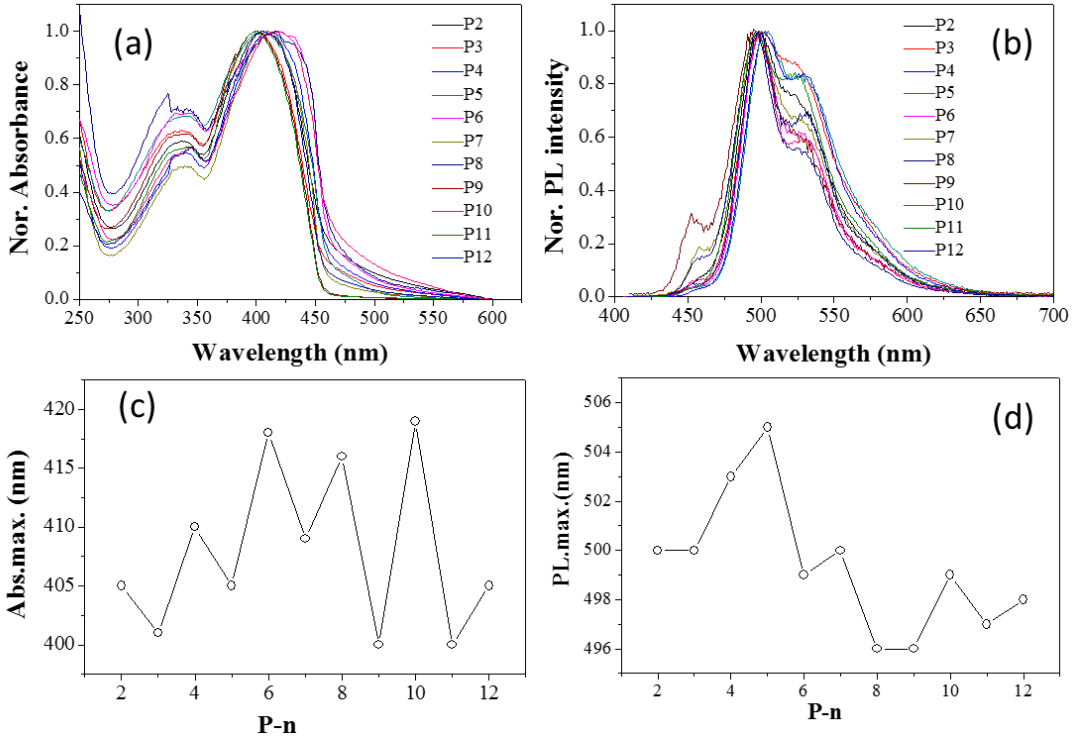

Figure 2.15. *Absorbance (a) and emission (b) spectra of the segmented polymers in thin film. (c) Plots of absorbance maxima vs the number of carbon atoms in the alkyl spacer in P-n. (d) Solid state photoluminescence quantum yield (PLQY) of the polymers was determined by integrating sphere setup and these values are plotted against the number of carbon atoms in the alkyl spacer in P-n.*

The PLQY was done according to the method given by Palsson et al.[34] using the Yvon Horiba Fluorolog-3 instrument. The PLQY of the polymers are shown in Figure 2.16. The quantum yields of the polymers varied from 16 to 26 % with ± 5 % with respect to the neighboring counterparts. Interestingly, the odd-polymers showed slightly higher PLQY compared to that of even-polymers. The comparison of the

absorbance maxima (see Figure 2.15), PLQY (see Figure 2.16) and enthalpy of polymers (see Figure 2.8) revealed that the strongly packed semicrystalline OPV even-polymers showed slightly less quantum yield compared to the weakly packed odd-polymers (amorphous polymers). This trend is attributed to the luminescence quenching by the crystalline domains that are present in the even-polymers.

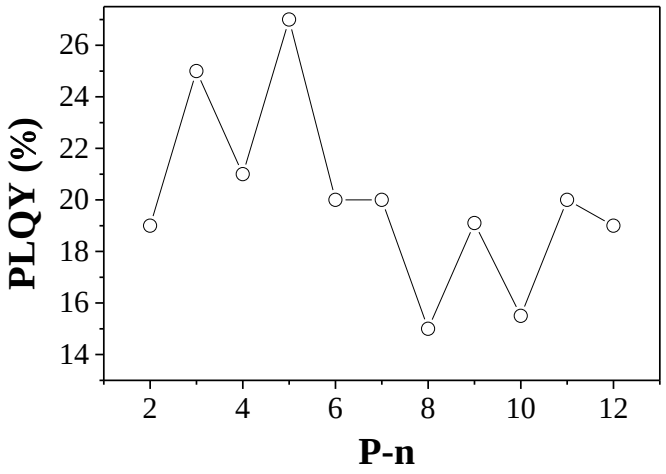

Figure 2.16. *Plotted PLQY (film) vs P-n*

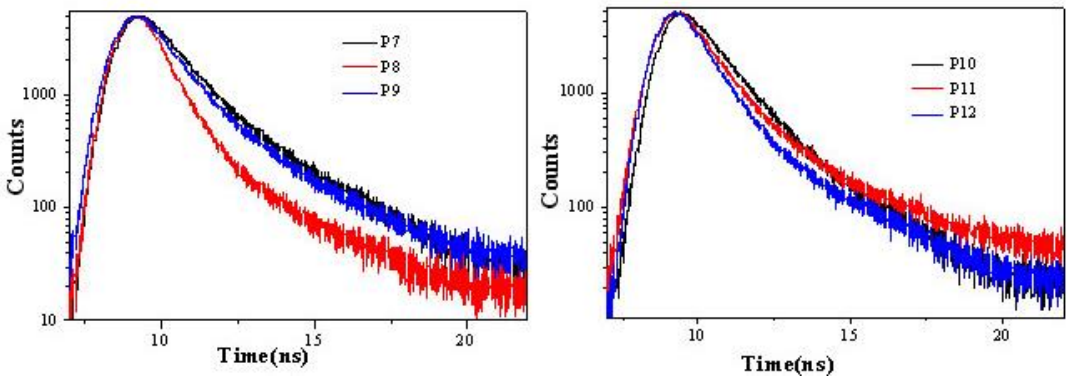

Figure 2.17. *Representative TCSPC decay profiles of polymers film*

Table 2.6. Fluorescence life time of the polymers in thin film using Nano LED, excitation λ = 371 nm. The film were optimized as 0.1 O.D.

Sample	τ_1(ns)	τ_2(ns)	A_1	A_2	χ^2
P2	0.7	3.0	73.43	26.57	1.2
P3	0.9	2.5	73.03	26.97	1.1
P4	0.8	2.7	74.63	25.37	1.3
P6	0.8	2.7	74.17	25.83	1.2
P7	1.0	2.9	70.58	29.42	1.2
P8	0.6	2.4	81.24	18.76	1.2
P9	1.0	3.9	85.24	14.76	1.2
P10	0.9	2.2	64.51	35.49	1.2
P11	0.9	3.3	78.61	21.39	1.2
P12	0.7	2.9	77.49	22.51	1.3

To further understand the excited state decay emission dynamics of the polymers, they were subjected to fluorescence lifetime analysis in thin film (see Figure 2.17) by time-correlated single photon counting (TCSPC) technique. The polymers were excited with 371 nm light-emitting diode excitation source, and the decay profiles were fitted with DAS 6 program to determine the excitation life time. The decay profiles were fitted with biexponential decay and their decay rate constants are given in table-6. All the polymers have the decay constants τ_1 = 0.7 – 1.0 ns and τ_2 = 2.2 – 3.3 ns which were comparable to that of reported poly(2-methoxy-5-(2-ethylhexyloxy)-1,4-phenylenevinylene) (MEH-PPV).[17] There is no large difference among the decay excited state emission dynamics of the segmented polymers irrespective of their semicrystalline or amorphous natures. Thus, the current polymer design provides the following important observations: (i) the spacer lengths largely influence on the packing of the polymer chains, (ii) even-spacer polymer are semi-crystalline, (iii) odd-spacer polymer are highly amorphous, and (iv) the odd-even effect induces small difference in the photophysical characteristics; however, the

color of the emission, solid state quantum yield and excited state decay dynamics are almost comparable. This is a very important finding since one can easily tune the semicrystalline or amorphous nature of the polymers without compromising on the photophysical characteristics of the π-conjugated system. Unfortunately, the semicrystalline polymers were found to be sluggish to flow in the molten state which hampered their processability. This was partially associated with the formation of thick submicrometer fibers and also the unavoidable chain entanglement as observed in FESEM images (see Figure 2.13). This suggests that alternative methods are required to process π-conjugated semicrystalline polymers into desired objects for loading such as in the narrow glass capillaries for testing their photonic switching capabilities.

2.3.5. Anisotropic π-conjugated Polymer Gels

Organogels of semicrystalline polymers are important classes of materials, and they preserve the self-organization of the polymer chains in the sub-micron to nanometer level in the gel state without compromising on their processability.[35] A large number of π-conjugated oligophenylenevinylene oligomers based organogels[36-43] and MEH-PPV polymer organogel[44] have been reported in the literature. The orgnanogel formation ability of the segmented polymers was investigated in variety of solvents (hexane, dichloromethane, THF, cyclohexane, chloroform and toluene) and toluene was found to be more suitable for gelation. About 10 mg of the polymer was dissolved in 1 mL of toluene in hot condition, filtered and subsequently allowed to cool to produce the organogel.

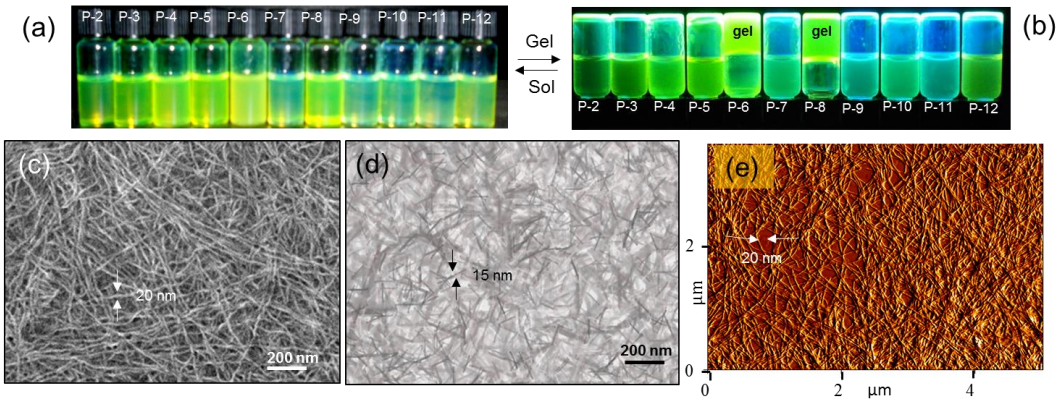

Figure 2.18. *Sol (a) and gel state (b) of the segmented polymers in toluene (10 mg/mL). (c) FE-SEM, (d) HR-TEM and (e) AFM images of the P-8 organogel.*

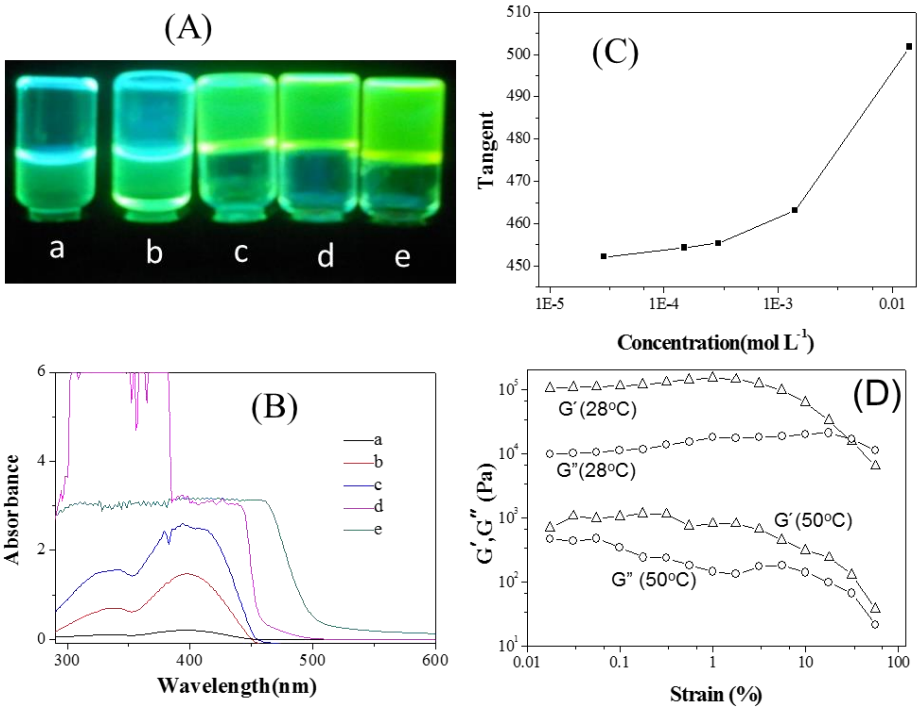

Figure 2.19. *(A) The photographs of the vials showed the existance of gel nature at higher concentation. (B) Absorbance spectra of the P-8 gel at various concentation in toluene. (c) The plot of on-set of the absroption versus the concnetrtaion. (C) Rheology experimental data of P-8 organogel in the gel (28 ℃) and sol state (50 ℃). The absorbance at various concentration of gel: (a) 3.0× 10^{-5} mol L^{-1} , (b) 1.5× 10^{-4} mol L^{-1} (c) 3.0× 10^{-4} mol L^{-1}, (d) 1.4× 10^{-3} mol L^{-1} and (e) 1.4× 10^{-2} mol L^{-1}. 3 mm path length and 200 μL quartz cuvette is used for this experiment. The on-set of the absorbance was determined by drawing a tangent. The on-set was plotted against the concentrations and this plot showed the 1x10^{-4} mol/L as minimum gel concentration.*

The photographs of the vials containing the polymer in the sol and gel state are shown in Figures 2.18a and 2.18b. All odd-polymers did not self-organize in the solvent and they did not produce organogel. In the even polymers series, those with low semicrystallinity (P-2, P-4, P-10 and P-12, see Figure 2.8d) did not produce stable organogels and only those with high crystallinity, namely, P-6 and P-8, produced organogel. Thus, the present investigation provides direct evidence that the semi-crystallinity in the π-conjugated polymer indeed facilitates the formation of stable organogels. The concentrations of the polymers were varied to study their gelation ability and these results indicated that the polymer P-8 produced more stable organogel (see Figure 2.19). The polymer P-6 required large amount of the samples and the gel was also not stable during the storage; thus, the most stable P-8 organogel was used for the subsequent studies. To visualize morphology of the organogel, the

sample was subjected to FESEM, atomic force microscope (AFM) and high resolution transmission electron microscope (HR-TEM) analysis. FESEM image of the polymer organogel showed the formation of nanofibers of 20 ± 5 nm width and length up to 5.2 ± 0.4 μm (see Figure 2.18c). HR-TEM image (see Figure 2.18d) of organogel confirmed that the size and shape of the nano-fibers as observed in the FE-SEM images. AFM image showed the nano-fiborus morphology and the fibres were found to be helical twist with length upto few micrometers (see Figure 2.18e).

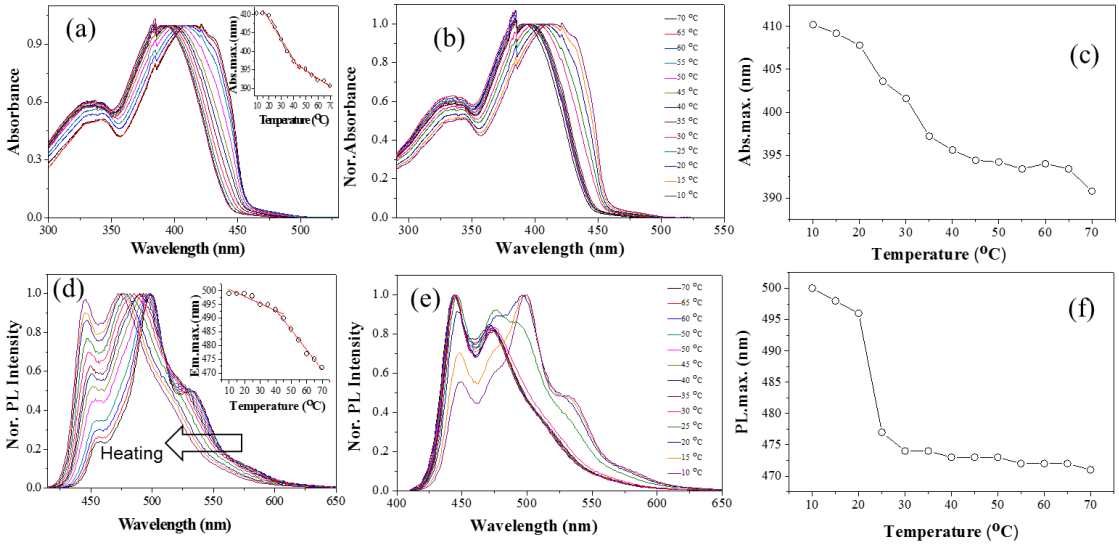

Figure 2.20. *(a) Temperature dependent absorbance spectra of P-8 gel in heating and (b) cooling cycle. (b) Temperature dependent emission spectra of P-8 Gel in heating and (d) cooling cycle. (Concentration of the polymer =1.0× 10^{-4} mol L^{-1})*

The photophyscial and thermal stability of the organogel was investigated by variable temperature absorbance and fluorescence spectroscopy. The absorbance spectra of the gel blue shifted while heating (see Figure 2.20) and red-shifted while cooling with respect to the unlocking and locking of π-aggregation of the OPV chromophore in the polymer backbone, respectively. The emission spectra also showed similar trend for the reversible aggregation in the heating (see Figure 2.20) and cooling cycles. The plots of absorbance and emission maxima of the gel versus the temperature (see in set in Figure 2.20a and 2.20b) showed break points at 42 - 44 °C as gel→sol transition temperature. Mechanical stability of the organogel was studied by dynamic rheological measurement at gel-state (28° C) and sol-state (50 °C). The plot of dynamic rheological properties of gel is shown in Figure 2.19. In the

gel state (at 28 °C), the polymers showed 100 times higher values for storage modulus G′and loss modulus G′′at 28 °C compared to that of the sol-state (at 50 °C). Further, both G' and G'' are showed plateau-region with increase in strain as indication of strong network among the nanofibers in the gel state.[45] DSC analysis of the xerogel (see Figure 2.21) indicated that the enthalpies of thermal transitions of the xerogel were slightly higher than their semicrystalline polymer. The higher enthalpies were attributed to the better packing of xerogel by the solvent assisted gelation process. The powder XRD analysis of the xerogel (see Figur 2.21) showed periodic d-spacing with respect to the layered solid state ordering as similar to that of semicrystalline sample (see Figure 2.9a).

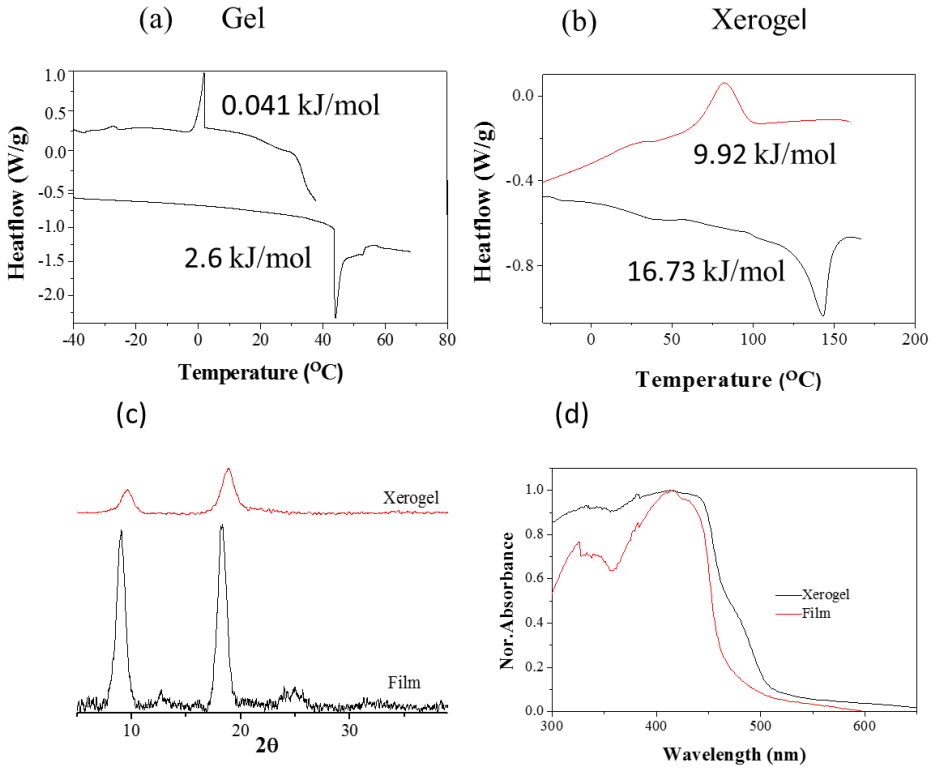

Figure 2.21. *DSC thermograms of P-8 organogel (a) and P-8 xerogel (b). (c) Powder wide angle X-ray diffraction (WXRD) pattern of P-8 polymer in the powder and xerogel state. (d) Absorbance of P-8 polymer in xerogel state and film state.*

Photophysical experiments revealed that the P-8 xerogel retained the characteristics of its semicrystalline polymer sample (see Figure 2.21). The π-conjugated polymers with even number of carbon atoms in the alkyl spacers have tendency to pack uniformly in the alternative zigzag confirmation to introduce semicrystallinity. On the other hand, the odd number of carbons introduce mismatch

for this zigzag arrangement which produces the amorphous polymer. Thus, this structural diversity in the segmented polymer design makes the even-polymer semicrystalline whereas the odd-polymer became amorphous (see Figure 2.6). Further, the higher degree of packing in the even-polymers drove them to aggregate together to produce organogel while cooling their polymer solution from hot toluene. The aligned polymer chains in the organogel produced anisotropic nanofibrous assembly. The amorphous polymer lacks perfect chain alignment and did not produce polymer organogel.

2.3.6. Organic Photonic Switches

Segmented polymer P-8 organogel was transferred into a narrow glass capillary of 1 mm diameter by immersing the capillary into the precooled viscous gel. The gel was uniformly sucked into the tube by capillary action and by this process polymer chains are aligned unidirectionally along the axis of the cylindrical capillary. The gel was allowed to stay without disturbance for 5 h at 25 °C. The aligned gel was tested for the photonic switching studies using PLM instrument as described in an earlier report[5] and the details are as shown in Figure 2.22. The capillary was placed on the sample holder which can rotate 360°. The instrument has fixed polarizer and an analyzer which was rotatable 90° at either side of the sample holder. Plane polarized light generated by the polarizer was employed as incident light source for the experiments. Anisotropic soft materials like polymer organogel in the present case refract the plane polarized light differently into slow and fast light waves with right angle to one another. The fast and slow waves emerged from the polarizer showed phase difference which was observed as optical retardance. Depending upon the nature and the angle at which the sample interacts with the incident plane polarized light; the fast and slow light waves produced either $\lambda/2$ or $\lambda/4$ switching of the incident wave. This phenomenon was traced by keeping the analyzer and polarizer perpendicular to each other and rotates the capillary from 0 to 90° in the sample plate (see Figure 2.22). When the sample was kept on the same path of the incident plane polarized light (parallel to the polarizer); no light passes through the analyser (polarizer perpendicular to analyzer). Further, the rotation of the sample from $\theta = 0$ to 45° showed the increase in the intensity of the light from the capillary followed by the interaction of the organogel with incident light. Further increase in the rotation of the sample from $\theta = 45$ to 90° produced the decrease in the intensity of the light from the

anisotropic organogel and the sample became dark at θ = 90°. The intensity of the lights from the sample was measured using imageJ software and it was plotted against the sample rotation angle, θ (see Figure 2.22b). This plot clearly indicates that the intensity of the light is maximum at 45° with respect to the typical nature of the λ/4 type optical switching (or wave plates) of the polymer anisotropic gel.

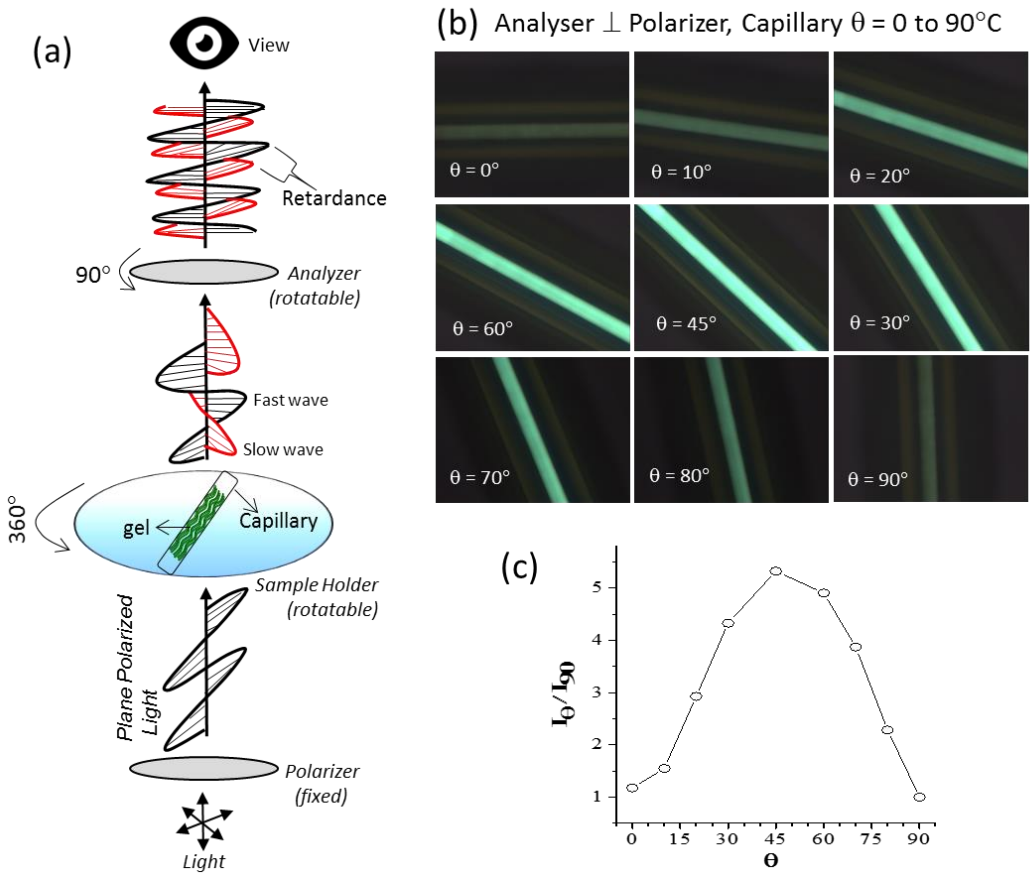

Figure 2.22. *(a) PLM instrument setup used for the studies. The organogel loaded in the glass capillary was placed on the sample holder. (b) Images of the organogel captured at various sample rotation from 0 to 90°. (c) Plot of the intensity of light from the organogel vs the sample rotation θ.*

To further confirm the λ/4 wave plate behavior of the organogel, the capillaries were subjected to few control experiments as shown in Figure 2.23. Two P-8 gel capillaries were kept perpendicular to one another and visualized under the cross-polarizers. Interestingly, the point at which the two capillaries cross each other became dark due to the cancellation of the optical retardance of the slow and fast waves from the first capillary to the second one (see Figure 2.23). Further, a nongel polymer P-7 solution (in toluene) was filled in glass capillary (no gel formation) and it was placed alongside of the P-8 gel capillary. These two parallel capillaries were kept perpendicular to the P-8 gel capillary as shown in Figure 2.23. When these capillaries were visualized through the crossed-polarizers, the two P-8 gel capillaries cross-point appeared as dark whereas the P-7 (no-gel) and P-8(gel) cross-point appeared as bright. This experiment indicated that two anisotropic gels were required to cancel the optical retardance. The same three capillary arrangements under the illumination of light when the polarizer is parallel to the analyzer did not show the optical retardance (see Figure 2.23). These controlled experiments further confirmed that the polymer self-organization into anisotropic organogel is very crucial factor for the λ/4 wave plate behaviors. Further, the unidimensional alignment of the anisotropic gel in the glass capillary is also crucial factor for the photonic switching. For instance, the wave plate nature of the organol gel was lost when the gel was spread on two dimensional glass surfaces (see Figure 2.24).

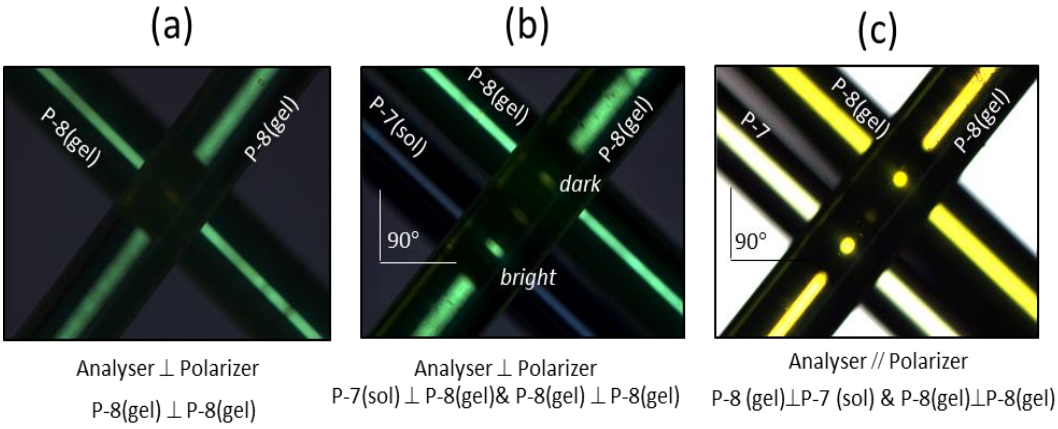

Figure 2.23. ***(a)*** *Images of the orthogonally aligned glass capillaries of P-8 organogel order orthogonally. (b) Images of P-8 (gel) orthogonal to P-8 (gel) and P-7 (sol) under cross polarizer. (c) Images of P-8 (gel) orthogonal to P-8 (gel) and P-7 under polarizer parallel analyzer. For all experiments, the angles of the polarizer and analyzer are given along with the images.*

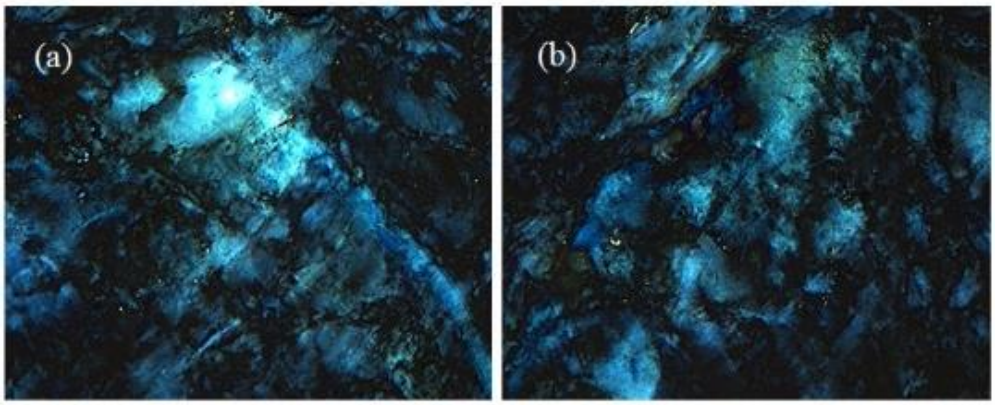

Figure 2.24. *PLM images of the P-8 gel drop caste on the glass susbtrate and image are captures at rotation angles (a) $\theta = 45^\circ$ and (b) $\theta = 0^\circ$*

2.3.7. Thermoreversible Optical Switches

The segmented polymer organogel showed thermoreversible self-assembly in the heating and cooling cycles and these were evident from the studies shown in Figure 2.22. The combination of the λ/4 photonic switching and thermoreversible behavior of the anisotropic polymer gel allowed us to develop new thermoresponsive optical wave plates or optical or photonic switches which may have potential application in the storage and optical transportation of information or sensing that are controllable by heat or thermal behaviours. To demonstrate the above feasibility in the present system; the polymer gel was subjected to variable temperature photonic switching studies using a temperature programmable hot stage attached to a polarizing light microscope as shown in Figure 2.25. The capillary was mounted on the hot stage at θ =45° and illuminated by plane polarized light under crossed polarizer. The capillary was subjected to control heat or cool at desired temperature. The images captured at the variable temperature above and below the gel melting temperature are shown in Figure 2.25. When the capillary was heated from 25 to 50 °C, the intensity of the sample slowly vanished and became dark above the gel temperature point. In the subsequent cooling, the sample has reassembled as anisotropic gel and behaved as λ/4 wave plates. The plot of temperature versus the intensity of the organogel (Figure 2.25b) revealed that the intensity of the light was reversible by more than 98 % in the heating and cooling cycles. This trend was reproducible in the subsequent heating and

cooling conditions. This indicates that the polymer organogel could be used as rewritable optical wave plate depending upon its sol-gel temperature region.

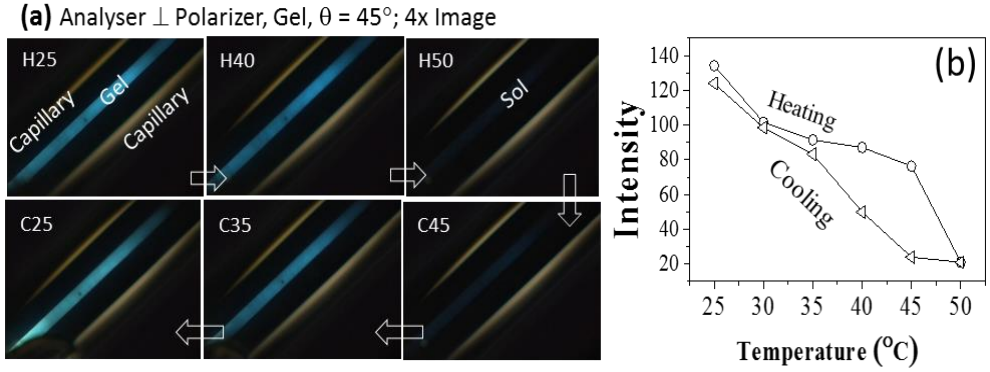

Figure 2.25. *Thermoreversible λ/4 photonic wave plates behaviors of P-8 organogel (a) and xerogel (c) in the heating and cooling cycles. Plot of the intensity of the organogel (b) and xerogel (d) vs the temperature in the heating and cooling cycles. In the Figures, H and C represents heating and cooling cycles, respectively.*

To further analyze the thermo-reversible nature of the anisotropic gel, the capillary was allowed to dry for 48 h and the xerogel were subjected to λ/4 switching studies. DSC analysis of the xerogel indicates that the sample become molten above 160 °C and aligned back (crystallization) in the subsequent cooling (see Figure 2.26). The images captured at various temperatures of capillary (at θ = 45°) containing the xerogel under crossed-polarizers are given in the Figure 2.26. While heating the intensity of the emission from the xerogel diminished and became dark at the molten state (at 160 °C). In the subsequent cooling the xerogel re-assembled to produce the brightness with λ/4 behaviour. However, the recovery of the intensity became better after annealing the sample at 25 °C for 48 h. The plot of temperature versus the intensity of the xerogel revealed that 30-40 % of the self-assembly was reversible (see Figure 2.26b) in the xerogel state. Thus, the gel is completely reversible for photonic switching in the organogel state; however, the reversibility became very slow in the case of the xerogel. The optical switching by the capillary filled with polymer organogel provides new optical switching possibility up to 160 °C in the neat conditions.

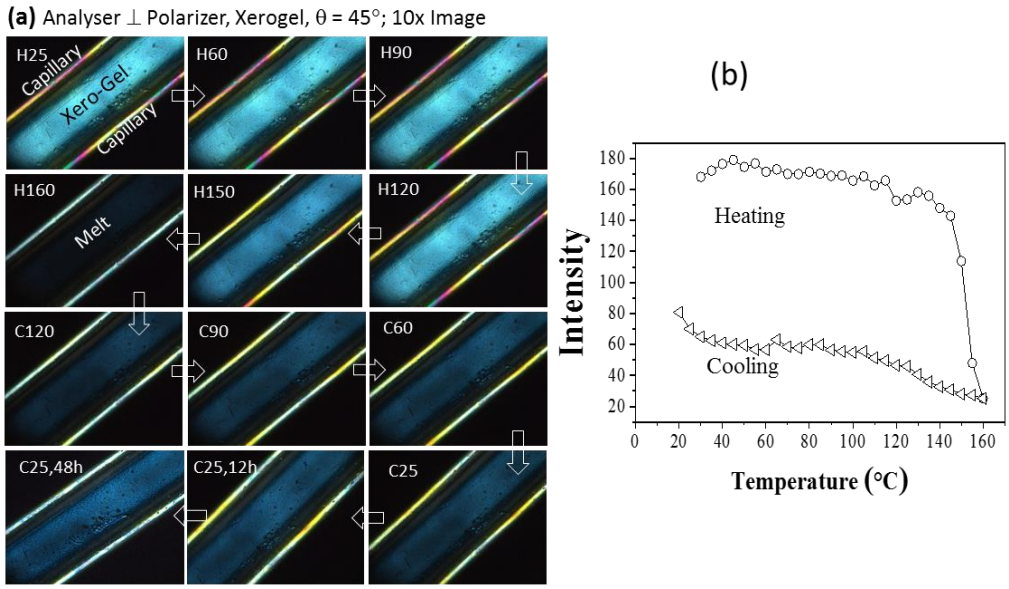

Figure 2.26. *Thermoreversible λ/4 photonic wave plates behaviors of P-8 organogel (a) and xerogel (c) in the heating and cooling cycles. Plot of the intensity of the organogel (b) and xerogel (d) vs the temperature in the heating and cooling cycles. In the Figures, H and C represents heating and cooling cycles, respectively.*

Further, semicrystalline polymers are very difficult to fill uniformly in a narrow capillary; however, in the present investigation the ability of the segmented polymer to produce organogel P-8 allow one to fill the narrow capillary devices at the gel state and subsequently remove the solvent to retain the alignment of the crystalline vectors in the xerogel state. The glass capillary device is a simple example developed in the laboratory to demonstrate the proof-of-concept. This photonic switching concept can be expandable to wide range of optical cables with pore size varying from few millimeters to micrometers for optical storage, transmission or communication. Further, synthetic polymer chemistry provides unlimited opportunity for designing wide variety of π-conjugates with tunable optical band gaps (in the entire visible and near-IR region), electronic configuration (electron rich or deficient) and rigid and flexible backbones; thus, this concept may be explored in other π-conjugates.

2.4. Conclusion

In conclusion, we have designed new series of semicrystalline segmented π-conjugated polymers with rigid OPV core and flexible alkyl units to demonstrate the first organic photonic switches or organic λ/4 wave plates. These new classes of segmented polymers were found to be either semicrystalline or amorphous depending upon even or odd numbers of carbon atoms present in the alkyl spacers. Variable temperature WXRD studies revealed that the polymer chains packed as lamellar network in the solid state. Single crystal structure of OPV-oligomer was resolved to understand the packing of the lamellar-assemblies in the polymer backbone. Absorbance, emission, solid state photoluminescence quantum yield and fluorescence time studies facilitated the understanding of the segmented polymers with respect to even or odd carbon atoms. Interestingly, the even-polymer with highest crystallinity (P-6 and P-8) produced stable polymer organogel unlike their amorphous odd-polymers (no gel formation). The morphology of the P-8 polymer gel was characterized by FESEM, HR-TEM and AFM analysis. Variable temperature photophysical studies revealed that the organogel showed thermo-reversible sol→gel transition at 42-44 °C. Further, the rheology measurements were carried out to confirm the mechanical stability of the polymer organogel. The organogel was transferred into a glass capillary and the aligned gel was demonstrated as photonic switches. The polymer organogel was found to behave as λ/4 wave plates and showed highest intensity for incident plane polarized at θ = 45° under crossed-polarizers. The thermoreversibility of the polymer gel was explored to construct thermo-responsive photonic switches for the temperature range from 25 to 160 °C. The optical wave plate concept demonstrated is not restricted to the present segmented OPV polymer design and it can be adapted to wide range of other π-conjugated polymers to make futuristic optoelectronic molecular devices.

2.5. References

1. Clark, J.; Lanzani, G.; Organic Photonics for Communications. *Nat. Photonics*, **2010**, *4*, 438-446.
2. Zhang, C.; Yan, Y.; Yao, J.; Zhao, Y. S. ; Manipulation of Light Flows in Organic Color-Graded Microstructures towards Integrated Photonics Heterojunction Devices. *Adv. Mater*.**2013**, *25*, 2854-2859.
3. Benedetto, F. D.; Persano, L.; Cingolani, R.; Pisignano, D.; Mele, E.; Multilevel, Room-Temperature Nanoimprint Lithography for Conjugated Polymer-Based Photonics. *Nano Lett*., **2005**, *5*, 1915-1919.
4. Paschotta, R.; *Encyclopedia of Laser Physics and Technology*, Volume 2, Wiley-VCH, Berlin, **2008.**
5. Zhou, J.; Du, X.; Gao, Y.; Shi, J.; Xu, B.; Aromatic- Aromatic Interactions Enhance Interfiber Contacts for Enzymatic Formation of a Spontaneously Aligned Supramolecular Hydrogel. *J. Am. Chem. Soc.***2014**, *136*, 2970−2973.
6. Zhang, S.; Greenfield, M. A.; Mata, A.; Palmer, L. C.; Bitton, R.; Mantei, J. R.; Aparicio, C.; O.de la Cruz, M.; Stupp, S. I.; A Self –Assembly Pathway to Aligned Monodomain Gels. *Nat. Mater*., **2010**, *9*, 594-601.
7. Maki, Y.; Ito, K.; Hosoya, N.; Yoneyama, C.; Furusawa, K.; Yamamoto, T.; Dobashi, T.; Sugimoto, Y.; Wakabayashi, K.; Anisotropic Structure of Calcium-Induced Alginate Gels by Optical and Small-Angle X-ray Scattering Measurements. *Biomacromolecules*, **2011**, *12*, 2145–2152
8. Wu, Z. L.; Kurokawa, T.; Liang, S.; Furukawa, H.; Gong, J. P.; Hydrogels with Cylindrically Symmetric Structure at Macroscopic Scale by Self-Assembly of Semi-Rigid Polyion Complex. *J. Am. Chem. Soc*. **2010**, *132*, 10064-10069.
9. Kanibolotsky, A. L.; Perepichka, I. F.; Skabara, P. J.; Star-Shaped π-Conjugated oligomers and their Applications in Organic electronics and Photonics. *Chem. Soc. Rev*. **2010**, *39*, 2695-2728.
10. Ye, L.; Zhang, S.; Huo, L.; Zhang, M.; Hou, J.; Molecular Design toward Highly Efficient Photovoltaic Polymers Based on Two-Dimensional Conjugated Benzodithiophene. *Acc. Chem. Res*. **2014**, *47*, 1595-1603.
11. Ying, L.; Ho, C-L.; Wu, H.; Cao, Y.; Wong, W-Y.; White Polymer Light –Emitting Devices for Solid-State Lighting: Materials, Devices, and Recent Progress. *Adv. Mater*. **2014**, *26*, 2459-2473
12. Wang, C.; Dong, H.; Hu, W.; Liu, Y.; Zhu, D.; Semiconducting π-Conjugated Systems in Field-Effect Transistors: A Material Odyssey of Organic Electronics. *Chem. Rev.* **2012**, *112*, 2208–2267.
13. Akcelrud, L. Electroluminescent Polymers. *Prog. Polym. Sci*., **2003**, *28*, 875.
14. Ren, X-K.; Wu, Y-C.; Wang, S-J.; Jiang, S-D.; Zheng, J-F.; yang, S.; Chen, E-Q.; Wang, C-W.; Hsu, C-S.; Crystal Structure and Molecular Packing Behavior of Poly(2,3-diphenyl-1,4-phenylenevinylene) Derivatives Containing Alkyl Side-Chains. *Macromolecules*, **2013**, *46*, 155-163.

15. Speros, J. c.; Martinez, H.; Paulsen, B. D.; White, S. P.; Bonifas, A. D.; Goff, P. C.; Frisbie, C. D.; Hillmyer, M. A.; Effects of Olefin Content and Alkyl Chain Placement on Optoelectronic and Morphological Properties in Poly(thienylene vinylenes). *Macromolecules*, **2013**, *46*, 5184-5194.
16. Kuo. C-y.; Huang, Y-C.; Hsiow, C-y.; Yang, Y-W.; Huang, C-I.; Rwei, S-R.; Wang, H-L.; Wang, L.; Effect of Side-Chain Architecture on the Optical and Crystalline Properties of Two- Dimensional Polythiophenes. *Macromolecules*, **2013**, *46*, 5985-5997.
17. Amrutha, S. R.; Jayakannan, M. Probing the π-Stack Induced Molecular Aggregation in π-Conjugated Polymers, Oligomers and Their Blends of Poly(phenylenevinylene)s *J. Phys. Chem. B.* **2008**. *112*, 1119-1129.
18. Amrutha, S. R.; Jayakannan, M. Structure Control of π-Conjugated Polymers for Enhanced Solid State Luminescence: Synthesis, Liquid Crystalline and Photophysical Properties of New Bulky Poly (p-phenylenevinylene)s and Oligo-Phenylenevinylenes bearing Tricyclodecane Pendants. *Macromolecules,* **2007,** *40, 2380 – 2391*.
19. Amrutha, S. R.; Jayakannan, M. Control of π-Stacking for Highly Emissive Poly(p-phenylenevinylene)s: Synthesis and Photoluminescence of New Tricyclodecane Substituted Poly(p-phenylenevinylene)s and its Copolymers. *J. Phys. Chem. B.* **2006**, *110*, 4083-4091
20. Neill, M. O.; Kelly, S. M.; Ordered Materials for Organic Electronics and Photonics. *Adv. Mater*. **2011**, *23*, 566-584.
21. Yang, Z.; Sokolik, I.; Karasz, F. E.; A Soluble Blue-light-emitting Polymer. *Macromolecules*, **1993**, *26*, 1188-1190.
22. Pang, Y.; Li, J. Hu, B.; Karasz, F. E.; A Highly Luminescent Poly[(*m*-phenylenevinylene)-*alt*-(*p*-phenylenevinylene)] with Defined Conjugation Length and Improved Solubility. *Macromolecules*, **1999**, *32*, 3946-3950.
23. Chen, Y.; Xu, Y.; Perry, K.; Sokolov, A. P.; More, K.; Pang, Y.; Achieving Diameter-Selective Separation of Single-Walled Carbon Nanotubes by Using Polymer Conformation-Confined Helical Cavity. *ACS Macro Lett*. **2012**, *1*, 701-705.
24. Chen, Y.; Malkovskiy, A.; Wang, X-Q.; Lebron-Colon, M.; Sokolov, A. P.; Perry, K.; More, K.; Pang, Y.; Selection of Single-Walled Carbon Nanotube with Narrow Diameter Distribution by Using a PPE–PPV Copolymer. *ACS Macro Lett*. **2012**, *1*, 246-251.
25. Balamurugan, A.; Reddy, M. L. P.; Jayakannan, M. π-Conjugated Polymer-Eu^{3+} Complexes: A Versatile Luminescent Molecular probe for Temperature Sensing. *J. Mater.Chem. A.* **2013**, *1*, 2256-2266.
26. Balamurugan, A.; Kumar, V.; Jayakannan, M. Carboxylic Distilbene Fluorescent Polymer Chemosensor for Temperature, Metal-ion and Biomolecule. *Chem. Commun*. **2014**, *50*, 842-845.

27. Goel, M.; Narasimha, K.; Jayakannan, M.; Helical Self-assemblies of Segmented Poly(phenylenevinylene)s and their Hierarchical Donor-Acceptor Complexes. *Macromolecules* **2014**, *47*, 2592−2603.
28. Tan, T. A. T.; Clarke, T. M.; James, D.; Durrant, J. R.; White, J. M.; Ghiggino, K. P.; Synthesis and Photo-induced Charge Separation of Confined Conjugation length Phenylenevinylene Based Polymers. *Polym. Chem.* **2013**, *4*, 5305–5309.
29. Goel, M.; Jayakannan, M. Supramolecular Liquid Crystalline π-Conjugates: The Role of Aromatic π-stacking and van der Waals Forces on the Molecular Self-assembly of Oligo-Phenylenevinylenes. *J. Phys. Chem. B.* **2010**, *114*, 12508- 12519
30. Segmented polymers were also prepared with methoxy or tricyclodecanemethylene solubilising unit on the OPV core and varying the alkyl chain in the backbone C_2 to C_{12}. The polymers with methoxy substitution were found to insoluble. The tricyclodecanemethylene polymers were found to be soluble only for C_{12} alkyl units (see ref.27). The 2-ethylhexyl substitution is very crucial for complete solubility of segmented polymers in the entire series of C_2 to C_{12} spacers.
31. Goel M.; Jayakannan, M. CH/π Interaction Guided Molecular Self-assembly in π-Conjugated Oligomers. *Chem. Eur. J.* **2012**, *18*, 2867-2874.
32. Goel, M.; Jayakannan, M. Herringbone and Helical Self-assembly of π-Conjugated Molecules in Solid State through CH/π Hydrogen Bond. *Chem. Eur. J.* **2012**, *18*, 11987-11993.
33. Atkins, P. W. *Physical Chemistry*, Edition. 6, Oxford University Press, Oxford Melbourne Tokyo, **1998.**
34. Palsson, L.-O.; Monkma, A. P.; Measurements of Solid –State Photoluminescence Quantum Yields of Films Using a Fluorimeter. *Adv. Mater.* **2002**, *14*, 757-758.
35. Babu, S. S.; Praveen, V. K.; Ajayaghosh, A.; Functional π-Gelators and Their Applications. *Chem. Rev.* **2014**, *114*, 1973–2129.
36. Praveen, V. K.; Ranjith, C.; Bandini, E.; Ajayaghosh, A.; Armaroli, N.; Oligo(phenylenevinylene) Hybrids and Selfassemblies: Versatile Materials for Excitation Energy Transfer. *Chem. Soc. Rev.* **2014**,*43*, 4222
37. Ajayaghosh, A.; Praveen, V. K.; *π*-Organogels of Self-Assembled *p*-Phenylenevinylenes: Soft Materials with Distinct Size, Shape, and Functions. *Acc. Chem. Res.* **2007,** *40*, 644–656
38. Sakakibara, K.; Chithra, P.; Das, B.; Mori, T.; Akada, M.; Labuta, J.; Tsuruoka, T.; Maji, S.; Furumi, S.; Shrestha, L. K.; Hill, J. P.; Acharya, S.; Ariga, K.; Ajayaghosh, A.; Aligned 1‑D Nanorods of a π‑Gelator Exhibit Molecular Orientation and Excitation Energy Transport Different from Entangled Fiber Networks. *J. Am. Chem. Soc.* **2014**, *136*, 8548−8551.

39. Yao, C.; Lu, Q.; Wang, X.; Wang, F.; Reversible Sol−Gel Transition of Oligo (p‑phenylenevinylene) s by π−π Stacking and Dissociation. *J. Phys. Chem. B* **2014**, *118*, 4661−4668
40. Marciel, A. B.; Tanyeri , M.; Wall, B. D.; Tovar, J. D.; Schroeder, C. M.; Wilson, W. L.; Fluidic-Directed Assembly of Aligned Oligopeptides With π -Conjugated Cores. *Adv. Mater.* **2013**, *25*, 6398–6404
41. Yagai, S.; Satoru Okamura, S.; Nakano, Y.; Yamauchi1, M.; Kishikawa1, K.; Karatsu, T.; Kitamura1, A.; Ueno, A.; Kuzuhara, D.; Yamada, H.; Seki, T.; Hajime Ito, H.; Design Amphiphilic Dipolar π-Systems for Stimuli-responsive Luminescent Materials using Metastable States. *Nat. Commun.* **2014**, *5*, 4013
42. George, S. J.; Ajayaghosh, A.; Self-Assembled Nanotapes of Oligo (*p*-phenylene vinylene)s: Sol–Gel-Controlled Optical Properties in Fluorescent *p*-Electronic Gels. *Chem. Eur. J.* **2005**, *11*, 3217 – 3227
43. Ajayaghosh, A.; Praveen, V. K.; Srinivasan, S.; Varghese, R.; Quadrupolar p-Gels: Sol–Gel Tunable Red–Green–Blue Emission in Donor–Acceptor type Oligo (*p*-phenylenevinylene)s. *Adv. Mater.* **2007**, *19*, 411–415
44. Wang, P. S.; Lu, H. H.; Liu, C. Y.; Chen**,** S. A.; Gel Formation via Physical Cross-Linking in the Soluble Conjugated Polymer, Poly[2-methoxy-5-(2-ethylhexyloxy)-1,4-phenylenevinylene], in Solution by Addition of Alkanes. *Macromolecules* **2008**, *41*, 6500-6504
45. Park, J. S.; Jeong, S.; Chang, d. C.; Kim, J. P.; Kim, K.; Park, E-K.; Song, K-W. Lithium-induced Supramolecular Hydrogel. *Chem. Commun.* **2011**, *47*, 4736-4738.

Chapter 3

Color-Tunable Amphiphilic Segmented π-Conjugated Polymer Nano-Assemblies and Their Bioimaging in Cancer Cells

Abstract:

A unique color tunable amphiphilic segmented π-conjugated polymer is designed and demonstrated their π-stack self-assembled aqueous luminescent nanoparticles for imaging in cervical and breast cancer cells. Oligo-phenylenevinylene (OPV) was employed as rigid luminescent π-core and oligo-ethyleneoxy chains were used as flexible spacers to constitute new amphiphilic segmented π-conjugated polymers by Wittig-Horner polymerization route. The rigidity of the π-core was varied using tricyclodecanemethyloxy, 2-etheylhexyloxy or methoxy pendants and appropriate π-core geometry was optimized to achieve maximum aromatic π-stacking interactions. Solvent-induced chain aggregation of the polymers exhibited a morphological transition from one-dimensional helical nanofibrous to three-dimensional spherical nanoassemblies in good/bad solvent combinations. This morphological transformation was accompanied by the fluorescence color change from blue-to-white-to-yellow. CIE color coordinates exhibited x = 0.25 and y = 0.32 for the white light emission followed by the collective emission from aggregated and isolated OPV chromophores. Electron and atomic microscopes, steady state photophysical studies, time- resolved fluorescent decay analysis and dynamic light scattering method enabled us to establish the precise mechanism for the self-assembly of segmented OPV polymers. The polymers produced stable and luminescent nanoparticles of < 200 nm diameter in aqueous solution. Cytotoxicity studies in cervical and breast cancer cells revealed that these new aqueous luminescent polymer nanoparticles are highly biocompatible and nontoxic to cells up to 60 μg/mL. Cellular uptake studies by confocal microscope further exposed that these nanoparticles were internalized in the cancer cells and they were predominantly accumulated in the nucleus. The present investigation opens up new amphiphilic segmented π-conjugated polymer design for producing diverse supramolecular assemblies and also demonstrates their new application as biocompatible fluorescent nanoprobes for imaging in cancer cells.

3.1. Introduction:

Aqueous nanoassemblies of amphiphilic π-conjugated materials are emerging as important luminescent molecular probes for bioimaging,[1-2] and sensing toxic metals[3-8] and as nano-scaffolds for delivery of gene[9] and drugs.[10-12] Amphiphilicity in π-conjugated aromatic polymers was typically introduced by anchoring flexible oligo-(or poly) ethylene glycols as side chains in the π-conjugated backbones.[13] PEG-lated oligomers of thiophenes,[14-17] fluorenes,[18] phenylenes,[19-23] phenyleneethylenes,[24-25] phenylenevinylenes,[26-27]and peryelnebisimides[28-29] were synthesized and self-assembled as vesicles, nanoparticles and toroids[30-31]etc. Inspired by these self-assemblies of small molecular π-conjugates; recently, amphiphilic π-conjugated polymer based on rod-coil A-B-A triblock copolymer of oligo-phenylenevinylene (OPV) core and PEG corona were reported for nano-fibrous and micellar assemblies.[32] Luo et al. reported the crown ether pendants were anchored on the poly(phenylene vinylene) backbone and studied the role of K^+ ion binding to produce nano-ribbon morphology.[33] The effect of potassium ion on the helical nano-fiber morphology of A-B diblocks of poly(3-triethyelene glycol thiophene)-block-poly(3-hexylthiophene) was also reported (see figure 3.1).[34]

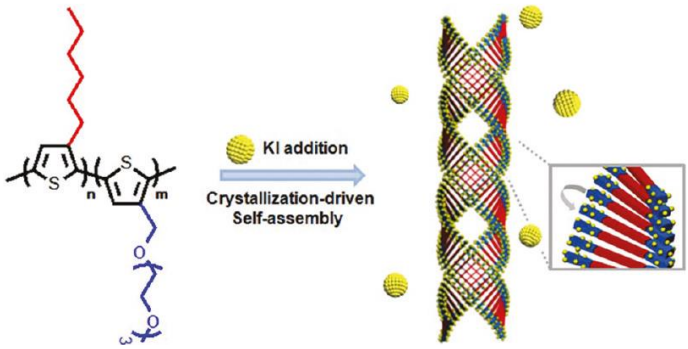

Figure 3.1. *Molecular structure of P3HT-b-P3(TEG)T diblock copolymers and schematic representation of their assembly into superhelical structures through crystallization in the presence of potassium ions (Adopted from Hayward et al. J. Am. Chem. Soc.* **2011**, *133*, 10390-10393).

Wu et al. reported the thermo and pH-responsive blocks of poly(3-hexylthiophene)-block-Poly(triethyeleneglycolallene)s demonstrated as white luminescent material shown in figure 3.2.[35] In most of these examples; the self-assembly was primarily

driven by the non-covalent interactions at the side chains and the π-conjugated polymer backbone was almost unaffected. Self-assembly of π-conjugated polymers that are responsive to change in the backbone is particularly important since it would provide new fundamental understanding of chain folding phenomena and also enabling the color-tuning via aromatic π-π stacking. Segmented π-conjugated polymers having rigid aromatic π-core and flexible alkyl or oligo ethyelene spacers in the backbone are unique classes of materials for the above purpose. In this design, the aromatic rigid core and flexible units can be selectively segregated in the polymer matrix by weak non-covalent forces such as aromatic π-stacking and van der Waals forces. Karasz and coworkers reported segmented polymers of oligo-(1,4-phenylenevinylene)s cores and demonstrated their application for blue light emitting diodes.[36] Pang and co-workers developed hybrid nano-composites based on 1,3-meta-phenylene-bridged conjugated polymer and single-walled carbon nanotubes.[37-38]

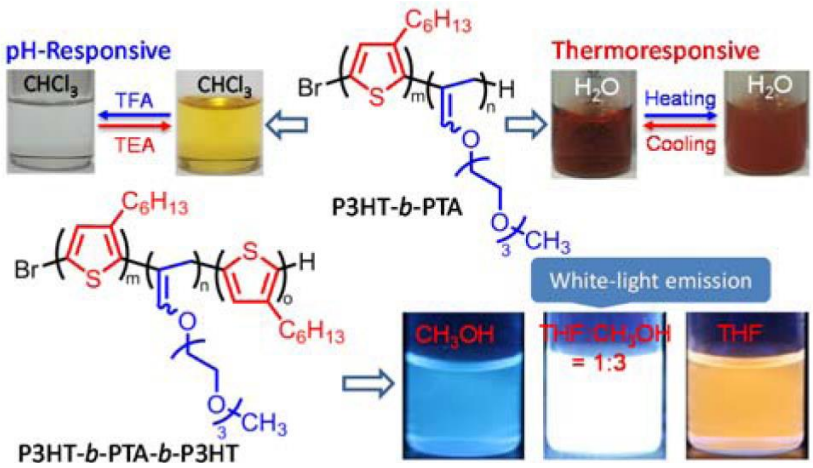

Figure 3.2. *Photographs of polymer in pH responsive, thermoresponsive, and in different solvents under room light UV light at 365 nm (Adopted from Wu et al. Macromolecules* **2015**, *48,* 5204-5212*).*

Segmented polymers with electron deficient and electron rich aromatic cores were self-assembled into helical amyliod-fibrils[39-40] and charger-transfer complexes.[41-43] Oligo-(1,4-phenylenevinylene)s segmented polymer and PCBM blends were prepared to study the photoinduced charge separation in solid state.[44] From our group, we reported segment π-conjugated polymers based on carboxylic substituted 1,3-oligo-phenyelenevinylenes as photosensitizer for Eu^{3+} ion [45] and their complexes were employed as triple detection probe for thermal, toxic metal ion and amino acids.[46] Further, oligo-1,4-phenyelenevinylenes (OPV) segmented polymers were studied for helical donor-acceptor assemblies.[47] Semicrystalline OPV segmented polymers were designed and self-assembled as organogels to demonstrate their photonic λ/4 wave plates for optical switching applications.[48]

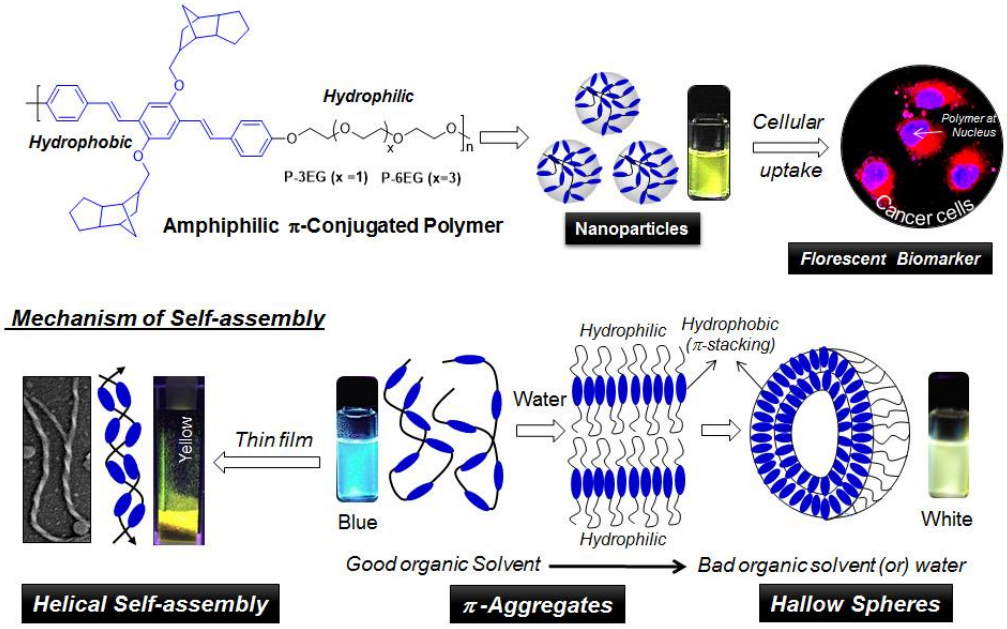

Figure 3.3. *Segmented π-conjugated design for diverse polymer self-assembly and demonstrate their luminescence nanoassemblies as biomarkers in cancer cell imaging.*

These studies emphasized the importance of segmented π-conjugated polymers for photonic and electronic applications. Unfortunately, no effort has been taken until now to study the aqueous self-assembly of segmented π-conjugated polymers for biomedical applications. This is partially associated with the limited solubility of segmented π-conjugated polymers in water. The present investigation is aimed to address this problem by designing new classes of water-soluble amphiphilic

π-conjugated OPV polymers and employ their aqueous stable nanoassemblies were demonstrated as nontoxic fluorescent biomarkers for cellular imaging in cancer cells. This new polymer design and imaging concept is shown in Figure 3.3.

The present investigation is emphasized to develop new classes of amphiphilic segmented π-conjugated polymers based on rigid and blue luminescent oligo-phenylenevinylene (OPV) π-core and variable oligo-ethyleneoxy flexible spacer. For this purpose, three OPV cores are chosen by varying the side chain anchoring groups as 2-ethylhexyloxy (EH, branched unit), tricyclodecanemethyleneoxy (TCD, rigid unit) and methoxy (Me) units. The selection of these pendants was done based on our recent efforts in resolving the crystal structures of OPVs to trace the role of substitution on the planarity of the molecules.[49-51] It was found that the substitution of TCD, EH and Me in the vertical position and long tails in the longitudinal positions of OPV aromatic core produced planar geometry. Thus, these three planar OPV cores were chosen here to make new classes of segmented polymers to study their self-assembly. Thus, the combination of these OPV cores and ethylene glycol spacers provide an excellent opportunity to fine-tune the correct structural design to study the self-assembly process of segmented π-conjugated polymers. The photophysical studies revealed that emission characteristics of the polymers were highly specific to their structure and the solvent compositions. The polymers underwent strong aromatic π-stacking and showed excellent color tunability from blue-to-white-to-yellow. This color tunability was accomplished by the morphological transition from nanofiber to spherical assemblies. The segmented polymers were found to produce stable aqueous luminescent nanoparticles. Cytotoxicity studies in cancer cells revealed that the polymer nanoparticles were non-toxic to cells and confocal microscopic analysis exhibited that the nanoparticles were readily taken by the cells and accumulated in the perinuclear environment. The overall investigation revealed that the new polymer design opens up a new opportunity to fine-tune their diverse nanoassemblies of segmented π-conjugated polymers and demonstrates their applications as fluorescent biomarker for the first time in cancer therapy.

3.2. Experimental Section

3.2.1 Materials: Hydroquinone, 4-hydroxybenzaldehyde, triethylene glycol, hexaethylene glycol, *p*-toluenesulfonyl chloride, triethylamine, triethyl phosphite,

dimethyl sulfate, and potassium tert-butoxide (1M in THF), were purchased from Aldrich Chemicals. HBr in glacial acetic acid, paraformaldehyde, K_2CO_3, and KOH were purchased locally. 1,8-Tricyclodecanemethanol was donated by Celanese Chemicals and Co. and has used without further purification. Solvents were purchased locally and purified by standard procedures. Tetraethyl ((2,5-bis((2-ethylhexyl)oxy)-1,4-phenylene)bis(methylene))bis(phosphonate) (**3**) reported in chapter 2 was used. Cervical cancer (HeLa) cells, breast cancer (MCF-7) cells were maintained in DMEM (phenol red, Gibco) containing 10% (v/v) fetal bovine serum (FBS) and 1% (v/v) penicillin–streptomycin at 37°C under a 5% CO_2 atmosphere. For all the assays, cells were rinsed with 40 % DPBS (Gibco), trypsinized using 0.05 % trypsin (Gibco) and seeded in 96 well or 6 well (as per experiment) flat bottomed plastic plates (Costar). Fluoromount was obtained from Southern Biotech.

3.2.2. Instrumentation:

^1H and ^{13}C NMR were recorded using 400 MHz JEOL NMR spectrometer. Infrared spectra were recorded using a Thermo-Scientific Nicolet 6700 FT-IR spectrometer in the solid state in KBr in the range of 4000-600 cm^{-1}. Mass analysis of precursors was determined by the Applied Biosystems 4800 PLUS MALDI TOF/TOF analyzer using TiO_2 as a matrix. The molecular weights of polymers were determined using gel permeation chromatography (GPC) which was performed by Viscotek triple detector setup and tetrahydrofuran as a solvent. TGA analysis was done using Perkin Elmer STA 6000 simultaneous Thermal Analyser. Differential scanning calorimetry (DSC) measurements had done by using TA Q20 DSC. The data were recorded at heating and cooling rate of 10 °C/min. The first heating cycle data were discarded since they possessed prehistory of the sample. Absorption spectra were recorded by using a PerkinElmer Lambda 45 UV spectrophotometer. Steady state emission and excitation spectra were recorded using Fluorolog-3 HORIBA JOBIN VYON fluorescence spectrophotometer. The quantum yields of the polymer aggregates were determined using quinine sulfate in 0.1 M H_2SO_4 ($\boldsymbol{\phi}$ = 0.546) as standards, respectively. The solvent induced aggregation studies were performed using methanol (MeOH) and water as bad-solvents, respectively, for P-TCD-6EG by making different good-solvent/bad-solvent combinations. The stock solution was prepared by dissolving the polymer in THF, and chloroform and various combinations of water/THF and methanol/ chloroform samples were prepared by maintaining the

absorbance at ≈0.1. The time-resolved fluorescence lifetime measurements (TCSPC) were performed using a Fluorolog HORIBA JOBIN VYON fluorescence spectrophotometer. Fluorescence intensity decays were collected by a time-correlated single photon counting technique (TCSPC) setup from Horiba Jobin Yvon. 371 nm LED used for sample excitation. FE-SEM images were recorded using Zeiss Ultra Plus scanning electron microscope and the samples were prepared by drop casting on silicon wafers and coated with gold. Atomic force microscope images were recorded for drop-cast samples using Agilent instruments. The sample was drop cast on a freshly cleaved mica surface. The imaging was carried out in tapping mode using TAP-190AL-G50 probe from Budget sensors with a nominal spring constant of 48 N/m and the resonance frequency of 190. Dynamic light scattering (DLS) was performed using a Nano ZS-90 apparatus utilizing 633 nm red laser (at 90° angle) from Malvern Instruments. High Resolution-Transmission Electron Microscopy (HR-TEM) images were recorded using Technai-300 instrument by drop casting aqueous sample on Formvar-coated copper grids. LSM confocal microscope was used for cell uptake images.

Synthesis of (Ethane-1,2-diylbis(oxy))bis(ethane-2,1-diyl) Bis(4-methylbenzenesulfonate) (13a): Triethylene glycol (5.0 g, 33.33 mmol) and p-toluenesulfonylchloride (13.9 g, 73.33 mmol) were dissolved in dry DCM (50.0 mL). The solution was cooled (<5 °C) and powdered KOH (14.9 g, 266.00 mmol) was slowly added under nitrogen atmosphere. The reaction mixture was stirred for 4 h at 0 °C. Water (60.0 mL) was added and the product was extracted into DCM (100.0 mL). The organic layer was dried over anhydrous Na_2SO_4 and the solvent was removed to get product as white solid. The product was further purified by passing through silica gel column using ethyl acetate (30 % v/v) in hexane as eluent. Yield= 13.7 g (90 %). ^{1}H -NMR (400 MHz, $CDCl_3$) δ ppm: 7.79 (d, 4H, Ar - **H**), 7.35 (d, 4H, Ar - **H**), 4.11 (t, 4H, Ar-$SO_2OC\mathbf{H}_2CH_2$), 3.66 (t, 4H, Ar-$SO_2OCH_2C\mathbf{H}_2$), 3.50 (s, 4H, Ar-$SO_2OCH_2CH_2$-$OC\mathbf{H}_2$), and 2.45 (s, 6H, Ar-$C\mathbf{H}_3$). ^{13}C -NMR (100 MHz, $CDCl_3$) δ ppm: 144.86, 132.87, 129.8, 127.9, 70.65, 69.18, 68.71 and 21.63. FT-IR (cm-1): 2869, 1744, 1448, 1344, 1293, 1170, 1124, 1014, 978, 906, 849, 807, 772, 704, and 660. MALDI-TOF TOF: calculated MW = 458.55 and found m/z = 481.09 (M^++Na^+) and m/z =497.43 (M^++K^+).

Synthesis of 3, 6, 9, 12,15-pentaoxaheptadecane-1,17-diyl bis(4-methylbenzenesulfonate) (13b): Hexaethylene glycol (2.0 g, 7.10 mmol) was reacted with p-toluenesulfonyl chloride (3.0 g, 15.60 mmol) in the presence of KOH (3.2 g, 56.80 mmol) in dry DCM (30 mL) as described for **13a**. The product was further purified by column chromatography using ethyl acetate (60 % v/v) in hexane as eluent. Yield= 3.14 g (75 %). ^{1}H -NMR (400 MHz, $CDCl_3$) δ ppm: 7.80 (d, 4H, Ar - **H**), 7.35 (d, 4H, Ar - **H**), 4.16 (t, 4H, Ar-$SO_2OC\mathbf{H}_2CH_2$), 3.69 (t, 4H, Ar-$SO_2OCH_2C\mathbf{H}_2$), 3.61-3.58 (m, 16H, Ar-$SO_2OCH_2CH_2$-$OC\mathbf{H}_2$-), and 2.45 (s, 6H, Ar-$C\mathbf{H}_3$). ^{13}C -NMR (100 MHz, $CDCl_3$) δ ppm: 144.79, 132.82, 129.78, 127.90 , 70.63, 70.49, 70.43, 70.39, 69.22, 68.58, and 21.59. FT-IR (cm-1): 3394, 2878, 1719, 1646, 1600, 1453, 1351, 1294, 1215, 1171, 1097, 1031, 1005, 916, 813, 770 and 660. MALDI-TOF TOF: calculated MW = 590.69 and found m/z = 613.69 ($M^+ + Na^+$) and m/z = 629.02 ($M^+ + K^+$).

Synthesis of 4,4'-(((ethane-1,2-diylbis(oxy))bis(ethane-2,1-diyl))bis(oxy))dibenzaldehyde (14a): 4-Hydroxybenzaldehyde (2.9 g, 24.0 mmol) and anhydrous K_2CO_3 (6.0 g, 44.0 mmol) were taken in dry acetonitrile (40.0 mL) and it was refluxed under nitrogen atmosphere. **13a** (5.0 g, 11.0 mmol) was added and the reaction was continued for 48 h at 80 °C under nitrogen atmosphere. The reaction mixture was poured into the water and then extracted with ethyl acetate. The organic layer was dried over anhydrous Na_2SO_4 and the solvent was evaporated to get product as white solid. It was further purified by column chromatography using 40 % ethyl acetate/ pet ether system. Yield= 2.7 g (69 %). ^{1}H-NMR (400 MHz, $CDCl_3$) δ ppm: 9.88 (s, 2H, Ar - C**H**O), 7.80 (d, 4H, Ar - **H**), 7.01 (d, 4H, Ar - **H**), 4.21 (t, 4H, Ar-$OC\mathbf{H}_2CH_2$), 3.90 (t, 4H, Ar-$OCH_2C\mathbf{H}_2$), and 3.77 (s, 4H, Ar-OCH_2CH_2-$OC\mathbf{H}_2$). ^{13}C -NMR (100 MHz, $CDCl_3$) δ ppm: 190.70, 163.78, 131.90, 130.11, 114.85, 71.93, 69.54, and 67.74. FT-IR (cm-1): 2887, 1687, 1600, 1598, 1571, 1506, 1457, 1425, 1392, 1352, 1303, 1249, 1213, 1147, 1099, 951, 916, 826, 791, and 647. MALDI-TOF TOF: calculated MW = 358.39 and found m/z = 381.10 ($M^+ + Na^+$) and m/z = 397.07 ($M^+ + K^+$).

Synthesis of 4,4'-((3,6,9,12,15-pentaoxaheptadecane-1,17-diyl)bis(oxy))dibenzaldehyde (14b): 4-Hydroxybenzaldehyde (0.91 g, 7.4 mmol) was reacted with compound **13b** (2.00 g, 3.4 mmol) using anhydrous K_2CO_3 (1.87 g, 13.6 mmol) in dry acetonitrile (40 mL) as described for **14a**. It was further purified by

column chromatography using ethylacetate and pet ether mixture (1:1 v/v). Yield= 1.0 g (58 %). ^{1}H-NMR (400 MHz, $CDCl_3$) δ ppm: 9.88 (s, 2H, Ar - C**HO**), 7.82 (d, 4H, Ar - **H**), 7.02 (d, 4H, Ar - **H**), 4.21 (t, 4H, Ar-OC**H**$_2$CH$_2$), 3.88 (t, 4H, Ar-OCH$_2$C**H**$_2$), and 3.66-3.72 (m, 16H, Ar-OCH$_2$CH$_2$-OC**H**$_2$). ^{13}C-NMR (100 MHz, $CDCl_3$) δ ppm: 191.00, 163.78, 132.92, 130.00, 114.82, 70.85, 70.57, 70.53, 69.41, and 67.70. FT-IR (cm-1): 2870, 2740, 1690, 1600, 1590, 1510, 1450, 1430, 1390, 1350, 1310, 1260, 1220, 1160, 1100, 1050, 951, 835 and 615. MALDI-TOF TOF: calculated MW = 490.55 and found m/z = 513.14 ($M^+ + Na^+$) and m/z = 529.10 ($M^+ + K^+$).

Synthesis of 1, 8-tricyclodecanemethylenetosylate (TCD-OTs) (9): 1, 8 Tricyclodecanemethanol (5.8 g, 0.035 mol) and p-toluenesulfonylchloride (6.7 g, 0.035 mol) were dissolved in DCM (30 ml). Triethyamine (12.2 ml, 0.09 mol) was slowly added to the above solution under ice cold conditions. The above solution was stirred at room temperature for 24 h. The product was extracted in DCM and dried over anhydrous sodium sulphate. It was purified by passing through silica gel column using 2% ethyl acetate in hexane as eluent. Yield = 79 %. ^{1}H NMR ($CDCl_3$, 400 MHz) δppm: 7.81 (d, 2H, Ar-H), 7.37 (d, 2H, Ar-H), 3.84 (m, 2H, -OCH$_2$), 2.45 -0.79 (m, 18H, cyclic and aliphatic H). ^{13}C-NMR ($CDCl_3$ 100 MHz) δ: 144.4, 133.5, 129.7, 127.9 (Ar-C), 73.7(-OCH$_2$), 45.4, 44.9, 43.3, 41.1, 39.9, 34.1, 28.8, 27.5, 26.8, 26.3, 21.6 ppm (cyclic-C). FT-IR (KBr, cm^{-1}): 2925, 1600, 1508, 1458, 1366, 1229, 1178, 1101, 1027, 959, 831, 821 and 666. GC-MS (MW =320.4): 321.1 (M+1).

Synthesis of 1, 4-bis (1, 8-tricyclodecanemethyleneoxy) benzene (10): Hydroquinone (4.4 g, 0.04 mol) and NaOH (3.2 g, 0.08 mol) were dissolved in a mixture of water (4.8 mL) and ethanol (40 mL). TCD- tosylate (26.8 g, 0.08 mol) was added and the reaction mixture was refluxed for 24 h. The reaction mixture was poured into large amount of water, extracted in DCM and dried over anhydrous sodium sulphate. It was further purified by passing through silica gel column using 0.5 % ethyl acetate in hexane as eluent. Yield = (45 %). ^{1}H NMR ($CDCl_3$, 400 MHz) *δ*: 6.7 ppm (s, 4H, Ar-H); 3.6 ppm (m, 4H, -OCH$_2$); 2.5-0.88 ppm (cyclic H, 30 H). ^{13}C NMR ($CDCl_3$, 100 MHz): 153.2, 115.4 (Ar-C), 72.8 (Ar-OCH$_2$), 45.5, 45.2, 43.7, 41.2, 40.1, 34.5, 28.9, 28.0, 26.9, 26.4 (cyclic-C). FT-IR (KBr, cm^{-1}): 2946, 2866, 2357, 1643, 1508, 1466, 1390, 1282, 1283, 1109, 1028 and 824. GC-MS (MW = 406.60): 407.1 (M+1).

Synthesis of 1, 4-bis (bromomethyl)-2, 5-di-(1, 8-tricyclodecanemethyleneoxy) benzene (11): 1,4-bis(1,8-tricyclodecanemethyleneoxy)benzene (3.0 g, 7.39 mmol) and *p*-HCHO (0.8 g, 29.30 mmol) were taken in 100 ml of glacial acetic acid and HBr in glacial acetic acid (5.5ml, 20.35mmol) was added using a pressure equalizing funnel. The reaction mixture was then refluxed for 8 h, cooled to room temperature and poured into large amount of water. The product precipitated as white solid, which was repeatedly washed with cold water to remove acidic impurities. The product was filtered and recrystallised from a hot saturated solution of acetone. Yield = 95 %. m. p. = 135-136 °C. ^{1}H NMR ($CDCl_3$, 400 Hz) δ: 6.8 ppm (s, 2H, Ar-H), 4.5 ppm (s, 4H, -CH_2Br), 3.7 ppm (m, 4H, -OCH_2), 2.5-1 (m, 30H, cyclic H and aliphatic-H). ^{13}C NMR δ: ($CDCl_3$, 100 MHz): 150.6, 127.5, 114.7 (Ar-C), 72.9 (Ar-OCH_2), 45.6, 45.2, 43.8, 41.3, 40.3, 34.6, 29.0, 28.7, 27.9, 27.0, 26.5 (cyclic-C). FT-IR (KBr, cm^{-1}): 2946, 2863, 1510, 1442, 1405, 1313, 1225, 1028 and 688. GC-MS (MW = 592.45): 593.12 (M+1).

Synthesis of 1, 4-bis (tricyclodecanemethyleneoxy)-2, 5-Xylenetetraethyldiphosphonate (12): 1,4-bis(bromomethyl)-2,5-di-(1,8-tricyclodecanemethyleneoxy)benzene (2.9 g, 5.00 mmoL) and triethyl phosphite (1.6 g, 10 mmol) were refluxed at 150 °C and excess triethyl phosphite was removed by applying high vacuum. The product separated as thick yellow oil. Yield = (90 %). ^{1}H-NMR ($CDCl_3$, 400 MHz) δ: 6.8 ppm (s, 2H, Ar-H), 3.9 ppm (m, 8H, -PO-OCH_2), 3.6 ppm (m, 4H, Ar-OCH_2), 3.2 ppm (m, 4H, Ar-CH_2P), 2.5-0.8 ppm (m, 42H, aliphatic). ^{13}C-NMR ($CDCl_3$, 100 MHz): 150.3, 119.4, 115 (Ar-C), 72.9 (Ar-OCH_2), 61.9(P-O-C), 45.6, 45.2, 43.8, 41.3, 40.3, 34.6, 29.0, 28.7, 27.9, 27.0, 26.5 ppm (cyclic-C and aliphatic carbon). FT-IR (cm^{-1}): 2944, 1515, 1472, 1395, 1247, 1219, 1032, 957, 900, 831, 646 and 533.4. GC-MS (MW = 706.83): 707.62 (M+1).

Synthesis of 1, 4-dimethoxybenzene (6): 4-methoxy phenol (20.0 g, 0.161 mol) and KOH (18.0 g, 0.322 mol) were taken in methanol (70 mL) under ice cold conditions. Dimethyl sulphate (30.5 g, 0.242 mol) was added dropwise to this reaction mixture. This reaction mixture was stirred at room temperature for 48 h, extracted into dichloromethane, and washed with 5 % NaOH solution. The organic layer was dried over anhydrous sodium sulphate and condensed to get white solid. The product was

further purified by passing through silica gel column using ethyl acetate (1 % v/v) in hexane as eluent. Yield = 75 % (13.3g). ^{1}H-NMR ($CDCl_3$, 400 MHz) δ: 6.9 ppm (s, 4H, **Ar-H**) and 3.8 ppm (s, 6H, **OCH$_3$**). ^{13}C-NMR ($CDCl_3$, 100 MHz) δ: 153.7, 114.6 (Ar-**C**) and 55.7 (**OCH$_3$**). FT-IR (KBr, cm^{-1}): 3012, 2947, 2910, 2827, 1977, 1866, 1505, 1450, 1414, 1293, 1210, 1182, 1109, 1035, 804 and 582. MALDI-TOF-TOF-MS (MW = 138.16): *m*/*z* = 138.88 (M^+).

Synthesis of 1, 4-bis (bromomethyl)-2, 5-dimethoxy benzene (7) : 6 (5.0 g, 0.0362 mol) and paraformaldehyde (4.3 g, 0.145 mol) were reacted with HBr in acetic acid (35.0 mL, 0.072 mol) following the procedure as described for **11**. It was recrystallised from hot acetone. Yield = 66 % (11.7 g). ^{1}H-NMR ($CDCl_3$, 400 MHz) δ: 6.8 ppm (s, 2H, **Ar-H**); 4.5 ppm (s, 2H, **CH$_2$**Br) and 3.8 ppm (s, 6H, O**CH$_3$**). ^{13}C-NMR ($CDCl_3$, 100 MHz) δ: 151.2, 127.3, 113.8 (Ar-**C**), 56.2 (O**CH$_3$**) and 28.6 (**CH$_2$**Br) ppm. FT-IR (KBr, cm^{-1}): 1505, 1460, 1427, 1401, 1317, 1225, 1204, 1177, 1147, 1038, 889, 873, 717 and 663. MALDI-TOF-TOF-MS (MW = 324.01): *m*/*z* = 363.12 (M^+ + 39).

Synthesis of tetraethyl (2, 5-dimethoxy-1, 4-phenylene)bis (methylene) di phosphonate (8): 7 (3 g, 6.2 mmol) and triethyl phosphite (9 mL, 51.6 mmol) were reacted as described for **12**. Yield = 78 % (5.3 g). ^{1}H-NMR ($CDCl_3$, 400 MHz) δ: 6.8 ppm (s, 2H, aromatic), 4.0 ppm (m, 8H, PO**CH$_2$**CH_3), 3.7 ppm (s, 6H, **OCH$_3$**), 3.1 ppm (d, 4H, Ar-**CH$_2$**P) and 1.2 ppm (t, 12H, $POCH_2$**CH$_3$)**. ^{13}C-NMR ($CDCl_3$, 100 MHz) δ: 150.9, 119.3, 113.9 (Ar-**C**), 61.8 (PO**CH$_2$**CH_3), 56.1 (O**CH$_3$**), 27.1, 25.7, and 16.3 ppm. FT-IR (KBr, cm^{-1}): 2980, 2899, 2834, 1511, 1470, 1409, 1389, 1262, 1216, 1026, 959, 877, 813, 762, 722, 697, 627 and 582. MALDI-TOF-TOF-MS (MW = 438.16): *m*/*z* = 461.20 (M^+ + 23).

Synthesis of Segmented π-Conjugated OPV polymers:

Typical procedure is explained for P-TCD-3EG and other polymers were synthesized following similar procedure. Compound **12** (0.5 g, 0.7 mmol) and compound **14a** (0.25 g, 0.7 mmol) were dissolved in dry THF (12 mL). The mixture was stirred under nitrogen atmosphere about 15 min at 25 °C. Potassium tert-butoxide (5 mL in 1 M THF) was added dropwise to the polymerization mixture under a nitrogen atmosphere and the stirring was continued at 25 °C for 24 h. The resultant yellow-green polymer solution was concentrated using rotavapor and it was poured into a large amount of methanol (50 mL). The yellow-green polymer was filtered and washed with large

amount of methanol. The polymer was re-dissolved in tetrahydrofuran, filtered and precipitated into methanol. The purification procedures were followed at least twice. Yield = 0.55 g (91 %). ^{1}H-NMR ($CDCl_3$, 400 MHz) δ ppm: 7.45 (d, 4H, **Ar-H**), 7.32 (d, 2H, J = 16 Hz, C**H**=C**H**), 7.13 (d, 2H, J = 20 Hz, C**H**=C**H**), 7.05 (s, 2H, **Ar-H**), 6.92 (d, 4H, **Ar-H**), 4.17 (t, 4H, OC**H₂**), 3.89 (t, 4H, OC**H₂**), 3.78 (d, 4H, OC**H₂**-TCD), and 2.5 to 1.50 (m, 30H, **aliphatic-H**). ^{13}C-NMR ($CDCl_3$, 100 MHz) δ ppm: 158.27, 151.11, 131.11, 128.30, 127.58, 126.77, 121.80, 114.80, 111.04, 73.61, 70.89, 69.81, 67.46, 45.67, 45.27, 43.96, 41.27, 40.30, 34.74, 29.07, 27.98, 27.00, and 26.51. FT-IR (cm^{-1}): 2940, 2867, 1602, 1508, 1458, 1419, 1385, 1345, 1294, 1249, 1178, 1125, 1055, 1019, 967, 922, 848, and 818.

Synthesis of P-TCD-6EG: Compound **12** (0.5 g, 0.7 mmol) was reacted with compound **14b** (0.343 g, 0.7 mmol) using potassium tert-butoxide (5 mL in 1 M THF) in dry THF (10 mL) as described for **P-TCD-3EG.** Yield = 0.61 g (87 %). ^{1}H-NMR ($CDCl_3$, 400 MHz) δ ppm: 7.44 (d, 4H, **Ar-H**), 7.31 (d, 2H, J = 16 Hz, C**H**=C**H**), 7.12 (d, 2H, J = 16 Hz, C**H**=C**H**), 7.04 (s, 2H, **Ar-H**), 6.91 (d, 4H, **Ar-H**), 4.16 (t, 4H, OC**H₂**), 3.87 (t, 4H, OC**H₂**), 3.74 (m, 16H, OC**H₂**), 3.72 (d, 4H, OC**H₂**-TCD), and 2.5 to 1.50 (m, 30H, **aliphatic-H**). ^{13}C-NMR ($CDCl_3$, 100 MHz) δ ppm: 158.25, 151.08, 131.06, 128.30, 127.55, 126.63, 121.72, 114.78, 111.0, 73.60, 70.76, 70.55, 69.70, 67.43, 45.64, 45.24, 43.95, 41.26, 40.27, 34.73, 29.05, 28.0, 27.0, and 26.51. FT-IR (cm^{-1}): 2936, 2864, 1647, 1600, 1506, 1457, 1417, 1382, 1349, 1292, 1241, 1178, 1102, 1019, 959, 844, and 814.

Synthesis of P-Me-6EG: Compound **8** (0.5 g, 1.1 mmol) was reacted with compound **14b** (0.56 g, 1.1 mmol) using potassium tert-butoxide (6 mL in 1 M THF) in dry THF (10 mL) as described for **P-TCD-3EG.** Yield = 0.48 g (77 %). ^{1}H-NMR ($CDCl_3$, 400 MHz) δ ppm: 7.47 (d, 4H, **Ar-H**), 7.34 (d, 2H, J = 16 Hz, C**H**=C**H**), 7.10 (s, 2H, **Ar-H**), 7.05 (d, 2H, J = 16 Hz, C**H**=C**H**), 6.90 (d, 4H, **Ar-H**), 4.14 (t, 4H, OC**H₂**), 3.90 (s, 6H, OC**H₃**), 3.86 (t, 4H, OC**H₂**), and 3.73-3.67 (m, 16H, OC**H₂**). ^{13}C-NMR ($CDCl_3$, 100 MHz) δ: 158.34, 151.29, 130.82, 128.23, 127.70, 126.44, 121.14, 114.74, 108.84, 70.78, 70.58, 70.54, 69.69, 67.41, and 56.31. FT-IR (cm^{-1}): 2969, 1688, 1598, 1503, 1456, 1404, 1348, 1293, 1239, 1209, 1098, 1033, 953, and 810.

Synthesis of P-EH-6EG: Compound **3** (0.5 g, 0.8 mmol) was reacted with compound 14b (0.386 g, 0.8 mmol) using potassium tert-butoxide (5 mL in 1 M THF) in dry

THF (10 mL) as described for **P-TCD-3EG.** Yield = 0.58 g (90 %). ^{1}H-NMR ($CDCl_3$, 400 MHz) δ ppm: 7.45 (d, 4H, **Ar-H**), 7.35 (d, 2H, J = 16 Hz, C**H**=C**H**), 7.08 (d, 2H, J = 16 Hz, C**H**=C**H**), 7.10 (d, 2H, **Ar-H**), 6.91 (d, 4H, **Ar-H**), 4.15 (t, 4H, OC**H**$_2$), 3.87 (t, 4H, OC**H**$_2$), 3.67 (m, 16H, OC**H**$_2$), 3.94 (d, 4H, OC**H**$_2$-EH), 2.02 (m, 4H, OCH2-C**H**$_2$- C**H**$_2$), 1.82 (m, 2H, OCH$_2$-C**H**-CH$_2$), 1.64-1.38 (m, 18H, **aliphatic-H**), 0.98 (t, 6H, C**H**$_3$**),** and 0.92 (t, 6H, C**H**$_3$). ^{13}C-NMR ($CDCl_3$, 100 MHz) δ ppm: 158.29, 151.00, 131.04, 128.00, 127.56, 126.69, 121.50, 114.79, 111.08, 71.76, 70.82, 70.61, 70.57, 69.72, 67.45, 39.76, 30.92, 29.25, 23.10, 14.12, and 11.31. FT-IR (cm^{-1}): 2922, 2866, 1682, 1602, 1508, 1460, 1419, 1383, 1348, 1292, 1243, 1200, 1106, 1032, 959, 847, 818, 729, and 643.

Aqueous Self-Assembly of P-TCD-6EG Polymer: In a typical experiment, 2.0 mg of the polymer was dissolved in DMSO (1.5 mL) and THF (0.5 mL). Deionized water (3.0 mL) was added dropwise into the polymer solution. The resulting solution was stirred at 25 °C under dark conditions for 4 h. The solution was transferred to the semipermeable membrane having MWCO 1000 and then dialyzed against a large amount of deionized water for 48 h. Fresh water was replenished periodically to ensure the removal of THF and DMSO from the dialysis membrane. The dialyzed solution was filtered, lyophilized, and stored at 4 °C for further usage.

Cell-Viability Assay: The tetrazolium salt, 3-(4,5-dimethylthiazol-2-yl)-2,5-diphenyltetrazolium bromide (MTT) assay was employed in order to study the cytotoxic effect of the P-TCD-6EG polymer nanoparticles in HeLa Cells. For this experiment, a 96-well plate (Corning, USA) was used and each of its wells were seeded with 1000 cells in 100 μL of DMEM with 10% FBS (fetal bovine serum) and these were allowed to adhere for 16 h. The media from each well was aspirated followed by addition of various concentrations of the polymer to each well. These were added in triplicates corresponding to individual experiments. Cells in DMEM with FBS in the absence of polymer were also maintained in triplicates as a blank control. The 96 well plate was incubated for 72 h without changing the media. After 72 h medium from each well was aspirated and 100 μL of MTT solution (a freshly prepared stock of MTT in sterile PBS (5 mg/mL) diluted to 50 μg/mL in DMEM) was added. These were allowed to incubate for another 4 h at 37 °C. The formation of purple formazan crystals was observed that developed due to the reduction of MTT by

mitochondrial dehydrogenase enzyme from viable cells, and the media from each well was aspirated and 100 μL of DMSO was added to the resultant crystals giving purple solutions in each well. The absorbance from formazan crystals was immediately recorded using microplate reader at 570 nm (Varioskan Flash), which gave a representative of the number of viable cells per well. Values corresponding to each triplicate (of control and polymer treated cells) were determined and their mean was used for calculations. In the triplicates, any value that deviated from rest two were discarded. The mean of blank control set as 100% (corresponding to viable cells) and relative percentage values for polymer nanoparticle were calculated with respect to this (Cell viability assay was done by my lab mate Dr. Bapurao and Nilesh.

Cellular Uptake Studies: Flame dried coverslips were taken in 6 well plate in DMEM medium containing 10 % FBS. On the surface of these coverslips, HeLa cells were seeded at a density of 1×10^5 cells and these were incubated at 37 ºC for 16 h. The cells in each well, thus grown, were treated with required concentrations of P-TCD-6EG polymer nanoparticles. This was incubated at 37 °C for 4 h under CO_2 environment and then the media was aspirated from each well, and the cells were washed twice with PBS (2×1 mL) and fixed with 4% paraformaldehyde solution in PBS for 10 min at room temperature. The cells were washed twice with PBS (2×1 mL) and stained with phalloidin (red) conjugated to Alexa 610 (Invitrogen) diluted 1:100 in 5% BSA solution in PBS. These were incubated for 2 min, at room temperature in dark conditions, and then the excess dye was washed from the plate and the cells were gently rinsed with PBS. The coverslips were mounted on slides using Fluoromount mounting medium (Southern Biotech) and were left for drying overnight at room temperature in the dark. The cells were imaged using a confocal microscope using the λ **405** nm (blue channel) and λ **560** nm (red channel) lasers. Images thus obtained were analyzed using ImageJ analysis software and the image for each channel was separated and merged (Confocal microscopy imaging was done by my lab mate Sonashree).

3.3. Results and Discussions:

3.3.1. Synthesis and Characterization of Segmented Polymers

New classes of segmented polymers were synthesized through multistep reactions as shown in scheme-3.1. ω- Bis-benzaldehydes (compounds 14**a-14b**) were synthesized by reacting 4-hydroxybenzaldehyde with appropriate tosylates of oligo-ethylene glycols (compounds **13a-13b**). Three bisphosphonate esters having variable aliphatic and cycloaliphatic substitutions such as methoxy (**8**), 2-ethylhexyloxy (**3**) and tricyclodecanemethyleneoxy (**12**) were synthesized following our earlier procedure.[48-49] The polymerization of monomers **3 or 8 or 12** with equimolar amounts of bis-benzaldehydes (**14a-14b**) under Wittig-Horner conditions produced respective segmented polymers consisting of rigid oligo-phenylenevinylenes and oligo-ethyleneoxy flexible spacers in the polymer backbone.

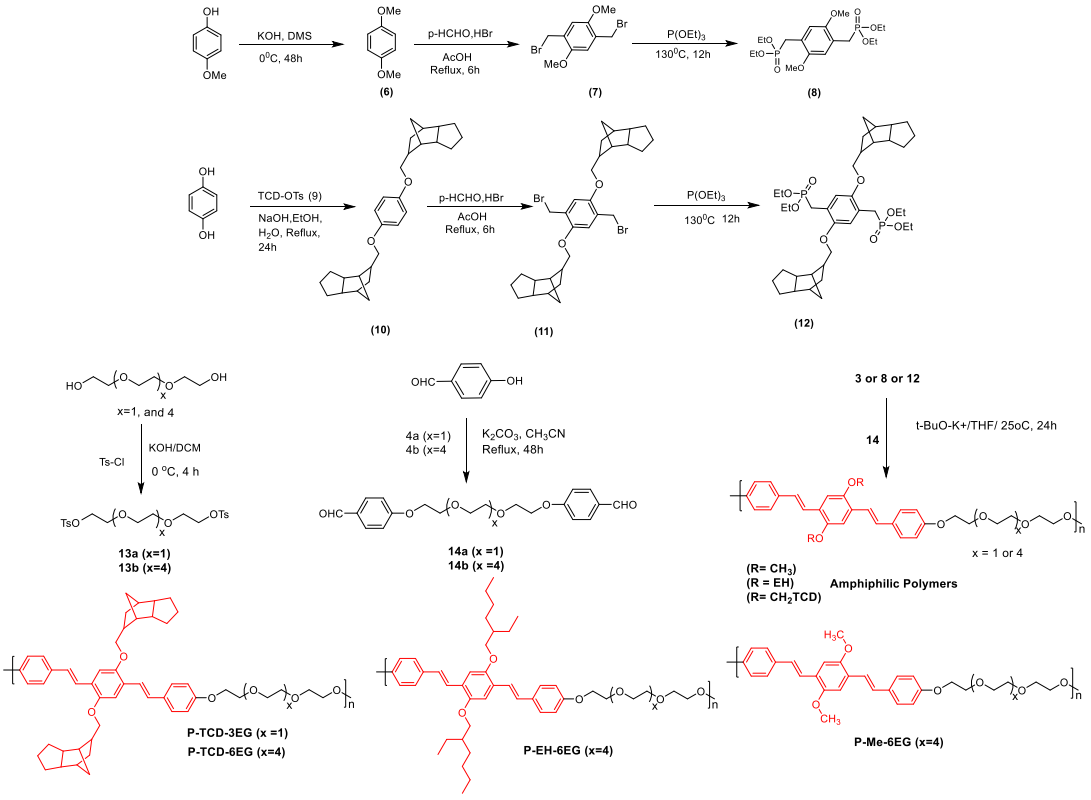

Scheme 3.1. *Synthesis of the main chain segmented polymers having rigid OPV core and flexible oligo-ethyleneoxy spacers.*

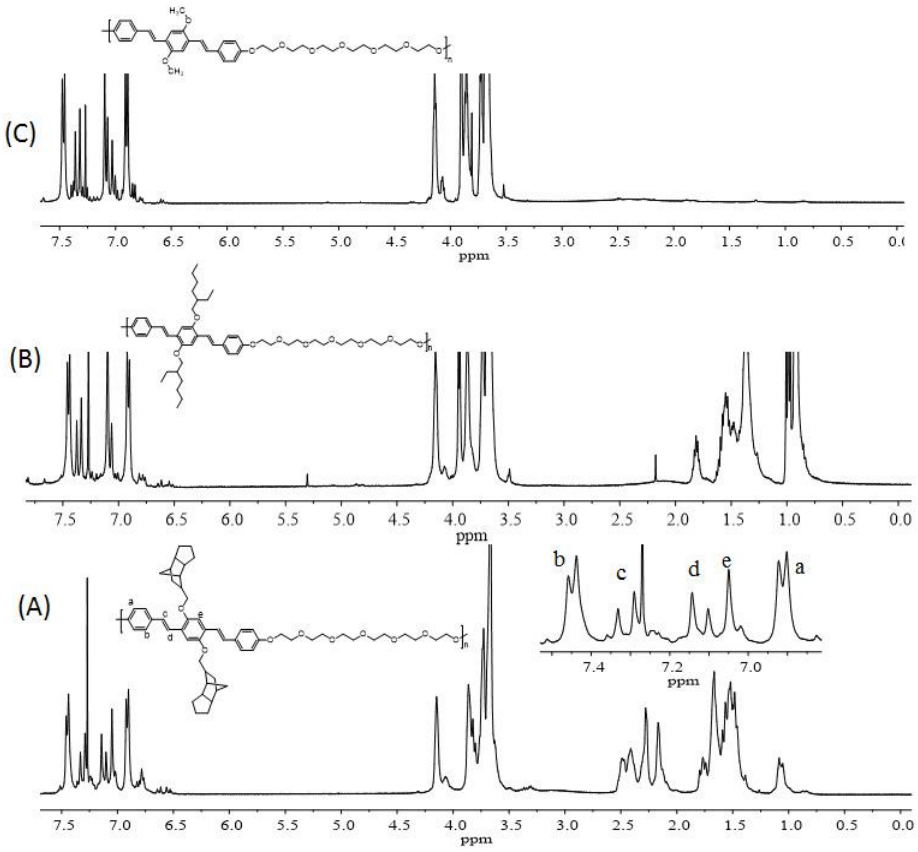

Figure 3.4. *^{1}H-NMR spectrum of P-TCD-3EG (A), P-EH-6EG (B), and P-Me-6EG polymer (C) in $CDCl_3$*

(a)

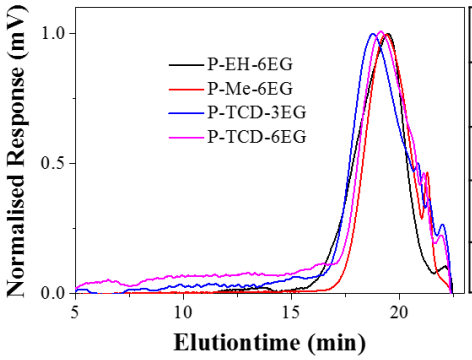

(b)

Sample	M_p	M_n	M_w	M_w/M_n
P-TCD-3EG	24,500	6,900	24,600	3.58
P-TCD-6EG	17,500	9,500	19,000	2.0
P-EH-6EG	12,200	10,000	28,000	2.78
P-Me-6EG	13,600	6,200	16,800	2.7

Figure 3.5. *GPC chromatograms of the segmented polymers in THF (a). Molecular weights of the segmented polymers (b)*

These polymers were referred as **P-Y-X**, where Y-represents ME, EH or TCD for the methoxy, ethylhexyloxy or tricyclodecanemethyleneoxy units, respectively, and X-for a number of oligoether units present in the flexible alkyl chains such as triethylene glycol (3EG) and hexaethylene glycol (6EG), respectively. For example, the TCD polymer with 6-EG unit is referred as P-TCD-6EG. The chemical structures of all the polymers are shown in scheme-1. The structures of the polymers were characterized by ^{1}H-NMR, ^{13}C-NMR, and FT-IR. ^{1}H-NMR spectra of the P-TCD-6EG polymer are showed in Figure 3.4A and different types of protons in the chemical structure are assigned by alphabets (see Figure 3.3 for NMR spectra of other polymers). The ^{1}H-NMR spectrum of the P-TCD-6EG polymer showed peaks from 7.46 to 6.90 ppm with an appropriate splitting pattern corresponding to aromatic phenylenevinylene protons (see Figure 3.4A). The two doublets belonged to trans-vinylene protons (c and d protons) appeared at 7.36 and 7.09 ppm (coupling constant J = 16 Hz). The peaks appeared at 7.43, 7.11 and 6.90 ppm were assigned to protons b, e, and a, respectively. The broad triplets at 4.10 ppm, 3.86 ppm were attributed to Ar-OC**H**$_2$C**H**$_2$ and 3.78 ppm is belonging to Ar-OC**H**$_2$-TCD protons, respectively. Among the two doublets in the vinyl protons, one of them merged with solvent peak at 7.26 ppm (see Figure 3.4a). TCD protons appeared below 3.5 ppm. The molecular weights of the polymers were determined by gel permeation chromatography (GPC) in tetrahydrofuran using polystyrene standards. The GPC chromatograms of the polymers appeared as mono-modal distribution except for P-TCD-3EG which showed was partially soluble in THF (see Figure 3.5a). The molecular weights of the polymers were obtained as M_w = 16800 to 28000 g/mol with a polydispersity of 2.0 to 3.5 (see figure 3.5b). Wittig-Horner polymerization route is typically known to produce polymers with 10-15 repeating units as observed by us[51,47] and others.[36] For biomedical applications, polymer molecular weights of < 40000 g/mol are preferred due to their easy clearance through the kidney. Hence, the custom designed polymers have molecular weight < 28,000 g/mol which is less than the acceptable range for biomedical imaging applications. Thermogravimetric analysis (TGA) of the polymers showed that the polymers were thermally stable up to 350 °C (see Figure-3.6a).

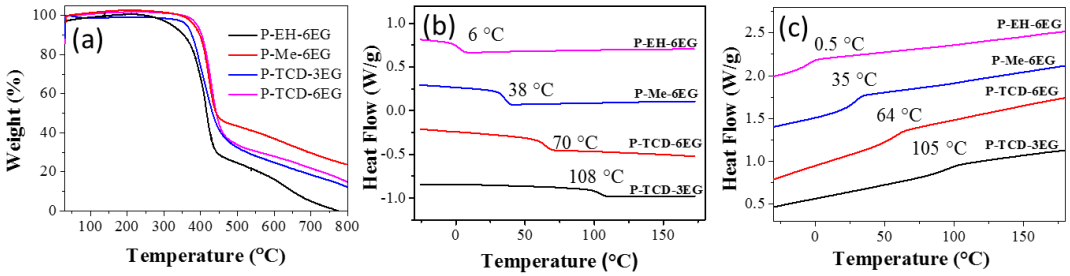

Figure 3.6. *TGA of the polymers under nitrogen at 10 ℃/min heating (a). DSC thermograms of polymers in heating (b) and cooling (c) cycles at 10 ℃/min .*

Differential scanning calorimetry (DSC) analysis of polymers was carried out at the heating/cooling cycle rate of 10 °C/min. DSC thermograms of the polymers at 10 ^{o}C/min heating are shown in Figure 3.6b. All the polymers were found to be completely amorphous and the DSC thermograms have shown only glass transition temperature (T_g) in cooling and heating cycles (see Figure-3.6c for their cooling cycles). The T_g's of the polymers gradually decreased from 108 to 70 °C upon increasing the length of the oligoethylene glycol segment from 3EG to 6EG in P-TCD-3EG to P-TCD-6EG. This trend is attributed to the increase in the flexibility of the polymer chains with an increase in the number of oligo-ethyleneoxy units in the segmented polymer chain. Further, the comparison among the 6EG spacer polymers revealed that the T_g values decreased with a decrease in the rigidity of the polymers in the following order TCD >ME>EH from 70 to 6 °C. This observation indicates that the cycloaliphatic TCD units introduced much higher rigidity in the OPV core compared to other two side chains. The variation of T_g values from 108 to 6 °C in the segmented polymers are clear indication that the rigidity of the π-conjugated units and varying the EG-spacers in the backbone are crucial factor for the rigidity of the structure. Among all these polymers, TCD units appeared to be very unique in producing highly rigid polymers with higher T_g values.

3.3.2. Aromatic π-Stack Aggregation and Emission Color-Tuning

The segmented OPV polymers are designed with different substitution in the central aromatic ring and flexible oligoethyelneoxy chains. This arrangement facilitates the strong aromatic π-stacking interaction among the OPV chromophores to maximize the self-assembly process. To study this effect in solution and solid state (in a thin film); the polymer samples were subjected to steady state photophysical studies and time-resolved fluorescent decay properties. The absorbance and emission spectra of P-TCD-3EG and P-TCD-6EG polymers were found to be almost identical in solution (see Figure 3.7a). In the solid state, the emission spectra of the hexaethylene glycol segmented P-TCD-6EG polymer showed 50 nm red-shift compared to the P-TCD-3EG polymer (see absorbance spectra in Figures 3.7a). This suggests that the TCD-substituted OPV chromophores became more facile to undergo self-assembly via aromatic π-interaction when they were separated by longer segmented spacers.

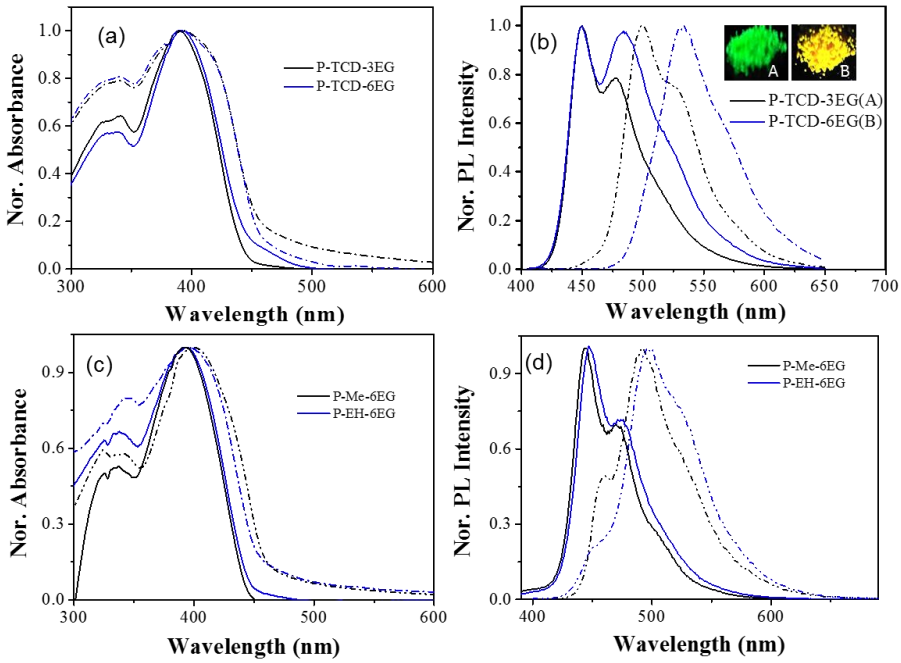

Figure 3.7 *The absorbance of P-TCD-3EG and P-TCD-6EG in $CHCl_3$ (solid line) and thin film (dotted line) (a). Emission of P-TCD-3EG and P-TCD-6EG in $CHCl_3$ (solid line) and thin film (dotted line) (b). The absorbance of P-Me-3EG and P-EH-6EG in $CHCl_3$ (solid line) and thin film (dotted line) (c). Emission of P-Me-3EG and P-EH-6EG in $CHCl_3$ (solid line) and thin film (dotted line) (d).*

The photographs of these polymer samples in Figure 3.7b showed greenish and yellow emission for P-TCD-3EG and P-TCD-6EG with respect to the 50 nm shift in their emission wavelength. This suggests that the increasing oligoethyleneoxy

segments between the adjacent OPVs increased the π-stacking interaction among the chromophores. The strong π-π stacking among the OPV cores induced emission-shift. This trend is attributed to the increasing the OPV self-aggregation with an increase in the segmented spacer length. Unlike P-TCD-6EG, the other 6EG-spacer polymers P-EH-6EG and P-ME-6EG did not show any significant color change in their emission spectra (see Figure 3.7d). Thus, the aromatic π-stacking interaction in the segmented polymer was mainly driven by the types of the OPV chromophores and in the present case TCD-OPV was very unique in exhibiting maximum packing among the various OPV π-cores. The segmented polymer with hexaethylene glycol (6EG) was found to more flexible than triethylene glycol spacer (3EG) which was evident from their T_g values (see Figure 3.6). The highly flexible chains possess high degree of freedom for both intrachain and interchain folding; as a result, the OPV could undergo strong aromatic π-stacking interactions. On the other hand, the shorter spacers (3EG) did not have sufficient flexibility to bend the chains which restrict the overlap between the OPV chromophores. These studies suggested that the longer segmented OPV polymers (> 6 EG units) have high tendency to undergo self-organization via aromatic π-stacking interaction. On the other hand, the shorter segmented lengths (< 3 EG units) did not provide enough flexibility for TCD-OPV chromophores in the polymer backbone for π-stacking induced self-assembly.

Typically polymer chains are expected to adopt either expanded or coil-like conformation with respect to the solvents in which they are present. For instance, a good solvent maximizes the solvent-polymer interaction and solvate the polymer chains in the expanded chain conformation whereas in poor solvents the polymer chains predominately adopt coil-like confirmation and precipitate the polymers.[47,50] Therefore, by appropriately choosing the combination of good and poor solvents; one can easily control the expanded or coil-like conformation in polymer chains. Since the segmented polymers showed very good spacer dependent self-assembly in the solid state, their solvent induced aggregated self-assembly were studied to trace their chain folding phenomena. For this purpose, two solvent combinations are chosen: (i) methanol/chloroform and tetrahydrofuran/water. Absorbance spectra of polymers (see Figures 3.8 and 3.10) showed a decrease in absorbance with an increase in methanol content in the solvent mixture. This trend is attributed to the variation in the molar extinction coefficient of OPV chromophores in the solvent combination.[51]

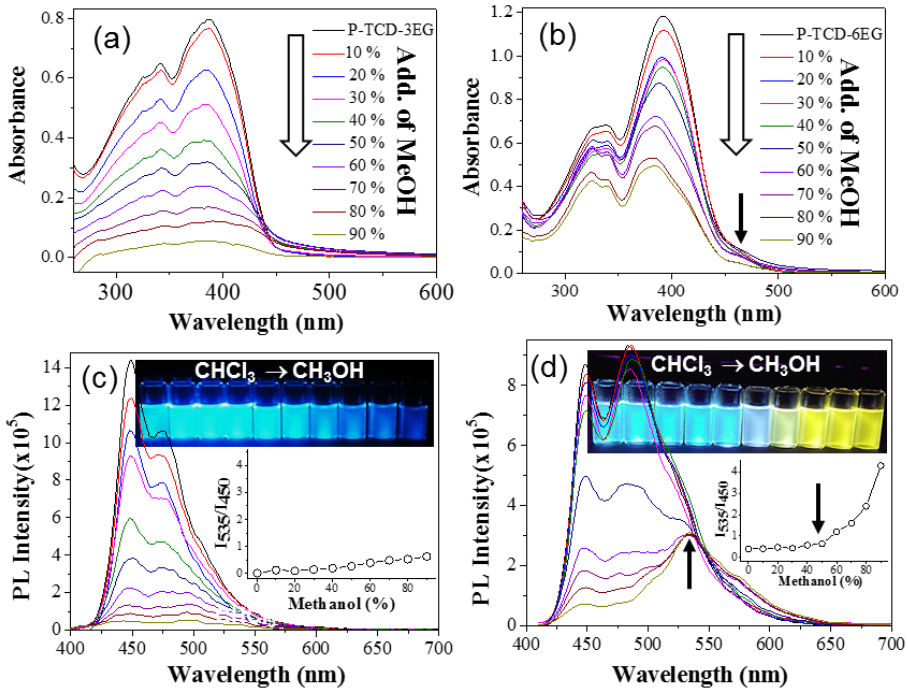

Figure 3.8 *Absorbance spectra of P-TCD-3EG (a) and P-TCD-6EG (b) in methanol/chloroform mixture. Emission spectra of P-TCD-3EG (c) and P-TCD-6EG (d) in methanol/chloroform mixture. The photographs are taken for polymer solutions in vials upon photo-excitation by UV-light at 365 nm. The concentration of the polymers were maintained as 2.5 x10^{-5} M.*

Interestingly P-TCD-6EG polymer showed an additional peak at 470 nm (shown by the arrow) with respect to the formation of π-induced OPV aggregates. This trend clearly indicates that P-TCD-6EG polymers have a high tendency for π-induced aggregation upon increasing the amount of methanol in the polymer solution. The emission spectra of P-TCD-3EG and P-TCD-6EG polymers in methanol/chloroform solvent combinations are shown in Figures 3.8c and 3.8d, respectively (see Figure 3.9 for P-EH-6EG and P-ME-6EG). The drastic decrease in the emission intensity of the spectra was attributed to the reduction in their molar extinction coefficient in their absorbance spectra. Interestingly, the long segmented P-PCD-6EG polymer showed excellent color tuning ability with the formation of new emission peak at higher wavelength region (which was absent in their lower counterpart P-TCD-3EG, see Figure 3.8c). The emission peak at λ_{em} =450 nm was assigned to isolated OPV chromophores and the new peak at λ_{em} =535 nm was assigned to OPV chromophore in the aggregated state (shown by the arrow). The comparison of the solid state emission maxima of P-TCD-6EG at 535 nm (see Figure

3.7b) and solvent induced aggregated emission peak at 537 nm (see Figure 3.8d) revealed that the OPV chromophores had attained maximum aromatic π-staking in methanol + chloroform mixture as equivalent to that of their interaction in the solid state. Further, to quantify the extent of aggregation in P-TCD-6EG (also P-TCD-3EG figure 3.8c), the ratio of the peaks λ_{em} = 535 /450 nm were plotted against the solvent composition and shown as an inset in Figures 3.8d. These plots showed distinct break points at 40-50 % methanol in chloroform for long segmented polymer for P-TCD-6EG (see Figure 3.8d) whereas the change is insignificant in short segmented polymer P-TCD-3EG (see Figure 3.8c). Additionally, the polymer solution of P-TCD-6EG showed excellent color tuning from blue-to-white-to-yellowish with an increase in the methanol composition in the solvent mixture (see the photographs in Figure 3.8).

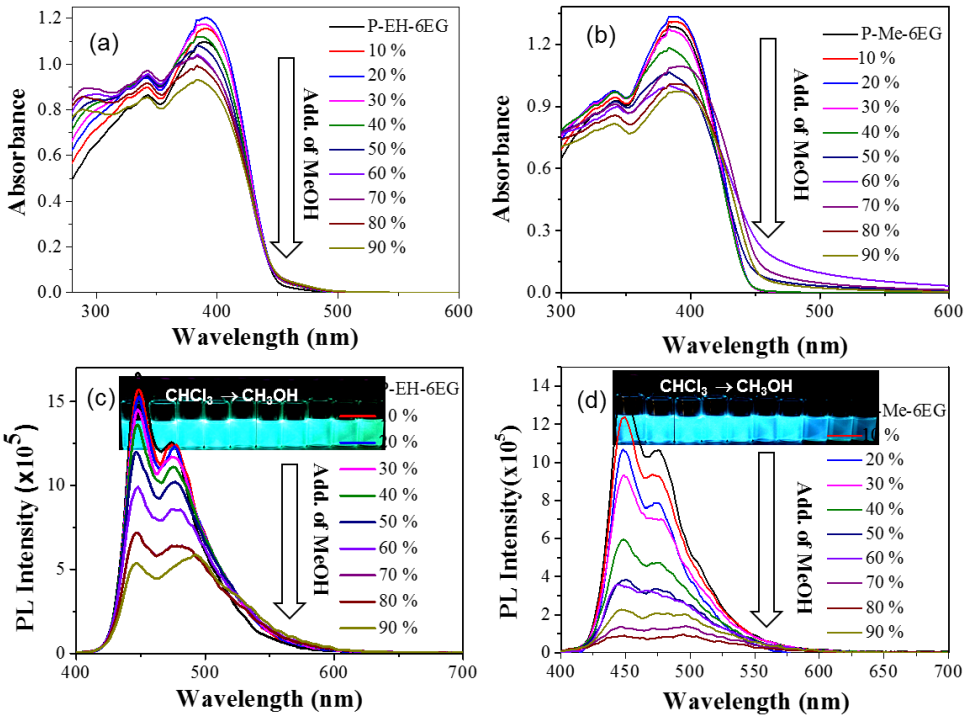

Figure 3.9. *The absorbance of P-EH-6EG in methanol/chloroform mixture (a). The absorbance of P-Me-6EG in methanol/chloroform mixture (b). Emission of P-EH-6EG in methanol/chloroform mixture (c). Emission of P-Me-6EG in methanol/chloroform mixture (d). In various solvent compositions and the photograph is taken upon photoexcitation by a UV-light source at 365 nm.*

Similar solvent induced aggregation experiments were carried out for P-EH-6EG and P-ME-6EG and these studies indicated that these polymers did not show π-stacking

interaction unlike P-TCD-6EG (see Figure 3.9). Based on these studies, it can be concluded that the TCD-OPV chromophores exhibited excellently π-induced aggregation compared to ethylhexyl and methoxy units in the segmented polymers. Furthermore, it is rather clear that the placing of the π-conjugated chromophores apart in the segmented backbone maximize the π-stack induced aggregation in segmented π-conjugated polymers.

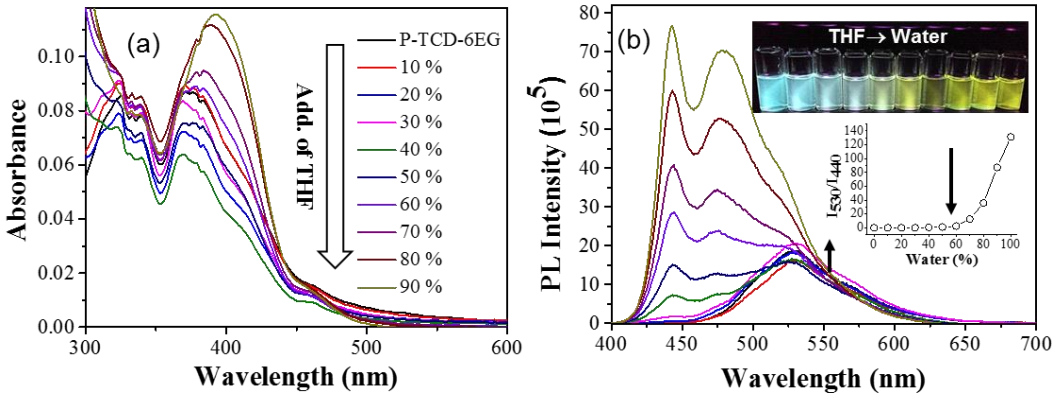

Figure 3.10 *Absorbance (a), and Emission (b) spectra of P-TCD-6EG in water/tetrahydrofuran solution. The photographs are taken for polymer solutions in vials upon photo-excitation by UV-light at 365 nm.*

In order to study the aqueous self-assembly of π-induced aggregation, the P-TCD-x polymers were dialyzed against large amount of water using cellulose semipermeable membrane of MWCO of 2000 g/mol for 48 h. The reservoir was continuously replenished with fresh water to ensure the removal of DMSO and THF from the polymer solution. Among the two segmented polymers, only P-TCD-6EG was found to produce stable aqueous solution whereas P-TCD-3EG (also P-ME-6EG) precipitated from water and not stable during the dialysis in water. The optical density of P-TCD-6EG was chosen as 0.1 and the composition of the solutions were varied from 10 to 90 v/v of THF+ water. The emission spectra of the P-TCD-6EG (see Figure 3.10b) showed the decrease in the emission intensity of the isolated OPV chromophores (at λ_{em} =450 nm) and new emission peak appeared for aggregated OPV chromophores (at λ_{em} =535 nm). The comparison of emission characteristics in water+THF combinations (see Figure 3.10b) with its solid state emission spectra of P-TCD-6EG (see Figure 3.7b) [or its aggregation in $CHCl_3$+methanol in Figure 3.8] revealed that TCD-OPV chromophores attained maximum aromatic π-staking in > 50 % water in THF or in 100 % water. Further, to quantify the extent of aggregation in P-

TCD-6EG the ratio of the peaks λ_{em} =535 /450 nm were plotted against the THF composition and shown as an inset in Figure 3.10b. This plot showed a distinct break point at 40-50 % of THF in water for P-TCD-6EG. The polymer P-TCD-6EG showed excellent color tuning from blue to white to yellowish with an increase in the water content in the solution (see Figure 3.10b) or in water. The emission spectra of P-TCD-6EG in the solvent combinations were fed into CIE color coordinate diagram and the details are shown in Figure 3.11. It is very interesting to notice that the P-TCD-6EG chains could be transforming its emission color from blue-to-white-to-yellow. At the intermediate solvent combination (50:50 %), both expanded and coil-like conformation coexisted in the polymer solution to produce white emission. This was further supported by the break points seen in the inset in Figures 3.8d and 3.10b. White light emission in the present system is observed due to the merging of blue and greenish yellow emission of isolated and aggregated OPV chromophores, respectively.

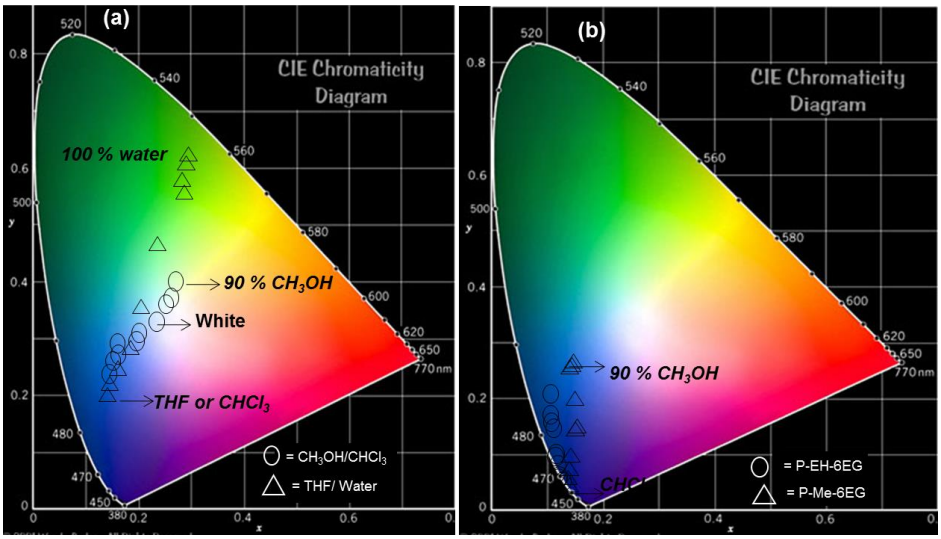

Figure 3.11. *CIE color coordinates of P-TCD-6EG polymer solution in THF+water (Δ) and $CHCl_3$+methanol (O) (a). CIE color coordinates of P-Me-6EG polymer in methanol/chloroform (Δ) and CIE color coordinates of P-EH-6EG polymer in methanol/chloroform (O) (b). The concentrations of the polymers were maintained as $2.5x10^{-5}$ M.*

The CIE color coordinates for the white emission was obtained as x = 0.25 and y= 0.36 which is in accordance for white emission as reported by us and others.[52-53,35] On the other hand, other polymers P-TCD-3EG, P-Me-6EG, and P-EH-6EG did not show such variation in the emission color in the CIE coordinates (see Figure 3.11). The

segmented polymers with P-Me-6EG polymers did not show the color tuning unlike the P-TCD-6EG polymers (both polymer have same spacer length; however, their substitution in the OPV cores varied). The difference for these behaviors can be correlated based on their structural arrangements from the single crystal data of methoxy substituted OPVs.[49] The three aryl rings in the methoxy substituted OPVs do not occupy the same plane and they were titled at either side by more than 34.02°. As a result, the OPVs became non-planar and expected to have less probability for the aromatic π-stacking for color tune-ability. On the other hand, the π-core consisting of the aryl rings in TCD substituted OPVs showed planar geometry in the single crystal structure.[50] Thus, strong aromatic π-stacking interactions were feasible among the TCD-OPVs for their unique color tuning-ability in the present segmented polymer system. This observation clearly supports that the P-TCD-6EG segmented polymer is very unique in structural design to undergo aromatic π-stacking to produce diverse luminescent colors. It is important to note that the present segmented OPV polymer design is one of the first examples to report color tuning in single π-conjugated polymer system. The fluorescence quantum yields for the polymer solutions were determined using quinine sulfate as standard.[47,51] The data quantum yields are plotted for both chloroform+methanol and THF+water solvent combinations. The quantum yields were found to decrease with the increase in the poor solvent amount (methanol or water) in the polymer solutions. The decrease in the quantum yield is attributed to the aggregated induced fluorescence quenching of the π-conjugated OPV chromophores.[54]

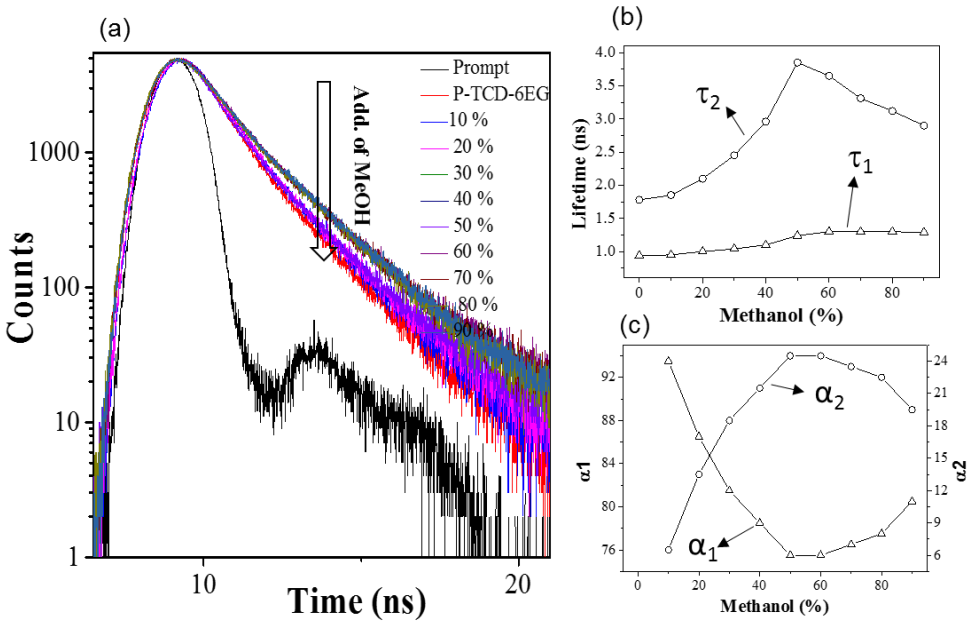

Figure 3.12. *TCSPC decay profiles of P-TCD-6EG polymers in methanol+chloroform solvent mixtures (a). Plots of fluorescent lifetime τ_1 and τ_2 (b) and fractional contribution α_1 and α_2 (c) of the polymers in methanol+chloroform solvent mixtures. The concentrations of the polymers were maintained as $2.5x10^{-5}$ M*

Table 3.1. Fluorescence lifetime (using Nano LED, excitation λ = 371nm) collected emission maximum of the P-TCD-6EG polymer in MeOH/$CHCl_3$.

Composition of MeOH (%)	τ_1 (ns)	τ_2 (ns)	A_1	A_2	χ^2
0	0.94	1.78	64.84	35.16	1.05
10	0.95	1.85	62.40	37.61	1.01
20	1.00	2.1	70.33	29.67	1.12
30	1.04	2.45	76.14	23.86	1.14
40	1.10	2.96	78.80	21.20	1.10
50	1.24	3.85	83.80	16.20	1.11
60	1.30	3.65	85.58	14.42	1.11
70	1.30	3.31	83.30	16.70	1.12
80	1.30	3.12	82.89	17.11	1.20
90	1.29	2.90	77.26	22.74	1.20

Time correlated single photon counting (TCSPC) was employed to study the excited state luminescent life times of P-TCD-6EG polymer in methanol/chloroform solvent combinations. The OPV chromophore was excited with 371 nm Nano LED source and the TCSPC decay profiles of the polymer are shown in Figure 3.12. The decay profiles of the polymer did not show many changes; however, a small decrease in the decay with an increase in the methanol compositions could be observed (see Figure 3.12a). These luminescence decay profiles were fitted with biexponential decay and their lifetime values are given in Table -3.1. The τ_1 and τ_2 values and their fractional contributions are plotted and shown in Figures 3.12b and 3.12c. The τ_1 and τ_2 represent the decay rate constant for isolated and aggregated OPV chromophores respectively. On increasing the methanol concentration, the value of τ_2 increased up to 60% MeOH/$CHCl_3$ and then attained a plateau. The higher τ_2 values indicate that the aggregated species indeed can fluorescence for a longer period. The fractional contributions were also showed break-points at 40-50 % methanol in the solvent mixtures. Hence, it may be concluded that the TCSPC decay studies supported the color tuning ability of the P-6EG polymer with a high luminescent lifetime in all three colors blue, white and yellow. On the basis of the photophysical studies, it may be concluded that the segmented OPV polymer possessed unique polymer geometry to undergo chain folding by the strong aromatic π-stacking on the backbone of the polymer chains.

3.3.3. Nanofibers, Hollow Spheres, and Nanoparticles

It is very clear from the photophysical studies that the P-TCD-6EG chains are capable of undergoing π-induced aggregation for color tuning from blue-to-white-to-yellow. To visualize the size and shape of the polymer aggregates accompanied by the above transition, the P-TCD-6EG samples in $CHCl_3$+methanol solvent combinations were subjected to FE-SEM and AFM analysis. These morphological features are given in Figure 3.13. The polymer showed nanofibrous morphology in chloroform alone (see Figure 3.13) and the length of helical nanofibers was estimated to be 10 µm to 20 µm and their widths were determined to be 20 nm to 50 nm in diameter. The closer observation revealed that thin and highly helical nano-fibres were produced by the longer segmented P-TCD-6EG. HR-TEM image was also further confirmed the existence of nanofibrous morphology in P-TCD-6EG (see Figure 3.13c). The P-TCD-6EG chains showed an excellent morphological transition from nano-fibers to

spherical nanoassemblies upon increasing the methanol amount in the solvent mixture (see Figure 3.13). The closer observation of spherical assemblies in 3.13e revealed that they are hollow. The observation was attributed to the folding or collapsing of the nano-fibres into hollow spheres. At higher methanol content, the morphology was turned completely into a spherical particle in nature (see Figure 3.13f).

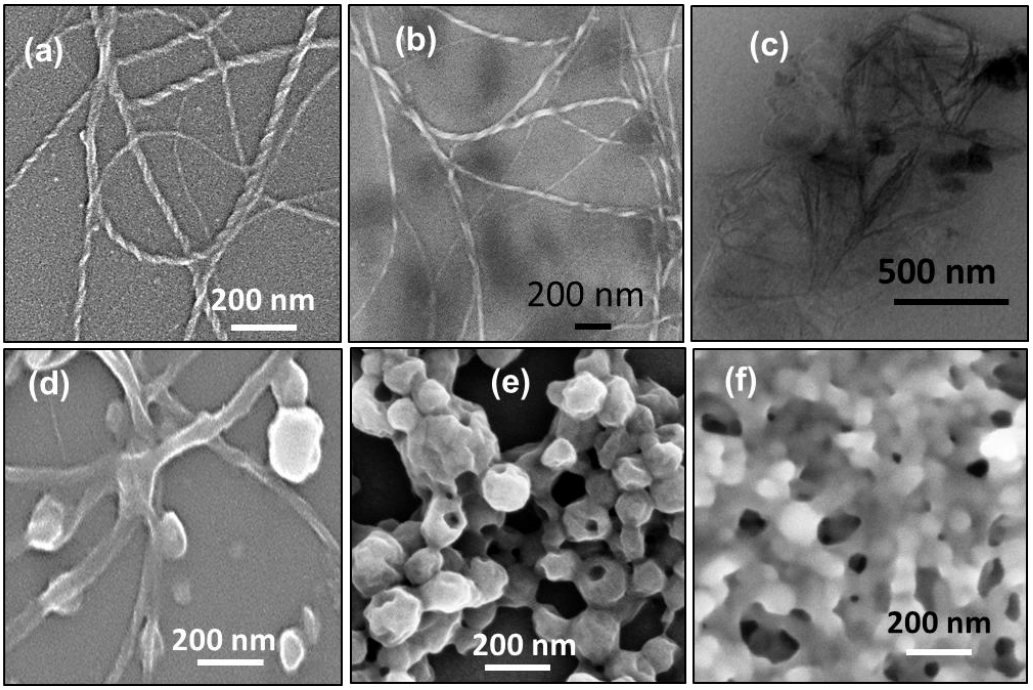

Figure 3.13. *FE-SEM images of P-TCD-6EG polymer (a) and (b) in chloroform; HR-TEM image of polymer; 20 % (b); 40 % (c) and 60 % (d) of methanol in chloroform. The concentrations of the polymers were maintained as* $1x10^{-5}$ *M.*

Atomic force microscope (AFM) images of P-TCD-6EG in chloroform showed highly twisted helical nano-fibrous (see Figure 3.14a) as seen in their FE-SEM images. AFM analysis showed the length of the fibres 5 to 10 µm with a thickness of 60 nm. AFM images of the polymer samples in solvent mixtures were recorded and shown in see Figures 3.14b to 3.14d. At 20 % methanol compositions, the polymer exhibited both helical nanofibers and hollow spheres (see Figure 3.14b). Upon increasing the methanol amount, the formation of hollow spheres became predominant and the nanofibrous morphology vanished completely (see Figures 3.14c and 3.14d). At 40 - 60 % methanol, the polymer chains produced exclusively hollow spheres of 400 nm in size. The depth profile of these objects clearly confirms their hollow structures (see inset in Figure 3.14d).

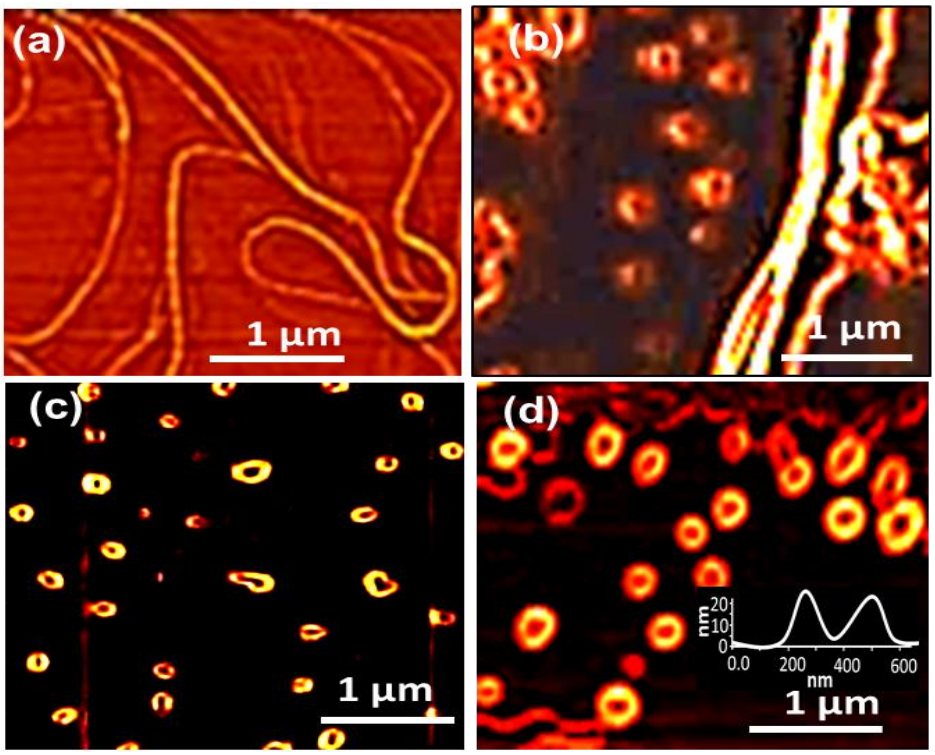

Figure 3.14. *AFM images of P-TCD-6EG polymer in chloroform (a); 20 % (b); 40 % (c) and 60 % (d) methanol in chloroform/methanol. The concentrations of the polymers were maintained as* $1x10^{-5}$ M.

The P-TCD-6EG polymer was also showed an excellent morphological transition from nano-fibers to spherical nanoassemblies in THF+water solvent mixture (see Figure 3.15b to 3.15f). FE-SEM and AFM images showed that the polymer chains exhibited the helical nanofibrous morphology in THF (see Figures 3.15a). Upon increasing the THF amount in the solvent mixture, the polymer transformed into hollow spherical assemblies as evident from their AFM images in Figures 3.15c to 3.15f. At 60 and 80 % THF in water, the polymer produced exclusively hollow-spheres (see Figures 3.15c and 3.15d). At 40 % THF in water (see Figure 3.15e) and the dialyzed aqueous solution (see Figure 3.15f, in water alone), the polymers were self-assembled into < 200 nm tiny nanoparticles which was confirmed by AFM image in Figure 3.15f. FE-SEM and high resolution TEM (HR-TEM) images of the dialyzed nanoparticles were recorded and showed in see Figure 3.16. These electron microscopic images exhibited the formation of spherical nanoparticles.

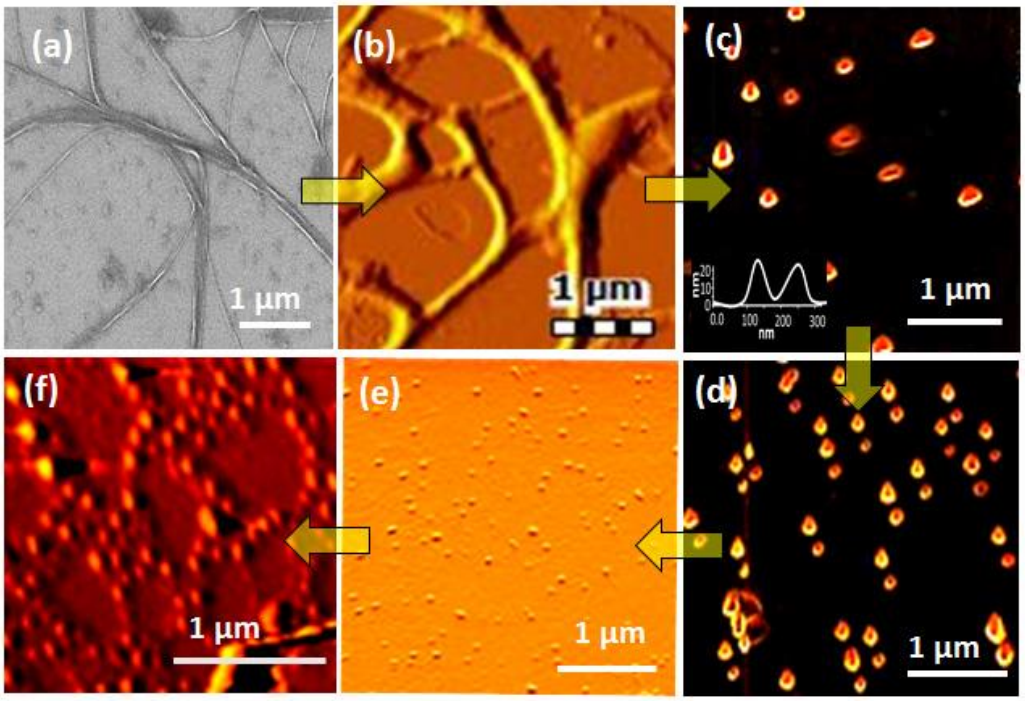

Figure 3.15. *P-TCD-6EG polymer FE-SEM image in THF (a); AFM image in THF (b); 20 % (c); 40 % (d); 60 % (e) water/THF composition, and in water (f). The concentrations of the polymers were maintained as* $1x10^{-5}$ *M.*

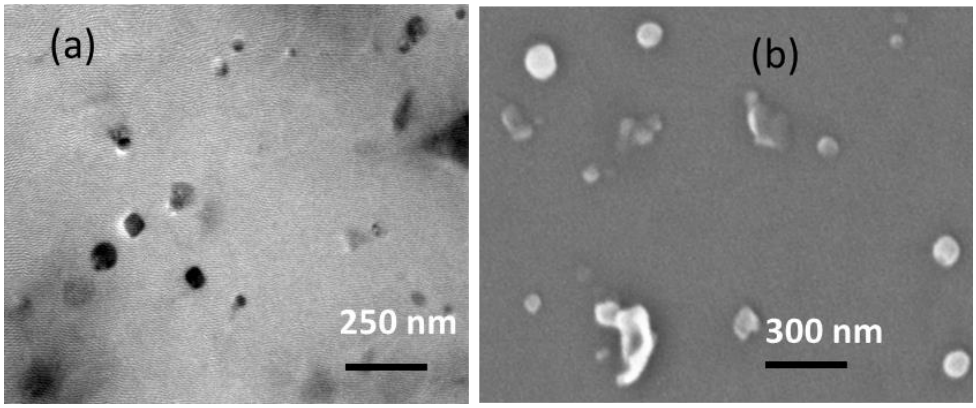

Figure 3.16. *HR-TEM image of P-TCD-6EG polymer (a) and FE-SEM image of P-TCD-6EG dialyzed polymer samples in water (b).*

In order to prove that the spherical nanoassemblies were pre-existed in the polymer solution and visualized as individual objects during imaging rather than they were produced during the solvent evaporation process; the polymer solutions were subjected to dynamic light scattering analysis. DLS histograms of THF+water and chloroform+methanol mixtures are shown in Figures 3.17 and 3.18. The dialyzed aqueous solution exhibited monomodal distribution with respect to particles in the

ranges of 200 ±20 nm (see Figure 3.21a). DLS histograms retained its mono-modal; however the size of the spherical objects became larger with a decrease in the amount of water in THF+water combinations. The size of the particles increase from 200 nm to 1.0 μm for 60 and 40 % of water in THF (see Figures 3.21b and 3.21c). This trend clearly suggests that upon increasing the THF concentration, the tightly packed nanoparticles slowly un-coiled into large size aggregates. The DLS histograms of chloroform+methanol solvent combination is also exhibited similar trend (see Figures 3.17a to 3.17f). For example, the polymers were self-assembled as mono-modal aggregated species in 60 % and 40 % methanol/chloroform (see Figures 3.17c and 3.17e) and it became multimodal larger aggregates in 20 % methanol/chloroform (see Figure 3.21f). These trends indicate that the polymer self-assembled as tightly packed spherical objects in bad solvents (in methanol or water) and expanded to larger sizes in good solvents (THF or chloroform) (The DLS histograms of other good and bad solvent combination see Figures 3.17 and 3.18). Thus, the DLS data directly evident that the morphological transition from spherical to nano-fibrous and vice versa are indeed occurred by the ability of the polymer chains to pre-assemble in the solvent combinations and not occurred by the solvent evaporation process while sample preparation for imaging.

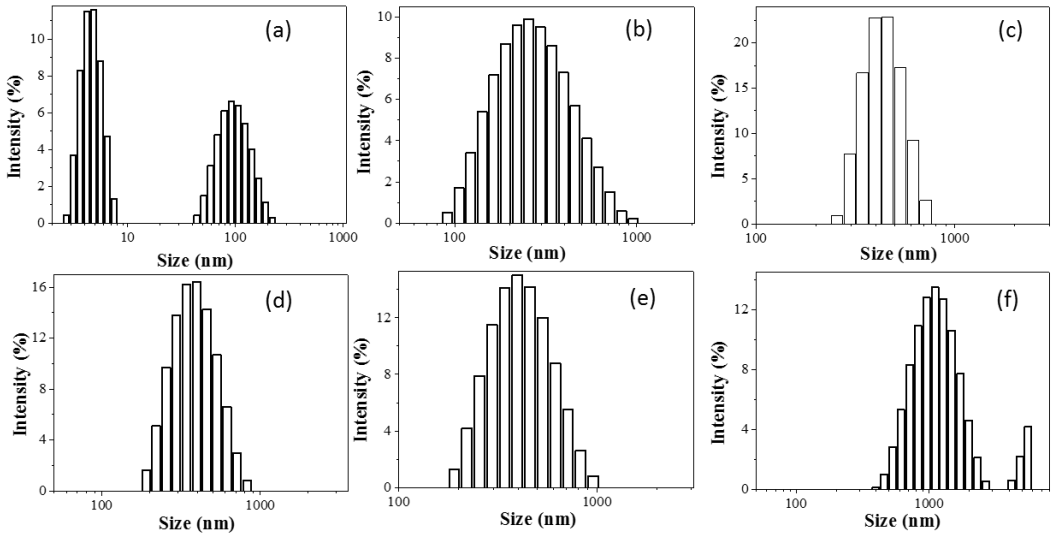

Figure 3.17. *DLS histograms of P-TCD-6EG 20 % (a), 30 % (b), 40 % (c), 50 % (d), 60 % (e), and 70 % (f) methanol/chloroform composition. The concentrations of the polymers were maintained as 2.5x10^{-4} M.*

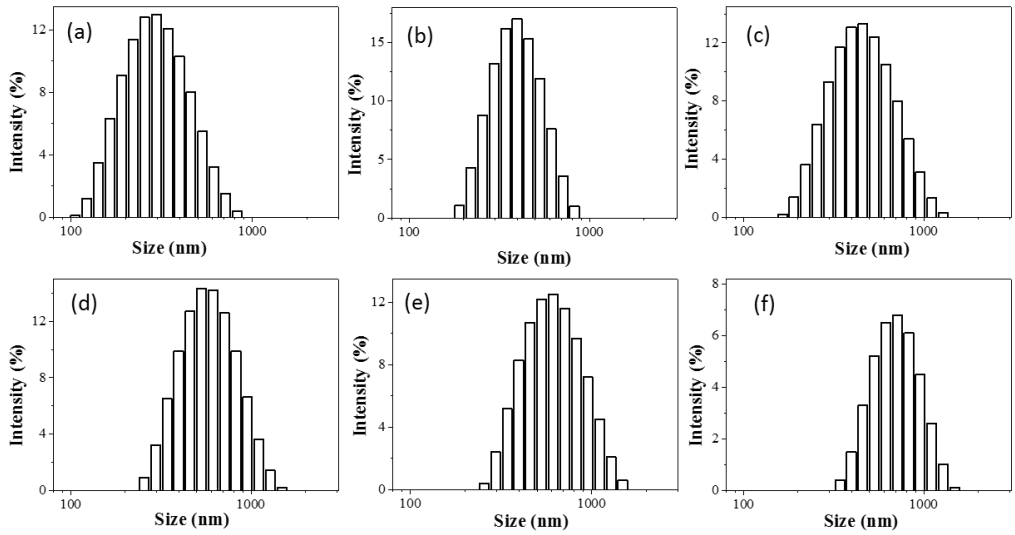

Figure 3.18. *DLS histograms of P-TCD-6EG in water (a), 20 % (b), 30 % (c), 40 % (b), 50 % (c), and 60 % (d) water/THF solvent mixture.*

The segmented polymer chains were solvated in good solvents (like chloroform and THF) in expanded chain conformation. These solvated chains undergo inter-chain aggregation to produce long fibril structure in the dropcaste films (see figures 3.13, 3.14, and 3.15). On the other hand, in poor solvents (like methanol and water), the polymer chains are collapsed to adapt coil-like conformation and these coiled chains would prefer to aggregates together to produce nanoparticles (see figures 3.13, 3.14, and 3.15). Thus, polymer topology played a crucial role on the self-assembly of these custom designed segmented OPV polymers. Based on the photophysical studies, color-tuning ability, morphological evidence, and DLS studies; the self-assembly of the segmented polymers are schematically drawn and shown in Figure 3.3. The following conclusion may be drawn for the unique self-assembly of custom-designed segmented TCD-OPV polymer. The polymer existed as solvated chains in good solvents (THF or chloroform) and exhibits blue-luminescence. The dropcaste film from the good solvent produces helical nanofibrous morphology. Upon increasing the bad solvent composition (water or methanol) in the polymer solution (THF+water or chloroform+methanol); the polymer chains experienced strong aromatic π-π stacking and produced layered intermediates via hydrophobic and hydrophilic interaction by the amphiphilic backbones. At this stage, the OPV π-core exists both in the aggregated (greenish yellow) and isolated form (blue) and their combination produced white color emission. The increase in the bad solvent amount

(methanol or water) increase the packing further and the layered assembly folded as spherical hollow particles and emit greenish yellow emission. The dialyzed polymer solution (in water alone); self-assembled structure appeared as tiny nanoparticles (no hollow structures are observed in the microscopic analysis) and luminescence as bright yellow color. Hence, the present segmented polymer design is very unique in producing diverse nanoassemblies such as nanofibres and hollow spheres and further capable of exhibiting luminescence color-tuning from blue-to-white-to-yellow in a single π-conjugated system.

3.3.4. Cytotoxicity and Bio-imaging

Water soluble π-conjugated polymers are emerging as important classes of luminescent probes for cellular imaging in biological system.[1-2, 55] The custom designed segmented TCD-OPV polymer produced very stable luminescent aqueous nano-particles. Thus, these nano-particles were employed as a bio-imaging probe for cancer cells. The cytotoxicity of the polymer nanoparticles were investigated in cervical (HeLa) and breast cancer (MCF 7) cell lines. The cytotoxicity of the polymer was tested in these cell lines by varying their concentration up to 60 μg/mL and the data are summarized in Figure 3.19. The nascent polymer nanoparticles were found to be non-toxic to cells and more than 90 % cell viability was observed in both cell lines. This data confirmed that the amphiphilic nanoparticles made by the segmented TCD-OPV polymers are very good biocompatible probes for cancer cells.

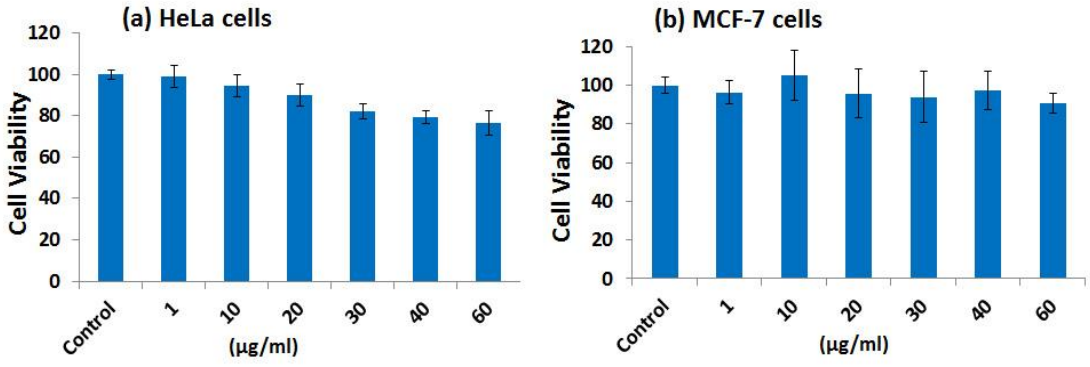

Figure 3.19. *Cytotoxicity of P-TCD-6EG polymer nanoparticles (a) in HeLa cells and (b) in MCF-7 cells.*

For cellular imaging, the polymer nanoparticle was administrated to HeLa cells and their confocal images were recorded and shown in Figure 3.20. Since the polymer nanoparticles are blue fluorescent, the cytoplasm of the cell was stained with Phalloidin (red fluorescent dye) and merged images distinctly showed the nucleus and cytoplasm. To study the influence of the incubation period on the polymer nanoparticles uptake; the cells were treated at various time intervals of 4 h, 8 h and 12 h with the polymer nanoparticles. The comparison of these images revealed that the cellular uptake of the polymer nanoparticles at 4h is almost similar to that of 8h and 12 h.

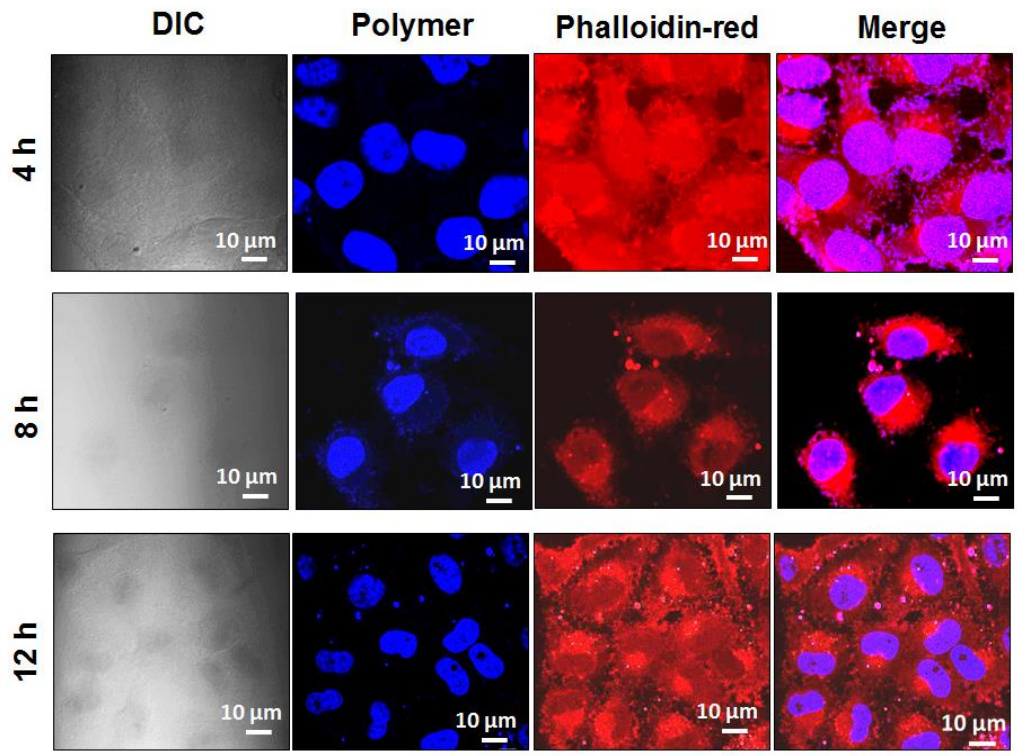

Figure 3.20. *Confocal images of HeLa cells incubated with P-TCD-6EG polymer at 4 h, 8 h, and 12 h. The cells were observed through the blue channel to locate the polymer (OPV chromophore) fluorescence. The actin cytoskeleton network in cells was stained with phalloidin (red).*

Most of the polymer nanoparticles are typically uptaken by the cells through endocytosis process. Our recent studies on the polymer nanoparticles in the treatment of the breast and colon cancer cell lines supported the similar observation.[56] Typically polyaromatic drugs or nuclear staining agents bind to the DNA in the nucleus by intercalation and aromatic π-stacking interaction.[56] Thus, the newly designed OPV

aromatic π-core may be underwent similar binding mechanism at the nucleus. Very recently we observed a similar trend for the binding of OPV based biodegradable block copolymer nanoassemblies.[55] These nanoparticles were found to be selectively accumulated in the nucleus of the cells. The merged image did not show any trace of the polymer particles in the cytoplasm. This observation makes these segmented OPV nanoparticles as ideal markers for the nucleus. These experiments confirmed that the blue luminescent nascent polymer nanoparticles are highly cell penetrable and very useful for cellular imaging applications in cancer diagnostics. Since OPV cores are very new entries for cellular imaging and the present manuscript explored their reproducibility in both cervical (HeLa) and breast (MCF 7) cell lines; the nuclear staining of OPVs would be expected to be similar for other cells as well. Further detail studies of DNA-OPV chromophores interactions are required to confirm this hypothesis. Owing to their biocompatibility, the structure of the segmented polymer can be further improvised to them as efficient anticancer drug carries along with intrinsic fluorescence as dual function delivery-cum-biomarkers in cancer therapy. Currently, the research work is focused on these directions to explore these segmented conjugated polymers in cancer therapy.

3.4. Conclusion

In summary, a new series of amphiphilic segmented π-conjugated polymers were designed and developed for studying their solvent-mediated diverse supramolecular assemblies and employed their aqueous nanoassemblies as a fluorescence probe for bio- imaging in cancer cells. The π-conjugated core was constituted by oligo-phenylenevinylene (OPV) units with variable anchoring units at the periphery to tune their rigidity and solubility for self-organization. The flexible segments were chosen from oligoethyleneoxy units and they were placed in the backbone of the chains to yield amphiphilic segment OPV polymers. Solvent induced aggregation ability of the segmented polymers were investigated in chloroform+methanol, THF+water and water alone. The π-conjugated OPV core was found to undergo strong aromatic π-π stacking upon increasing the composition of the bad solvent (water or methanol) in the polymer solution. Both the types of the OPV cores as well as the oligoethyleneoxy chain lengths were found to play an important role in directing the segmented polymers for diverse self-assembly. The polymer P-TCD-6EG was found to produce helical nanofibrous morphology in good solvents (chloroform or THF) and it underwent a morphological transition from fibres to hollow spheres upon varying the solvent composition. This morphological transition was also accompanied by the fluorescence color tuning by the OPV core. It was found that the chromophores exhibited blue-to-white-to-yellow color change along with the morphological transitions. Dynamic light scattering studies confirmed that the segmented polymers indeed produced stable spherical nano-aggregates of 200 nm in the solution. Steady state fluorescence studies and time-resolved fluorescent decay dynamic analysis confirmed the color tunability in the segmented π-conjugated polymers. The polymers produced stable nanoparticles assemblies in water with luminescent properties. Cytotoxicity in cervical and breast cancer cells revealed that these segmented polymer nanoparticles are non-toxic to cells. Confocal microscopy imaging revealed that the polymer nanoparticles selectively accumulated in the nucleus. The present design explored new segmented π-conjugated polymers for producing stable aqueous nanoparticles which are successfully demonstrated as potential candidates for bio-imaging applications. The segmented polymer design reported here not only restricted to OPV π-core, and in general it can be expanded to

wide ranges of other π-conjugated systems to explore this new concept for material and biomedical applications.

3.5. References

1. Li, K.; Liu, B. Polymer-encapsulated organic nanoparticles for fluorescence and photoacoustic imaging. *Chem. Soc. Rev.* **2014**, *43*, 6570−6597.
2. Zhu, C.; Liu, L.; Yang, Q.; Lv, F.; Wang, S. Water-Soluble Conjugated Polymers for Imaging, Diagnosis, and Therapy. *Chem. Rev*. **2012**, *112*, 4687−4735.
3. Bunz, U. H. F.; Seehafer, K.; Bender, M.; Porz, M. Poly(aryleneethynylene)s (PAE) as paradigmatic sensor cores. *Chem. Soc. Rev.* **2015**, *44*, 4322-4336.
4. Thomas III, S. W.; Joly, G. D.; Swager, T. M. Chemical Sensor Based on Amplifying Fluorescent Conjugated Polymers. *Chem. Rev*. **2007**, *107*, 1339-1386.
5. Kim, H. N.; Ren, W. X.; Kim, J. S.; Yoon, J. Fluorescent and colorimetric sensors for detection of lead, cadmium, and mercury ions. *Chem. Soc. Rev.* **2012**, *41*, 321-3244.
6. Wu, Y.; Tan, Y.; Wu, J.; Chen, S.; Chen, Y. Z.; Zhou, X.; Jiang, Y.; Tan, C.; M. Fluorescence Array-Based Sensing of Metal Ions Using Conjugated Polyelectrolytes. *ACS Appl. Mater. Interfaces* **2015**, 7, 6882−6888.
7. McQuade, D. T.; Pullen, A. E.; Swager, T. M. Conjugated Polymer-Based Chemical Sensors. *Chem. Rev*. **2000**, *100*, 2537−2574.
8. Bunz, U. H. F. Poly(aryleneethynylene)s: Syntheses, Properties, Structures, and Applications. *Chem. Rev*. **2000**, *100*, 1605-1644.
9. Xu, X.; Liu, R.; Li, L. Nanoparticles made of π-conjugated compounds targeted for chemical and biological applications. *Chem. Commun.* **2015** *51*, 16733-16749.
10. Ding, D.; Li, K.; Zhu, Z.; Pu, K.; Hu, Y.; Jiang, X.; Liu, B. Conjugated polyelectrolyte–cisplatin complex nanoparticles for simultaneous in vivo imaging and drug tracking. *Nanoscale*, **2011**, *3*, 1997-2002.
11. Feng, L.; Liu, L.; Lv, F.; Bazan, G.C.; Wang, S. Preparation and Biofunctionalization of Multicolor Conjugated Polymer Nanoparticles for Imaging and Detection of Tumor Cells. *Adv. Mater.* **2014**, *26*, 3926-3930.
12. Feng, X.; Tang, Y.; Duan, X.; Liu, L.; Wang, S. *J.* Lipid-modified conjugated polymer nanoparticles for cell imaging and transfection. *Mater. Chem.* **2010**, *20*, 1312-1316.
13. Akcelrud, L. Electroluminescent polymers *Prog. Polym. Sci*. **2003**, *28*, 875.

14. Kilbinger, A. F. M.; Schenning, A. P. H. J.; Goldoni, F.; Feast , W. J.; Meijer, E. W. Chiral Aggregates of α,ω-Disubstituted Sexithiophenes in Protic and Aqueous Media. *J. Am. Chem. Soc.* **2000,** *122,* 1820-1821.
15. Jiang, L.; Hughes, R. C.; Sasaki, D. Y. Supramolecular assembly of a quaterthiophene surfactant. *Chem. Commun.* **2004**, 1028-1029.
16. Henze, O.; Feast, W. J.; Gardebien, F.; Jonkheijm, P.; Lazzaroni, R.; Leclere, P.; Meijer, E. W.; Schenning, A. P. H. J. Chiral Amphiphilic Self-Assembled α,α‘-Linked Quinque-, Sexi-, and Septithiophenes: Synthesis, Stability and Odd−Even Effects. *J. Am. Chem. Soc.***2006** , *128* , 5923
17. Schenning, A. P. H. J.; Kilbinger, A. F. M.; Biscarini, F.; Cavallini, M.; Cooper, H. J.; Derrick, P. J.; Feast, W. J.; Lazzaroni, R.; Leclere, P.; McDonell, L. A.; Meijer, E. W.; Meskers, S. C. J. Supramolecular Organization of α,α‘-Disubstituted Sexithiophenes. *J. Am. Chem. Soc.* **2002,** *124,* 1269.
18. Abbel, R.; Weegen, R. V. D.; Meijer, E. W.; Schenning, A. P. H. J. Multicolor self-assembled particles of fluorene-based bolaamphiphiles. *Chem. Commun.* **2009**, 1697.
19. Shin, S.; Lim, S.; Kim, Y.; Kim, T.; Choi, T.; Lee, M. Supramolecular Switching between Flat Sheets and Helical Tubules Triggered by Coordination Interaction. *J. Am. Chem. Soc.***2013,** *135,* 2156-2159.
20. Lee, E.; Jeong, Y.; Kim, J.; Lee, M. Controlled Self-Assembly of Asymmetric Dumbbell-Shaped Rod Amphiphiles: Transition from Toroids to Planar Nets. *Macromolecules.* **2007**, *40,* 8355-8360.
21. Ryu, J.; Lee, M. Transformation of Isotropic Fluid to Nematic Gel Triggered by Dynamic Bridging of Supramolecular Nanocylinders. *J. Am. Chem. Soc.* **2005,** *127,* 14170-14171.
22. Moon, K.; Kim, H.; Lee, E.; Lee M.; Self-Assembly of T-Shaped Aromatic Amphiphiles into Stimulus-Responsive Nanofibers. *Angew. Chem. Int. Ed.* **2007**, *46,* 6807.
23. Moon, K.; Lee, E.; Lee M.; Synthesis and self-assembly of propeller-shaped amphiphilic molecules. *Chem. Commun.* **2008**, 3061-3063.
24. Rest, C.; Mayoral, M. J.; Fucke, K.; Schellheimer, J.; Stepanenko, V.; Ferna`ndez, G.; Self-Assembly and (Hydro)gelation Triggered by Cooperative π–π and Unconventional C[BOND]H···X Hydrogen Bonding Interactions. *Angew. Chem., Int. Ed.,* **2014,** *53,* 700-705.

25. Ajayaghosh, A.; Varghese, R.; Mahesh, S.; Praveen, V. K.; From Vesicles to Helical Nanotubes: A Sergeant-and-Soldiers Effect in the Self-Assembly of Oligo(p-phenyleneethynylene)s. *Angew. Chem. Int. Ed.* **2006**, *45*, 7729.
26. Shin, S.; Gihm, S. H.; Park, C. R.; Kim, S.; Park, S. Y. Water-Soluble Fluorinated and PEGylated Cyanostilbene Derivative: An Amphiphilic Building Block Forming Self-Assembled Organic Nanorods with Enhanced Fluorescence Emission. *Chem. Mater.* **2013**, *25*, 3288-3295.
27. Hulvat, J. F.; Sofos, M.; Tajima, K.; Stupp, S. I. Self-Assembly and Luminescence of Oligo(p-phenylene vinylene) Amphiphiles. *J. Am. Chem. Soc.* **2005**, *127*, 366-372.
28. Zhang, X.; Gorl, D.; Wurthner, F.; White-light emitting dye micelles in aqueous solution. *Chem. Commun.* **2013**, *49*, 8178-8180.
29. Zhang, X.; Chen, Z.; Wurthner, F.; Morphology control of fluorescent nanoaggregates by co-self-assembly of wedge- and dumbbell-shaped amphiphilic perylene bisimides. *J. Am. Chem. Soc.* **2007**, *129*, 4886-4887.
30. Kim, Y.; Ll, W.; Shin, S.; Lee, M.; Development of Toroidal Nanostructures by Self-Assembly: Rational Designs and Applications. *Acc. Chem. Res*. **2013**, *46*, 2888-2897.
31. Rahaman, M.; Ghosh, S.; Aqueous self-assembly of chromophore-conjugated amphiphiles. *Phys. Chem. Chem. Phy.* **2014**, 16, 26672-26683.
32. Wang, H.; Wang, H. H.; Urban, V. S.; Littrell, K. C.; Thiyagarajan, P.; Yu, L.; Syntheses of Amphiphilic Diblock Copolymers Containing a Conjugated Block and Their Self-Assembling Properties. *J. Am. Chem. Soc.* **2000**, *122*, 6855-6861.
33. Luo, Y.; Liu, H.; Xi, F.; Li, L.; Jin, X.; Han, C. C.; Chan, C.; Supramolecular Assembly of Poly(phenylene vinylene) with Crown Ether Substituents To Form Nanoribbons. *J. Am. Chem. Soc.* **2003**, *125*, 6447-6451.
34. Lee, E.; Hammer, B.; Kim, J. K.; Page, Z.; Emrick, T.; Hayward, R. C. Hierarchical Helical Assembly of Conjugated Poly(3-hexylthiophene)-block-poly(3-triethylene glycol thiophene) Diblock Copolymers. *J. Am. Chem. Soc.* **2011**, *133*, 10390-10393.
35. Hu, Y.; Su, M.; Ma, C.; Yu, Z.; Liu, N.; Yin, J.; Ding, Y.; Wu, Z.; Multiple Stimuli-Responsive and White-Light Emission of One-Pot Synthesized Block Copolymers Containing Poly(3-hexylthiophene) and Poly(triethyl glycol allene) Segments. *Macromolecules* **2015**, *48*, 5204-5212.

36. Yang, Z.; Sokolik, I.; Karasz, F. E. A Soluble Blue-Light-Emitting Polymer. *Macromolecules*, **1993**, *26*, 1188-1190.
37. Chen, Y.; Xu, Y.; Perry, K.; Sokolov, A. P.; More, K.; Pang, Y. Achieving Diameter-Selective Separation of Single-Walled Carbon Nanotubes by Using Polymer Conformation-Confined Helical Cavity. *ACS Macro Lett*. **2012**, *1*, 701-705.
38. Chen, Y.; Malkovskiy, A.; Wang, X-Q.; Lebron-Colon, M.; Sokolov, A. P.; Perry, K.; More, K.; Pang, Y. Selection of Single-Walled Carbon Nanotube with Narrow Diameter Distribution by Using a PPE–PPV Copolymer. *ACS Macro Lett*. **2012**, *1*, 246-251.
39. Lokey, R. S.; Iverson, B.L. Synthetic molecules that fold into a pleated secondary structure in solution. *Nature* **1995**, *375*, 303-305.
40. Gabriel, G. J.; Sorey, S.; Iverson, B. L., Altering the Folding Patterns of Naphthyl Trimers. *J. Am. Chem. Soc.***2005**, *127*, 2637-2640.
41. Ghosh, S.; Ramakrishnan, S.; Structural Fine-Tuning of (Donor-spacer-acceptor-spacer)$_n$ Type Foldamers. Effect of Spacer Segment Length, Temperature, and Metal-Ion Complexation on the Folding Process. *Macromolecules* **2005**, *38*, 676-686.
42. Ghosh, S.; Ramakrishnan, S. Aromatic donor-acceptor charge-transfer and metal-ion-complexation-assisted folding of a synthetic polymer. *Angew. Chem. Int. Ed.* **2004**, *43*, 3264-3268
43. Ghosh, S.; Ramakrishnan, S. Small molecule induced folding of a synthetic polymer. *Angew. Chem. Int. Ed.* **2005**, *44*, 5441-5447.
44. Tan, T. A. T.; Clarke, T. M.; James, D.; Durrant, J. R.; White, J. M.; Ghiggino, K. P. Synthesis and photo-induced charge separation of confined conjugation length phenylene vinylene-based polymers. *Polym. Chem.* **2013**, *4*, 5305–5309.
45. Balamurugan A.; Reddy, M. L. P.; Jayakannan, M. π-conjugated Polymer-Eu3+ Complexes: A Versatile Luminescent Molecular probe for Temperature Sensing. *J. Mater. Chem. A.* **2013**, *1*, 2256-2266.
46. Balamurugan, A.; Kumar, V.; Jayakannan, M. Triple action Polymer Probe: Carboxylic Distilbene Fluorescent Polymer Chemosensor for Temperature, Metal-ion and Biomolecules. *Chem. Commun.* **2014**, *50*, 842−845.

47. Goel, M.; Narasimha, K.; Jayakannan, M. Helical Self-assemblies of Segmented Poly(phenylenevinylene)s and their Hierarchical Donor-Acceptor Complexes. *Macromolecules* **2014**, *47*, 2592−2603.
48. Narasimha, K.; Jayakannan, M. π-Conjugated Polymer Anisotroipic Organogel Nano-fibrous Assemblies for Thermo-responsive Photonic Switches. *ACS Appl. Mater. Interfaces* **2014**, 6, 19385−19396.
49. Goel, M.; Narasimha, K.; Jayakannan, M**.** Direct Evidence for Secondary Interactions in Planar and Nonplanar Aromatic π-Conjugates and Their Photophysical Characteristics in Solid-State Assemblies. *J. Phys. Chem. B.* **2015**. *119*, 5102-5112.
50. Goel, M.; Jayakannan, M. Herringbone and Helical Self-assembly of π -conjugated Molecules in Solid State through CH/π Hydrogen Bond. *Chem. - Eur. J*. **2012**, *18*, 11987−11993.
51. Amrutha, S. R.; Jayakannan, M**.** Probing the π -stack Induced Molecular Aggregation in π-Conjugated Polymers, Oligomers and Their Blends of Poly(phenylenevinylene)s. *J. Phys. Chem. B.* **2008**. *112*, 1119-1129.
52. Sonawane, S. L.; Asha, S.K. Blue, Green, and Orange-Red Emission from Polystyrene Microbeads for Solid-State White-Light and Multicolor Emission. *J. Phys. Chem. B*. **2014**, *118*, 9467-9475.
53. Balamurugan, A. Reddy, M. L. P.; Jayakannan, M. Single polymer Photosensitizer for Tb3+ and Eu3+ ions: A Novel Approach for White Light Emission based on Carboxylic Functionalized poly(m-phenylenevinylene)s. *J. Phys. Chem. B*. **2009**, *113*, 14128-14138.
54. Resta, C.; Pietro, S. D.; Elenkov, M. M.; Hamersak, Z.; Pescitelli, G.; Bari, L. D. Consequences of Chirality on the Aggregation Behavior of Poly[2-methoxy-5-(2′-ethylhexyloxy)-p-phenylenevinylene] (MEH-PPV). *Macromolecules,* **2014,** *14, 4847-4850.*
55. Kulkarni, B.; Surnar, B.; Jayakannan, M. Dual Functional Nanocarrier for Cellular Imaging and Drug Delivery in Cancer Cells Based on π -Conjugated Core and Biodegradable Polymer Arms. *Biomacromolecules,* **2016,** *17, 1004*-1016.
56. Pramod, P. S.; Shah, R.; Sonali, C.; Balasubramanian, N.; Jayakannan, M. Polysaccharide Nano-vesicular Multidrug Carrier for Synergistic Killing of Cancer Cells. *Nanoscale*, **2014**, *6*, 11841- 11855.

Chapter 4

Segmented π-Conjugated Polymer-Arylenebisimide Based Room Temperature Charge-Transfer Complexes and Their Color Tunability

Abstract:

New room temperature stable solid state charge transfer (CT) complexes based on electron rich oligo-phenylenevinylene (OPV) and electron deficient arylenebisimides were reported. Semi-crystalline and amorphous segmented OPV polymers are chosen and they were complexed with naphthalene (NDI) and phenylene (PDI) biimides to produce red and green coloured CT complexes absorbance from the visible to NIR region in the solar spectrum. The CT complexes exhibited 1:1 complexation for donor polymers and acceptor NDI (or PDI) molecules with respect to long range order o D-A-D-A-D-A π-stacked supramolecular assemblies. Interestingly, the solid state alignment of the D-A interaction was controlled by the types of the electron deficient acceptor units; as a result OPV polymer-NDI complex was found to exhibit two dimensional lamellar packing. Electron microscope, polarizing microscope and X-ray diffraction analysis provided direct evidence for the lamellar D-A self-assembly. The role of macromolecular effect on the D-A complexation in the CT complex was investigated using structurally identical small molecular OPV analogues. The OPV-NDI and OPV-PDI complexes were found to exhibit CT band in the solution; however, the phase separation of individual D and A crystalline domains of these small molecules hampered the CT self-assembly in the solid state. Interestingly, the superior ability of supramolecular organization of long chain polymers produced stable CT complexes under atmospheric conditions at room temperature. Due to OPV containing segmented polymer-NDI or PDI complexes were found to exhibit. This enabled the accomplishment of first examples of room temperature CT complexes in π-conjugated polymer system having absorption from 350 to 1100 nm based on OPV-NDI and OPV-PDI diads. Additionally, these stable room temperature donor-acceptor CT self-assemblies can be processed under solvent free melt crystallization process; thus, they are very important futuristic materials for directly processing in optoelectronics. The present investigation open up a new platform for D-A CT complexes in π-Conjugated polymers, more exclusively based on segmented polymer concept which are new entries in the literature.

4.1. Introduction

Supramolecular assembly of electron rich donor (D) and deficient acceptor (A) molecules have been widely explored for energy generation devices.[1-5] Electron rich donor-type semiconducting polymers such as poly(pheynelevinylene)s (PPV), poly(3-alkylthiophenes), and polyfluorenes were blended with electron deficient molecules like fullerene (C_{60}) derivatives, perylenebisimide, and naphthalene derivatives for photo induced charge separation in organic solar cells.[6-12] Charge-transfer (CT) interactions between alternately stacked electron donor (D) and electron acceptor (A) molecules have been cleverly employed for the construction of various molecular and macromolecular assemblies such as foldamers,[13-17] catenanes/rotaxanes[18-19] and supramolecular polymers.[20-21] Charge-transfer D-A single crystal and hydrogels are being used for room-temperature organic ferroelectric devices.[22-23] The donor (D) and acceptor (A) used for highly ordered D-A assembly have being exploited to measure the photoconductivity and ambipolar charge transport of D-A material.[24-26] Donor-acceptor assemblies based on small organic chromophores were developed to mimic the long chain polymers through covalent linkage or noncovalent interactions. Quadruple hydrogen bond interactions, organo gels, aromatic π-stacking, and metal−ligand coordination are some of the approaches that are widely reported for making D−A arrays and donor-acceptor CT complexes in solution and gel state.[27-32] Carboxylic acid substituted segmented 1, 3-polyoligophenylenevinylene with the acceptor perylene bisimide molecule having pyridine moiety, and hydrogen bonded D-A assembles were reported for white light emission and thermosensitive emission.[33] Ghiggino and co-workers[34] recently reported the photoinduced charge separation in oligo-1,4-phenylenevinylenes (OPV) segmented polymers with PCBM and alt-*co*-MEH-PPV:PCBM blends. Our research group reported TCD based oligo-1,4-phenylenevinylenes (OPV) segmented polymers and studied their helical donor-acceptor assemblies using perylene-bisimide derivative.[35]

Charge transfer complexes that are stable in solid state (or thin-film) are particularly important since these materials can be used for energy generation and storage devices. Nazario Martín and co-workers[24] recently demonstrated the formation of highly ordered functional materials from π-extended tetrathiafulvalene (exTTF) as electron-donor and perylene-bisimide (PBI) as electron-acceptor. A controlled alignment of the n/p-material was bestowed by the electrostatic co-

assembly of two complementary self-assembling nanofibers which results in high values of photoconductivity. Ajayaghosh and co-workers[25] studied the D-A assembly of p-type π-gelator trithienylenevinylene derivative (TTV) with an n-type semiconductor perylene-bisimide (PBI) derivative and resulted in the formation of self-sorted fibers. By using flash photolysis time-resolved microwave conductivity (FP-TRMC) technique, the anisotropic photoconductivity of D-A (TTV/PBI) was measured. Helin Huang et al.[36] reported the morphology control of nanofibril D-A assemblies and measured their photoconductivity. Jian Pei and co-workers[37] reported the synthesis of C_3 symmetric donor–acceptor truxene derivative (Tr_3) and it's oxidized counterpart, the truxenone derivative (TrO_3) and studied one-dimensional microwires formed by the co-assembly of complementary aromatic donors and acceptors. Edward A. McGehee et[38] al reported studies of cocrystalisation of complementary C_3-symmetric donor-acceptor components like hexaalkoxytriphenylene (D) and mellitic triimide (A) in 1:1 ratio and studied the mesophase behaviour of D-A assembly in solid state. These systems are described in detail in the introduction chapter.

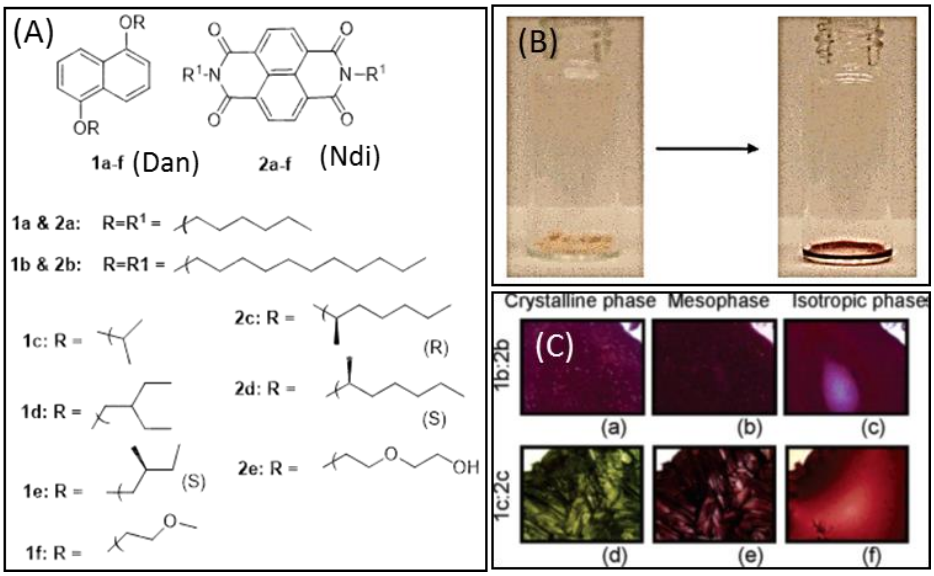

Figure 4.1. *(A) Structures of Dan and Ndi.* ***(B)*** *Color change from light yellow to deep red upon melting of the 1:1 Dan:Ndi mixture 1b:2b, which is characteristic of CT mixtures. (C) Color of bulk samples of 1:1 mixtures (a) Deep red 1b:2b crystalline phase (60°C). (b) Deep red 1b:2b mesophase (110 °C). (c) Deep red 1b:2b liquid phase (160 °C). (d) Light yellow 1c:2c crystalline phase (60 °C). (e) Deep red 1c:2c mesophase (110 °C). (f) Deep red 1c:2c liquid phase (160°C) (adapted from. J. Am. Chem. Soc.* ***2006,*** *128 7995-8002)*

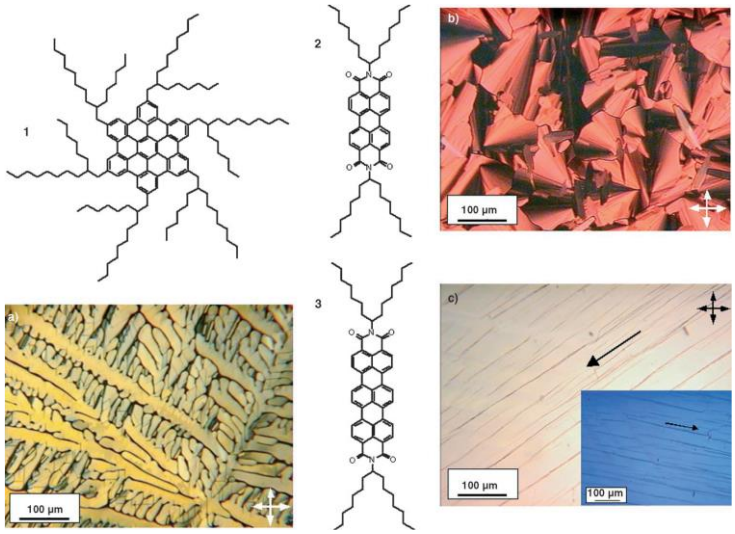

Figure 4.2*. Chemical structures and polarized optical microscopic images of (a) 1, (b) 2, and (c) 3. The crossed arrows indicate the orientation of the polarization filters in the optical microscope (adapted from Angew. Chem., Int. Ed.* ***2006****, 45, 819).*

Bent L. Iverson and co-workers[39-40] reported studies of cocrystallisation of Complementary C_2-Symmetric electron rich 1,5-dialkoxynaphthalene (Dan) donors and relatively electron deficient 1,4,5,8-naphthalenetetracarboxylic diimide (Ndi) acceptors in 1:1 ratio and studied alternating stacks of Dan and Ndi derivatives produced columnar mesophase with a deep red color with charge transfer band and predictable mesophase transition showed in figure 4.1. Klaus Mullen and co-workers[41] reported studies of columnar mesophase behaviour of donor-acceptor assembly of the derivative of hexaperihexabenzocoronene and derivative of perylenediimide in the solid state showed in figure 4.2. Recently Joseph J. Reczek and co-workers[42] reported a series of aromatic donor-acceptor columnar liquid crystal materials (see figure 4.3.) was developed whose charge-transfer absorption completely spans the visible spectrum.

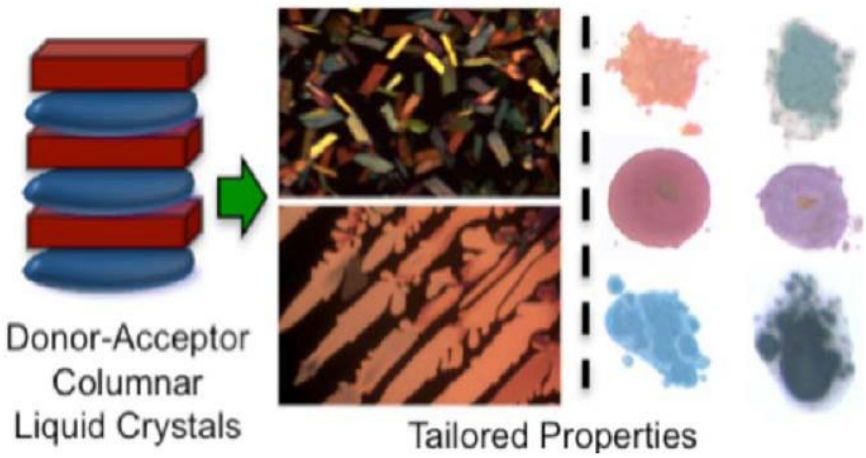

Figure 4.3. *Schematic representation of arrangement of donor and acceptor and forms columnar liquid crystals with color change (adapted from Chem. Mater.* ***2012****, 24, 3318– 3328).*

The above CT materials are largely reported based on small or oligomeric π-conjugated systems and they have to undergo harsh processing conditions in thin film devices. Further, most of the CT complexes were stable only in their molten state or high temperature (> 100 °C); thus, the solid state CT materials that are stable at for room temperature are very rare. This limitation directly limits the device fabrication of CT organic complexes which are required to be stable at room temperature. Additionally, it is also important to make CT materials that are capable of harvesting light in the entire the solar spectrum to enhance the device efficient. This emphasized the need for the development of new classes of CT complexes with following desirable criteria: (i) π-conjugated polymer CT complexes with stability in room temperature, (ii) soluble in organic solvents so that processable into thin films, (iii) should possess structural diversity to for light absorbance characteristics in solar spectrum to enhance the harvesting efficiency and so on forth. Unfortunately, there are no reports known for the room temperature CT in the literature; thus, new efforts are required to address this important problem.

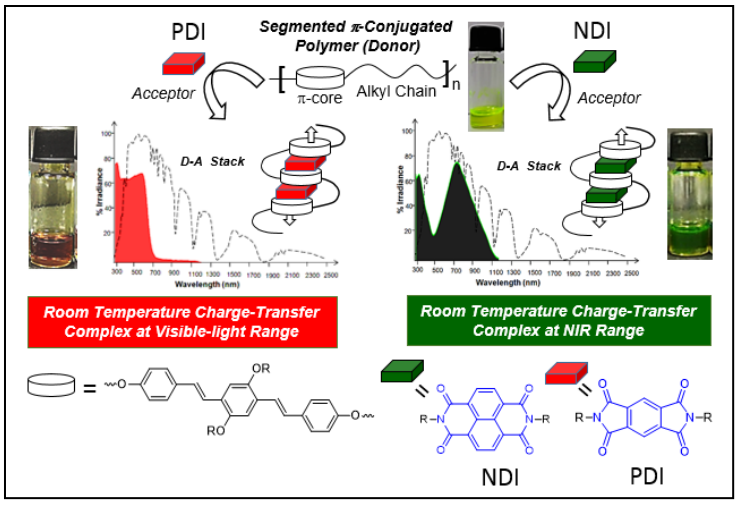

Figure 4.4. *Approaches to develop the first organic D-A material based on segmented π-conjugated polymer and CT band covering visible and NIR region.*

The present investigation is emphasized to develop new classes of donor-acceptor type charge transfer complexes based on segmented OPV polymers and very well known electron deficient molecules such as naphthalene diimide (NDI) and phenylene diimide (PDI). The solubility of the donor-acceptor system was

accomplished by substituting 2-ethylehexyl side chains both in the donor polymer and acceptor molecules. The segmented OPV polymer produced instant CT complexes upon mixing with NDI and PDI molecules, and these complexes were produced as red and green colour with respect to their absorption in the visible and NIR region, respectively (see Figure 4.4). Thermal behaviours such as melting and crystallization processes were studied by DSC and PLM. The solid state packing of the CT complexes were further studied by powder X-ray diffraction. Detailed photophysical studies enabled the determination of the D-A complex ratio, thermo-reversibility, etc. Structurally identical small molecular OPV CT complexes were also designed to study the role of the macromolecular complexation ability compared to small molecules. The overall findings revealed that the segmented OPV polymer-NDI complexes (also PDI complexes) were turned to be one of the first examples for stable room temperature CT in the literature.

4.2. Experimental Section

4.2.1. Materials: Pyromellitic dianhydride, 1,4,5,8-Naphthalenetetracarboxylic dianhydride, 2-ethyl-1-hexylamine, acetic acid, 4-propoxybenzaldehyde, 4-hydroxybenzaldehyde, bromoalkanes, and zinc acetate. Solvents were purchased locally and purified by standard procedures. Segmnetd polymer P-5 to P-10 reported in the chapter 2 were used.

4.2.2. General Procedures. ^{1}H and ^{13}C NMR were recorded using 400 MHz JEOL and 100 MHz NMR spectrometer respectively. Infrared spectra were recorded using a Thermo-Scientific Nicolet 6700 FT-IR spectrometer in the solid state in KBr in the range of 4000-600 cm^{-1}. TGA analysis was done using PerkinElmer STA 6000 simultaneous thermal analyser. High resolution mass spectra of PDI and NDI were recorded using a micro mass ESI-TOF MS Spectrometer. Mass analysis of precursors were determined by the Applied Biosystems 4800 PLUS MALDI TOF/TOF analyser using TiO2 as matrix. Differential scanning calorimetry (DSC) measurements had done by using TA Q20 DSC. The data were recorded at heating and cooling rate of 10 °C/min. The first heating cycle data was discarded since they possessed prehistory of the sample. Absorption spectra were recorded by using a PerkinElmer Lambda 45 UV spectrophotometer. Steady state emission and excitation spectra were recorded using Fluorolog-max HORIBA JOBIN VYON fluorescence spectrophotometer. In solution state DA material carried out by using 200 µL cuvette with 3 mm path length. Powder

X-ray diffraction patterns were recorded by Philips Analytical Diffractometer using Cu Kα emission. The spectra were recorded in the range of 2θ = 5−40° and analysed using X'pert software. Variable-temperature X-ray diffraction studies were performed using a Rigaku Dmax 2500 diffractometer with a copper target.

Polarized Light Microscope (PLM) imaging: To study the temperature dependent mesophase or crystalline textures of all samples, LIECA DM2500 P polarized light microscope equipped with Linkam TMS 94 heating-freezing stage was used. A pinch of sample was placed on the glass substrate, heated to melt at 10 °C/min, and kept isothermally at 20 °C above their melting temperature for 2-3 minutes. The melt was subsequently cooled at 10 °C/min which leads to nucleation and further growth patterns and these images were continuously captured using camera.

Synthesis of 4-(heptyloxy)benzaldehyde (15): 4-Hydroxybenzaldehyde (0.5 g, 4 mmol), 1-bromoheptane (0.96 mL, 6 mmol) and powdered anhydrous K_2CO_3(1.1 g, 8 mol) were taken in dry acetonitrile (30 mL) and refluxed for 1 h under nitrogen atmosphere. 1-Bromoheptane (0.96 mL, 6 mmol) was added drop wise to the above hot reaction mixture. The reaction mixture was further refluxed for 24 h under nitrogen atmosphere. The product was extracted in DCM and dried over anhydrous sodium sulphate. The product was further purified by passing through silica gel column using ethyl acetate (5% v/v) in hexane as eluent. Yield = 77 %. ^{1}H-NMR ($CDCl_3$, 400 MHz) δ ppm: 9.88 (s, 2H, C**H**O), 7.83 (d, 2H, **Ar-H**), 7.0 (d, 2H, **Ar-H**), 4.05 (t, 2H, O**CH$_2$**), 1.82 (m, 2H, C**H$_2$)**, 1.47 (m, 2H, C**H$_2$)**, 1.32 (m, 6H, C**H$_2$)** and 0.9 (t, 3H, C**H$_3$**). ^{13}C-NMR ($CDCl_3$, 100 MHz) δ ppm: 190.83, 164.25, 132.0, 129.7, 114.72, 68.41, 31.73, 29.03, 29.0**,** 25.90, 22.58, and 14.06. FT-IR (KBr, cm^{-1}): 2932, 2853, 2731, 1423, 1393, 1311, 1258, 1215, 1159, 1100, 1016, 856, 721, and 651. High resolution mass spectrometry (HRMS) (MW=220.31): 221.11 (M+1).

Synthesis of 4-(octyloxy)benzaldehyde (16): 4-Hydroxybenzaldehyde (2 g, 16 mmol) was reacted with 1-bromooctane (2.5 mL, 20 mmol) , and K_2CO_3 (2.7 g, 20 mmol) as described for above. The product was further purified by passing through silica gel column using ethyl acetate (5% v/v) in hexane as eluent. Yield = 80 %. ^{1}H-NMR ($CDCl_3$, 400 MHz) δ ppm: 9.88 (s, 2H, C**H**O), 7.83 (d, 2H, **Ar-H**), 7.0 (d, 2H, **Ar-H**), 4.05 (t, 2H, OC**H$_2$**), 1.82 (m, 2H, C**H$_2$)** 1.47 (m, 2H, C**H$_2$),** 1.32 (m, 8H, C**H$_2$)** and 0.9 (t, 3H, C**H$_3$**). ^{13}C-NMR ($CDCl_3$, 100 MHz) δ ppm: 190.87, 164.25, 132.0, 129.67, 114.72, 68.41, 31.77, 29.28, 29.18, 29.03, 25.94, 22.64, and 14.09. FT-IR

(KBr, cm^{-1}): 2932, 2855, 2733, 1572, 1026, 856, 832, 721, and 651. High resolution mass spectrometry (HRMS) (MW=234.33): 235.10 (M+1).

4,4'-((1E,1'E)-(2,5-bis((2-ethylhexyl)oxy)-1,4-phenylene)bis(ethane 2,1diyl))bis((octyloxy)benzene): (OPV-8): Compound 3 (0.3 g, 0.47 mmol) was reacted with 4-octyloxybenzaldehyde (0.27 g, 1.2 mmol) were taken in dry THF (15 mL), purged nitrogen in 30 min. and kept under ice cold condition. Potassium *tert*-butoxide (6.0 mL, 1M THF solution) was added dropwise to the reaction mixture under a nitrogen atmosphere and the stirring was continued at 30 °C for 12 hrs. The resultant yellow green solution was concentrated and poured into a large amount of methanol. The yellow green precipitate was filtered and washed with a large amount of methanol. The product was further purified by passing through silica gel column using ethyl acetate (5 % v/v) in hexane as eluent. Yield =0.31 g (84 %). ^{1}H NMR ($CDCl_3$, 400 MHz), δ ppm : 7.46 (d, 4H, Ar-H), 7.36 (d, 2H, CH=CH), 7.11 (s, 2H, Ar-H), 7.09 (d, 2H, CH=CH), 6.90 (d, 4H, Ar-H),4.0 (t, 4H, OCH_2), 3.95 (d, 4H, OCH_2), 1.81 (m, 6H,2CH, $2CH_2$), 1.64-1.27 (m, 36H, CH_2), 1.0 (t, 6H, CH_3), and 0.95-0.89 (m, 12H, CH_3) .^{13}C-NMR ($CDCl_3$, 100 MHz) δ ppm: 158.7, 151.0, 130.67, 128.03, 127.58, 126.70, 121.27, 114.67, 110.04, 71.75, 68.07, 39.78, 31.82,30.93,29.37, 29.26, 26.06, 24.22,23.12, 22.66, 14.13,14.11 and 11.33. FT-IR (KBr, cm^{-1}): 3785, 2921, 2854, 2278, 1602, 1507, 1462, 1420, 1386, 1292, 1240, 1197, 1027, 966, 848, 812, 724, and 668. MALDI-TOF-MS (MW =794.6): *m*/*z* = 794.5 (M^+).

4,4'-((1E,1'E)-(2,5-bis((2-ethylhexyl)oxy)-1,4-phenylene)bis(ethene-2,1-diyl))bis((heptyloxy)benzene): (OPV-7): Compound **3** (0.3 g, 0.47 mmol) was reacted with 4-heptyloxybenzaldehyde (0.26 g, 1.2 mmol) **as described for OPV-8**. The product was further purified by passing through silica gel column using ethyl acetate (5 % v/v) in hexane as eluent. Yield = 0.29 (80 %). ^{1}H NMR ($CDCl_3$, 400 MHz), δ ppm: 7.46 ppm (d, 4H, **Ar-H**), 7.36 ppm (d, 2H, C**H**=C**H**), 7.11 ppm (s, 2H, **Ar-H**), 7.09 ppm (d, 2H, C**H**=C**H**), 6.90 ppm (d, 4H, Ar-**H**),4.0 ppm (t, 4H, OC$\mathbf{H_2}$), 3.95 ppm (d, 4H, OC$\mathbf{H_2}$),1.81 (m, 6H, 2C**H,** 2C$\mathbf{H_2}$), 1.64-1.27 ppm (m, 32H, C$\mathbf{H_2}$), 1.0 ppm (t, 6H, C$\mathbf{H_3}$), and 0.95-0.89 ppm (m, 12H, C$\mathbf{H_3}$) .^{13}C-NMR ($CDCl_3$, 100 MHz) δ ppm: 158.7, 151.0, 130.66, 128.02, 127.57, 126.70, 121.26, 114.66, 110.03, 71.74, 68.06, 39.76, 31.80,30.92,29.28, 29.26, 29.07,26.01, 24.21,23.11, 22.61, 14.13,14.10 and 11.32 ppm. FT-IR (KBr, cm^{-1}): 3788, 3046, 2923, 2857, 1600, 1504,

1460, 1419, 1384, 1288, 1239, 1191, 1120, 1072, 1031, 962, 846, 813, 728, and 665. MALDI-TOF-TOF-MS (MW = 767.2): *m*/*z* = 766.6 (M^+).

Synthesis of Pyromelletic diimide (PDI): Pyromellitic dianhydride (5.0 g, 22.9 mmol) and 2-ethylhexylamine (6.5 g, 50.4 mmol) were taken in acetic acid (50 mL). The reaction mixture was stirred at 100 °C for 12 h. After completion of the reaction, it was poured into water and stirred. The solid product was filtered, washed with methanol and it was further purified by silica gel column using ethyl acetate (30 % v/v) in hexane as eluent. Yield = 70 % (8.6 g). ^{1}H-NMR ($CDCl_3$, 400 MHz) δ ppm: 8.27 (s, 4H, **Ar-H**), 3.65 (d, 4H, NC**H**$_2$), 1.86 (m, 2H, OCH_2C**H**), 1.37 -1.29 (m, 16H, **aliphatic-H**) and 0.94-0.87 (m, 12H, C**H**$_3$). ^{13}C-NMR ($CDCl_3$, 100 MHz) δ ppm: 166.59, 137.13, 118.12, 42.50, 38.22, 30.45, 28.41, 23.80, 22.94, 14.02, and 10.35. FT-IR (KBr, cm^{-1}): 3872, 3737, 3606, 3205, 2928, 2864, 2311, 1765, 1695, 1514, 1453, 1392, 1352, 1153, 1061, 945, 893, 788, and 729. Molecular formula: $C_{26}H_{36}N_2O_4$, high resolution mass spectrometry (HRMS) (MW = 440.267): *m*/*z* = 441.274 $(M+H)^+$.

Synthesis of Naphthalene diimide (NDI): 1, 4, 5, 8- Naphthalenetetracarboxylic dianhydride (5.0 g, 22.9 mmol) and 2-ethylhexylamine (5.3 g, 40.1 mmol) were taken in aceticacid (50 mL). The reaction mixture was stirred at 100 °C for 12 h. After completion of the reaction, it was poured into water and stirred. The solid product was filtered, washed with methanol and further purified by silica gel column using ethyl acetate (40 % v/v) in hexane as eluent. Yield = 80 % (7.3 g). ^{1}H-NMR ($CDCl_3$, 400 MHz) δ ppm: 8.76 (s, 4H, **Ar-H**), 4.15 (d, 4H, NC**H**$_2$), 1.95 (m, 2H, OCH_2C**H**), 1.42 - 1.26 (m, 16H, **aliphatic-H**) and 0.96-0.87 (m, 12H, C**H**$_3$). ^{13}C-NMR ($CDCl_3$, 100 MHz) δ ppm: 163.24, 131.02, 126.73, 126.58, 77.00, 44.59, 37.92, 30.67, 28.61, 24.01, 23.03, 14.07, and 10.59. FT-IR (KBr, cm^{-1}): 3943, 3883, 3825, 3740, 3609, 3074, 2926, 2862, 1698, 1650, 1579, 1452, 1373, 1332, 1240, 1180, 1084, 981, 893, 769, and 718. Molecular formula: $C_{30}H_{38}N_2O_4$, high resolution mass spectrometry (HRMS) (MW = 490.283): *m*/*z* = 491.291 $(M+H)^+$.

Synthesis of donor-acceptor complexes: To make donor-acceptor complexes, equimolar amounts of segmented OPV polymer and NDI (or PDI) were taken in toluene (10 wt %) and mixed very well by constant stirring. Immediate appearance of red and green color solution was observed for OPV polymer+PDI and OPV polymer+

NDI complex, respectively. The resultant donor-acceptor blend was filtered and solvent was removed to yield the powder blend samples.

4.3. Results and Discussion

4.3.1. Synthesis and Characterization of Donor-acceptor Complexes

The chemical structure of the segmented OPV polymers (P-x) and electron deficient naphthalene diimide (NDI) and pyromellitic diimide (PDI) are shown in scheme-4.1. The PDI and NDI were synthesized by reacting their corresponding dianhydrides with ethylhexylamine using $Zn(OAC)_2$ as catalyst.[44] In the present design, 2-ethylhexyl pendent units were retained in both polymer and NDI (also PDI) in order to maintain the solubility of the species in organic solvents and also to maintain the structural similarity among the π-conjugated species. To make donor-acceptor complexes, equimolar amounts of segmented OPV polymer P-4 to P-10 (synthesized in chapter 2) and NDI (or PDI) were taken in toluene and mixed very well by constant stirring. The color of the solutions immediately changed into red and green for OPV polymer+PDI and OPV polymer+ NDI complex, respectively.

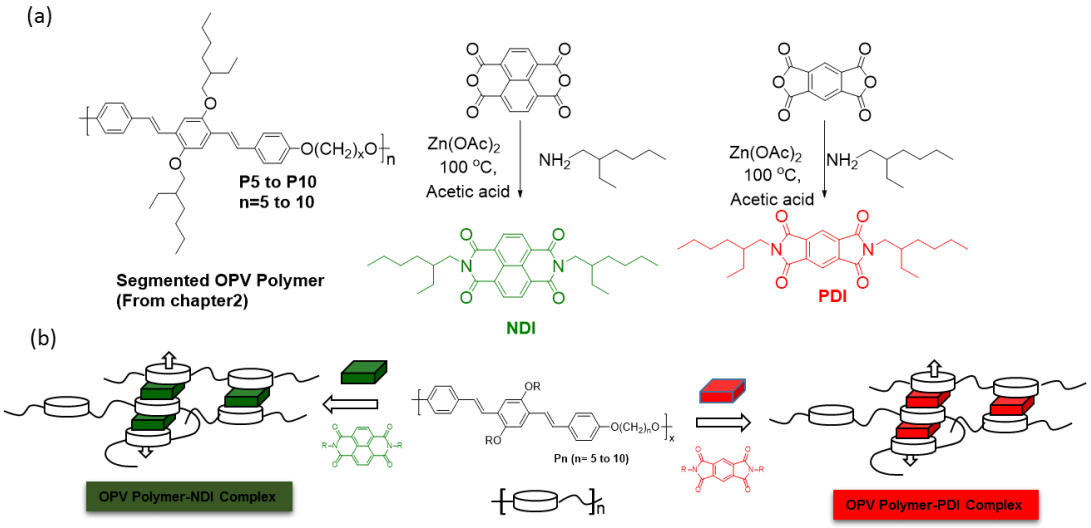

Scheme-4.1. *(a) Synthesis of segmented OPVs, NDI and PDI molecules and (b) their donor-acceptor complexes.*

Differential scanning calorimetry (DSC) thermograms of PDI, NDI, few segmented OPV polymers and their complexes are given in figure 4.5. NDI showed melting transition with respect to larger aromatic ring structure at 205.2 °C and 192.6

°C, respectively (see Figure 4.5a). The PDI showed melting and crystalline transition at 102.2 °C and 85.6 °C, respectively (see Figure 4.7b). The OPV segmented polymers having even numbers of carbon atoms in the spacers were found to be semicrystalline whereas odd-spacers were highly amorphous (see chapter-2). This suggested that the carbon atoms in the alkyl spacers directed the molecular self-assembly of segmented polymers towards highly crystalline solids. The even number of carbon atoms seemed to controlling packing ability of the polymer chains in the present system. Interestingly, the NDI complexation with amorphous odd-spacer polymers (P-5, P-7 and P-9) induced semicrystallinity in their complexes P-5+NDI, P-7+NDI and P-9+NDI (see Figure 4.5c and 4.5d). This trend was attributed to the aromatic donor-acceptor interaction driven crystallization process in fully amorphous polymers P-5 to P-9. These complexes showed broad melting and crystallization peaks in the heating and cooling cycles, respectively (see Figures 4.8c and 4.8d).

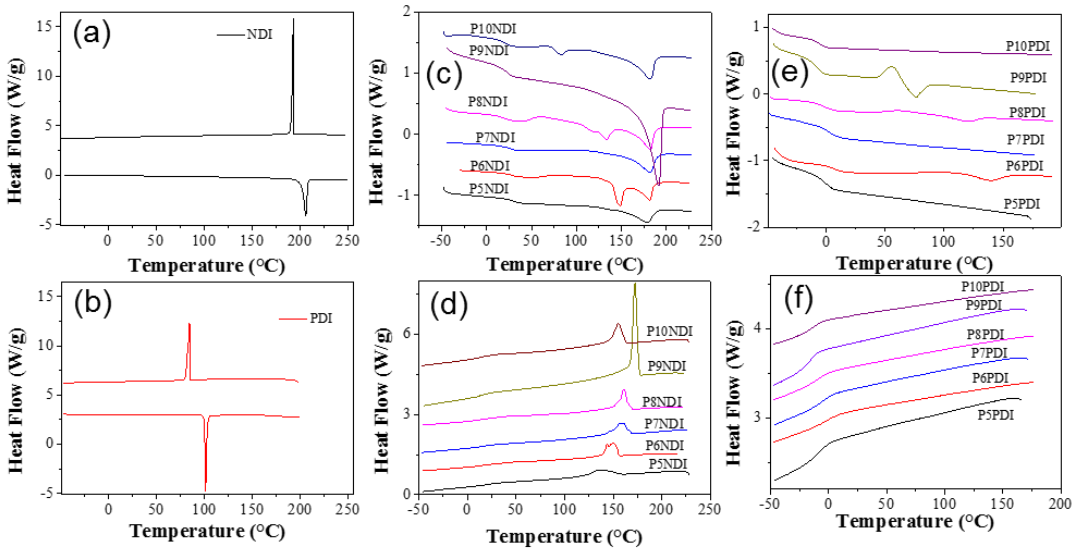

Figure *4.5.* *(a) DSC thermograms of NDI in the heating and cooling cycles. DSC thermograms of NDI complexes of P-5 to P-10 in heating (b), and cooling cycle (c). (d) DSC thermograms of PDI in the heating and cooling cycles. DSC thermograms of PDI complexes of P-5 to P-10 in heating (e), and cooling cycle (f). The heating and cooling cycles were programmed at 10 °/min rate under nitrogen.*

The NDI complexation with semi-crystalline polymers exhibited two melting transitions in P-6+NDI, P-8+NDI and P-10+NDI in the heating cycle and single crystallization in the cooling cycle (see Figures 4.8c and 4.8d). It is also important to mention that once the donor-acceptor complexes are crystallized from the molten state (in the cooling cycle), they retained the crystalline properties until they were heated

again above their melting transition (heating cycle). This property is particularly important since the donor-acceptor complexes can be readily aligned by simple thermal heating/cooling process in solvent free processing conditions and their aligned state could be retained for applications at ambient conditions. On the other hand, the OPV polymer + PDI complexes were predominately found to be amorphous in nature. These complexes showed very weak thermal transitions in the heating cycles (see Figure-4.8e) which are negligible compared to their even-polymer complexes showed in Figure 4.8c. However, these complexes did not show crystallization peak and they exhibit only glass transition in the heating and cooling cycle (see Figure 4.8f). These results suggested that the chain folding of segmented OPV polymers with arylene dimides were indirectly controlled by the types of the acceptor employed for the complexation. For instance, the NDI+OPV polymer interaction was found to be strong to induce macromolecular chain folding for semi-crystallinity which seems to be less efficient in the PDI+OPV polymer complexes.

Table 4.1. DSC thermal data of all polymer+NDI complexes in the heating and cooling cycles at 10°/min.

Sample	**T_m (K)**	**T_c (K)**	**T_g(c) (K)**	**T_g(m) (K)**	**ΔH_m (kJ /mol)**	**ΔH_c (kJ /mol)**
P5NDI	451.4	410.7	294.5	303.7	14.66	13.54
P6NDI	454.9	422.4	291.6	301.5	20.93	19.16
P7NDI	455.1	433.6	292.3	299.0	16.30	15.44
P8NDI	455.3	434.2	285.4	294.2	21.31	18.17
P9NDI	464.8	445.1	288.8	296.4	21.46	21.56
P10NDI	455.3	428.1	288.3	293.0	18.06	17.28
NDI	476.6	468.6	-	-	41.33	40.21
PDI	374.0	357.2	-	-	24.78	22.84

The DSC data for PDI, NDI and their other polymer complexes are given in the Table 4.1. To further confirm the above trend, the crystallization temperature (T_C), enthalpies of melting and crystallization of the complexes are plotted and showed in figures 4.6. The T_C of the complexes decreased from 445 K to 410 K upon decreasing

the spacer from C10 to C5 carbon atoms (see Figure 4.6a). The T_g of the complexes were also decreased from 294 k to 281 K with decrease in the spacer length from C10 to C5 (see Table 4.1). The decrease in T_g with increase in the spacer length was attributed to the higher flexibility in the long segmented OPV polymers. The enthalpies of melting were not showing any specific trend (see Figure 4.6b). The enthalpies of crystallization in the OPV polymer-NDI complexes were compared with their nascent polymers in Figure 4.6 (data for the nascent polymer was taken from our earlier chapter-2 for comparison purpose). Since the polymers P-5, P-7 and P-9 are amorphous; their enthalpies were taken as zero. The polymers P-6, P-8 and P-10 showed enthalpies of crystallization in the range of 3.8 to 7.5 kJ/mol. On the other hand, their donor-acceptor complexes showed higher enthalpies in the range of 13.5 to 21.5 kJ/mol indicating highly packed (ordered) in solid state. Further, it is important to note that the amorphous polymer complexes P-5, P-7 and P-9 were also turned into semi-crystalline in the solid state as similar to that of their even-spacer polymer complexes. This unique property of the odd-spacer OPV polymers indicated that the donor-acceptor interaction indeed facilitate the nucleation process in the polymer matrix and result them into semi-crystalline.

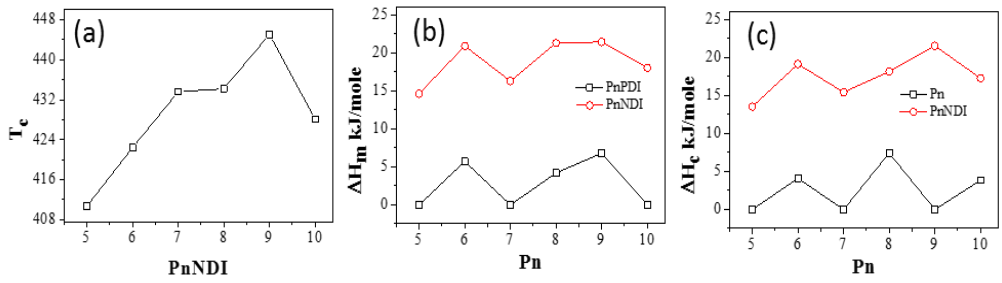

Figure 4.6. *(a) Plots of T_c and versus the number of carbon atoms in the spacer for polymer + NDI complexes (PnNDI, n=5 to 10). (b) Plots of enthalpies of melting versus the number of carbon atoms in the spacer for polymer +NDI and polymer +PDI complexes (PnNDI, PnPDI n=5 to 10). (c) Plots of enthalpies of crystallization versus the number of carbon atoms in the spacer for polymer and their NDI complexes.*

4.3.2. PLM Morphology and WXRD Patterns

To morphological features of crystallization process in the donor-acceptor complexes were studied by polarizing light microscope (PLM) attached with programmable hot stage. The sample was placed on the glass substrate and heated to melt (at 10 °C/min) and it was subsequently cooled at 10 °C/min to capture the morphological features. PLM images of NDI and PDI in the crystallization process were captured and summarized in figure 4.7. The samples showed typical long and sharp crystalline domains with respect to crystalline solids.

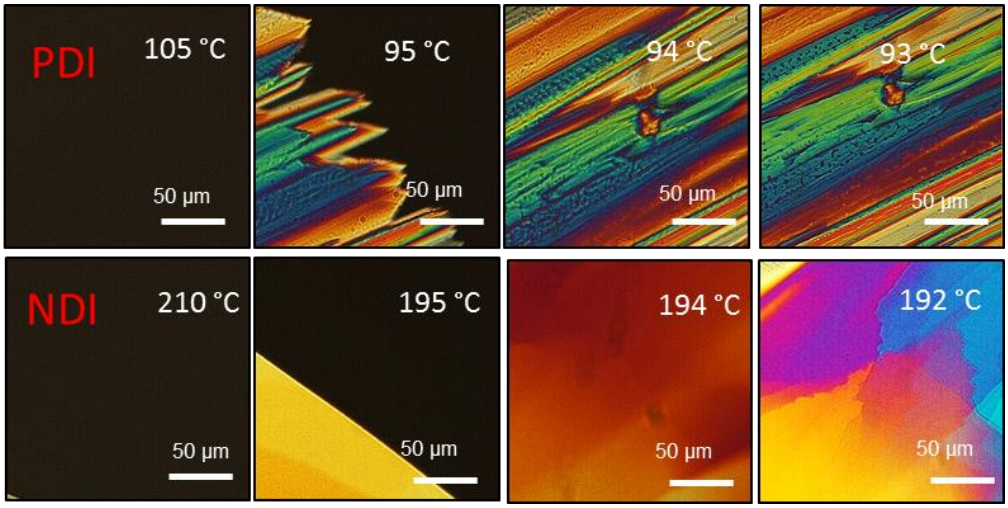

Figure 4.7. *(a) PLM images of PDI and NDI on glass cover slips in the cooling cycles were programmed at 10 °/min rate.*

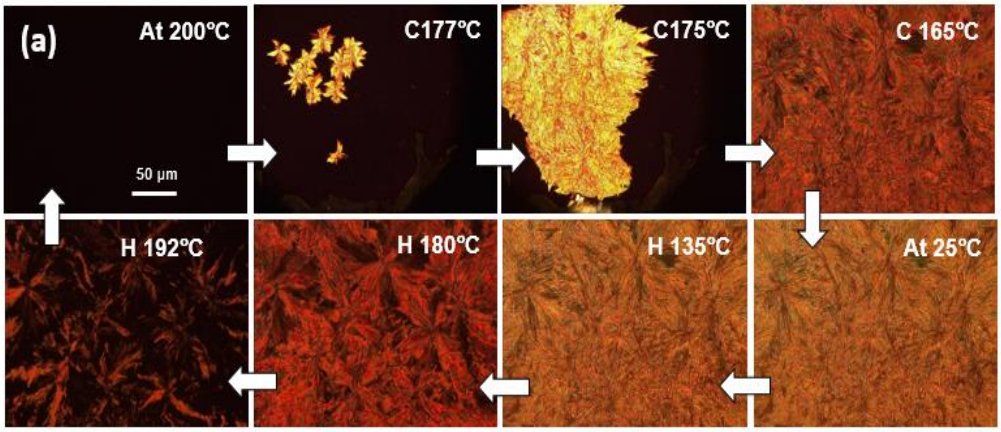

Figure 4.8. *(a) PLM images of P-8+NDI complex on glass cover slips in the cooling and heating cycles. The terminology C and H before the temperatures are used for representing cooling and heating cycles, respectively.*

The PLM images of P-8+NDI complexes are shown in Figure 4.8. At 200 °C, the complex showed dark image under cross polarisers clearly indicating the completely molten state (see Figure 4.8a). Upon cooling (at 10°/min), the nucleation started at 187 °C and the crystal growth was completed within a minute at 175 °C. The PLM image was retained same up to 25 °C and the crystalline vectors gradually disappeared while melting them above 150 °C. The entire morphological features were reproducible in the subsequent heating and cooling cycles.

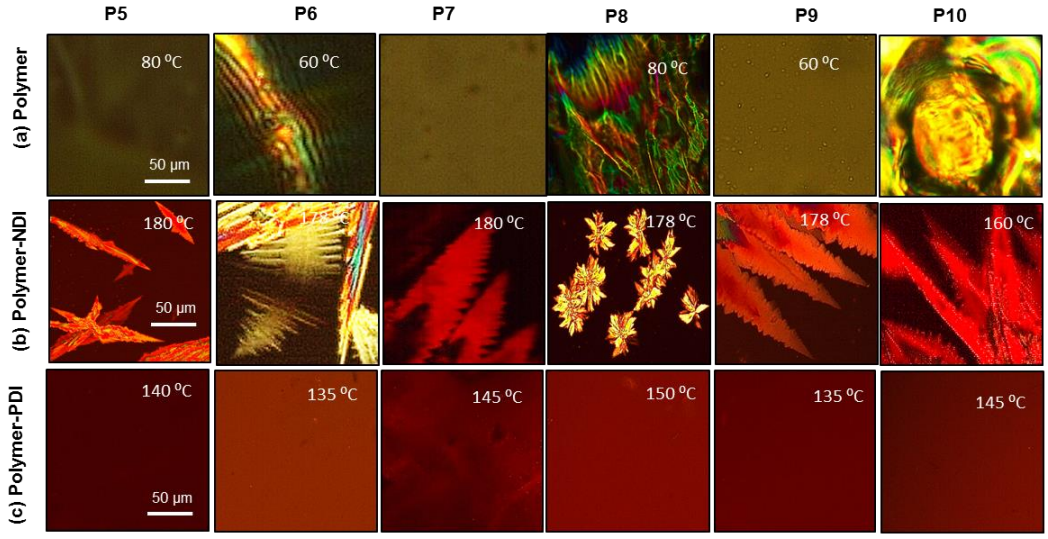

Figure 4.9. *(a) PLM images of OPV polymers P-5 to P-10 (b), OPV polymer + NDI complexes (c) and OPV polymer + PDI complexes (d) in the cooling cycles. The heating and cooling cycles were programmed at 10 °/min rate.*

The PLM morphologies P-5 to P-10 polymers and their NDI and PDI complexes are shown in Figure 4.9. In figure 4.9, the crystalline vectors were visible in the OPV segmented polymers P-6, P-8 and P-10 whereas the P-5, P-7 and P-9 polymers showed molten features with respect to amorphous solid. Interestingly, the NDI-complexes exhibited well-defined crystalline domains for the polymers P-5 to P-10 irrespective of their amorphous or crystalline nature of the parent polymer. This observation is very well matched with the DSC data in Figures 4.5c. On the other hand, the PDI-complexes showed no crystalline vectors as the indication of absence of crystallization even after the complexation. It is also important to mention that the even-spacer crystalline polymers P-6, P-8 and P-10 also lost their crystallization ability in the presence of PDI. These results were very well corroborated with DSC

data in Figures 4.5f. Hence, the crystallization process in segmented CT complexes is highly controlled by the donor-acceptor interaction. NDI complexes were found to be very unique in producing semi-crystalline CT complexes.

Wide angle x-ray diffraction patterns for PDI and NDI samples (see Figure 4.10a) showed sharp transitions with respect to highly crystalline solids. WXRD patterns of semi-crystalline polymers (P-6 and P-8) showed peaks at 2θ = 10 and 18 with respect to ordered crystalline structures whereas amorphous polymers (P-7 and P-9) did not show any sharp crystalline peaks (the WXRD patterns of P-6 to P-9 were taken from our previous chapter for comparison purpose). The PDI complexes did not show any crystalline peak (see Figure 4.10) which matched with the DSC thermograms and PLM images for completely amorphous nature. Upon complexation, the WXRD patterns of NDI complexes with polymers P-5 to P-10 showed well-ordered crystalline domains with d-spacing of layered structures (see Figure 4.11). In A series the peaks at 2θ = 5.13, 14.63, 19.6, 25.76,... etc followed the 001, 003, 004, 006... sequences indicating the formation of layered assemblies and in B series 2θ = 11.55, 17.22, 22.55,... etc. On the other hand,

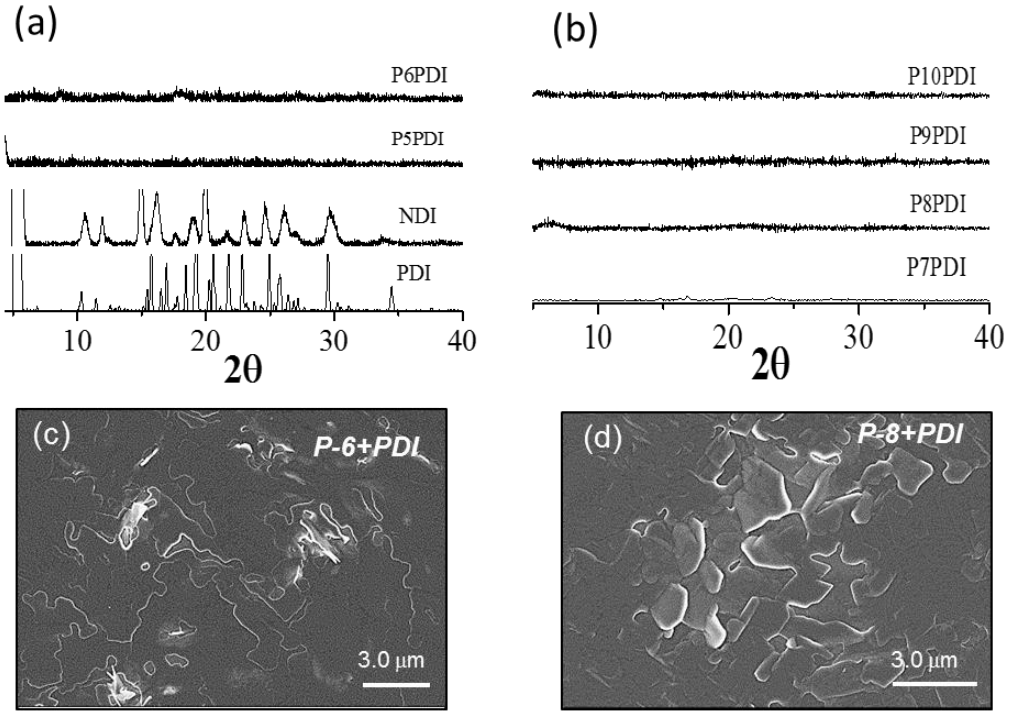

Figure 4.10. *(a) WXRD patterns of PDI, NDI, polymer+PDI complexes. (b) WXRD patterns of polymer+PDI Complexes. FESEM images of thin films (c) P-6+NDI and (d) P-8+PDI processed under 10°/min cooling rate on silicon wafers.*

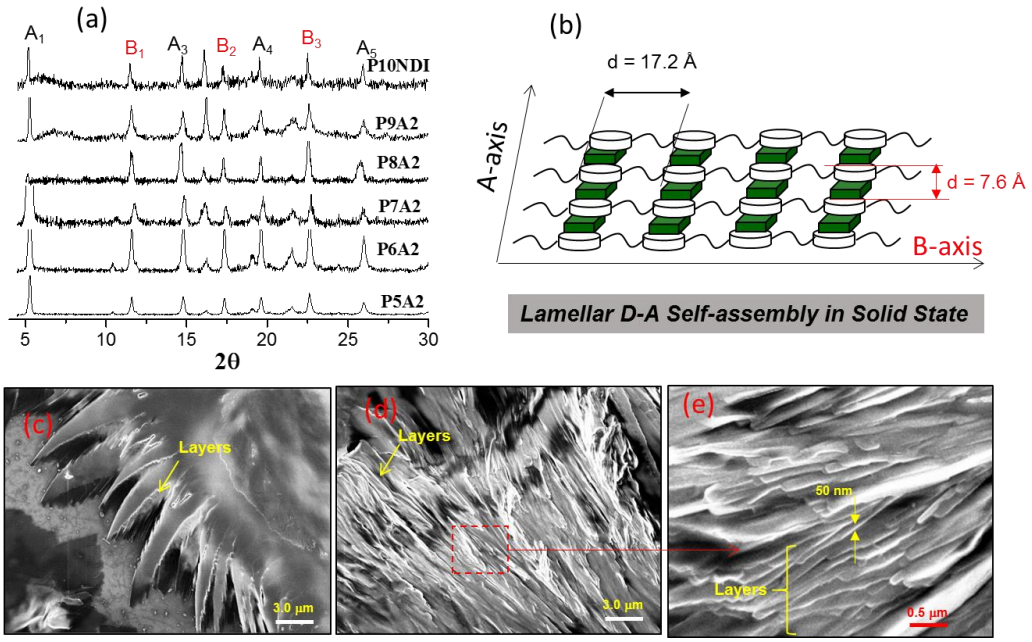

Figure 4.11. *(a) WXRD patterns of of polymer+NDI complexes. (b) Schematic representation of WXRD patterns of polymer+NDI complexes lamellar arrangement in solid state. FESEM images of thin films (c) P-6+NDI and (d) P-8+NDI processed under 10°/min cooling rate on silicon wafers. (e) Zoomed area from P-8+NDI.*

To get more insight into the morphological features at the micro-meter domain, the NDI and PDI complexes of P-6 and P-8 polymers were subjected to sample preparation on silicon wafer using hot stage at 10°/min cooling rate. Field emission SEM images of these aligned samples are shown in figures 4.10 and 4.11. The PDI complexes exhibited morphology with respect to amorphous film formation (see figures 4.10c and 4.10d). Interestingly, the NDI complexes showed bundles of sharp crystalline vectors which were further aligned in the layered structures (see figures 4.11c and 4.11d). This morphological trend followed the observation in the WXRD pattern. Based on the DSC data, PLM images, FESEM images and WXRD patterns, it may be concluded that the newly developed donor-acceptor complexes between the OPV segmented polymers and NDI and PDI were highly controlled by the selection of the appropriate chromophores: (i) NDI is very good acceptor for all OPV polymers P-5 to P-10 and produce stable semicrystalline donor-acceptor self-assemblies irrespective of the amorphous or crystalline nature of the polymers, and (ii) PDI was found to influence on the packing of the segmented polymers; however, the resultant complexes were produced as completely amorphous solid. Hence, in the present investigation the solid state assemblies of the donor-acceptor complexes could

be readily tuned with the selection of appropriate NDI or PDI molecules. Additionally, the crystalline NDI and amorphous PDI complexes were found to be highly stable at ambient conditions; thus, they can be further exploited for futuristic electronic or energy storage devices which have to be studied separately.

4.3.3. Donor-Acceptor CT Complexes in Solution

To study the donor-acceptor interaction of OPV segmented polymer with NDI and PDI, detail photophysical studies like absorbance, and emission measurements were performed. Absorbance spectra of PDI, NDI and OPV chromophores showed maxima at 320 nm, 380 nm, and 400 nm, respectively (see Figure 4.12a). The absorbance of the chromophores were retained as O.D = 0.1 to record their emission spectra (see Figure 4.12b).

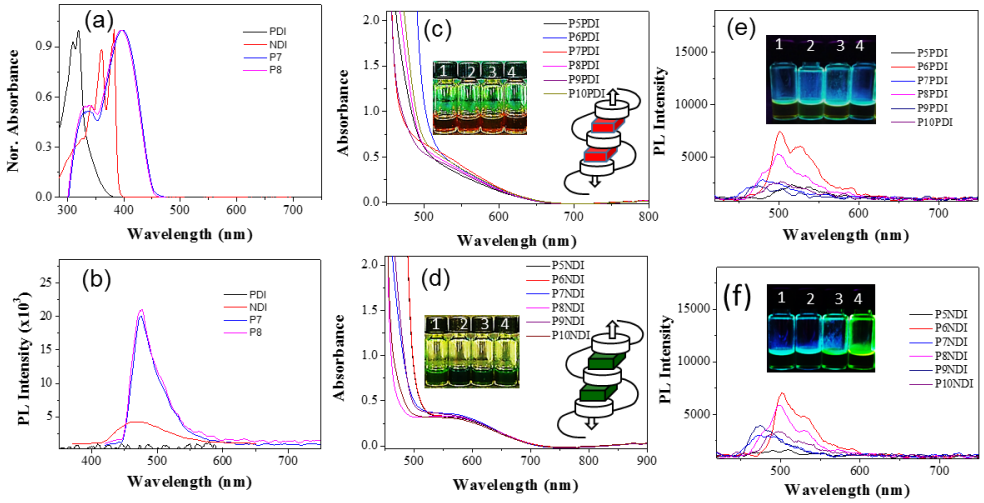

Figure 4.12. *Absorbance (a) and emission spectra (b) of NDI, PDI, P-7 and P-8 at 10^{-5} M in toluene. Absorbance spectra of OPV polymer+PDI complexes (c) and OPV polymer+NDI complexes (d) at $3.0x10^{-2}$ M in toluene. The donor acceptor ratio was maintained as 1:1. Emission spectra of OPV polymer+PDI complexes (e) and OPV polymer+PDI complexes (f) at $3.0x10^{-2}$ M in toluene (λ_{ex} = 400 nm). The photographs in vials show the colour of the complexes in normal light and excited with UV-light. Vials 1, 2, 3 and 4 contains the polymers P-5, P-6, P-7 and P-8, respectively, in their PDI and NDI complexes.*

The PDI showed very weak emission signal) whereas the NDI showed blue emission with maxima at 480-490 nm which is almost similar to that of OPV polymers. To measure the donor-acceptor interactions, the concentrations of OPV chromophore in the polymer, PDI and NDI were taken as 3.0 $x10^{-2}$ M in toluene. As

soon as mix the donor and acceptor in toluene, the color of the OPV polymer+PDI and OPV polymer+NDI immediately tuned into red and green, respectively (see vials in Figure 4.12c and 4.12d). Both the OPV chromophore and NDI (or PDI) do not have absorbance above 400 nm; thus, the emerging of red and green colour in the PDI and NDI complexes were attributed to the formation of charge transfer (CT) complexes. The absorbance spectra of the OPV polymer complexes with NDI and PDI were measured using 200 μL cuvett and high concentration of the donor-acceptor was required (10^{-2} M) to identify the CT band. The CT bands in the OPV polymer+PDI and OPV polymer+NDI were observed at 525 nm and 600 nm, respectively (see Figures 4.12c and 4.12d). The emission spectra of these charge transfer complexes showed very negligible fluorescence (or no fluorescence) compared to nascent OPV polymer which again confirmed the formation of the efficient CT complexes (see Figures 4.12e and 4.12f). Further, the tendencies for the CT band formation in the complexes were not influenced by the variable alkyl chain length in the segmented polymers. This suggested that the electrostatic interactions between the chromophores were controlled OPV donor and NDI (or PDI) acceptor and not the topology of the polymer chains.

To determine the donor-acceptor complex ratio, concentration dependent absorbance measurements were carried out by keeping the OPV polymer donor constant (3.0×10^{-2} M) and varied number of equivalent of acceptor (NDI or PDI) from 5.0×10^{-3} M to 6.0×10^{-2} M. The additions of NDI into P-8 polymer in toluene showed increase in absorbance for CT band at 580 nm with increase in the amount of NDI amount (see Figure 4.13b). A similar trend was observed for addition of PDI into P-8 polymers and the data are summarized in Figure 4.13a. The plot of absorbance at 580 nm versus the amount of NDI (see in-set in figure 4.13b) showed a break point with respect to the formation of 1:1 complex. The 1:1 ratio in the donor-acceptor complex implies the formation long range of alternative ...D-A-D-A... arrangements in continuum. Emission spectra of complexes were also recorded for the addition of NDI or PDI into the P-8 polymer for the above mentioned concentration range. The OPV segmented P-8 polymer is highly luminescent and it underwent fluorescence quenching followed the formation of CT band between OPV-NDI or OPV-PDI interactions (see Figures 4.13c and 4.13d). The plots of OPV emission intensity versus the NDI or PDI concentration showed sharp break points at 1:1 ratio of both

OPV polymer-NDI and OPV polymer-PDI complexes (in set figure 4.13c and 4.13d). Thus, based on the above experiments, it may be concluded that segmented OPV polymers possessed unique polymer topology to make extended D/A assemblies with 1:1 composition ratio.

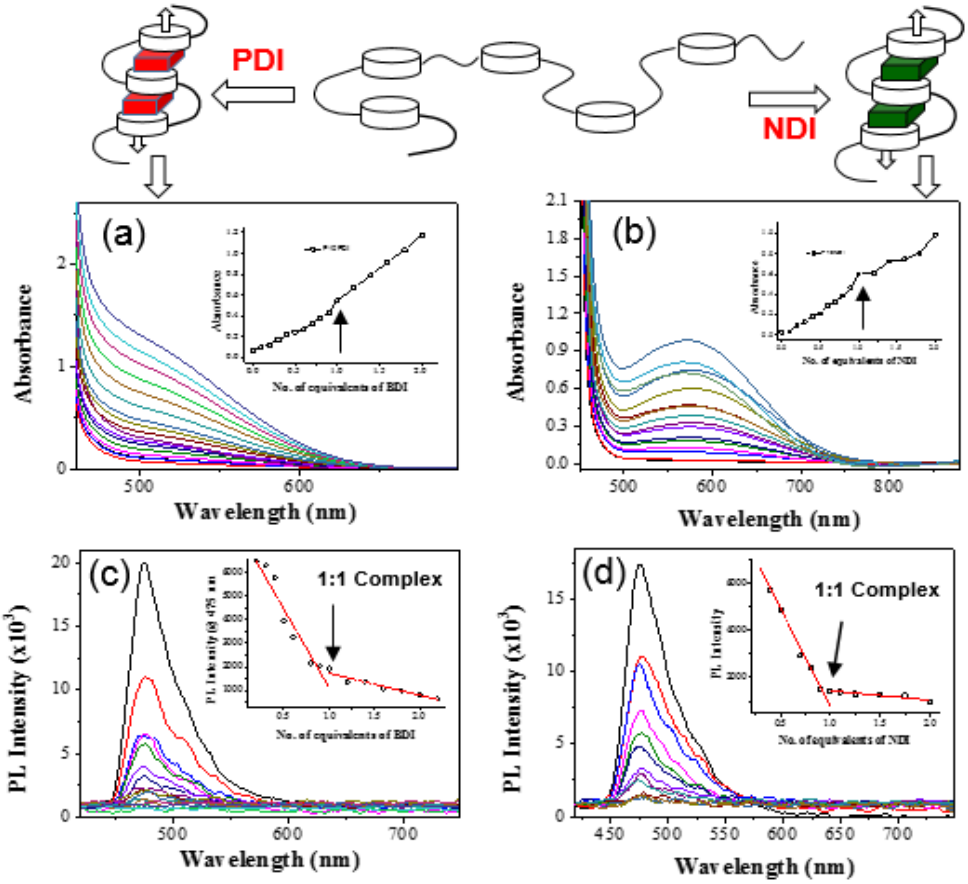

Figure 4.13. *(a) Absorbance spectra of P-8 polymer to followed by the addition of various amounts of PDI in toluene. (b) Absorbance spectra of P-8 polymer to followed by the addition of various amounts of NDI in toluene. Emission spectra of P-8 polymer followed by the addition of PDI (c) and NDI (d) in toluene. The concentration of P-8 was maintained as* $3.0x10^{-2}$ *M and the amount of NDI or PDI were varied from* $5.0x10^{-3}$ *M to* $6.0\ x10^{-2}$ *M for the above experiments.*

The reversibility of these D-A complexes was checked by variable temperature photophysical absorbance and emission studies. P-8+NDI complex with 1:1 ratio was subjected to heating (from 5 to 90 °C) and cooling (from 90 to 5 °C) and their absorbance and emission spectra are shown in Figure 4.14. The plot of absorbance maxima versus temperature showed decrease in the intensity of CT band in the heating cycle and increase in the CT band in the cooling cycle; however no

clear break point could be observed. The CT band was reversible in the subsequent cooling cycles. These experiments confirmed the reversibility of D/A self-assemblies and the existence of the CT band in the OPV polymer donor-acceptor systems.

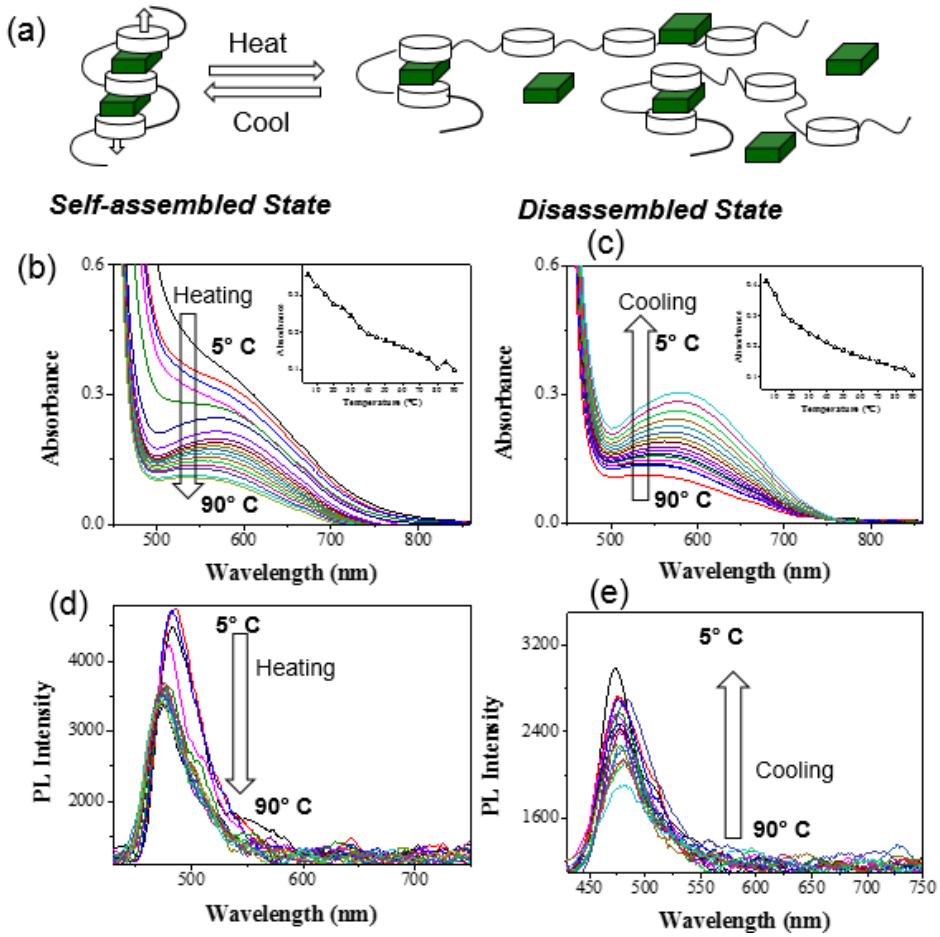

Figure 4.14. *(a) Schematic representation of D-A complex with temperature. Absorbance and (b) emission spectra of P-8+NDI in (b) heating and (c) cooling cycles. Emission spectra of P-8+NDI in (d) heating and (e) cooling cycles. The concentration of P-8 was maintained as 3.0x10^{-2} M and the donor-acceptor mole ratio was maintained as 1:1.*

4.3.4. Oligomer CT Band Formation

Structurally identical oligo-phenylenevinylene (OPV)s were synthesized and complexed with NDI and PDI to produce OPV-NDI and OPV-PDI CT complexes. These small molecular complexes provided additional opportunity to trace the role of macromolecular chain effect on the CT complexes stability. For this purpose, two OPVs having C_7 and C_8 side chains were synthesized as shown in Figure 4.15a. DSC analysis of OPV_n, was carried out at the heating/cooling cycle rate of 10 °C/min and

OPV7 and OPV8 showed simple single sharp melting and crystallization transition in heating and cooling cycles (see figure 4.15b). The data of OPVs and their complexes with PDI and NDI summarised in table 4.2. DSC thermograms showed in Figures 4.15.

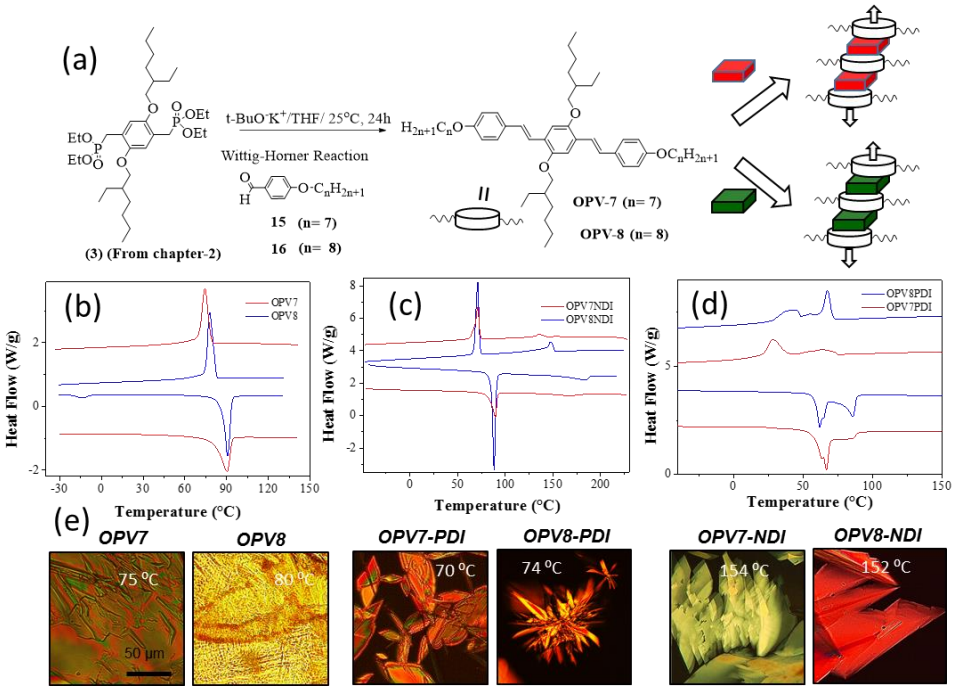

Figure 4.15. *(a) Synthesis of OPVs and schematic representation of donor-acceptor complexation with PDI, and NDI. (b) DSC thermograms of OPV7, OPV8 in heating cycle and cooling cycle. DSC thermograms of (c) PDI and (d) NDI complexes of OPV7, and OPV8 in heating cycle and cooling cycle. (e) PLM images of OPV7, OPV8 and their complexes with PDI and NDI on glass cover slips in the cooling and heating cycles. The heating and cooling cycles were programmed at 10 °/min rate.*

OPVs and their complexes were subjected to PLM analysis with a programmable hot stage. Both OPVs showed sharp melting and crystalline transition in heating and cooling cycles. The OPVs started with needle like nucleation and rapid growth of crystalline vectors and their PLM images were showed in Figures 4.15. The oligomer complexes were also found to be crystalline. The OPV+PDI and OPV+NDI complexes showed two transitions in heating and cooling cycles and these two transitions were not belonging to either of individual components. The PLM images of OPV+PDI and OPV+NDI complexes showed in Figure 4.15. The D-A complexes showed flower like textures followed by crystalline phase as reported earlier reports.[39-42]

Table 4.2. DSC thermal data of OPVs, OPV+PDI and OPV+NDI complexes the heating and cooling cycle at 10°/min.

Sample	T_{M1} (K)	T_{M2} (K)	ΔH_{M1} (kJ/mol)	ΔH_{M2} (kJ/mol)	T_{C1} (K)	T_{C2} (K)	$\Delta H_1^{(c)}$ (kJ/mol)	$\Delta H_2^{(c)}$ (kJ/mol)
OPV7	363.8	-	37.67	-	347.4	-	40.34	-
OPV8	363.7	-	40.1	-	351.7	-	44.7	-
OPV7PDI	339.9	346.8	28.2	4.04	337.2	301.0	7.6	24.26
OPV8PDI	335.2	359.2	23.3	23.1	339.8	316.2	22.10	15.62
OPV7NDI	362.8	441.5	35.95	7.92	410.2	344.2	9.0	36.80
OPV8NDI	361.7	456.7	65.21	0.93	441.4	343.2	3.74	62.73

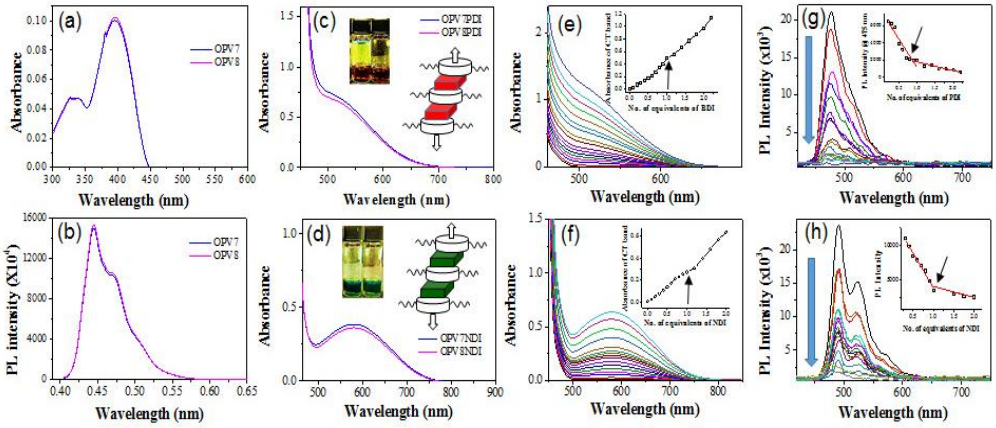

Figure 4.16. *(a) Absorbance and (b) Emission spectra of OPV7 and OPV8. (c) Absorbance spectra of OPV+PDI complexes at 3.0x10^{-2} M in toluene. (d) Absorbance spectra of OPV+NDI complexes. The donor-acceptor mole ratio was maintained as 1:1. Absorbance spectra of OPV8 to followed by the addition of various amounts of (e) PDI and (f) NDI in toluene. Emission spectra of OPV8 followed by the addition of (g) PDI, and (h) NDI in toluene. The concentration of OPV8 was maintained as 3.0x10^{-2} M and the amount of PDI or NDI was varied from 5.0x10^{-3} M to 6.0 x10^{-2} M for the above experiments.*

The photophysical properties of the OPVs were studied in solution (toluene) as well as in solid state (in film). In toluene, at dilute concentration, the OPVs showed almost identical absorbance and emission maxima (see Figure 4.16) with respect to their polymer samples (see Figure 4.12). To measure the donor-acceptor interactions, the concentrations of OPV chromophore was taken as 3.0 x10^{-2} M in toluene and

mole ratio of the donor-to-acceptor was retained as 1: 1. Both the OPV chromophore do not have absorbance above 400 nm; thus, the emerging of red and green colour in the PDI and NDI complexes were attributed to the formation of charge transfer (CT) complexes. The CT bands in the OPV +PDI and OPV +NDI were observed at 525 nm and 600 nm, respectively (see Figures 4.16c and 4.16d). Further, the tendencies for the CT band formation in the complexes were not influenced by the variable alkyl chain length in the OPV molecules. This suggested that it was purely electrostatic interactions between the chromophores drive the CT band and not the topology of the OPV chromophore. To determine the donor-acceptor complex ratio, concentration dependent absorbance measurements were carried out by keeping the OPV donor constant ($3.0x10^{-2}$ M) and varied number of equivalent of acceptor (NDI or PDI) from $5.0x10^{-3}$ M to $6.0 x10^{-2}$ M. The plot of absorbance at 580 nm versus the amount of NDI (see in-set in figure 4.16f) showed a break point with respect to the formation of 1:1 complex. The 1:1 ratio in the donor-acceptor complex implies the formation infinite extension of alternative D-A-D-A arrangements in continuum. Emission spectra of complexes were also recorded for the addition of NDI or PDI into the OPV8 for the above mentioned concentration range. The plots of OPV emission intensity versus the NDI or PDI concentration showed sharp break points at 1:1 ratio of both OPV-NDI and OPV-PDI complexes (see insert Figure 4.16g and 4.16h). Thus, based on the above experiments, it may be concluded the OPV possessed unique polymer topology to make extended D/A assemblies with 1:1 composition ratio as similar to that of polymer-NDI or PDI complexes. Hence, the ability to produce D-A CT complexes in solution by OPV chromophores was not restricted to oligomeric or polymeric systems.

The quenching constant or association constant calculated for poymer+NDI and OPV8+NDI by using Stern-Volmer equation.

$$I_0/I=1+K_{SV}[Q]$$

Where, I_0 and I are the fluorescence intensities observed in the absence and presence of quencher. K_{SV} is the Stern-Volmer quenching constant or association constant for the charge transfer complex. In some cases, the fluorophore can form a stable complex with another molecule. From the concentration dependent fluorescence data (see Figure 4.13 and 4.16), the K_{SV} constants for P8+NDI complex and OPV8+NDI

complex were determined as 310 g/mol and 103 g/mol, respectively. The K_{SV} determination is shown in Figure. 4.17. The higher K_{SV} for the polymer complex confirmed that the macromolecular complexation effect in the present CT complex was almost 3 times higher their small oligomer CT complexes.

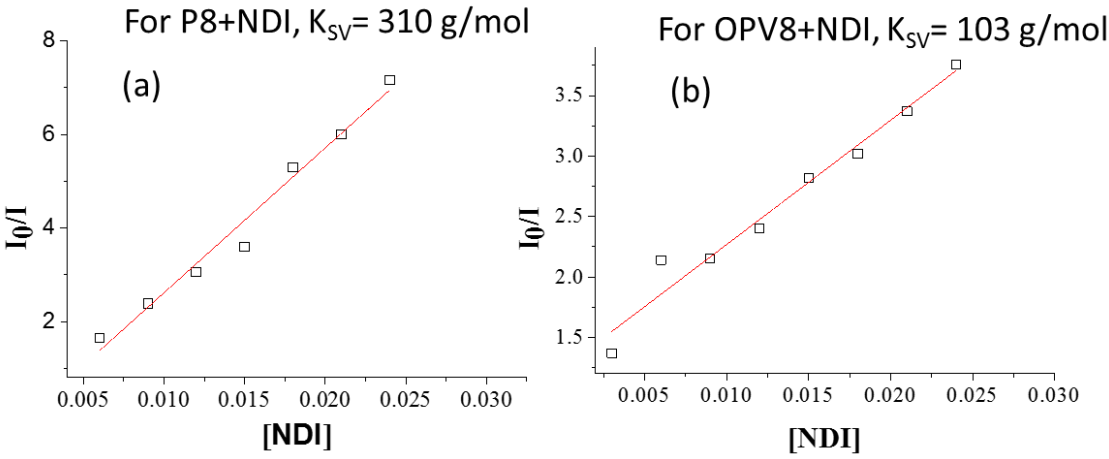

Figure 4.17 *Stern-volume plot for (a) P-8+NDI and (b) OPV8+NDI complexes.*

4.3.5. Charge Transfer Complexes in Solid State

The ability to form stable CT complex in the solid state (or thin film) is highly dependent on their close packing of chromophore which is completely different from solution state. For instance in the solution, the chromophores are completely solvated by the solvent molecules and the dissolved molecules can easily diffused in the medium to get associated to maximize the donor-acceptor interactions. On the other hand, in the solid state many factors controlled the molecular interactions and some important ones are: (i) restricted diffusion of the electron deficient molecules in the electron rich OPV donor polymer, (ii) segregation of individual chromophores due like-like interactions, and (iii) phase separation donor and acceptor phase chromophores followed by the crystallization in the polymer matrix either by the acceptor molecules or polymer chains. To study the solid state charge transfer complex properties, thin films of the CT complexes were prepared on thin glass slide using the PLM hot stage setup. A pinch of the sample as planed between two glass cover-slips and it was melted above the melting temperature and allowed to cool at 10 °C/min to make uniform thin film. During this film preparation, the images were recorded to make sure the reproducibility of the data.

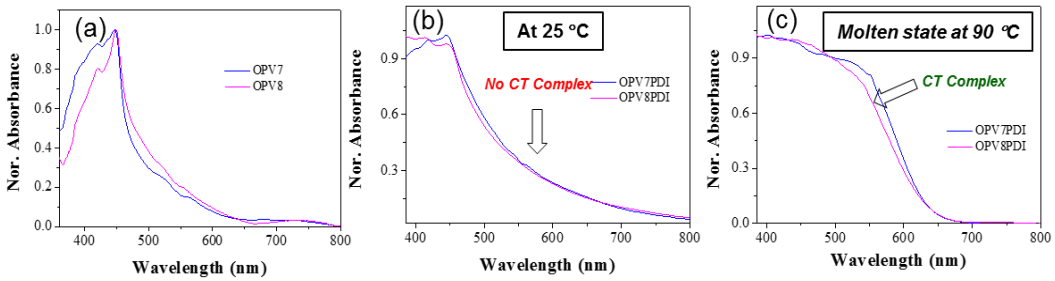

Figure 4.18*. (a) Absorbance spectra of OPV at room temperature. (b) Absorbance spectra of OPV+PDI complexes (c) at 25 °C and (d) at 90 °C in film/solid state. The donor-acceptor mole ratio was maintained as 1:1.*

Solid state absorbance spectra of the OPVs and their NDI and PDI complexes are given in Figure 4.17. The OPVs showed absorbance maxima at 450 nm, and the peaks were slightly red-shifted in compared to their solution spectra (see Figure 4.16a). The emission spectra of the OPVs showed strong bluish-green emission whereas both NDI and PDI did not show any fluorescence (spectra not shown). The absorbance spectra of OPV+PDI complexes did not show with respect to CT band at 25°C. The thin-film was measured absorbance at 90°C using the temperature controller set-up in the UV-Vis spectrophotometer. At 90 °C, the spectra showed strong absorbance at 600 nm with respect to the existence of CT band (see figure 4.18c). DSC analysis in Figure. 4.15 revealed that the OPV-PDI CT complex has melting transition at 80°C; thus above this temperature the complex existed as molten state. Thus, the absorbance spectra at 90 °C showed CT band due to the free mixing of donor and acceptor molecules in the molten state (molten state is similar to solution for free movement of molecules). A similar experiment for NDI-OPV complex could not be performed due to the limitation in the temperature controller in the UV-Vis spectrophotometer as110 °C upper limit. The OPV-NDI complexes melt above 180 °C (see DSC plots in Figure 4.15); thus, we could not able to record the spectra in their molten state. Nevertheless, the OPV-PDI complex clearly revealed that the OPV base CT complexes were completely absent at room temperature (at 25 °C) due to the crystallization of individual donor and acceptor components and phase separation of D and A. The miscibility of the D and A enhanced in the molten state which exhibits CT band. This process is schematically shown in Figure 4.19.

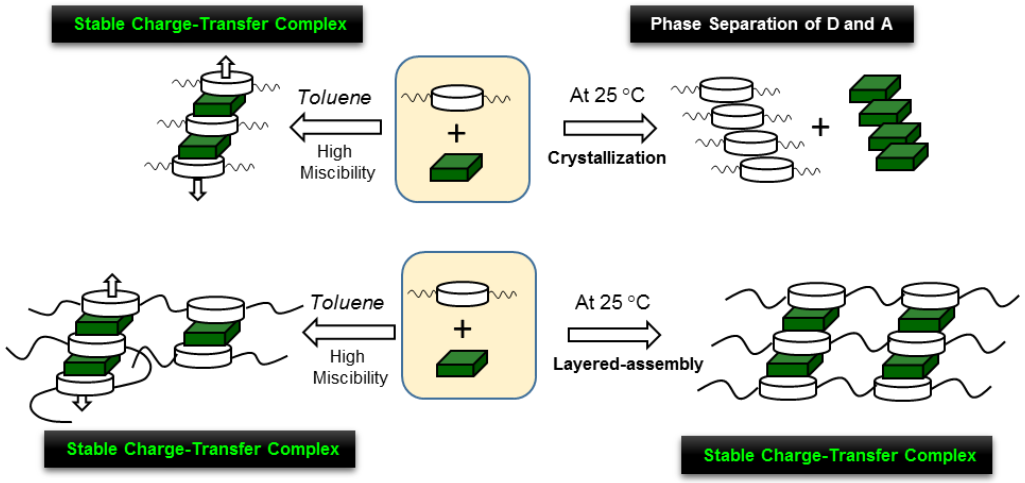

Figure 4.19. *Schematic representation of arrangement of donor-acceptor complex in solution and solid state at different temperatures.*

To study the solid state charge transfer properties of the segmented OPV polymer with NDI or PDI, their 1:1 complexes were processed as thin films on glass substrate using the method described for OPV complexes. Solid state absorbance spectra of PDI and polymer complexes are given in figure in 4.20a. The PDI (also NDI) chromophores and OPV polymers showed absorbance spectra < 500 nm. These peaks were slightly red-shifted in compared to their solution spectra (see Figure 4.12a). The emission spectra of the P-7 and P-8 polymers showed strong bluish-green emission whereas both NDI and PDI did not show any fluorescence (see figure 4.20b). The absorbance spectra of OPV polymer + PDI complexes thin films were recorded at 25 °C and reported in figure 4.20c. These spectra showed peak at 580 nm with respect to the strong CT band covering entire visible region (see figure 4.20c). The comparison of the CT complexes of OPV-PDI and segmented OPV polymer-PDI complexes clearly evident that, the polymer CT complexes were very unique and produce stable CT complexes at 25 °C. The absorbance spectra of OPV polymer-NDI complexes showed board absorbance staring form 580 nm to 1100 nm covering the visible to NIR range (see figure 4.19d). Further, the longer segmented OPV polymer P-8 to P-10+NDI showed much higher red shift in the absorbance spectra compared to the P-5 to P-7 +NDI complexes. This trend is attributed to the increase in the packing efficiency of the D-A assemblies with increase in the aliphatic unit in the segmented polymer chains. The emission spectra of the D-A assemblies in the solid state did not show any fluorescence confirming the observation of CT band in Figure 4.20a. To

infer more insight into the absorbance range of the polymer-PDI and polymer-NDI CT band harvesting the entire solar spectrum, the absorbance spectra of the complexes plotted along with solar spectra AMI..... and shown in figures 4.20e and 4.20f, respectively.

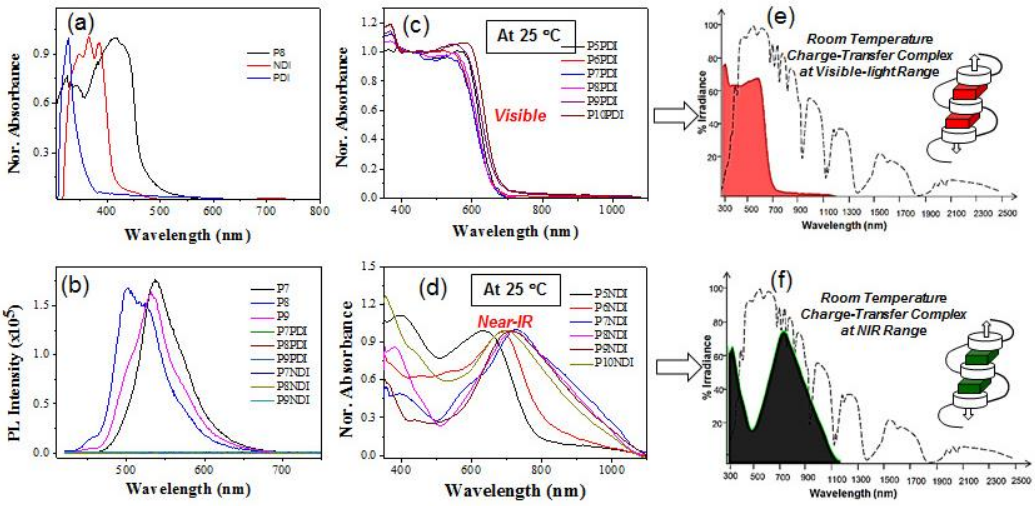

Figure 4.20. *(a) Absorbance spectra of NDI, PDI, and P-8 in film/solid state. (b) Emission spectra the polymers P-7, P-8 and P-9, respectively, in their PDI and NDI complexes. Absorbance spectra of the (c) OPV polymers+PDI, and (d) OPV polymer+NDI complexes in film/solid state. Schematic representation of absorbance spectra of (e) P8+PDI complex, and (f) and P8+NDI complexes. The donor-acceptor mole ratio was maintained as 1:1.*

The OPV polymer+PDI complexes absorbed the light mostly in the visible light corresponding to red-region whereas the OPV polymer+ NDI complexes covered the visible to NIR region from 300 to 1100 nm. It is important to highlight that the charge transfer complexes of OPV polymer + PDI and OPV polymer+NDI was very stable and observed at room temperature. Further, the solid state CT band absorbance was found to be much higher in intensity compared to their solution CT band (compare figure 4.12c and 4.12d). The stability of the CT band in the polymer complex was attributed to the macromolecular chain effect in the supramolecular assemblies of donor-acceptor system. The WXRD data for OPV polymer-NDI complex further supported that the complexes were existed in the well defined 2D layers assembly. Thus, the OPV polymers chains could able to fold in such a manner to tarp the acceptors molecules in their matrix to retain the CT band at room temperature. This macromolecular chain effect on the CT band stabilization is shown

in Figure 4.18. Hence, it may be concluded that the new combination of OPV polymer+NDI donor-acceptor solid state assemblies is one of the first examples to produce CT band capable of absorption the light entire solar spectrum at the room temperature. The CT band the D-A complexes in the solid state was observed to very stable for more than 6 months at room temperature in normal laboratory conditions. This unique stable CT complexes can be used for harvesting efficient solar energy in photovoltaics, etc which has to be explored in future endowers.

4.3.6. Energy calculation for CT band

To understand the charge transfer complexes formation in segmented OPV polymers with PDI and NDI, the energy HOMO (S_0) and LUMO (S_1) energy levels were compared. The S_1 energy level of OPV, PDI and NDI chromophores were reported by other groups based on DFT calculation (from vacuum level) are directely used.[45-47] The S_1 energy level (or LUMO) of OPV, PDI and NDI chromophores were reported as -2.60 eV, -2.95 eV and -3.56 eV, respectively. The optical energy gapes (E_g) of the P-8 (having OPV), PDI and NDI were determined from their ons-set of their thin-film absorbance spectra (see Figure 4.20.) as 2.30 eV, 3.20 eV and 2.58 eV, respectively. This facilitated the determination of HOMO levels of OPV, PDI and NDI chromophores using the formula; $S_0 = S_1 + E_g$ and the values were obtained as -4.97, -6.15, and -6.14, for OPV, PDI and NDI chromophores, respectively and the values are reported in Table 4.3.

Table. 4.3. Energy calculations

Sample	Optical Band gap E_g, (eV)[a]	S_1 (eV) (LUMO)	$S_0 = S_1 + E_g$ (eV), (HOMO)
P8 (OPV)	2.30	- 2.60[b]	- 4.97
PDI	3.20	- 2.95[c]	-6.15
NDI	2.58	- 3.56[d]	-6.14
P8+PDI	1.76	-4.39[e]	-6.15[e]
P8+NDI	1.13	-5.02[e]	-6.15[e]

a) Determined from on-set of the absorbance spectra in thin film

[b] Adapted from Janssen et al. *J. Phys. Chem. B* **2000**, *104*, 10174.

[c] Adapted from Schab-Balcerzak et al. *J. Phys. Chem. C* **2014**, *118*, 13070

[d] Adapted from Singh et al. *Org. Electron*. **2006**, *7*, 480.

[e] Determined using the formula $S_1 = S_0 - E_g$ since the energy levels of HOMO of the charge separate states cannot be lower than that of acceptor chromophores NDI or PDI in the CT complex

The optical band gap of the charge transfer complexes were determined as 1.76 and 1.13 eV (from absorbance spectra Figure 4.20) for P-8+PDI and P-8+NDI, respectively. Since the S_0 levels of NDI and PDI were already very low in the range of -6.15 eV, their charge transfer complexes S_0 state most unlikely expected to have lower than this energy level. Hence, the S_0 of P-8+PDI and P-8+NDI complexes were taken as -6.15 eV. The S_1 state of these CT complexes were determined using the formula: $S_1 = S_0 - E_g$ and these values were found to be 1.76 and 1.13 eV for P8+PDI and P-8+NDI complexes, respectively these values are given in table 4.3.

These energy levels are plotted and shown for P-8, PDI, NDI, P-8+PDI and P-8+NDI in Figure 4.20. The charge transfer complexes can be formed in the donor-acceptor system by two independent pathways: (i) initial photoexcitation of donor D*A followed by the indirect charge transfer process D^+A^-(path-1) or (ii) the direct charge separation process (path-2). If the D-A assemblies follow the path-1, then this excitation energy could be used for the fluorescence from the acceptor molecule. In the present system both NDI and PDI complex did not show any fluorescent; thus, the possibility for path-1 process is negligible. Thus, we presume that the direct charge separation would be the most acceptable mechanism for the formation of the CT complex between the segmented OPV polymer and arylenebisimide acceptors (see the figure 4.21). The energy gap of the P-8+PDI was relatively high (1.76 eV) which account for the red-colour absorption. On the other hand, the Eg for the P-8+NDI is very low in the range of 1.1 eV which produced CT absorption in the NIR region. Hence, the present polymer design provides unique opportunity to tune the colour of the CT complexes both in the visible and NIR region. Further, it is worth to mention that the red and green colour absorption of the CT bands stabilized both solution and in solid state exclusively by the segmented OPV polymers through macromolecular

complexation effect which is one of the first examples for room temperature CT complexes based on π-conjugated polymers. The segmented OPV polymer based CT complexes reported here are not only restricted to OPV π-core, and in general it can be expanded to wide ranges of other π-conjugated systems to explore this new concept for material applications.

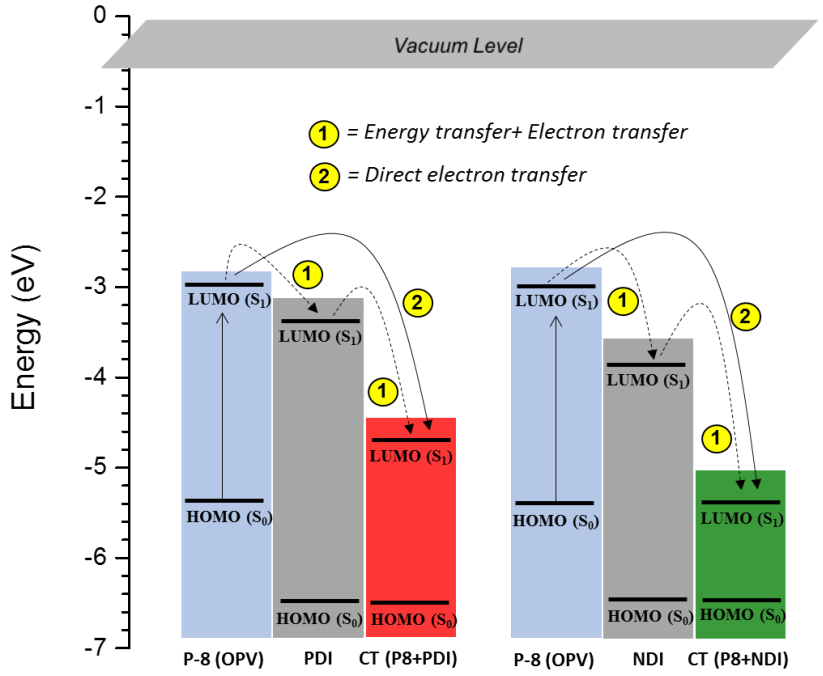

Figure 4.21. *The energy transfer and the indirect (1, shown dotted line) and direct (2, shown solid line) charge-separation processes.*

4.4. Conclusion

In conclusion, the charge transfer interaction is driven by self-assemblies of segmented poly(phenylenevinylene)s with electron deficient molecules by solvent free as well as solvent assisted self-organization. New series of segmented OPV polymer based supramolecular donor-acceptor complexes have been designed by choosing PDI and NDI as acceptors. Semi-crystalline or amorphous segmented OPV polymers have been chosen and they were complexed with NDI that produced green coloured CT complexes spanning the absorbance range from visible to NIR region and with PDI produced red covering the visible region. The CT complexes showed 1:1 complexation for donor polymers and acceptor NDI (or PDI) molecules with respect to long range order of D-A-D-A-D-A π-stacked supramolecular assemblies. Interestingly, the solid state alignment of the D-A interaction was controlled by the type of the acceptor units; as a result OPV polymer-NDI complex arranged in lamellar fashion in solid state confirmed by Electron microscope, polarizing microscope and X-ray diffraction analysis. To study the macromolecular effect on the D-A complexation in the CT complex, structurally identical small molecule OPV analogues were synthesized. The OPV-NDI and OPV-PDI complexes were found to exhibit CT band in the solution; however, the phase separation of individual donor and acceptor in solid state was observed at room temperature. Interestingly, charge transfer interaction between OPV polymers and acceptor produced stable CT complexes at room temperature. The polymer + PDI complexes showed broad CT band in the range of 500-700 nm and the polymer + PDI complexes showed broad CT band in the range of 500-1100 nm band in solid state. Hence, it may be concluded that the new combination of OPV polymer+NDI donor-acceptor solid state assemblies is one of the first examples to produce CT band capable of absorbing the light in the entire solar spectrum at the room temperature. Additionally, these stable room temperature donor-acceptor CT self-assemblies can be processed under solvent free melt crystallization process; thus, they are very important futuristic materials for direct processing in optoelectronics. The segmented OPV polymer based CT complexes reported here are not only restricted to OPV π-core, and in general it can be expanded to wide ranges of other π-conjugated systems to explore this new concept for material applications.

4.5. References

1. Wang, C.; Dong, H.; Hu, W.; Liu, Y.; Zhu, D. *Chem. Rev.* **2012**, *112*, 2208-2267.
2. Hoeben, F. J. M.; Jonkheijm, P.; Meijer, E. W.; Schenning, A. P. H. J. *Chem. Rev*. **2005**, *105*, 1491-1546.
3. Sommer, M.; Huettner, S.; Thelakkat, M. *J. Mater. Chem.* **2010**, *20*, 10788-10797.
4. Hunter, C. A.; Lawson, K. R.; Perkins, J.; Urch, C. J. *J. Chem. Soc. Perkin Trans.* **2001**, *2*, 651–669.
5. Tayi, A. S.; Kaeser, A.; Matsumoto, M.; Aida, T.; and Stupp, S. I. *Nature Chem.* **2015**, *7*, 281
6. Huettner, S.; Hodgkiss, J. M.; Sommer, M.; Friend, R. H.; Steiner U.; Thelakkat, M. *J. Phys. Chem. B* **2012**, *116*, 10070−10078.
7. Eckert, J. F.; Nicoud, J. F.; Nierengarten, J. F.; Liu, S. G.; Echegoyen, L.; Barigelletti, F.; Armaroli, N.; Ouali, L.; Krasnikov, V.; Hadziioannou, G. *J. Am. Chem. Soc.* **2000**, *122,* 7467-7479.
8. Peeters, E.; Hal, P. A. V.; Knol, J.; Brabec, C. J.; Sariciftci, N. S.; Hummelen, J. C.; Janssen, R. A. J. *J. Phys. Chem. B* **2000,** *104*, 10174-10190.
9. Wang, L.; Wu, C-F.; Wang, H-Y.; Chen, Q-D.; Han, W.; Qin, W-P.; McNeill, J.; Sun, H-B. *Nanoscale*, **2013**, *5*, 7256-7270
10. Neuteboom, E. E.; Meskers, S. C. J.; Hal, P. A. V.; Duren, J. K. J. V.; Meijer, E. W.; Janssen, R. A. J.; Dupin, H.; Pourtois, G.; Cornil, J.; Lazzaroni, R.; Bredas, J. L.; Beljonne, D. *J. Am. Chem. Soc.* **2003**, *125*, 8625-8638.
11. L. Ouali, L.; Krasnikov V. V., Stalmach, U.; Hadziioanno, G. *Adv. Mater.* **1999**, *11*, 1515-1518.
12. Asha, S. K.; Schenning, A. P. H. J.; Meijer, E. W. *Chem. Eur. J.* **2002**, *8*, 3353-3361.
13. Jalani, K.; Kumar, M.; George, S. J. Chem. Commun. 2013, 49, 5174 –5176;
14. Scott Lokey, R.; Iverson, B. L. *Nature* **1995**, *375*, 303 –305;
15. Ghosh, S.; Ramakrishnan, S.; *Macromolecules* **2005**, *38*, 676-686.
16. Ghosh, S.; Ramakrishnan, S. *Angew. Chem. Int. Ed.* **2004**, *43*, 3264-3268
17. Ghosh, S.; Ramakrishnan, S. *Angew. Chem. Int. Ed.* **2005**, *44*, 5441-5447.

18. Kaiser, G.; Jarrosson, T.; Otto, S.; Ng, Y.-F.; Bond, A. D.; Sanders, J. K. M. *Angew. Chem. Int. Ed*. **2004,** *43*, 1959 –1962;
19. Vignon, S. A.; Jarrosson, T.; Iijima, T.; Tseng, H.-R.; Sanders, J. K. M.; Stoddart, J. F. *J. Am. Chem. Soc.* **2004**, *126*, 9884 – 9885.
20. De Greef, T. F. A.; Smulders, M. M. J.; Wolffs, M.; Schenning, A. P. H. J.; Sijbesma,; R. P., Meijer, E. W. *Chem. Rev.* **2009**, *109*, 5687.
21. Huang, F.; Scherman, O. A. *Chem. Soc. Rev*. **2012**, *41*, 5879.
22. Pandeeswar. M.; Senanayak. S. P.; Narayan. K. S.; Govindaraju. T. *J. Am. Chem. Soc.* **2016**, *138*, 8259−8268.
23. Tayi, A. S.; Shveyd, A. K.; Sue, A. C.-H.; Szarko, J. M.; Rolczynski, B. S.; Cao, D.; Kennedy, T. J.; Sarjeant, A. A.; Stern, C. L.; Paxton, W. F.; Wu, W.; Dey, S. K.; Fahrenbach, A. C.; Guest, J. R.; Mohseni, H.; Chen, L. X.; Wang, K. L.; Stoddart, J. F.; Stupp, S. I. *Nature* **2012**, *488*, 485
24. López-Andarias, J.; Rodriguez, M. J.; Atienza, C.; López, J. L.; Mikie, T.; Casado, S.; Seki, S.; Carrascosa, J. L.; Martín, N *J. Am. Chem. Soc.* **2015**, *137*, 893-897.
25. Prasanthkumar, S.; Ghosh, S.; Nair, V. C.; Saeki, A.; Seki, S.; Ajayaghosh, A. *Angew. Chem., Int. Ed*. **201**5, *54*, 946-950.
26. Diez-Perez, I.; Li, Z. H.; Guo, S. Y.; Madden, C.; Huang, H. L.; Che, Y. K.; Yang, X. M.; Zang, L.;Tao, N. J. *ACS Nano* **2012**, 6, 7044-7052
27. Das, A.; Ghosh, S. *Angew Chem. Int. Ed.* **2014**, *53*, 2038–2054.
28. Kumar, M.; Venkata Rao, K.; George, S. J. *Phys. Chem. Chem. Phys.* **2014**, 16, 1300.
29. Chakraborty, S.; Kar, H.; Sikder, A.; Ghosh, S. *Chem. Sci **2017**, 8*, 1040.
30. Sikder, A.; Ghosh, B.; Chakraborty, S.; Paul, A.; Ghosh, S.; *Chem. Eur. J.* **2016**, *22*, 1908-1913.
31. Kar, H.; Ghosh, S.; *Chem. Commun.* **2014**, *50*, 1064-1066.
32. Kumar, M.; George, S. J. Chem. Asian J. 2014, 9, 2427-2431.
33. Shinde. S.; Asha. S. K.; *Macromolecules* **2016**, *49*, 8134−8145.
34. Tan, T. A. T.; Clarke, T. M.; James, D.; Durrant, J. R.; White, J. M.; Ghiggino, K. P.; *Polym. Chem.* **2013**, *4*, 5305–5309.

35. Goel, M.; Narasimha, K.; Jayakannan, M. *Macromolecules* **2014**, *47*, 2592−2603.
36. Che, Y.; Huang, H.; Xu, M.; Zhang, C.; Bunes, B. R.; Yang, X.; Zang, L. *J. Am. Chem. Soc.* **2011**, 133, 1087–1091.
37. Wang, J.-Y.; Yan, J.; Ding, L.; Ma, Y.; Pei, J. *Adv. Funct. Mater*. **2009**, *19*, 1746.
38. Park. L. Y.; Hamilton. D. G.; McGehee. E. A.; McMenimen. K. A. *J. Am. Chem. Soc.* **2003**, *125*, 10586-10590.
39. Alvey, P. M.; Reczek, J. J.; Lynch, V.; Iverson, B. L. *J. Org. Chem.* **2010**, *75*, 7682- 7690.
40. Reczek, J. J.; Villazor, K. R.; Lynch, V.; Swager, T. M.; Iverson, B. L. J. Am. Chem. Soc. **2006,** *128* 7995-8002
41. Pisula, W.; Kastler, M.; Wasserfallen, D.; Robertson, J. W. F.; Nolde, F.; Kohl, C.; Müllen, K. *Angew. Chem., Int. Ed.* **2006**, *45*, 819.
42. Leight, K. R.; Esarey, B. E.; Murray, A. E.; Reczek, J. J. *Chem. Mater*. **2012**, *24*, 3318– 3328.
43. Narasimha, K.; Jayakannan, M. *ACS Appl. Mater. Interfaces* **2014**, 6, 19385−19396.
44. Sharma, S.; Kolhe. N. B.; Gupta, V.; Bharti, V.; Sharma, A.; Datt, R.; Chand, S.; Asha, S. K. *Macromolecules* **2016**, *49*, 8113−8125.
45. Peeters, E.; van Hal, P. A.; Knol, J.; Brabec, C. J.; Sariciftci, N. S.; Hummelen, J. C.; Janssen, R. A. J. *J. Phys. Chem. B* **2000**, *104*, 10174.
46. Grucela-Zajac, M.; Bijak, K.; Kula, S.; Filapek, M.; Wiacek, M.; Janeczek, H.; Skorka, L.; Gasiorowski, J.; Hingerl, K.; Sariciftci, N. S.; Nosidlak, N.; Lewinska, G.; Sanetra, J.; Schab-Balcerzak, E. *J. Phys. Chem. C* **2014**, *118*, 13070.
47. Singh, T. B.; Erten, S.; Zafer, C.; Turkmen, G.; Kuban, B.; Teoman, Y.; Sariciftci, N. S.; Icli, *Org. Electron*. **2006**, *7*, 480.

Summary and Future directions

The thesis entitled **"*Segmented π-Conjugated Polymers for Optical and Biomedical Applications*"** deals with design and development of segmented OPV polymer diverse self-assembly for optical and biomedical applications. The thesis is aimed to develop unique classes of semicrystalline segmented π-conjugated polymers with rigid OPV core and flexible alkyl units to demonstrate the organic photonic switches. Amphiphilic segmented π-conjugated polymers with color tunability in good and bad solvent combination and employ for bio imaging. Further, these polymers complexed with acceptors like PDI and NDI forms color tunable CT complexes covering visible and NIR region.

In chapter 2, In conclusion, a unique new series of semicrystalline segmented π-conjugated polymers designed with rigid OPV core and flexible alkyl units to demonstrate the organic photonic switches or organic λ/4 wave plates. These classes of segmented polymers were found to be either semicrystalline or amorphous depending upon even or odd numbers of carbon atoms present in the alkyl spacers length. Variable temperature WXRD studies revealed that the polymer chains packed as lamellar network in the solid state. Single crystal structure of OPV-oligomer was resolved to understand the packing of the lamellar-assemblies in the polymer backbone. Absorbance, emission, solid state photoluminescence quantum yield and fluorescence life time studies facilitated the understanding of the segmented polymers with respect to even or odd carbon atoms. Interestingly, the even-polymer with highest crystallinity (P-6 and P-8) produced stable polymer organogel unlike their amorphous odd-polymers. The morphology of the P-8 polymer gel was characterized by FESEM, HR-TEM and AFM analysis. Variable temperature photophysical studies revealed that the organogel showed thermo-reversible and sol→gel transition at 42-44 °C. Further, mechanical stability of the polymer organogel confirmed by the rheology measurements. The organogel was transferred into a glass capillary and the aligned gel was demonstrated as photonic switches. The polymer organogel was found to behave as λ/4 wave plates and showed highest intensity for incident plane polarized at θ = 45° under crossed-polarizers. The thermoreversibility of the polymer gel was explored to construct thermo-responsive photonic switches for the temperature range from 25 to 160 °C.

In chapter 3, a new series of amphiphilic segmented π-conjugated polymers having π-conjugated core was constituted by oligo-phenylenevinylene (OPV) units with variable anchoring units at the periphery to tune their rigidity and solubility for self-organization. The flexible segments were chosen from oligoethyleneoxy units and they were placed in the backbone of the chains to yield amphiphilic segment OPV polymers. Solvent induced aggregation ability of the segmented polymers were investigated in chloroform+methanol, THF+water and water alone. The π-conjugated OPV core was found to undergo strong aromatic π-π stacking upon increasing the composition of the bad solvent (water or methanol) in the polymer solution. The polymer P-TCD-6EG was found to produce helical nanofibrous morphology in good solvents (chloroform or THF) and it underwent a morphological transition from fibres to hollow spheres upon varying the solvent composition. This morphological transition was also accompanied by the fluorescence color tuning by the OPV core. It was found that the chromophores exhibited blue-to-white-to-yellow color change along with the morphological transitions. Dynamic light scattering studies confirmed that the segmented polymers indeed produced stable spherical nano-aggregates of 200 nm in the solution. Steady state fluorescence studies and time-resolved fluorescent decay dynamic analysis confirmed the color tunability in the segmented π-conjugated polymers. The polymers produced stable nanoparticles assemblies in water with luminescent properties. Cytotoxicity in cervical and breast cancer cells revealed that these segmented polymer nanoparticles are non-toxic to cells. Confocal microscopy imaging revealed that the polymer nanoparticles selectively accumulated in the nucleus.

In chapter 3, The charge transfer interaction driven by self-assemblies of segmented poly(phenylenevinylene)s with electron deficient molecules by solvent free as well as solvent assisted self-organization. New series of segmented OPV polymer based supramolecular donor-acceptor complexes made by choosing PDI and NDI as acceptors. Semi-crystalline or amorphous segmented OPV polymers have chosen and they were complexed with NDI produced green coloured CT complexes covering the absorbance visible and NIR region and with PDI produced red covering the absorbance visible region. The CT complexes showed 1:1 complexation for donor polymers and acceptor NDI (or PDI) molecules with respect to long range order of D-A-D-A-D-A π-stacked supramolecular assemblies. Interestingly, the solid state

alignment of the D-A interaction was controlled by the type of the acceptor units; as a result OPV polymer-NDI complex arranged in lamellar fashion in solid state confirmed by Electron microscope, polarizing microscope and X-ray diffraction analysis. To study the macromolecular effect on the D-A complexation in the CT complex, structurally identical small molecular OPV analogues were synthesized. The OPV-NDI and OPV-PDI complexes were found to exhibit CT band in the solution; however, the phase separation of individual donor and acceptor in solid state at room temperature. Interestingly, CT transfer interaction between OPV polymers and acceptor produced stable CT complexes at room temperature. The polymer + PDI complexes showed broad CT band in the range of 500-700 nm and The polymer + PDI complexes showed broad CT band in the range of 500-1100 nm band in solid state. Additionally, these stable room temperature donor-acceptor CT self-assemblies can be processed under solvent free melt crystallization process; thus, they are very important futuristic materials for directly processing in optoelectronics.

Future Directions

This thesis is mainly focused on the synthesis of segmented π-conjugated polymers and these polymers were completely characterized using standard techniques. These polymers exhibited diverse self-assembly that was exploited for the organic photonic switches application, and their aqueous self-assembly was utilized for bio imaging applications. Lastly, these polymers were complexed with acceptors like PDI and NDI resulting in color tunable CT complexes spanning the visible and NIR region. Donor-acceptor complexes that are made by blending process often phase separate after some time that is one of the limiting factors in D-A acceptor complexes. With the knowledge of the work done in this thesis we can develop D-A based random copolymers from alcohol derivative of OPV and naphthalene via isocyanate route. These random copolymers can form CT band in solution and solid state without adding any external molecule. This broad CT band would encompass the visible and NIR region. These polymers can avoid phase separation at any time. Lastly the ferroelectricity of D-A complexes, which is forming CT band will be studied.

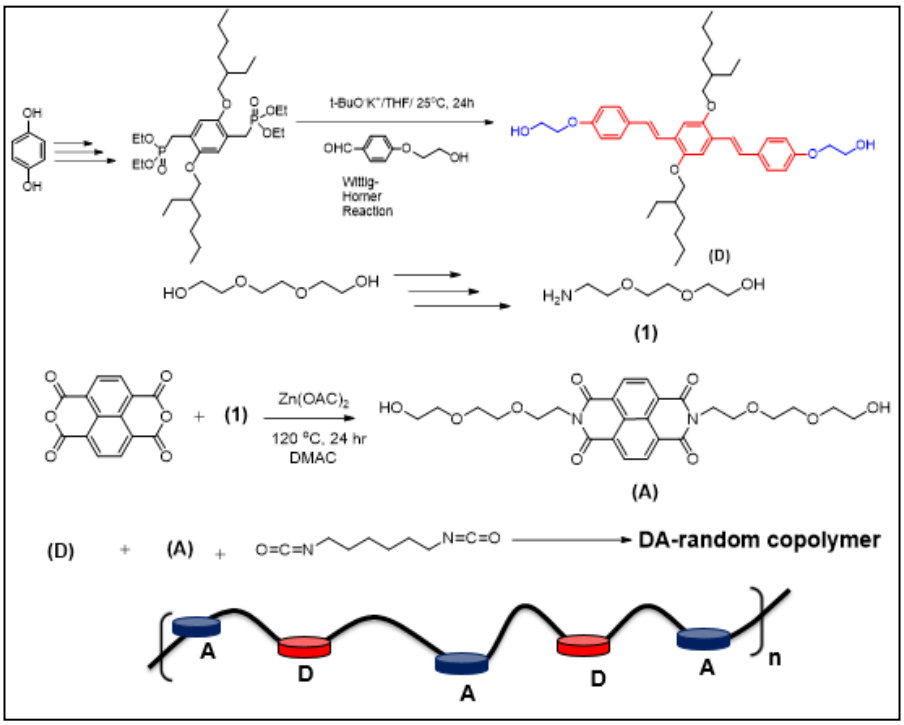

Figure 5.1: *Schematic representation of the synthesis of donor-acceptor random copolymer for the future work.*

List of publications

Publications in International Journals:

List of Publications:

1. Narasimha, K.; Jayakannan, M. Colour-tunable Amphiphilic Segmented π-Conjugated Polymer Nano-Assemblies and their Bio-imaging in Cancer Cells. ***Macromolecules*, 2016**, *49*, 4102-4114.
2. Narasimha, K.; Jayakannan, M. π-Conjugated Polymer Anisotroipic Organogel Nano-fibrous Assemblies for Thermo-responsive Photonic Switches, ***ACS Appl. Mater. Interfaces***., **2014**, *6*, 19385-19396
3. Goel, M.; **Narasimha, K.;** Jayakannan, M. Helical Self-assemblies of Segmented Poly(phenylenevinylene)s and their Hierarchical Donor-Acceptor Complexes. ***Macromolecules***, **2014**, *47*, 2592-2603.
4. Goel, M.; **Narasimha, K.;** Jayakannan, M. Direct Evidence for Secondary Interactions in Planar and Nonplanar Aromatic π-Conjugates and Their Photophysical Characteristics in Solid-State Assemblies. ***J. Phys. Chem. B***. **2015**, 119, 5102-5112.
5. Narasimha, K.; Jayakannan, M. Segmented π-Conjugated Polymer-Arylenebisimide Based Room Temperature Charge-Transfer Complexes and Their Color Tunability. *Manuscript Submitted to* ***Macromolecules.***
6. Narasimha, K.; Jayakannan, M. Donor-Acceptor Charge Transfer Complexes in Organogel Matrix (*Manuscript under preparation).*

Publications in International Conference Proceedings:

1. Narasimha, K.; Jayakannan, M. Colour-tunable Amphiphilic Segmented π-Conjugated Polymer Nano-Assemblies and their Bio-imaging in Cancer Cells, *ICONSAT-2016*, IISER PUNE, March 2016.
2. Karnati, N.; Jayakannan, M. π-Conjugated Polymer Anisotroipic Organogel Nano-fibrous Assemblies for Thermo-responsive Photonic Switches, *MACRO-2015*, IACS Kolkata, Jan-2015.
3. Karnati, N.; Jayakannan, M. π-Conjugated Polymer Anisotroipic Organogel Nano-fibrous Assemblies for Thermo-responsive Photonic Switches, *"International meet on Advances in Polymer Science",* NCL Pune, Oct-2014.